Investigations on the synthesis of silicon-arsenic double bonds and the preparation of M_xE_y nanoparticles from single-source-precursors (M = Ga, Ge, Sn; E = P, As)

Zur Erlangung des

DOKTORGRADES DER NATURWISSENSCHAFTEN

(Dr. rer. nat.)

der Fakultät für Chemie und Pharmazie

der Universität Regensburg

DISSERTATION

Vorgelegt von

Daniela Meyer

aus Neumarkt in der Oberpfalz

Regensburg 2019

Diese Arbeit wurde angeleitet von Prof. Dr. Manfred Scheer.

Promotionsgesuch eingereicht am: 02. April 2019

Tag der mündlichen Prüfung: 02. Mai 2019

Vorsitzender: Prof. Dr. Hubert Motschmann

Prüfungsausschuss: Prof. Dr. Manfred Scheer

Prof. Dr. Henri Brunner

Prof. Dr. Frank-Michael Matysik

Universität Regensburg

Eidesstattliche Erklärung

Ich erkläre hiermit an Eides statt, dass ich die vorliegende Arbeit ohne unzulässige Hilfe Dritter und ohne Benutzung anderer als der angegebenen Hilfsmittel angefertigt habe; die aus anderen Quellen direkt oder indirekt übernommenen Daten und Konzepte sind unter Angabe des Literaturzitats gekennzeichnet.

Daniela Meyer

This thesis was elaborated within the period from January 2014 until April 2019 in the Institute of Inorganic Chemistry at the University of Regensburg, under the supervision of Prof. Dr. Manfred Scheer.

Dedicated to my family

“The secret to do anything is believing, that you can do it. Anything, that you believe you can do strong enough, you can do. Anything. As long as you believe.“

Bob Ross

Table of Contents

1. Introduction

1.1. Phosphorus – a versatile element

1.1.1. Industrial preparation, modifications and applications

Due to its oxophilic character phosphorus[1] can solely be found as phosphatic minerals in nature, so that for the first time in 1669 the alchemist Hennig Brand was able to obtain it in its elemental form as white phosphorus.[2] After the discovery, this element with its greenish-blue luminescence was produced from urine and bone ash for further use as fertilizer in the early agricultural industry. Today P_4 is prepared according to the method of Readman by the reaction of fluorapatite $Ca_5(PO_4)_3(OH, F, Cl)$ (= $3\ Ca_3(PO_4)_2 \cdot Ca(OH, F, Cl)_2$) with coal and quartzite in an electric arc furnace.[3,4,5] Thereby, elemental phosphorus shows four main modifications with several submodifications.

The most accessible and most important modification of phosphorus in industry is white phosphorus P_4 consisting of tetrahedral molecules in the solid state (Figure 1 - 1 centre).[6,7,8] P_4 is at room temperature metastable to the transformation into more stable modifications[9,10] as well as it is oxidized to P_2O_5 when exposed to air. The oxidation is accompanied by chemiluminescence which gave the element its name φωσφόρος (*phōsphóros*), meaning *light-bearer*.[11-14] Apart from this interesting phenomenon white phosphorus also shows three crystalline sub-modifications with different orientations of the P_4 tetrahedra. α-P_4, the modification at room temperature, exhibits a random cubic solid state structure, changing into triclinic β-P_4 at –76.9°C and to γ-P_4 with a distorted *bcc*-structure at –170°C.[15-18]

The most important phosphorus containing compounds in industry[19] are fertilizers and herbicides like glyphosate and its derivatives that are processed via H_3PO_2 and H_3PO_3.[20] P_4 itself is annealed to P_{red}[21] for further application. Furthermore, it is used in the synthesis of species like PCl_3 and $POCl_3$, which is utilized for example as chlorinating agent in drug manufacturing and the synthesis of fine chemicals, etc.[21,22,23] Examples are sulphur compounds like P_4S_{10} applied as anticorrosive and anti-wear additives in lubricating oil.[24,25] P_4 was used as rat poison,[26] while it can still be found in smoke grenades and in firebombs,[27] which gained notoriety in World War II.

As already mentioned the high-temperature modification and the second most important form of phosphorus in industry, red phosphorus, can be obtained by the irradiation or the annealing of P_4 at 200 – 400°C (Figure 1 - 1 bottom left). After its discovery by Schrötter in 1848,[28,29] a highly polymeric and amorphous solid state structure with random strands of P_2-bridged P_{10}-cages was revealed by crystallization experiments.[30,31]

Experiments proved P_{red} to be less reactive than P_4 which becomes already apparent in the fact that P_{red} is not pyrophoric. But by boiling P_{red} in PBr_3 it is possible to isolate a more reactive sub-modification called Schenck's phosphorus with a bromine content up to 30%.[30,32]

Due to its reduced reactivity P_{red} is preferred towards P_4 in pyrotechnics or ammunition manufacturing, but it also finds application in drug manufacturing, in safety matches, which occurred after the discovery of the toxicity of white phosphorus, as flame inhibitor in plastic materials or as potential anode for sodium ion batteries. [26,27,33-35]

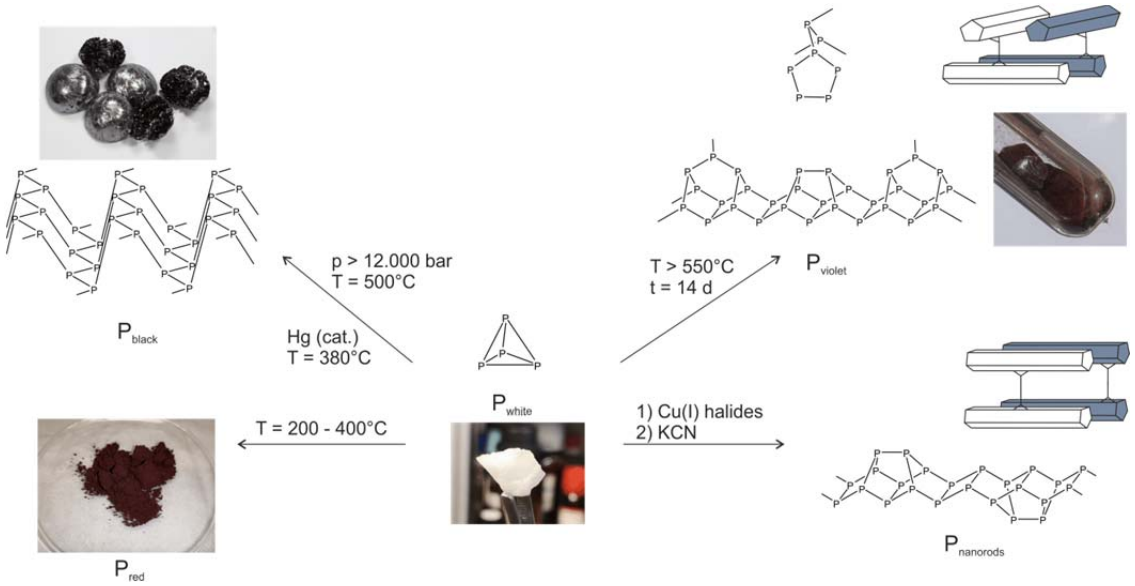

Figure 1 - 1: The different modifications of phosphorus and their preparation methods starting from P_4 (centre). From the bottom left to the bottom right: Red phosphorus, annealed at T = 200 – 400°C; black phosphorus, achieved at high pressure (> 12.000 bar) and elevated temperatures (picture P_{black} © Juergen Bauer – smart-elements.com); nanorods of phosphorus, synthesized with copper halides; Hittorf's phosphorus, prepared during long heating periods (picture P_{violet} from commons.wikimedia.org, CC BY 3.0).

Not even twenty years after the discovery of red phosphorus Hittorf reported on the synthesis of a new modification he observed during crystallisation experiments of P_{red} in liquid lead.[36] In 1969, Krebs *et al*. finally succeeded in the solution of the solid state structure as they were able to show that P_{violet} consists of polymeric strands of alternating P_8- and P_9-units connected by P_2-bridges. Thereby, the superimposed polymers are arranged perpendicular to each other (Figure 1 - 1 top right).[37]

In 2004 Pfitzner *et al.* synthesized phosphorus nanorods by reacting P_4 with copper(I) halides which first leads to the formation of the two copper phosphorus polymers $(CuI)_8P_{12}$ and $(CuI)_3P_{12}$. With addition of KCN it is possible to isolate the polymers $^1_\infty$[P8]P4(4)[and $^1_\infty$[P10]P2[that are very similar to those of P_{violet} and also to those of P_{red} (Figure 1 - 1 bottom right). But in contrast to the perpendicular orientation of P_{violet}, all strands of $P_{nanorods}$ are parallel to each other.[38]

The most stable modification of phosphorus at room temperature[39] is the high pressure modification P_{black} discovered by Bridgman in 1914. Usually it is prepared from P_4 at 200°C and pressures of at least 12.000 bar, but only recently a new low pressure synthesis was reported starting from P_{red}, Au, Sn and SnI_4 via Au_3SnP_7.[15,40,41] The first low pressure approach to black phosphorus was introduced by Krebs *et al.* in 1955 with Hg as a catalyst.[42] In contrast to P_{red} and P_{violet} the solid state structure of P_{black} consists of heavily waved double-layers in an orthorhombic crystal system (Figure 1 - 1 top left),[43] which can be transferred into a cubic form at 10 GPa[44] and a hexagonal system at 137 GPa.[45] Furthermore, P_{black} shows semiconducting properties and a variable band gap of about 0.3 eV[46] depending on the number of layers of phosphorus,[47] making it applicable in batteries, transistors, sensor techniques and printing devices.[48-52] Because of these interesting features theoretical calculations were performed leading to the hypothetical modifications P_{blue} and P_{green} with crystal structures very similar to the one of P_{black} and tunable band gaps of about 3 eV (P_{blue}) and 0.7 – 2.4 eV (P_{green}).[47,53]

1.1.2. Phosphorus in nature

1.1.2.1. Biological importance

Although the different modifications of elemental phosphorus do not occur in nature, the element itself plays a significant role as it can be found in the cells of each creature.[54] It forms the phosphate backbone of the DNA double helix[55] which acts as storage device of genetic information.[56] Also the RNA, whose task is the translation of genetic information into amino acids, holds an analogous backbone. Additionally, phosphorus can be found as phospholipids in cell membranes, as $Ca_3(PO_4)_2$ in bones,[57] or in 2,3-bisphosphoglycerate, modulating the O_2-affinity of haemoglobin. However, the most important phosphorus compound in organisms is the universal energy currency adenosine triphosphate ATP[58-60] with its three energy-rich anhydride bonds. During phosphoryl group transfer reactions the energy is used to activate different molecules for various metabolisms. Additionally, ATP is a signalling molecule in numerous signalling cascades of metabolic regulation and it's synthesized in the respiratory chain by oxidative phosphorylation or in photosynthesis by photophosphorylation.[56]

1.1.2.2. The phosphorus cycle

Because of the essential role of this element for animals and plants the phosphorus cycle evolved as one of the slowest biogeochemical processes in the world since the majority of the phosphate movement takes place over soil and through oceans. The phosphorus cycle holds two reservoirs which are constantly exchanging phosphate. First, organic PO_4^{3-} is stored in each organism on earth. This PO_4^{3-} is released with the death of a creature resulting in the organic phosphorus compounds to be transferred into inorganic, poorly soluble phosphates over a long period of time. These phosphates enclosed in rocks are eroded into the oceans, where they deposit as sediments and therefore are excluded from the range of almost all organisms until tectonic events lift the seabed. Subsequently, rain, bacteria and fungi are able to release orthophosphate from the rocks whereby it is available as a fertilizer for plants with which the phosphorus is again incorporated into the organic part of the phosphorus cycle.[61-65]

1.1.3. Chemical behaviour

Beyond its miscellaneous applications and its significance in nature phosphorus also offers a broad spectrum of reactions. P_4 is a reducing agent which not only self-ignites in the open air but is also capable of reducing H_2SO_4 to SO_2 and precipitating metals from their salt solutions.[1] Although it is a rather poor ligand, white phosphorus forms various complexes with Lewis-acidic metals or metal fragments acting as end-on[66,67] or bidentate ligand.[68-71] In literature there are also numerous examples for compounds exhibiting single- and double-bridging bicyclo[1.1.0]butane (butterfly) structural motifs[69,72-74] or for reactions in which the P_4 tetrahedron is transformed into P_3-,[75-78] cyclo-P_4-,[74,79] cyclo-P_5-,[80-82] or P_6-fragments.[83-86] In contrast to the just described rich chemistry of white phosphorus the other modifications of this element are distinctly less reactive.

1.1.4. The toxicity of phosphorus

Of all modifications of elemental phosphorus only P_4 leads to severe symptoms of poisoning after exposure to high doses or repeatedly to low doses.[26] The repetitive intake may lead to severe

damage of tissue and organs like necrosis of the soft tissue of the mouth, termed as phosphonecrosis or phossy jaw. This painful disease affected especially the workers of match stick factories around the turn of the last century when match sticks were still made of pastes containing about 4% of P_4.[87] With this in view, the use of white phosphorus in cod-liver oil to cure toddlers with the bone disease rickets till the beginning of the 20th century seems like lunacy. The reason for the "effectivity" of this dubious treatment is the formation of condensed bone structures in growing bone tissue due to P_4 counteracting the softening of the bones. Still, the children suffered from decreased appetite and growth during the treatment. Unlike the long-term exposition the intake of one large dose of white phosphorus results in severe vomiting and abdominal cramps followed by symptoms like collapse of blood vessels or fatty infiltration into all tissues until death by multi-organ failure occurs.[88,89]

1.2. Arsenic – the notorious one

1.2.1. The Queen of poisons

In contrast to phosphorus arsenic is commonly known for its toxicity[90,91] as especially its trivalent compounds were used as poisons (As_2O_3 "white arsenic") in assassinations driven by political motivations or base motives throughout the centuries. The element even became a star in films like "Arsenic and Old Lace" by Frank Capra or in books as "Strong Poison" by Dorothy L. Sayers in which a particularly insidious murder demands the entire expertise of gentleman detective Lord Peter Wimsey. Only with the discovery of the Marsh test, invented by James Marsh in 1836,[92] and the associated chances to verify arsenic, the element and its compounds vanished from the list of coveted toxins on which it was due to its symptoms of poisoning.

These resemble the gastric flu as both conditions come along with severe abdominal cramps, diarrhoea and vomiting being caused by the ability of As compounds to tarnish cellular membrane processes leading to an abnormal water and electrolyte balance.[93,94] But also the reactivity of AsO_4^{3-} and AsO_3^{3-} towards the SH-groups in the active sites of enzymes is dangerous as the concerned enzymes are shut down. This impedes cellular energy generation or disrupts nuclear mechanisms like gene expression or DNA repair which might end in tumours turning arsenic into a cocarcinogen with mutagenic porperties. Furthermore, As interferes with the endogenous synthesis of the energy carrier ATP (chapter 1.1.2.1), because the involved enzymes are not able to differentiate between phosphorus and its heavier homologue leading to the production of adenosine triarsenate ATAs. However, ATAs is highly instable and prone to hydrolysis by which the energy supply in the cells finally collapses.[56] Due to these risks protection sequences in the DNA evolved which code the synthesis of the enzyme arsenic(+3)-methyltransferase catalysing the degradation of inorganic As(III) species.[93-101] Over the time different detoxification pathways occurred, as some marine organisms are able to synthesize inert arsenosugars[102] but also species like methyl arsonate, arsenocholine and arsenobetaine have been identified.[103,104] Scientists even found evidences for arsenic to play a role in the metabolism of the amino acid methionine.[105]

1.2.2. Natural occurrence, modifications and industrial preparation

Although there are only very little examples for the role of arsenic in nature it can be found as ore like realgar As_4S_4 as well as in metal arsenides like arsenopyrite Fe[AsS] (= $FeAs_2 \cdot FeS_2$). It even exists in pure form. In 1250, the monk Albertus Magnus from Cologne successfully isolated elemental As from an arsenic compound.[1] The name arsenic originates from the Arabic word *al zernikh* or *al zarnikh* meaning *golden coloured* which initially was the name for orpiment As_2S_3.[106,93,1]
The most stable modification of arsenic As_{grey} that shows a rhombohedral solid state structure[107,108] similar to the theoretical P_{blue}[53] with waved double layers of six-rings in chair conformation and metalloid properties (Figure 1 - 2 centre).[109-112,6] These properties lead to a huge band gap that occurs as soon as the crystallinity vanishes leaving an amorphous material probably suitable for semiconductor applications.[113,114]
In industry, the most important modification of arsenic is prepared from arsenopyrite Fe[AsS] or loellingite $FeAs_2$ by sublimating As from the ore at 650 – 700°C and precipitating it onto cold condensers or by the reduction of As_2O_3 with activated carbon at 700 – 800°C. Additionally emerging impurities as there are As_2O_3 or As_2S_3 are removed by a second sublimation step. Exceptionally pure As_{grey} which is needed in solid-state technology can be achieved by sublimation from molten lead, by crystallization of molten arsenic or the decomposition of pure AsH_3.[1]

If arsenic is evaporated and quenched on a cold surface or in solvents it is possible to obtain a second modification, the metastable yellow arsenic[115] which is the heavier analogue of P_4. The first who managed to achieve this allotrope was Bettendorff in 1867.[116] As_4, which is prepared at temperatures of 750°C, tends to polymerize to As_{grey} in solution and solid state above 20°C and especially, when it's exposed to light. Due to this facts, single crystal X-ray studies are highly difficult with the result that till today no molecular structure of free yellow arsenic exists.[117,118] Nevertheless, X-ray analyses of vapour-deposited or encapsulated As_4 revealed a tetrahedral setup[7,119-123] as well as there are differential thermal analysis studies that give hints of at least two sub-modifications where the As_4 tetrahedra are arranged in different ways.[124]

Beside gray and yellow arsenic an orthorhombic modification called black arsenic exists but up to date it was only possible to synthesize it at high temperatures or with incorporated stabilizing impurities like Hg[125,126] or O.[125] Up to date, all attempts to cool pure As_{black} to room temperature failed which might be due to the fact that this allotrope is not as energetically favoured as As_{grey} or As_4.[127] However, the mineral arsenolamprite seems to contain pure black arsenic.[128]

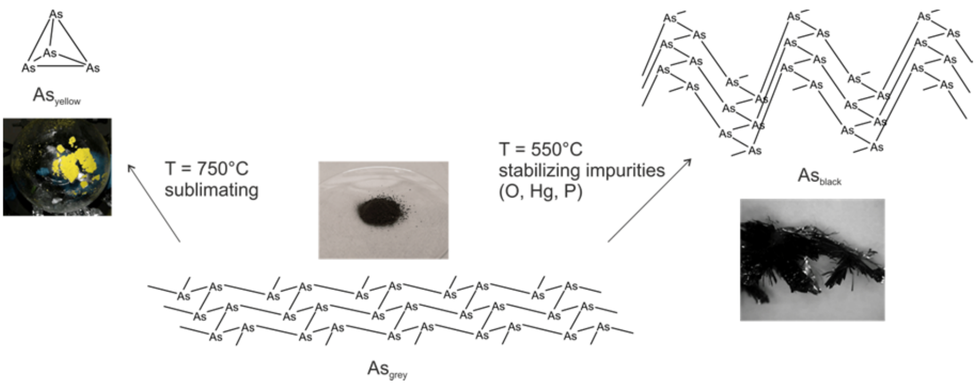

Figure 1 - 2: Modifications of arsenic starting from grey arsenic (centre). Left: Yellow As, prepared by sublimating As_{grey} at 750°C (picture by Maria Haimerl and Martin Weber). Right: P-stabilized black arsenic, achieved at 550°C (Picture reprinted from Angewandte Chemie International Edition with permission from Whiley, „Synthesis and Identification of Metastable Compounds: Black Arsenic – Science or Fiction“, O. Osters, T. Nilges, F. Bachhuber, F. Pielnhofer, R. Weihrich, M. Schöneich, P. Schmidt, Vol. 51, 2994 – 2997, Copyright 2013.).

1.2.3. The chemistry of arsenic

The chemical behaviour of grey arsenic compared to its yellow allotrope is similar to the reactivity of P_{red} and P_{black} compared to P_4, as As_{grey} does not decompose in the air but needs elevated temperatures to burn to As_2O_3 and As_2O_5. On the other hand, a reaction with F_2 or Cl_2 occurs already at room temperature just like the conversion with oxidizing acids with which arsenous acid is formed.[1] In contrast to As_{grey}, As_4 is neither stable in the air nor under light nor heat as the latter cause polymerisation above 20°C (chapter 1.2.2). As_4 is an even weaker ligand than its lighter homologue P_4, but nevertheless, it reveals a rich complex chemistry as it is able to coordinate as an intact tetrahedron end-on[129] or side-on[122,130] to metal centres, likewise it is able to bind in a bridging manner[131]. Similar to P_4 also in the case of As_4 a butterfly structural motif[132,133] can be found just as As_2-,[134,135] As_3-,[75,136] cyclo-As_4-,[131,137,138] As_5-[139] and As_6-ligands[138].

1.2.4. Surprising applications

When thinking of toxic elements and compounds the first usage that comes to one's mind is the application as pesticidal or insecticidal agent or as chemical weapon like it was the case for methylarsinechloride or Lewisit utilized in World War I and II.[93,140,141] Interesting is the application in the wall paint Paris Green in the 19th century consisting of $CuAc_2 \cdot 3\ Cu(AsO_2)_2$ that was unfortunately transformed to highly toxic and volatile As(III) compounds by mould and H_2 emerging from gas lamps.[141] In contrast to this non-voluntary poisoning the use of arsenic compounds as beauty aid for the ladies of ancient times who aimed for noble paleness and a healthy look doesn't seem to be the best idea.[140] But even more surprising is the application of mostly organic As-compounds as medicine like Melarsoprol[140] for African sleeping sickness or especially as chemotherapeutic agents as there are Salvarsan[142,143,144] and As_2O_3.[142] Also in industry a wide range of usage for arsenic exists. Like phosphorus it is used as wood preservative, or it is an additive to bronze in order to increase the degree of hardness, or to molten lead for a higher surface tension.[142] In the last few decades another field of application emerged as very pure arsenic is an important part of solid-state technology as well as the direct semiconductor GaAs and its heavier homologue InAs are utilized in lasers[145] or fluorescence sensors,[146] whereas GaInNAsSb,[147] Cu_3AsS_4 and $Cu_{12}As_4S_{13}$ are suitable for

photovoltaics.[148,149] These substances, especially GaAs and InAs are not only used as bulk-material but also in nanoparticles form offering enhanced and tuneable properties like for example GaAs exhibits an absorption and emission in the visible range at a particle radius below 10 nm.[150,151]

1.3. Nanoparticles

1.3.1. The definition

Nanoscale materials are not only interesting for compounds of arsenic as they are a versatile and fascinating class of matter. First, the term *nanoparticles*, deriving from greek νάνος (*nános*) meaning *dwarf*, describes materials whose individual components exhibit a diameter of about 1 to 100 nm (Figure 1 - 3). The comparison with a human hair, whose width is approximately 80.000 nm, clarifies the tiny dimensions where nanotechnology takes place, and which are also the reason for exceptional properties and countless applications.[152,153] Named by Taniguchi in 1974[154] nanotechnology as the science of nanoscopic matter has since then evolved to one of the most promising fields of research and industries.

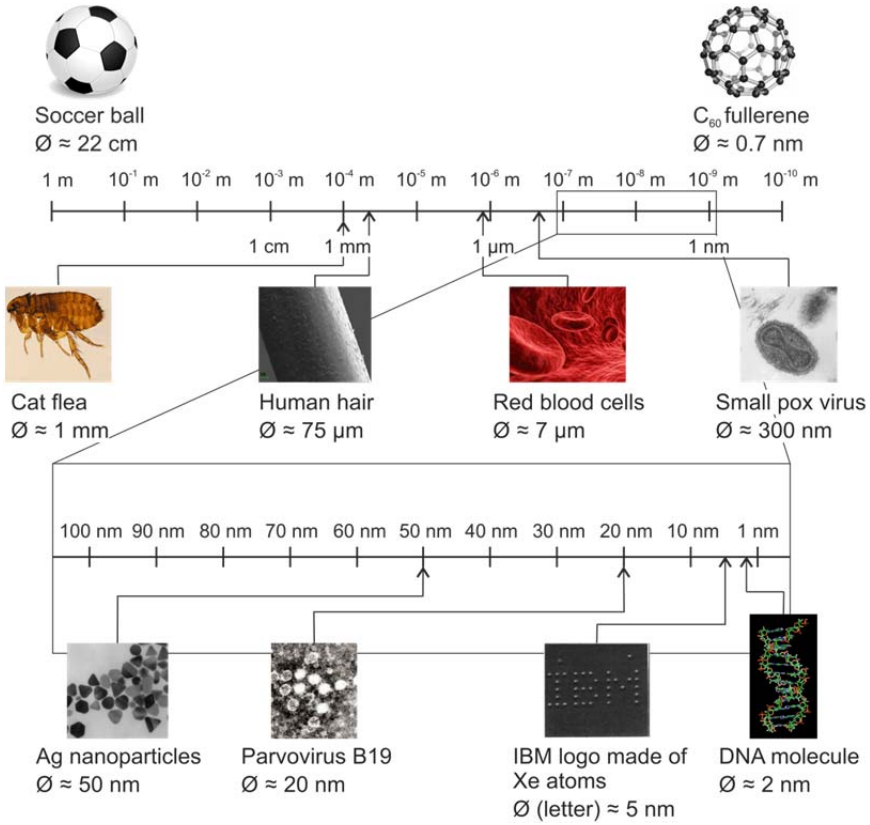

Figure 1 - 3: Size comparison ranging from 1 m to 0.1 nm on the top scale, while the bottom scale depicts the nanoparticles range from 100 nm to 1 nm. For a better understanding, some examples like a human hair or red blood cells are shown. Attention should be paid to the ratio of the C_{60} molecule to a football which is approximately the same as the ratio of a football to the earth, namely $1:100 \cdot 10^6$. The image was inspired by figure 2.1 in chapter 2 of the final report about nanoscience and nanotechnology by the Royal Society, the UK National Academy of Science and the Royal Academy of Engineering; http://www.nanotec.org.uk/index.htm. The image of the Ag nanoparticles is reprinted from Analyst with permission from The Royal Society of Chemistry: "Gold and silver nanoparticles: A class of chromophores with colors tunable in the range from 400 to 750 nm", Y. Sun, Y. Xia, Vol. 128, 686 – 691, Copyright 2003. The picture of the IBM logo was reprinted with permission from Springer, Nature: Springer, Nature, "Positioning single atoms with a scanning tunnelling microscope", D. M. Eigler, E. K. Schweizer, Copyright 1990. All other images are either from de.wikipedia.org, en.wikipedia.org or commons.wikimedia.org (CC BY-SA 3.0 and CC BY-SA 4.0).

1.3.2. A brief history

Nanoscale particles exist almost as long as the universe due to their formation in supernovae or planetary nebulae[155-159] (Figure 1 - 4) and as a consequence they are also abundant all over the earth where they can be found as inorganic compounds like aluminosilicate or iron oxide in rocks.[160] During forest fires or volcanic eruptions nanoscopic soot material is released in large amounts into the air.[161] But also organisms contain a wide variety of organic nanoparticles like proteins, the DNA or glycogen in their cells.[162]

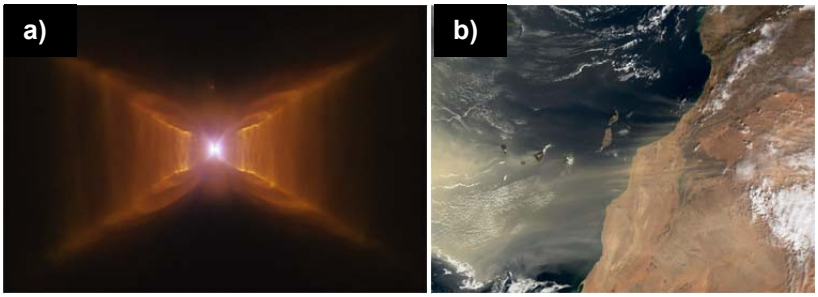

Figure 1 - 4: a): Image of the Red Rectangle proto-planetary Nebula, located in the monoceros constellation. Beside its red colour it also exhibits a blue luminescence that might derive from crystalline Si nanoparticles.[163] Image from https://de.wikipedia.org/wiki/Roter_Rechtecknebel (CC BY 2.0). b): Picture of a sandstorm blowing from the Sahara Desert over the Atlantic Ocean and the Canary Islands. Such phenomena are a source for naturally occurring nanoscale material similar to forest fires or volcanic eruptions. Image from https://earthobservatory.nasa.gov/NaturalHazards/view.php?id=2083.

But not all of the submicron material in nature derives from natural origins, ever since the industrial revolution let the amount of anthropogenic nanoparticles explode. Today, the unplanned release of anthropogenic nanoscale matter includes amongst others diesel exhaust and soot from welding or smelting processes leading to blankets of smog over big cities.[164,165] Despite these rather inconvenient consequences, nanoparticles offer numerous opportunities, so that their application has a surprisingly long history throughout the centuries as already the Romans were able to manufacture vessels containing nanoscale material. A spectacular example for this is the Lycurgus cup, a glass with beautiful ornaments that appears green in normal daylight, but changes its colour to red as soon as it is illuminated from the inside (Figure 1 - 5). This effect is caused by colloidal gold incorporated in the glass.[166] Similar to the gold nanoparticles other colloidal metals were used in ancient ceramics to give them unique decorations or colours.[167]

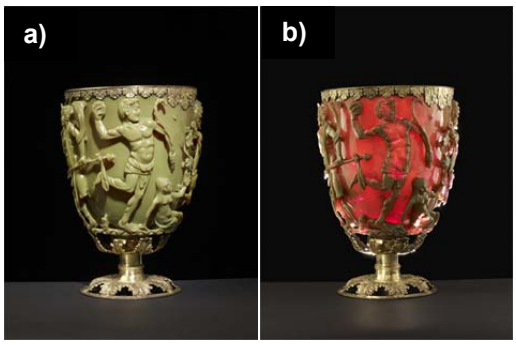

Figure 1 - 5: The Lycurgus cup is a glassy drinking cup garnished with scenes from the death of King Lycurgus and was manufactured in the Late Roman Empire around the 4th century AD. a): Image of the green cup in normal light. b): The cup is illuminated from inside displaying the red colour of nanoscopic gold incorporated in the glass. © 2017 Trustees of the British Museum.

The development of nanotechnology as a field of research slowly began in 1931 with the invention of the electron microscope, which allowed to take pictures in the nanoscale range for the first time.[168] About 30 years later Richard Feynman spoke about the multitudinous possibilities hidden in that world which is too small for our eyes.[169] Since the 1980s the progress in nanoscience proceeds faster and faster as new discoveries occurred, like the first synthesis of quantum dots,[170-172] or the invention of the scanning tunnel and the atomic force microscope, which provide far better images than the previous electronic microscopes.[168,173-175] Two other milestones in the history of nanoparticles are the discoveries of fullerenes[176] and carbon nanotubes,[177] which are as sensational as the IBM logo made of Xe atoms that were arranged by STM (Figure 1 - 6 c).[178] Today, the term *nanotechnology* contains a wide scientific field whose achievements shaped our modern world. Smartphones or high performance computers are not possible without the development of smaller and smaller transistors[179,180] or OLED-nano-polymer displays and even items of our everyday life comprise nanoparticles providing antibacterial or sturdy properties.[181]

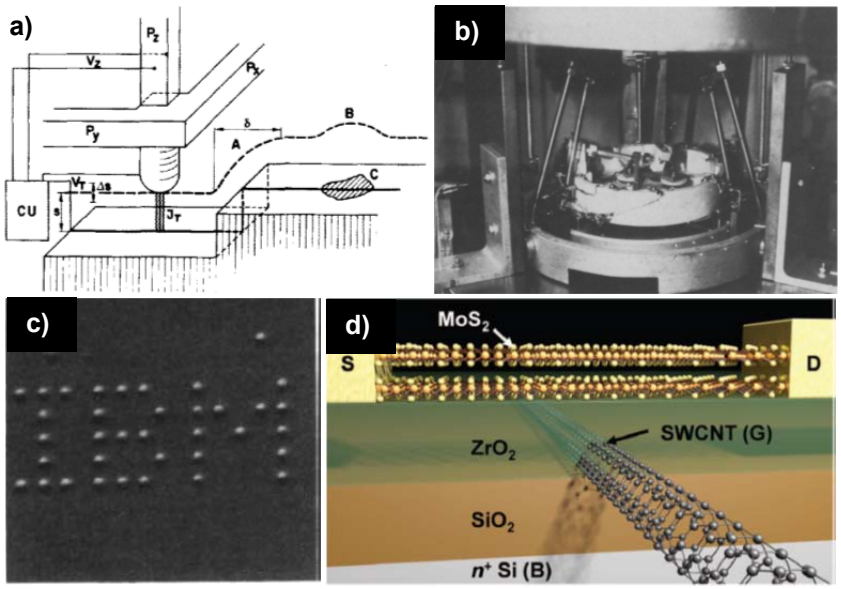

Figure 1 - 6: a): Schematic figure of the functional principle and b): image of the tunnel unit of Binnig's and Rohrer's scanning tunnelling microscope (Reprinted from "Scanning tunnelling microscopy", Vol. 126, G. Binning, H. Rohrer, 236 – 244, Copyright 1983, with permission from Elsevier). c): Image of the IBM logo made of Xe atoms (Reprinted by permission from Springer, Nature: Springer, Nature, "Positioning single atoms with a scanning tunnelling microscope", D. M. Eigler, E. K. Schweizer, Copyright 1990). d): Simulation of a nanoscale MoS_2-transistor with a gate length of 1 nm, one of the smallest transistors in the world (Reprinted by permission from The American Association for the Advancement of Science: Science, "MoS_2 transistors with 1-nanometer gate lenghts", S. B. Desai, S. R. Madhvapathy, A. B. Sachid, J. P. Llinas, Q. Wang, G. H. Ahn, G. Pitner, M. J. Kim, J. Bokor, C. Hu, H.-S. P. Wong, A. Javey, Copyright 2016).

1.3.3. Preparation of nanoscopic material

For the synthesis of nanoparticles two general approaches can be used which are based on opposed principles as the top-down preparation utilizes the physical comminution of a bulk material. On the other hand the bottom-up method starts from the self-organisation of atoms or molecules in chemical reactions.[182]

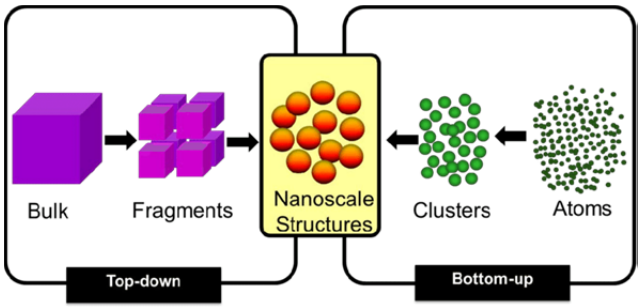

Figure 1 - 7: Top down approach by shredding larger materials vs bottom up methods in which nanoparticles are prepared by the self-organization of atoms and molecules. Image from Journal of Physics: Conference Series (CC BY 3.0).[183]

1.3.3.1. Top-down syntheses

The most obvious way to generate nanoscale substances is to mill a macroscopic material until its fragments have the desired size. This process is suitable for example for *bcc* and *hcp* metals that are quite hard and can be narrowed to the nanoparticle range, whereas the softer *fcc* metals are sintered as soon as the rising temperatures in the mills are high enough leading to an agglomeration of the hitherto hackled fragments.[182] During the synthesis by laser ablation the particles are removed through abrupt evaporation while the bulk is battered with a high-energy laser pulse.[184] The lithography method rather serves the preparation of defined nanoscopic structures on surfaces by using protective masks and an electron beam or extreme ultraviolet radiation to erase the unprotected parts of the material than to synthesize free nanoparticles.[185]

1.3.3.2. Bottom-up approaches

The bottom-up methods include the aerosol syntheses,[186-188] in which flame, plasma, electric or laser reactors[189] generate gaseous reagents that agglomerate to nanoparticles after being quenched by cold inert gas. During this process, the particle size and the size distribution are controlled by the velocity of evaporation as well as the temperature and pressure of the chilling gases. Nevertheless, the formation of metastable, crystalline phases at high temperatures might lead to phase changes during cooling and therefore to a loss of crystallinity or to agglomeration to larger units.[190]

A very similar preparation to the aerosol methods is the sol-gel approach where the products are not formed in gaseous reactions but in solution leading to materials of low density, which are applicable in ceramics after compression processes. However, in the course of compression undesired cracks in the material might occur due to compression ratios and the associated shrinkage.[190-192]

Another way for the preparation of nanoparticles is the use of the hot-injection method where the reagents are dissolved in a high-boiling and sometimes coordinating solvent followed by a fast heating step. Depending on the source materials used this approach can be divided into two sub-methods of which the first is the multi-source-precursor reaction.

Beside nanoparticular matter consisting of one element, like colloidal metals,[193] many nanoparticles are made of at least two components according to their applications as there are the CdS or CdSe quantum dots with their unique optical properties.[194] In the multi-source-precursor synthesis[195,196] each component of the eventual particle is present in a separate compound that are released by decomposition during heating to form the desired nanoscale material (Equation 1 - 1).

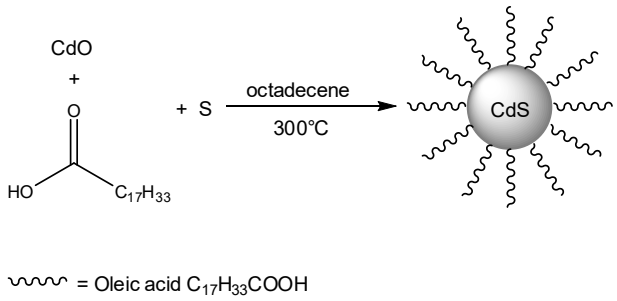

Equation 1 - 1: Preparation of CdS quantum dots via multi-source precursor synthesis using oleic acid as reagent and stabilizing agent to avoid an agglomeration of the particles.[197]

Familiar to this method is the single-source-precursor preparation. Here, all components of the nanoparticles are combined in one compound so that not only the stoichiometry is theoretically given but also the bonds between the components are preformed.[198,199] Other advantages are the avoidance of volatile and/or overly pyrophoric species, like P_4 or the highly toxic PH_3, as well as the preparation of solid precursors that are very easily purified to yield more pure nanoscopic materials. Also the need for harsh reaction temperatures is decreased (Equation 1 - 2).[200]

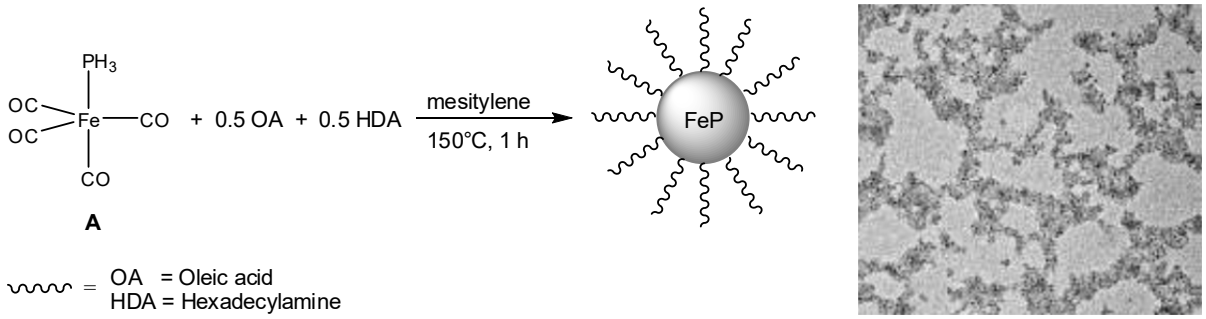

Equation 1 - 2: Single-source precursor synthesis of FeP nanoparticles by decomposition of $[(CO)_4Fe(PH_3)]$ (**A**) with oleic acid and hexadecylamine as hydrolizing and stabilizing agents.[201] Instead of the gaseous, flammable and highly toxic PH_3 complex **A**, which is a solid and therefore easier to handle, was used. Right: TEM picture of the obtained FeP particles. Reprinted from Chemical Communications, 49, C. Hunger, W.-S. Ojo, S. Bauer, S. Xu, M. Zabel, B. Chaudret, L.-M. Lacroix, M. Scheer, C. Nayral, F. Delpech, "Stoichiometry-controlled FeP nanoparticles synthesized from a single source precursor", p. 11788 – 11790, Copyright 2013, with permission from The Royal Society of Chemistry.

All these facts make the single-source-precursor method to an attractive approach although the synthesis of the precursor complexes itself can be quite challenging.

1.3.4. Unique properties

The reason for the preparation of nanoparticles is the fact that they exhibit fascinating characteristics which are caused by their small size leading to an increased amount of atoms located in an energetically unfavourable place at the particle's surface.[1,182] This results in an enlarged surface-to-bulk ratio which not only extends the total surface of a material consisting of nanoparticles many times over compared to the corresponding bulk. It also turns nanoscale substances into very energy-rich compounds with a boosted reactivity explaining their use as catalysts.

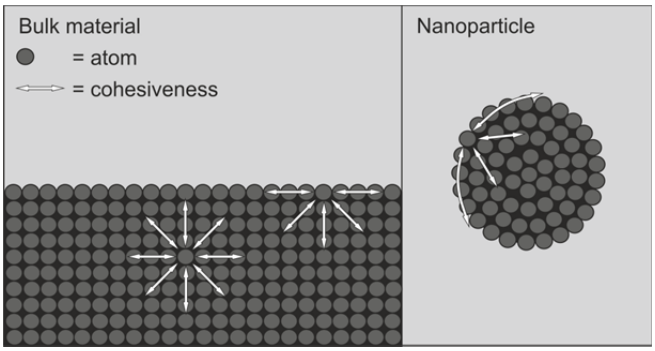

Figure 1 - 8: Comparison of the cohesiveness affecting the atoms within a bulk material and on its surface as well as affecting the atoms sitting on the surface of a nanoparticle. Image inspired by Figure 316 in „Hollemann, Wiberg – Lehrbuch der Anorganischen Chemie“, N. Wiberg, A. F. Hollemann, 2007, p 1430.

Nanoparticles also show a reduced melting point as a large number of atoms sits on the surface where they are weaker bound than the atoms in the bulk phase which are surrounded by binding partners from all sides (Figure 1 - 8). While in large crystalline materials lattice defects can be found repeatedly diminishing rigidity, the small size of nanoparticles prevents the formation of such defects resulting in resistant substances. Also accounted for by the size are the self-healing properties some coatings exhibit as the tiny units within such coatings are much easier relocated to fill a crack than bulk substances. On the first sight, the superior magnetic properties of nanoparticles, which allow their implementation in magnetic storage systems, have nothing to do with size, but on second thought this is not true. Similar to the highly ordered crystalline particles without any defects, magnetic nanoparticles exhibit a size in the range of a Weiss domain turning them into little permanent magnets. As it is less energy-consuming to influence a group of such flexible permanent magnets the magnetic capacity of nanoscale material is higher than the one of a comparable bulk substance with many rather immobile Weiss domains. But the most stunning characteristic nanoparticles display is their unique optical property that can be separated into two sub-features. The first part is the transparency which for example nano-Y_2O_3 reveals allowing the creation of ceramics made of this material whose constituent parts are to small to scatter the incoming VIS-light.[202] Nevertheless, UV-light is deflected making the transparent ceramics attractive as UV-absorbers. The second optical property of nanoparticles is the size-depending chromaticity like it can be seen in CdSe (Figure 1 - 9).[203]

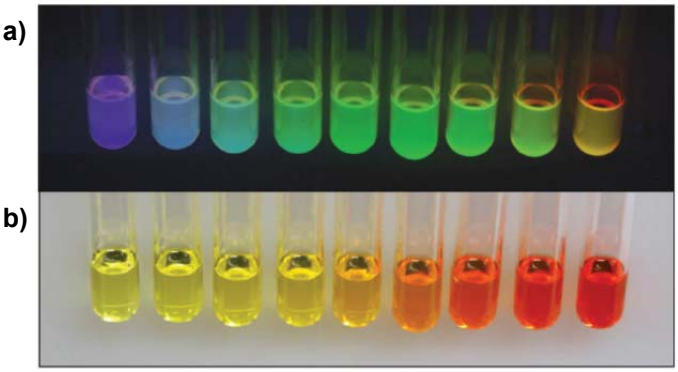

Figure 1 - 9: a): Suspensions of CdSe nanoparticles under UV light with an increasing size from left to right. b): Samples of the same CdSe nanoparticles under ambient light. Reprinted with permission from Journal of Chemical Education, 82, 11, K. J. Nordell, E. M. Boatman, G. C. Lisensky, “A Safer, Easier Faster Synthesis for CdSe Quantum Dot Nanocrystals”, pp 1697 – 1699, Copyright 2005, American Chemical society.

Again, due to the size of the individual particles, the charge carriers are constrained in all directions of space leading to a particle-in-the-box-like behaviour because of which the energetic orbitals are able to adopt only discreet values. This quantization of the energy levels is referred to as quantum confinement.[204-207] Therefore only certain wavelengths of light are absorbed or emitted which change as soon as the particle size is altered and with it the gaps between its energy levels. This behaviour offers a possibility to determine the size of the nanoparticles by analysis of the corresponding photometric and fluorimetric spectra.

1.3.5. Tools for the investigation of nanoparticles

Beyond the analysis outlined above a whole range of approaches to investigate nano-material has evolved since the development of the electron microscope in order to ascertain not only the size, but also the composition, the actual binding situation and the crystallinity within the particles.[182,208] The method of choice to make a point about the types of bonds between the components is the rather insensitive attenuated total reflectance FT-IR spectroscopy. Here, the analysis is based on the absorption and the excitation of different vibration modes by an IR-beam with the detected loss in energy being distinctive of the bonding types present in the sample.

Probably a little bit more interesting might be the elemental composition of the nanoscale substances which can be studied with a range of different methods like X-ray photoelectron spectroscopy (XPS), energy dispersive X-ray spectroscopy (EDX) or TOF-secondary ion mass spectrometry (TOF-SI-MS). In XPS and EDX a similar approach is used as in both examination methods nuclear electrons are utilized for detection. For XPS analyses an X-ray beam strikes nuclear electrons out of the sample's surface whose kinetic energy, which is representative for each element, is detected. In the same way, an electron beam is applied in EDX to again knock nuclear electrons out of a surface. But instead of studying their energy, the element-specific X-rays are recorded which originate from electrons of higher energy levels falling down to the now unoccupied lower ones while emitting radiation. In contrast to these two methods the very sensitive TOF-SI-MS exploits a completely different approach as here ionized Ga or Ar atoms are fired at a sample releasing fragments from its surface (sputtering) that are analysed after a second ionization step. The now charged fragments are detected in a time-of-flight-MS.

Structural investigations are performed by utilizing some classic inorganic methods as there are X-ray analysis, small angle X-ray and neutron scattering, extended X-ray absorption fine structure (EXAFS) or positron lifetime spectroscopy. The general crystallinity of a sample, including the detection if the nanoparticles are amorphous or crystalline or the determination of the size of the crystalline parts, is studied by X-ray analysis. However, small angle X-ray and neutron scattering is used to gain insight into the form and orientation of the individual crystallites as well as into number and location of the points of contact between them. Akin to this, by EXAFS questions about short-range orders within a single particle can be answered, while lattice defects and the associated structural fluctuations are detected by positron lifetime spectroscopy. Another method to study the defects within a crystalline nano-material is the Muon spin rotation which is limited to magnetic substances and used to identify the magnetic structure of a sample. The defects can be ascertained due to the muons that tend to accumulate in such disordered parts of the crystal lattice.

For the structural analysis of biological nanoparticles like proteins circular dichroism is utilized to determine the secondary structure due to the refractive indices that provide an indication of the amount of β-sheets and α-helices present in a protein. Furthermore, colorimetric approaches are applicable to quantify for example metallic cofactors as copper by transferring it into a coloured complex with bicinchoninic acid.

However, the most fascinating analytical methods concerning nanoparticles are the imaging techniques around the electron microscopy like the above mentioned scanning tunnel and atomic force microscopes, of which the latter generates 3D pictures of the samples, or the transmission and scanning electron microscopes. By the use of those form and size of nanoscale substances in a studied sample are easily determined.

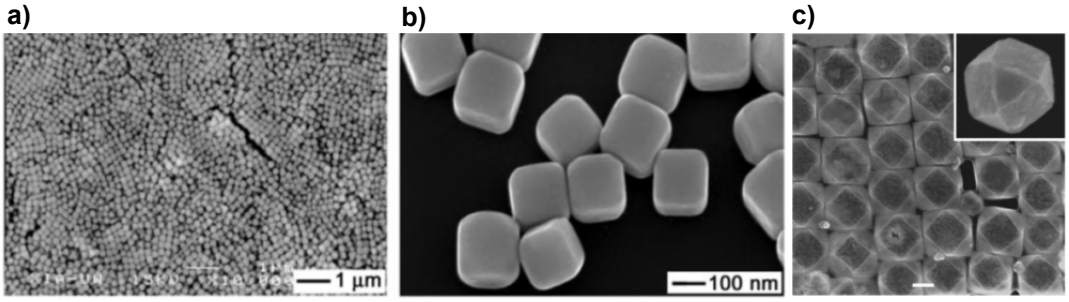

Figure 1 - 10: a), b): SEM Images of cubic Ag nanoparticles synthesized via polyol synthesis. c): Ag nanocubes after the reaction with 0.3 mL $HAuCl_4$.[209] Reprinted by permission from The American Association for the Advancement of Science: Science, "Shape-Controlled Synthesis of Gold and Silver Nanoparticles", Y. Sun, Y. Xia, Copyright 2002.

1.3.6. The toxicity of nanoscale materials

Beside the different preparation and detection methods also reports about the toxicity of nanoparticles gradually emerged assuming the small size of the particles might turn them into toxins due to the associated potential to overcome endogenous protective barriers.[161,164,210,211] But in fact the danger arising from such substances might not be as grave as feared because the reactive surface of airborne particles leads to the agglomeration to larger units, which are less dangerous. Nevertheless, regarding this outstanding reactivity the surface of nanoscale material seems to be a good indication for its hazardousness, because the substances might react readily within the human body exactly like they do with their provided reaction partners. This implies the generation of reactive nitrogen or oxygen species in the cells causing oxidative stress which eventually leads to severe damage. Thus, the intake of nanoparticles might lead to inflammation and fibroses up to death by tumours in one or more organs depending on their capability of being absorbed into the body.[164,212-216] The occurring macroscopic effects are caused by microscopic reasons due to the ability of nanoscopic matter to penetrate the cells and their compartments, where the reactivity of the foreign matter causes oxidative stress or damage to the cytoskeleton.[217,218]

1.3.7. Abundant fields of application and far more possibilities

Despite the not to be underestimated toxicity, today, nanoparticles find application in all aspects of life, starting with medicine,[219-221] energy techniques or material sciences through to micro-[187] and optoelectronic[194] as well as different data storage systems[222-224] and high-performance ceramics.[225,226] In medicine, magnetic nanoparticles are used in tumour treatment or as contrast agents for MRI,[227] while other therapeutic approaches base on gene transfer strategies[228] as well as they utilize nanoscopic polymers or micelles as vessels in drug delivery that can be synthesized exactly fitting to their application.[229,230] Likewise, the antibacterial effects[231] of nanoparticles are known for their applicability to stimulate responses of the immune system.[232,233] Very promising is the research concerning artificial skin[234,235] that might be used as a realistic coating for prosthetics (Figure 1 - 11 a), and tissue engineering.[236]

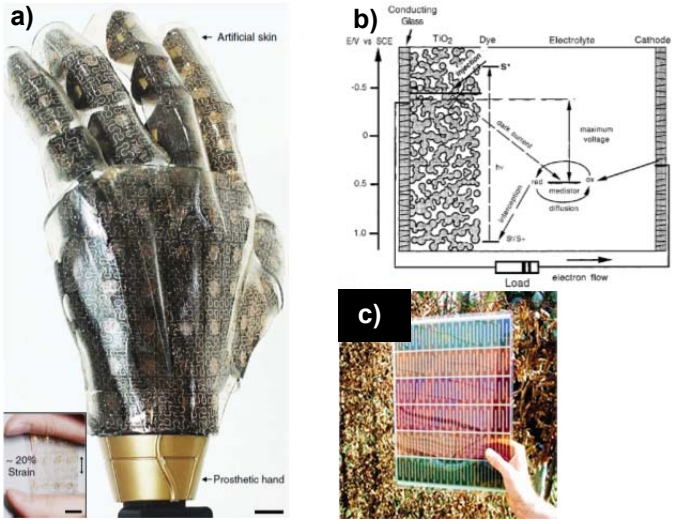

Figure 1 - 11: a): Image of a prosthetic hand covered in artificial skin made of stretchable Si nanoribbons, which is not only able to sense humidity, pressure or temperature, but can also produce "body warmth" by itself due to an implemented heater.[235] Reprinted by permission from Springer, Nature: Springer, Nature Communications, "Stretchable silicon nanoribbon electronics for skin prosthesis", J. Kim, M. Lee, H. J. Shim, R. Ghaffari, H. R. Cho, D. Son, Y. H. Jung, M. Soh, C. Choi, S. Jung, K. Chu, D. Jeon, S.-T. Lee, J. H. Kim, S. H. Choi, T. Hyeon, D.-H. Kim, Copyright 2014. b): Schematic figure of Grätzel's dye sensitized solar cell (DSSC). Reprinted by permission from: "Molecular Photovoltaics", A. Hegfeldt, M. Grätzel, *Acc. Chem. Res.* 2000, *33*, 269 – 277, Copyright 2000, American Chemical Society. c): Photo of DSSCs. © Winfried Hoffmann. Reprinted with permission from MIT Technology Review, https://www.technologyreview.com/s/406763/window-power/#comments.

Beside the interesting medical possibilities one of the main application fields of nanoscale material is catalysis as there are numerous examples for nanoparticles catalysts due to their reactive surface which leads to an increased reaction capacity at reduced temperatures,[237-242] being the reason why nanomaterials can also be found in various sensors.[243]

In the field of energy techniques, nanoparticles play an important role for light harvesting and the conversion of light energy into thermal[244] or electric energy, as it is the case in solar cells with Grätzel's dye sensitized solar cell (DSSC) being the first to exploit the advantages of the huge surface of nano-TiO_2 (Figure 1 - 11 b and c).[245-247] Another possibility for energy conversion and potential energy storage is the solar-based water splitting, where the energy is saved in the amount of formed H_2 retrievable by combustion.[248] In the same way, scientists all over the world work on solutions for the ineffectiveness of commercial Li-ion batteries and the opportunities of nanoparticles to improve

this state.[249,250] Moreover, nanoscopic substances provide the potential to be utilised in fuel cell technology in order to produce commercial cells operating at room temperature instead of 500 – 1000°C.[251]

In materials sciences nanoparticles often offer great alternatives to bulk compounds[241] as the nanoscale substances show for example comparable or better stability with a simultaneous loss of weight which is an interesting feature for automotive and aviation industry.[252-254] Promising for varnish and paint amongst others is the development of self-healing and pressure-sensitive coatings made of nano-material[255,256] which also might be a convenient property for the UV protective layers that are already used for wood,[257] plastics[258] or textiles.[259]

Beside all these interesting applications for industries nanoparticles are also used for the provision of clean water in the dry 3rd world countries with often contaminated groundwater resources,[260] to supply people after natural disasters or to help survivors in war zones where all infrastructure is destroyed.[261] It is similar with the decomposition of oil which is released during the averages of supertankers or within wastewaters of refineries and subsequently pollutes huge areas of the ocean killing thousands and thousands of marine creatures and birds. Thus, Ziolli *et al.* were able to report on a heterogenous nano-TiO_2 catalyst which corrodes the water-soluble fractions of crude-oil in seawater under UV irradiation.[262] However, nanoscale material is not only suitable to decompose pollutants in water, but it can also be incorporated in filters that destroy contaminants from the air.[263]

Beside the fascinating examples above there are also numerous applications for nanoparticles containing phosphorus and arsenic (chapter 1.2.4). Apart from fluorescence sensors, InAs[264] is incorporated in core shell nanoparticles along with ZnSe to form fluorescence markers that can be implanted *in vivo* into cells.[265] However, indium arsenide and its lighter analogue are mainly component units in optoelectronics[266-268] or solid-state technology,[269] where they serve as active substances or as support material. In the latter case GaAs is used in combination with Fe_3O_4 nanoparticles to form spintronic or magnetic storage devices,[270] with nano-MnAs for magnetic and memristive applications[271,272] or with ErAs nanoscale material which can be built in solar cells.[273,274] But not only arsenides exhibit numerous possibilities in different fields of usage, also phosphides can be versatilely utilised. Among the already described optical and magnetic devices especially transition metal phosphides like NiP, Ni_2P or Co_2P are qualified for catalysis[275] or photosensitizing[276] as well as for water splitting.[277-279] On the other hand, InP[280,281] and GaInP nanoparticles are applied including optoelectronics[282] or quantum computation[283], while GaP and the transition metal compound Zn_3P_2 were studied amongst others for their use as thermoelectrics.[284] Also very interesting are the phosphides and arsenides of the group 14 elements as calculations of Lin *et al.* in 2018 showed a broad suitability in photocatalysis, photovoltaics and nanoelectronics for 2D films of SiP, SiAs and SiSb which still has to be confirmed in experiments.[285] However, scientists have already proven SiP_2 to be a promising anode material for Li ion batteries although it was only tested as a bulk and not yet in nanoparticles form.[286] The same is true for germanium and tin phosphides.[287-289] Nevertheless, it is assumed that not only bulk material of silicon, germanium and tin phosphides display various potential applications, but also their nanoparticles might have many utilizations which need to be investigated.

1.4. References

[1] N. Wiberg, A. F. Hollemann **2007**, „Hollemann, Wiberg – Lehrbuch der Anorganischen Chemie“ 102nd Edition: de Gruyter Berlin.
[2] F. Krafft, *Angew. Chem. Int. Ed.* **1969**, *8*, 660 – 671.
[3] J. B. Readman, *J. Chem. Technol. Biotechnol.* **1890**, *9*, 163 – 211.
[4] A. D. F. Toy **1973**, „The Chemistry of Phosphorus“: Pergamon Press, Oxford.
[5] G. Villalba, Y. Liu, H. Schroder, R. U. Ayres, *J. Ind. Ecol.* **2008**, *12*, 557 – 569.
[6] C. N. Singman, *J. Chem. Educ.* **1984**, *61*, 137 – 142.
[7] L. R. Maxwell, S. B. Hendricks, V. M. Mosley, *J. Chem. Phys.* **1935**, *3*, 699 – 709.
[8] D. E. C. Corbridge, E. J. Lowe, *Nature* **1952**, *170*, 629.
[9] N. B. Goodman, L. Ley, D. W. Bullett, *Phys. Rev. B* **1983**, *27*, 7440 – 7450.
[10] F. Bachhuber, J. v. Appen, R. Dronskowski, P. Schmidt, T. Nilges, A. Pfitzner, R. Weihrich, *Angew. Chem. Int. Ed.* **2014**, *53*, 11629 – 11633; *Angew. Chem.* **2014**, *126*, 11813 – 11817.
[11] R. J. VanZee, A. U. Khan, *J. Am. Chem. Soc.* **1974**, *96*, 6805 – 6806.
[12] R. J. VanZee, A. U. Khan, *Chem. Phys. Lett.* **1975**, *36*, 123 – 125.
[13] P. A. Hamilton, T. P. Murrells, *J. Phys. Chem.* **1986**, *90*, 182 – 185.
[14] H.-B. Qian, P. B. Davies, P. A. Hamilton, *J. Chem. Soc. Faraday Trans.* **1995**, *91*, 2993 – 2998.
[15] P. W. Bridgman, *J. Am. Chem. Soc.* **1914**, *36*, 1344 – 1363.
[16] A. Simon, H. Borrmann, H. Craubner, *Phosphorus, Sulfur Silicon Relat. Elem.* **1987**, *30*, 507 – 510.
[17] A. Simon, H. Borrmann, J. Horakh, *Chem. Ber.* **1997**, *130*, 1235 – 1240.
[18] H. Okudera, R. E. Dinnebier, A. Simon, *Z. Kristallog. – Cryst. Mater.* **2005**, *220*, 259 – 264.
[19] Chemical Economic Handbook, Phosphorus and Phosphorus Chemicals, IHS February 2017.
[20] M. A. Dhansay, P. W. Linder, R. G. Torrington, T. A. Modro, *J. Phys. Org. Chem.* **1990**, *3*, 248 – 254.
[21] S. Hoerold, A. Ratcliff, *J. Pyrotech.* **2001**, *13*, 54 – 63.
[22] T. J. Connolly, M. Matchett, P. McGarry, S. Sukhtankar, J. Zhu, *Org. Process Res. Dev.* **2006**, *10*, 391 – 397.
[23] L. Chen, X. Li, Y. Pang, L. Li, X. Zhang, L. Yu, *J. Mater. Sci. Mater. Med.* **2007**, *18*, 2199 – 2203.
[24] J. D. Bartleson, *Vol. US2534217A*, Standard Oil Co, USA, **1950**, pp. 1 – 6.
[25] A. G. Papay, R. J. Hartley, *Vol. US4857214A*, Afton Chemical Corp, USA, **1989**, pp. 1 – 9.
[26] P. Duerksen-Hughes, P. Richter, L. Ingerman, W. Ruoff, S. Thampi, S. Donkin, U.S. Department of Health and Human Services - Public Health Service - Agency for Toxic Substances and Disease Registry, USA, **1997**, pp. 1 – 248.
[27] E.-C. Koch, *Propellants Explos. Pyrotech.* **2008**, *33*, 165 – 176.
[28] A. Schrötter, *Liebigs Ann. Chem.* **1848**, *68*, 247 – 253.
[29] A. Schrötter, *J. Prakt. Chem.* **1850**, *51*, 155 – 158.
[30] R. Schenck, *Ber. dtsch. chem. Ges.* **1902**, *35*, 351 – 358.
[31] W. L. Roth, T. W. DeWitt, A. J. Smith, *J. Am. Chem. Soc.* **1947**, *69*, 2881 – 2885.
[32] R. Schenck, *Ber. dtsch. chem. Ges.***1903**, *36*, 979 – 995; 4202 – 4209.
[33] U. Braun, B. Schartel, *Macromol. Chem. Phys.* **2004**, *205*, 2185 – 2196.
[34] V. Alagarsamy **2012**, “Pharmaceutical Chemistry of Natural Products” 1st Edition: Elsevier India.
[35] Y. Zhu, Y. Wen, X. Fan, T. Gao, F. Han, C. Luo, S.-C. Liou, C. Wang, *ACS Nano* **2015**, *9*, 3254 – 3264.
[36] W. Hittorf, *Ann. Phys.* **1865**, *202*, 193 – 228.
[37] H. Thurn, H. Krebs, *Acta Crystallogr. Sect. B: Struct. Sci.* **1969**, *25*, 125 – 135.
[38] A. Pfitzner, M. F. Bräu, J. Zweck, G. Brunklaus, H. Eckert, *Angew. Chem. Int. Ed.* **2004**, *43*, 4228 – 4231; *Angew. Chem.* **2004**, *116*, 4324 – 4327.
[39] P. A. G. O'Hare, B. M. Lewis, I. Shirotani, *Thermochim. Acta* **1988**, *129*, 57 – 62.
[40] P. W. Bridgman, *Physic. Rev.* **1914**, *3*, 126 – 141; 153 – 203.
[41] a) S. Lange, P. Schmidt, T. Nilges, *Inorg. Chem.* **2007**, *46*, 4028 – 4035; b) T. Nilges, M. Kersting, T. Pfeifer, *J. Solid State Chem.* **2008**, *181*, 1707 – 1711.
[42] H. Krebs, H. Weitz, K. H. Worms, *Z. Anorg. Allg. Chem.* **1955**, *280*, 119 – 133.
[43] H. Thiel, *Ann. Phys.* **1956**, *452*, 122 – 125.
[44] T. Kikegawa, H. Iwasaki, *Acta Crystallogr. Sect. B: Struct. Sci.* **1983**, *39*, 158 – 164.
[45] Y. Akahama, M. Kobayashi, H. Kawamura, *Phys. Rev. B* **1999**, *59*, 8520 – 8525.
[46] Y. Maruyama, S. Suzuki, K. Kobayashi, S. Tanuma, *Physica B+C* **1981**, *105*, 99 – 102.
[47] W. H. Han, S. Kim, I.-H. Lee, K. J. Chang, *Condensed Matter* **2017**, 1 – 5.
[48] H. Liu, A. T. Neal, Z. Zhu, Z. Luo, X. Xu, D. Tománek, P. D. Ye, *ACS Nano* **2014**, *8*, 4033 – 4041.
[49] L. Li, Y. Yu, G. J. Ye, Q. Ge, X. Ou, H. Wu, D. Feng, X. H. Chen, Y. Zhang, *Nat. Nanotech.* **2014**, *9*, 372 – 377.

[50] S. P. Koenig, R. A. Doganov, H. Schmidt, A. H. C. Neto, B. Özyilmaz, *Appl. Phys. Lett.* **2014**, *104*, 103106-1 – 103106-4.
[51] R. Gusmao, Z. Sofer, M. Pumera, *Angew. Chem. Int. Ed.* **2017**, *56*, 8052 – 8072.
[52] G. Hu, T. Albrow-Owen, X. Jin, A. Ali, Y. Hu, R. C. T. Howe, K. Shehzad, Z. Yang, X. Zhu, R. I. Woodward, T.-C. Wu, H. Jussila, J.-B. Wu, P. Peng, P.-H. Tan, Z. Sun, E. J. R. Kelleher, M. Zhang, Y. Xu, T. Hasan, *Nature Commun.* **2017**, *8*, 278-1 – 278-10.
[53] Z. Zhu, D. Tománek, *Phys. Rev. Lett.* **2014**, *112*, 176802-1 – 176802-5.
[54] F. H. Westheimer, *Science* **1987**, *235*, 1173 – 1178.
[55] J. D. Watson, F. H. Crick, *Nature* **1953**, *171*, 737 – 738.
[56] J. M. Berg, J. L. Tymoczko, G. J. Gatto jr., L. Stryer **2018**, „Stryer Biochemie" 8. Auflage: Springer Verlag, Berlin.
[57] K. J. Quelch, R. A. Melick, P. J. Bingham, S. M. Mercuri, *Arch. Oral Biol.* **1983**, *28*, 665 – 674.
[58] K. Lohmann, *Naturwissenschaften* **1929**, *17*, 624 – 625.
[59] F. Lipmann, *Adv. Enzymol* **1941**, *1*, 99 – 162.
[60] J. Baddiley, A. M. Michelson, A. R. Todd, *J. Chem. Soc.* **1949**, 582 – 586.
[61] P. N. Froelich, M. L. Bender, N. A. Luedtke, G. R. Heath, T. DeVries, *Am. J. Sci.* **1982**, *282*, 474 – 511.
[62] K. B. Föllmi, *Earth-Sci. Rev.* **1996**, *40*, 55 – 124.
[63] J. Elser, E. Bennett, *Nature* **2011**, *478*, 29 – 31.
[64] D. Cordell, S. White, *Sustainability* **2011**, *3*, 2027 – 2049.
[65] Z. Yuan, S. Jiang, H. Sheng, X. Liu, H. Hua, X. Liu, Y. Zhang, *Environ. Sci. Technol.* **2018**, *52*, 2438 – 2450.
[66] P. Dapporto, S. Midollini, L. Sacconi, *Angew. Chem. Int. Ed.* **1979**, *18*, 469.
[67] S. Heinl, E. V. Peresypkina, A. Y. Timoshkin, P. Mastrorilli, V. Gallo, M. Scheer, *Angew. Chem. Int. Ed.* **2013**, *52*, 10887 – 10891; *Angew. Chem.* **2013**, *125*, 11087 – 11091.
[68] I. Krossing, *J. Am. Chem. Soc.* **2001**, *123*, 4603 – 4604.
[69] Y. Xiong, S. Yao, M. Brym, M. Driess, *Angew. Chem. Int. Ed.* **2007**, *46*, 4511 – 4513; *Angew. Chem.* **2007**, *119*, 4595 – 4597.
[70] G. Prabusankar, A. Doddi, C. Gemel, M. Winter, R. A. Fischer, *Inorg. Chem.* **2010**, *49*, 7976 – 7980.
[71] A. E. Seitz, U. Vogel, M. Eberl, M. Eckhardt, G. Balázs, E. V. Peresypkina, M. Bodensteiner, M. Zabel, M. Scheer, *Chem. Eur. J.* **2017**, *23*, 10319 – 10327.
[72] S. Heinl, S. Reisinger, C. Schwarzmaier, M. Bodensteiner, M. Scheer, *Angew. Chem. Int. Ed.* **2014**, *53*, 7639 – 7642; *Angew. Chem.* **2014**, *126*, 7769 – 7773.
[73] J. E. Borger, A. W. Ehlers, M. Lutz, J. C. Slootweg, K. Lammertsma, *Angew. Chem. Int. Ed.* **2015**, *55*, 613 – 617; *Angew. Chem.* **2015**, *128*, 623 – 627.
[74] J. Müller, S. Heinl, C. Schwarzmaier, G. Balázs, M. Keilwerth, K. Meyer, M. Scheer, *Angew. Chem. Int. Ed.* **2017**, *56*, 7312 – 7317; *Angew. Chem.* **2017**, *129*, 7418 – 7423.
[75] M. Di Vaira, S. Midollini, L. Sacconi, *J. Am. Chem. Soc.* **1979**, *101*, 1757 – 1763.
[76] M. Scheer, U. Becker, M. H. Chisholm, J. C. Huffman, F. Lemoigno, O. Eisenstein, *Inorg. Chem.* **1995**, *34*, 3117 – 3119.
[77] Y. H. Budnikova, A. G. Kafiyatullina, A. S. Balueva, R. M. Kuznetsov, V. I. Morozov, O. G. Sinyashin, *Russ. Chem. Bull.* **2003**, *52*, 2419 – 2423.
[78] B. Pinter, K. T. Smith, M. Kamitani, E. M. Zolnhofer, B. L. Tran, S. Fortier, M. Pink, G. Wu, B. C. Manor, K. Meyer, M.-H. Baik, D. J. Mindiola, *J. Am. Chem. Soc.* **2015**, *137*, 15247 – 15261.
[79] F. Dielmann, A. Timoshkin, M. Piesch, G. Balázs, M. Scheer, *Angew. Chem. Int. Ed.* **2017**, *56*, 1671 – 1675; *Angew. Chem.* **2017**, *129*, 1693 – 1698.
[80] O. J. Scherer, J. Schwalb, G. Wolmershäuser, W. Kaim, R. Gross, *Angew. Chem. Int. Ed.* **1986**, *25*, 363 – 364.
[81] M. Detzel, T. Mohr, O. J. Scherer, G. Wolmershäuser, *Angew. Chem. Int. Ed.* **1994**, *33*, 1110 – 1112.
[82] E. Mädl, M. V. Butovskii, G. Balázs, E. V. Peresypkina, A. V. Virovets, M. Seidl, M. Scheer, *Angew. Chem. Int. Ed.* **2014**, *53*, 7643 – 7646; *Angew. Chem.* **2014**, *126*, 7774 – 7777.
[83] M. Herberhold, G. Frohmader, W. Milius, *J. Organomet. Chem.* **1996**, *522*, 185 – 196.
[84] M. Fleischmann, F. Dielmann, L. J. Gregoriades, E. V. Peresypkina, A. V. Virovets, S. Huber, A. Y. Timoshkin, G. Balázs, M. Scheer, *Angew. Chem. Int. Ed.* **2015**, *54*, 13110 – 13115; *Angew. Chem.* **2015**, *127*, 13303 – 13308.
[85] O. J. Scherer, *Comments Inorg. Chem.* **1987**, *6*, 1 – 22.
[86] F. Spitzer, C. Graßl, G. Balázs, E. Mädl, M. Keilwerth, E. M. Zolnhofer, K. Meyer, M. Scheer, *Chem. Eur. J.* **2017**, *23*, 2716 – 2721.
[87] J. P. W. Hughes, R. Baron, D. H. Buckland, M. A. Cooke, J. D. Craig, D. P. Duffield, A. W. Grosart, P. W. J. Parkes, A. Porter, *Br. J. Ind. Med.* **1962**, *19*, 83 – 99.
[88] A. K. Ghoshal, E. A. Porta, W. S. Hartroft, *Am. J. Pathol.***1969**, *54*, 275 – 291.
[89] P. Pani, E. Gravela, C. Mazzarino, E. Burdino, *Exp. Mol. Pathol.* **1972**, *16*, 201 – 209.

[90] A. Gomez-Caminero, P. Howe, M. Hughes, E. Kenyon, D. R. Lewis, M. Moore, J. Ng, A. Aitio, G. Becking, World Health Organization, Geneva, **2001**, pp. 1 – 114.
[91] L. L. Brunton, R. Hilal-Dandan, B. C. Knollmann **2017**, „Goodmans & Gilman's The Pharmacological Basis of Therapeutics" 13. Edition, McGraw-Hill Education, USA, 1307 – 1310.
[92] J. Marsh, *Edinburgh New Philos. J.* **1836**, *V21*, 229 – 236.
[93] M. S. Gorby, *West. J. Med.* **1988**, *149*, 308 – 315.
[94] H. Marquardt, S. G. Schäfer, H. Barth **2013**, „Toxikologie" 3. Auflage: Wissenschaftliche Verlagsgesellschaft mbH, Stuttgart.
[95] M. J. Mass, A. Tennant, B. C. Roop, W. R. Cullen, M. Styblo, D. J. Thomas, A. D. Kligerman, *Chem. Res. Toxicol.* **2001**, *14*, 355 – 361.
[96] T. Hayakawa, Y. Kobayashi, X. Cui, S. Hirano, *Arch. Toxicol.* **2005**, *79*, 183 – 191.
[97] H. Naranmandura, N. Suzuki, K. T. Suzuki, *Chem. Res. Toxicol.* **2006**, *19*, 1010 – 1018.
[98] A. Hernández, N. Xamena, J. Surrallés, C. Sekaran, H. Tokunaga, D. Quinteros, A. Creus, R. Marcos, *Mutat. Res.***2008**, *637*, 80 – 92.
[99] T. Agusa, J. Fujihara, H. Takeshita, H. Iwata, *Int. J. Mol. Sci.* **2011**, *12*, 2351 – 2382.
[100] D. Sumi, S. Himeno, *Biol. Pharm. Bull.* **2012**, *35*, 1870 – 1875.
[101] C. M. Schlebusch, J. Cecil M. Lewis, M. Vahter, K. Engström, R. Y. Tito, A. J. Obregón-Tito, D. Huerta, S. I. Polo, Á. C. Medina, T. D. Brutsaert, G. Concha, M. Jakobsson, K. Broberg, *Environ. Health Perspect.* **2013**, *121*, 53 – 58.
[102] X.-M. Xue, J. Ye, G. Raber, B. P. Rosen, K. Francesconi, C. Xiong, Z. Zhu, C. Rensing, Y.-G. Zhu, *Environ. Sci. Technol.* **2019**, *53*, 634 – 641.
[103] M. Vahter, E. Marafante, L. Dencker, *Sci. Total Environ.* **1983**, *30*, 197 – 211.
[104] Y. Shibata, M. Morita, K. Fuwa, *Adv. Biophys.* **1992**, *28*, 31 – 80.
[105] E. O. Uthus, *J. Trace Elem. Exp. Med.* **2003**, *16*, 345 – 355.
[106] K. K. Bhargava, N. L. Trang, A. Cerami, J. W. Eaton, *Mol. Biochem. Parasitol.* **1983**, *9*, 29 – 35.
[107] H. Tokailin, T. Takahashi, T. Sagawa, K. Shindo, *Phys. Rev. B* **1984**, *30*, 1765 – 1772.
[108] J. H. Xu, E. G. Wang, C. S. Ting, W. P. Su, *Phys. Rev. B* **1993**, *48*, 17271 – 17279.
[109] H. Stöhr, *Z. Anorg. Allg. Chem.* **1939**, *242*, 138 – 144.
[110] H. Krebs, F. Schultze-Gebhardt, *Z. Anorg. Allg. Chem.* **1956**, *283*, 263 – 276.
[111] J.-P. Issi, *Aust. J. Phys.* **1979**, *32*, 585 – 628.
[112] X. Gonze, J.-P. Michenaud, J.-P. Vigneron, *Phys. Rev. B* **1990**, *41*, 11827 – 11836.
[113] M. J. Kelly, D. W. Bullett, *Solid State Commun.* **1976**, *18*, 593 – 595.
[114] Z. Zhu, J. Guan, D. Tomanek, *Condensed Matter* **2014**, arXiv:1410.6371v1, 1 – 5.
[115] J. Eiduss, R. Kalendarev, A. Rodionov, A. Sazonov, G. Chikvaidze, *Phys. Stat. Sol. B* **1996**, *193*, 3 – 23.
[116] A. Bettendorff, *Justus Liebigs Ann. Chem.* **1867**, *144*, 110 – 114.
[117] H. Erdmann, M. V. Unruh, *Z. Anorg. Allg. Chem.* **1902**, *32*, 437 – 452.
[118] Y. F. Zhukovskii, R. I. Kalendarev, *J. Mol. Struct. THEOCHEM* **2001**, *544*, 111 – 121.
[119] M. F. Daniel, A. J. Leadbetter, *Philos. Mag. B* **1981**, *44*, 509 – 529.
[120] A. V. Parygin, G. V. Chikvaidze, G. K. Semin, B. V. Lokshin, Y. A. Eiduss, *Phys. Stat. Sol. A* **1984**, *84*, K101 – K103.
[121] C. Schwarzmaier, A. Schindler, C. Heindl, S. Scheuermayer, E. V. Peresypkina, A. V. Virovets, M. Neumeier, R. Gschwind, M. Scheer, *Angew. Chem. Int. Ed.***2013**, *52*, 10896 – 10899; *Angew. Chem.* **2013**, *125*, 11097 – 11100.
[122] C. Schwarzmaier, M. Sierka, M. Scheer, *Angew. Chem. Int. Ed.* **2013**, *52*, 858 – 861; *Angew. Chem. Int. Ed.* **2013**, *125*, 891 – 894.
[123] D. Yang, J. Zhao, L. Yu, X. Lin, W. Zhang, H. Ma, A. Gogoll, Z. Zhang, Y. Wang, X.-J. Yang, B. Wu, *J. Am. Chem. Soc.* **2017**, *139*, 5946 – 5951.
[124] A. N. Rodionov, R. I. Kalendarev, G. V. Tchikvaidze, J. A. Eiduss, *Nature* **1979**, *281*, 60.
[125] P. M. Smith, A. J. Leadbetter, A. J. Apling, *J. Phil. Mag.* **1975**, *31*, 57 – 64.
[126] M. Puselj, Z. Ban, D. Grdenic, *Z. Anorg. Allg. Chem.* **1977**, *437*, 298 – 292.
[127] O. Osters, T. Nilges, F. Bachhuber, F. Pielnhofer, R. Weihrich, M. Schöneich, P. Schmidt, *Angew. Chem. Int. Ed.* **2012**, *51*, 2994 – 2997; *Angew. Chem.* **2012**, *124*, 3049 – 3052.
[128] A. H. Clark, *Mineralogical Magazine* **1970**, *37*, 732 – 733.
[129] C. Schwarzmaier, A. Y. Timoshkin, M. Scheer, *Angew. Chem. Int. Ed.* **2013**, *52*, 7600 – 7603; *Angew. Chem.* **2013**, *125*, 7751 – 7755.
[130] F. Spitzer, M. Sierka, M. Latronico, P. Mastrorilli, A. V. Virovets, M. Scheer, *Angew. Chem. Int. Ed.* **2015**, *54*, 4392 – 4396; *Angew. Chem.* **2015**, *127*, 4467 – 4472.
[131] M. Schmidt, A. E. Seitz, M. Eckhardt, G. b. Balázs, E. V. Peresypkina, A. V. Virovets, F. Riedlberger, M. Bodensteiner, E. M. Zolnhofer, K. Meyer, M. Scheer, *J. Am. Chem. Soc.* **2017**, *139*, 13981 – 13984.

[132] C. Schwarzmaier, A. Y. Timoshkin, G. Balázs, M. Scheer, *Angew. Chem. Int. Ed.* **2014**, *53*, 9077 – 9081; *Angew. Chem. Int. Ed.* **2014**, *126*, 9223 – 9227.
[133] S. Heinl, G. Balázs, A. Stauber, M. Scheer, *Angew. Chem. Int. Ed.* **2016**, *55*, 15524 – 15527; *Angew. Chem.* **2016**, *128*, 15751 – 15755.
[134] B. Sigwarth, L. Zsolnai, H. Berke, G. Huttner, *J. Organomet. Chem.* **1982**, *226*, C5 – C8.
[135] L. Y. Goh, W. Chen, R. C. S. Wong, *J. Organomet. Chem.* **1995**, *503*, 47 – 51.
[136] M. Di Vaira, S. Midollini, L. Sacconi, F. Zanobini, *Angew. Chem.* **1978**, *90*, 720 – 721.
[137] O. J. Scherer, J. Vondung, G. Wolmershäuser, *J. Organomet. Chem.* **1989**, *376*, C35 – C38.
[138] C. v. Hänisch, D. Fenske, F. Weigend, R. Ahlrichs, *Chem. Eur. J.* **1997**, *3*, 1494 – 1498.
[139] O. J. Scherer, C. Blath, G. Wolmershäuser, *J. Organomet. Chem.* **1990**, *387*, C21 – C24.
[140] K. A. Graeme, C. V. Pollack Jr., *J. Emerg. Med.* **1998**, *16*, 45 – 56.
[141] R. N. Ratnaike, *Postgrad. Med. J.* **2003**, *79*, 391 – 396.
[142] H. G. Seiler, H. Sigel, A. Sigel **1988**, „Handbook on Toxicity of Inorganic Compounds", Marcel Dekker, Inc., New York, 79 – 90.
[143] N. C. Lloyd, H. W. Morgan, B. K. Nicholson, R. S. Ronimus, *Angew. Chem. Int. Ed.***2005**, *44*, 941 – 944; *Angew. Chem.***2005**, *117*, 963 – 966.
[144] K. Haxton, *Nat. Chem.* **2011**, *3*, 744.
[145] O. Gauthier-Lafaye, P. Boucaud, F. H. Julien, S. Sauvage, S. Cabaret, J.-M. Lourtioz, V. Thierry-Mieg, R. Planel, *Appl. Phys. Lett.* **1997**, *71*, 3619 – 3621.
[146] J. P. Zimmer, S.-W. Kim, S. Ohnishi, E. Tanaka, J. V. Frangioni, M. G. Bawendi, *J. Am. Chem. Soc.* **2006**, *128*, 2526 – 2527.
[147] J. S. Harris. Jr., R. Kudrawiec, H. B. Yuen, S. R. Bank, H. P. Bae, M. A. Wistey, D. Jackrel, E. R. Pickett, T. Sarmiento, L. L. Goddard, V. Lordi, T. Gugov, *Phys. Stat. Sol. B* **2007**, *244*, 2707 – 2729.
[148] R. B. Balow, E. J. Sheets, M. M. Abu-Omar, R. Agrawal, *Chem. Mater.* **2015**, *27*, 2290 – 2293.
[149] R. B. Balow, C. K. Miskin, M. M. Abu-Omar, R. Agrawal, *Chem. Mater.* **2017**, *39*, 573 – 578.
[150] J. Hung, S.-c. Lee, C.-t. Chia, *J. Nanopart. Res.* **2004**, *6*, 415 – 419.
[151] J. P. Park, J.-j. Lee, S.-W. Kim, *J. Am. Chem. Soc.* **2016**, *138*, 16568 – 16571.
[152] The Royal Society and The Royal Academy of Engineering. *Nanoscience and Nanotechnology: Opportunities and Uncertainties* , The Royal Society, **2004**, available at http://www.nanotec.org.uk
[153] M. Auffan, J. Rose, J.-Y. Bottero, G. V. Lowry, J.-P. Jolivet, M. R. Wiesner, *Nat. Nanotechnol.* **2009**, *4*, 634 – 641.
[154] N. Taniguchi, **1974**, *„On the basic concept of „nanotechnology"" Proc. Intl. Conf. Prod. Eng. Part II*, Japan Society of Precision Engineering, Tokyo, 18 – 23.
[155] L. Becker, T. E. Bunch, L. J. Allamandola, *Lunar Planet.Sci. Conf.* **1999**, *30*, 1805.
[156] D. D. Clayton, E. A.-N. Deneault, B. S. Meyer, *Astrophys. J.* **2001**, *562*, 480 – 493.
[157] N. Dauphas, L. Remusat, J. H. Chen, M. Roskosz, D. A. Papanastassiou, J. Stodolna, Y. Guan, C. Ma, J. M. Eiler, *Astrophys. J.* **2010**, *720*, 1577 – 1591.
[158] B. T. Draine, B. Hensley, *Astrophys. J.* **2012**, *757*, 103 (1 – 9).
[159] D. A. García-Hernández, E. Villaver, P. García-Lario, J. A. Acosta-Pulido, A. Manchado, L. Stanghellini, R. A. Shaw, F. Cataldo, *Astrophys. J.* **2012**, *760*, 107 (1 – 16).
[160] H. Guo, A. S. Barnard, *J. Mater. Chem. A* **2013**, *1*, 27 – 42.
[161] C. Buzea, I. I. Pacheco, K. Robbie, *Biointerphases* **2007**, *2*, MR17 – MR71.
[162] S. Stanley, *Curr. Opin. Biotechnol.* **2014**, *28*, 69 – 74.
[163] M. H. Nayfeh, S. R. Habbal, S. Rao, *Astrophys. J. Lett.* **2005**, *621*, L121 – L124.
[164] A. D. Maynard, E. D. Kuempel, *J. Nanopart. Res.* **2005**, *7*, 587 – 614.
[165] S. T. Stern, S. E. McNeil, *Toxicol. Sci.* **2008**, *101*, 4 – 21.
[166] M. Faraday, *Phil. Trans. R. Soc. Lond.* **1857**, *147*, 145 – 181.
[167] P. Colomban, *J. Nano Res.* **2009**, *8*, 109 – 132.
[168] A. L. Robinson, *Science* **1986**, *234*, 821 – 822.
[169] R. P. Feynman, *Engineering and Science* **1960**, *23*, 22 – 36.
[170] A. I. Ekimov, A. A. Onushchenko, *Pis'ma v Zhurnal Eksperimental'noi i Teoreticheskoi Fiziki* **1981**, *34*, 363 – 366.
[171] R. Rossetti, R. Hull, J. M. Gibson, L. E. Brus, *J. Chem. Phys.* **1985**, *82*, 552 – 559.
[172] A. I. Ekimov, A. L. Efros, *Phys. Status Solidi B* **1988**, *150*, 627 – 633.
[173] G. Binnig, H. Rohrer, C. Gerber, E. Weibel, *Appl. Phys. Lett.* **1982**, *40*, 178 – 180.
[174] G. Binnig, H. Rohrer, *Surf. Sci.* **1983**, *126*, 236 – 244.
[175] G. Binnig, C. F. Quate, C. Gerber, *Phys. Rev. Lett.* **1986**, *56*, 930 – 933.
[176] H. Kroto, J. R. Heath, S. C. O'Brien, R. E. Smalley, *Nature* **1985**, *318*, 162 – 163.
[177] S. Iijima, *Nature* **1991**, *354*, 56 – 58.

[178] D. M. Eigler, E. K. Schweizer, *Nature* **1990**, *344*, 524 – 526.
[179] S. Lee, S. Jeong, D. Kim, B. K. Park, J. Moon, *Superlattices Microstruct.* **2007**, *42*, 361 – 368.
[180] I. Cho, B. J. Kim, S. W. Ryu, J. H. Cho, J. Cho, *Nanotechnology* **2014**, *25*, 505604-1 – 505604-11.
[181] S. Kumar, G. Pant, V. Sharma, P. Bisht, *Int. J. Inform. Comput. Technol.* **2014**, *4*, 1597 – 1603.
[182] H. Gleiter, *Prog. Mater Sci.* **1989**, *33*, 223 – 315.
[183] R. S. Rawat, *Journal of Physics: Conference Series* **2015**, *591*, 012021-1 – 012021-25.
[184] Y.-P. Sun, B. Zhou, Y. Lin, W. Wang, K. A. Shiral-Fernando, P. Pathak, M. J. Meziani, B. A. Harruff, X. Wang, H. Wang, P. G. Luo, H. Yang, M. E. Kose, B. Chen, L. M. Veca, S.-Y. Xie, *J. Am. Chem. Soc.* **2006**, *128*, 7756 – 7757.
[185] L. A. Ponomarenko, F. Schedin, M. I. Katsnelson, R. Yang, E. W. Hill, K. S. Novoselov, A. K. Geim, *Science* **2008**, *320*, 356 – 358.
[186] B. Xia, I. W. Lenggoro, K. Okuyama, *Adv. Mater.* **2001**, *13*, 1579 – 1582.
[187] I. Agranovski, *Aerosols - Science and Technology*, WILEY-VCH Verlag GmbH & Co. KGaA, Weinheim, **2010**, pp. 65 – 89.
[188] X. S. Lv, Y. Qiu, Z. Y. Wang, G. M. Jiang, Y. T. Chen, X. H. Xu, R. H. Hurt, *Environ. Sci. Nano* **2016**, *3*, 1215 – 1221.
[189] K. C. Patil, S. T. Aruna, S. Ekambaram, *Curr. Opin. Solid State Mater. Sci.* **1997**, *2*, 158 – 165.
[190] P. Bowen, C. Carry, *Powder Technol.* **2002**, *128*, 248 – 255.
[191] M. Kumagai, G. L. Messing, *J. Am. Ceram. Soc.* **1984**, *67*, C230 – C231.
[192] C. Legros, C. Carry, P. Bowen, H. Hofmann, *J. Eur. Ceram. Soc.* **1999**, *19*, 1967 – 1978.
[193] Y. Yu, L. Gu, C. Zhu, S. Tsukimoto, P. A. v. Aken, J. Maier, *Adv. Mater.* **2010**, *22*, 2247 – 2250.
[194] L. L. Beecroft, C. K. Ober, *Chem. Mater.* **1997**, *9*, 1302 – 1317.
[195] D. Kim, J. Park, K. An, N.-K. Yang, J.-G. Park, T. Hyeon, *J. Am. Chem. Soc.* **2007**, *129*, 5812 – 5813.
[196] S. Carenco, M. Demange, J. Shi, C. Boissière, C. Sanchez, P. L. Floch, N. Mézailles, *Chem. Commun.* **2010**, *46*, 5578 – 5580.
[197] W. W. Yu, X. Peng, *Angew. Chem. Int. Ed.* **2002**, *41*, 2368 – 2371.
[198] J. P. Carpenter, C. M. Lukehart, S. B. Milne, S. R. Stock, J. E. Wittig, B. D. Jones, R. Glosser, J. G. Zhu, *J. Organomet. Chem.* **1998**, *557*, 121 – 130.
[199] J. Park, B. Koo, Y. Hwang, C. Bae, K. An, J. G. Park, H. M. Park, T. Hyeon, *Angew. Chem. Int. Ed.* **2004**, *43*, 2282 – 2285; *Angew. Chem.* **2004**, *116*, 2332 – 2335.
[200] N. L. Pickett, P. O'Brien, *Chem. Rec.* **2001**, *1*, 467 – 479.
[201] C. Hunger, W.-S. Ojo, S. Bauer, S. Xu, M. Zabel, B. Chaudret, L.-M. Lacroix, M. Scheer, C. Nayral, F. Delpech, *Chem. Commun.* **2013**, *49*, 11788 – 11790.
[202] X. Hou, S. Zhou, T. Jia, H. Lin, H. Teng, *J. Alloys Compd.* **2011**, *509*, 2793 – 2796.
[203] G. Zlateva, Z. Zhelev, R. Bakalova, I. Kanno, *Inorg. Chem.* **2007**, *46*, 6212 – 6214.
[204] A. P. Alivisatos, *Science* **1996**, *271*, 933 – 937.
[205] H. Yu, J. Li, R. A. Loomis, L.-W. Wang, W. E. Buhro, *Nat. Mater.* **2003**, *2*, 517 – 520.
[206] D. V. Melnikov, J. R. Chelikowsky, *Phys. Rev. Lett.* **2004**, *92*, 046802-1 – 046802-4.
[207] Y. Son, M. Park, Y. Son, J.-S. Lee, J.-H. Jang, Y. Kim, J. Cho, *Nano Lett.* **2014**, *14*, 1005 – 1010.
[208] F. Haguenau, P. W. Hawkes, J. L. Hutchison, B. Satiat–Jeunemaître, G. T. Simon, D. B. Williams, *Microsc. Microanal.* **2003**, *9*, 96 – 138.
[209] Y. Sun, Y. Xia, *Science* **2002**, *298*, 2176 – 2179.
[210] S. F. Hansen, B. H. Larsen, S. I. Olsen, A. Braun, *Nanotoxicology* **2007**, *1*, 243 - 250.
[211] C. S. Yah, G. S. Simate, S. E. Iyuke, *Pak. J. Pharm. Sci.* **2012**, *25*, 477 – 491.
[212] A. Nemmar, M. F. Hoylaerts, P. H. M. Hoet, B. Nemery, *Toxicol. Lett.* **2004**, *149*, 243 – 253.
[213] A. Radomski, P. Jurasz, D. Alonso-Escolano, M. Drews, M. Morandi, T. Malinski, M. W. Radomski, *Br. J. Pharmacol.* **2005**, *146*, 882 – 893.
[214] A. Elder, R. Gelein, V. Silva, T. Feikert, L. Opanashuk, J. Carter, R. Potter, A. Maynard, Y. Ito, J. Finkelstein, G. Oberdörster, *Environ. Health Perspect.* **2006**, *114*, 1172 – 1178.
[215] Z. Chen, H. Meng, G. Xing, C. Chen, Y. Zhao, G. Jia, T. Wang, H. Yuan, C. Ye, F. Zhao, Z. Chai, C. Zhu, X. Fang, B. Ma, L. Wan, *Toxicol. Lett.* **2006**, *163*, 109 – 120.
[216] P. I. Jalava, R. O. Salonen, A. S. Pennanen, M. Sillanpää, A. I. Hälinen, M. S. Happo, R. Hillamo, B. Brunekreef, K. Katsouyanni, J. Sunyer, M.-R. Hirvonen, *Inhal. Toxicol.* **2007**, *19*, 213 – 225.
[217] W. Möller, T. Hofer, A. Ziesenis, E. Karg, J. Heyder, *Toxicol. Appl. Pharmacol.* **2002**, *182*, 197 – 207.
[218] N. Li, C. Sioutas, A. Cho, D. Schmitz, C. Misra, J. Sempf, M. Wang, T. Oberley, J. Froines, A. Nel, *Environ. Health Perspect.* **2003**, *111*, 455 – 460.
[219] H. Liu, T. J. Webster, *Biomaterials* **2007**, *28*, 354 – 369.
[220] J. Kreuter, *Int. J. Pharm.* **2007**, *331*, 1 – 10.
[221] S. Laurent, D. Forge, M. Port, A. Roch, C. Robic, L. V. Elst, R. N. Muller, *Chem. Rev.* **2008**, *108*, 2064 – 2110.

[222] R. F. Ziolo, E. P. Giannelis, B. A. Weinstein, M. P. O'Horo, B. N. Ganguly, V. Mehrotra, M. W. Russell, D. R. Huffman, *Science* **1992**, *257*, 219 – 223.
[223] G. Nair, S. Survase, *Int. J. Chem. Physi. Sci.* **2014**, *3*, 56 – 60.
[224] X. Zhang, Z. Lai, Z. Liu, C. Tan, Y. Huang, B. Li, M. Zhao, L. Xie, W. Huang, H. Zhang, *Angew. Chem. Int. Ed.* **2015**, *54*, 5425 – 5428; *Angew. Chem.* **2015**, *127*, 5515 – 5518.
[225] Y. Tian, Y. Gong, Z. Zhang, D. Meng, *J. Mater. Sci. - Mater. Electron.* **2014**, *25*, 5467 – 5474.
[226] H. Zhang, J. Yang, S. Gray, J. A. Brown, T. D. Ketcham, D. E. Baker, A. Carapella, R. W. Davis, J. G. Arroyo, D. A. Nolan, *ACS Omega* **2017**, *2*, 3739 – 3744.
[227] J. Gao, H. Gu, B. Xu, *Acc. Chem. Res.* **2009**, *42*, 1097 – 1107.
[228] K. E. Lundin, O. E. Simonson, P. M. D. Moreno, E. M. Zaghloul, I. I. Oprea, M. G. Svahn, C. I. E. Smith, *Genetica* **2009**, *137*, 47 – 56.
[229] P. Calvo, C. Remuñán-López, J. L. Vila-Jato, M. J. Alonso, *J. Appl. Polym. Sci.* **1997**, *63*, 125 – 132.
[230] J. Zhang, M. Saltzman, *Chem. Eng. Prog.* **2013**, *109*, 25 – 30.
[231] C.-N. Lok, C.-M. Ho, R. Chen, Q.-Y. He, W.-Y. Yu, H. Sun, P. K.-H. Tam, J.-F. Chiu, C.-M. Che, *J. Proteome Res.* **2006**, *5*, 916 – 924.
[232] A. Garapaty, J. A. Champion, *Biointerphases* **2015**, *10*, 030801-1– 030801-16.
[233] a) G. D. Crozals, D. Kryza, G. J. Sánchez, S. Roux, D. Mathé, J. Taleb, C. Dumontet, M. Janier, C. Chaix, *Bioconjugate Chem.* **2018**, *29*, 795 – 803; b) D. Kryza, G. D. Crozals, D. Mathe, J. Taleb, Sidi-Boumedine, M. Janier, C. Chaix, C. Dumontet, *Bioconjugate Chem.* **2018**, *29*, 804 – 812.
[234] Y. W. Chun, T. J. Webster, *Ann. Biomed. Eng.* **2009**, *37*, 2034 – 2047.
[235] J. Kim, M. Lee, H. J. Shim, R. Ghaffari, H. R. Cho, D. Son, Y. H. Jung, M. Soh, C. Choi, S. Jung, K. Chu, D. Jeon, S.-T. Lee, J. H. Kim, S. H. Choi, T. Hyeon, D.-H. Kim, *Nature Com.* **2014**, *5*, 5747-1 – 5747-11.
[236] S. A. Jamal, *Chem. Sci.* **2013**, *4*, CSJ-91 1 – 10.
[237] H. Bönnemann, G. Braun, W. Brijoux, R. Brinkmann, A. Schulze-Tilling, K. Seevogel, K. Siepen, *J. Organomet. Chem.* **1996**, *520*, 143 – 162
[238] A. B. R. Mayer, *Polym. Adv. Technol.* **2001**, *12*, 96 – 106.
[239] I. I. Moiseev, M. N. Vargaftik, *Russ. J. Gen. Chem.* **2002**, *72*, 512 – 522.
[240] R. Narayanan, M. A. El-Sayed, *J. Phys. Chem. B* **2005**, *109*, 4357 – 4460.
[241] M. Zäch, C. Hägglund, D.Chakarov, B.Kasemo, *Curr. Opin. Solid State Mater. Sci.* **2006**, *10*, 132 – 143.
[242] N. R. Shiju, V. V. Guliants, *Appl. Catal., A* **2009**, *356*, 1 – 17.
[243] R. Bogue, *Sens. Rev.* **2009**, *29*, 310 – 316.
[244] O. Neumann, A. S. Urban, J. Day, S. Lal, P. Nordlander, N. J. Halas, *ACS Nano* **2013**, *7*, 42 – 49.
[245] B. O'Regan, M. Grätzel, *Nature* **1991**, *353*, 737 – 740.
[246] A. Hagfeldt, M. Grätzel, *Acc. Chem. Res.* **2000**, *33*, 269 – 277.
[247] K. R. Catchpole, *Philos. Trans. R. Soc. London, Ser. A* **2006**, *364*, 3493 – 3503.
[248] R. Takakura, T. Oshikiri, K. Ueno, X. Shi, T. Kondo, H. Masuda, H. Misawa, *Green Chem.* **2017**, *19*, 2398 – 2405.
[249] Y. Yu, L. Gu, C. Zhu, S. Tsukimoto, P. A. v. Aken, J. Maier, *Adv. Mater.* **2010**, *22*, 2247 – 2250.
[250] L. Nie, H. Wang, S. Liu, *Chalcogenide Lett.* **2016**, *13*, 555 – 562.
[251] J. Garcia-Barriocanal, A. Rivera-Calzada, M. Varela, Z. Sefrioui, M. R. Díaz-Guillén, K. J. Moreno, J. A. Díaz-Guillén, E. Iborra, A. F. Fuentes, t. J. Pennycook, C. Leon, J. Santamaria, *ChemPhysChem* **2009**, *10*, 1003 – 1011.
[252] H. Ferkel, B. L. Mordike, *Mater. Sci. Eng., A* **2001**, *298*, 193 – 199.
[253] Y. Wang, S. Lim, J. L. Luo, Z. H. Xu, *Wear* **2006**, *260*, 976 – 983.
[254] A. Kockmann, J. C. Porsiel, R. Saadat, G. Garnweitner, *RSC Adv.* **2018**, *8*, 11109 – 11118.
[255] A. M. Atta, A. M. El-Saeed, H. I. Al-Shafey, G. A. El-Mahdy, *Int. J. Electrochem. Sci.* **2016**, *11*, 5735 – 5752.
[256] B. Qian, Z. W. Song, L. Hao, H. Q. Fan, *Mater. Corros.* **2017**, *68*, 717 – 724.
[257] M. Nikolic, J. M. Lawther, A. R. Sanadi, *J. Coat. Technol. Res.* **2015**, *12*, 445 – 461.
[258] D. Cheng, G. Cai, J. Wu, J. Ran, X. Wang, *Colloid. Polym. Sci.* **2017**, *295*, 2163 – 2172.
[259] S. Kathirvelu, L. D'Souza, B. Dhurai, *Indian J. Fibre Text. Res.* **2009**, *34*, 267 – 273.
[260] B. An, Q. Liang, D. Zhao, *Water Res.* **2011**, *45*, 1961 – 1972.
[261] T. Pradeep, Anshup, *Thin Solid Films* **2009**, *517*, 6441 – 6478.
[262] R. L. Ziolli, W. F. Jardim, *J. Photochem. Photobiol. A* **2002**, *147*, 205 – 212.
[263] D. Fukushi, A. Sato, K. Yoshida, M. Kitano, *Bull. Chem. Soc. Jpn* **2017**, *90*, 885 – 892.
[264] A. A. Guzelian, U. Banin, A. V. Kadavanich, X. Peng, A. P. Alivisatos, *Appl. Phys. Lett.* **1996**, *69*, 1432 - 1434.
[265] J. P. Zimmer, S.-W. Kim, S. Ohnishi, E. Tanaka, J. V. Frangioni, M. G. Bawendi, *J. Am. Chem. Soc.* **2006**, *128*, 2526 – 2527.
[266] Q. Gao, H. J. Joyce, S. Paiman, J. H. Kang, H. H. Tan, Y. Kim, L. M. Smith, H. E. Jackson, J. M. Yarrison-Rice, X. Zhang, J. Zou, C. Jagadish, *Phys. Status Solidi C* **2009**, *6*, 2678 – 2682.

[267] M.-H. Bae, B.-K. Kim, D.-H. Ha, S. J. Lee, R. Sharma, K. J. Choi, J.-J. Kim, W. J. Choi, J. C. Shin, *Cryst. Growth Des.* **2014**, *14*, 1510 – 1515.
[268] A. Krasnok, M. Caldarola, N. Bonod, A. Alú, *Adv. Opt. Mater.* **2018**, *6*, 1701094-1 – 1701094-22.
[269] F. E. Kruisa, H. Fissana, A. Peleda, *J. Aerosol Sci* **1998**, *29*, 511 – 535.
[270] S. Hihath, R. A. Kiehl, K. v. Benthem, *J. Appl. Phys.* **2014**, *116*, 084306-1 – 084306-9.
[271] M. F. H. Wolff, D. Görlitz, K. Nielsch, M. E. Messing, K. Deppert, *Nanotechnology* **2010**, *22*, 055602-1 – 055602-4.
[272] P. N. Hai, M. Tanaka, *Appl. Phys. Lett.* **2015**, *107*, 122404-1 – 122404-5.
[273] J. M. O. Zide, A. Kleiman-Shwarsctein, N. C. Strandwitz, J. D. Zimmerman, T. Steenblock-Smith, A. C. Gossard, *Appl. Phys. Lett.* **2006**, *88*, 162103-1 – 162103-3.
[274] M. A. Scarpulla, J. M. O. Zide, J. M. LeBeau, C. G. V. d. Walle, A. C. Gossard, K. T. Delaney, *Appl. Phys. Lett.* **2008**, *92*, 173116-1 – 173116-3.
[275] S. L. Brock, K. Senevirathne, *J. Solid State Chem.* **2008**, *181*, 1552 – 1559.
[276] S. Cao, Y. Chen, C.-J. Wang, P. He, W.-F. Fu, *Chem. Commun.* **2014**, *50*, 10427 – 10429.
[277] J. Masa, S. Barwe, C. Andronescu, I. Sinev, A. Ruff, K. Jayaramulu, K. Elumeeva, B. Konkena, B. R. Cuenya, W. Schuhmann, *ACS Energy Lett.* **2016**, *1*, 1192 – 1198.
[278] S. Surendran, S. Shanmugapriya, S. Shanmugam, L. Vasylechko, R. K. Selvan, *Appl. Energy Mater.* **2018**, *1*, 78 – 92.
[279] J. Liu, M. Meyns, T. Zhang, J. Arbiol, A. Cabot, A. Shavel, *Chem. Mater.* **2018**, *30*, 1799 – 1807.
[280] A. A. Guzelian, J. E. B. Katari, A. V. Kadavanich, U. Banin, K. Hamad, E. Juban, A. P. Alivisatos, *J. Phys. Chem.* **1996**, *100*, 7212 – 7219.
[281] S. Koh, T. Eom, W. D. Kim, K. Lee, D. Lee, Y. K. Lee, H. Kim, W. K. Bae, D. C. Lee, *Chem. Mater.* **2017**, *29*, 6346 – 6355.
[282] S. Prucnal, S. Zhou, X. Ou, H. Reuther, M. O. Liedke, A. Mücklich, M. Helm, J. Zuk, M. Turek, K. Pyszniak, W. Skorupa, *Nanotechnology* **2012**, *23*, 485204-1 – 485204-8.
[283] A. K. Nowak, M. D. Martín, H. P. v. d. Meulen, J. M. Ripalda, L. González, Y. González, L. Viña, J. M. Calleja, *Europhys. Lett.* **2014**, *108*, 17002-1 – 17002-5.
[284] J.-H. Pöhls, A. Faghaninia, G. Petretto, U. Aydemir, F. Ricci, G. Li, M. Wood, S. Ohno, G. Hautier, G. J. Snyder, G.-M. Rignanese, A. Jain, M. A. White, *J. Mater. Chem. C* **2017**, *5*, 12441 – 12456.
[285] S. Lin, J. Gu, Y. Wang, Y. Wang, S. Zhang, X. Liu, H. Zeng, Z. Chen, *J. Mater. Chem. A* **2018**, *6*, 3738 – 3746.
[286] H.-T. Kwon, C. K. Lee, K.-J. Jeon, C.-M. Park, *ACS Nano* **2016**, *10*, 5701 – 5709.
[287] Y. Kim, Y. Kim, A. Choi, S. Woo, D. Mok, N.-S. Choi, Y. S. Jung, J. H. Ryu, S. M. Oh, K. T. Lee, *Adv. Mater.* **2014**, *26*, 4139 – 4144.
[288] W. Li, H. Li, Z. Lu, L. Gan, L. Ke, T. Zhai, H. Zhou, *Energy Environ. Sci.* **2015**, *8*, 3629 – 3636.
[289] H.-S. Shin, K.-N. Jung, Y. N. Jo, M.-S. Park, H. Kim, J.-W. Lee, *Sci. Rep.* **2016**, *6*, 26195-1 – 26195-10.

2. Research Objectives

As it can be seen, especially in the last chapter of the introduction, even after 30 years of constant development nanoscience and nanotechnology still own unimagined potential for future application, which in particular is true in combination with the rich chemistry of arsenic and phosphorus. As the fields of solid-state technology and energy techniques are increasing with the energy thirst of modern society heretofore unexploited nanomaterial like particles containing P and As and elements of group 12 and 14 become more and more interesting. In this process, substances as SiP_2 already proved their suitability. Nevertheless, a lot effort needs to be put in the studies of group 12/15 and group 14/15 nanoscale compounds as well as in tests concerning their applicability. Also the synthetic methods should be considered, in order to avoid toxic or dangerous reagents. Therefore, the single-source-precursor approach seems to be very promising, as not only harsh reaction conditions are avoided but also an influence on the stoichiometry of the nanoparticles' components might be possible.

For this purpose the present work addresses two main topics of which the first covers the synthesis of single-source-precursors containing the elements Ge, Sn and Zn in combination with phosphorus or arsenic and investigations on their suitability for nanoparticles preparation. In order to stabilize the formed complexes two different kinds of ligands were used, namely the benzamidinato ligand $[PhC(N^tBu)_2]$ and the *β*-diketiminato ligand $[CH(C(Me)N(2,6\text{-}^iPr_2C_6H_3))_2]$.

But not only the heavier homologues of group 14 might be promising single source precursors, also compounds with a rare silicon-arsenic double bond could display fascinating and useful features. Thus, in the second topic novel Si=As compounds coordinated by a benzamidinato ligand were synthesized.

In detail the following tasks occurred:

- Studies on the reactivity of the system $[PhC(N^tBu)_2]SiCl/LiAs(SiMe_3)_2$.

- Synthesis of $[CH(C(Me)N(2,6\text{-}^iPr_2C_6H_3))_2]MP(SiMe_3)_2$ complexes (M = Ge, Sn) and their use as single-source-precursors for nanoparticles. Studies on the synthesis of the arsenic analogues and their use as single-source-precursors for nanoparticles.

- Synthesis of $[CH(C(Me)N(2,6\text{-}^iPr_2C_6H_3))_2]Ga(PH_2)_2$ for nanoparticles studies.

- Synthesis of zinc bromide complexes containing the benzamidinato ligand and studies on the reactivity of those compounds towards $LiE(SiMe_3)_2$ (E = P, As) for the preparation of single source precursors for Zn_2P_3 nanoparticles.

3. Reactivity of the Amidinate Stabilized Chlorosylilene Towards $LiAs(SiMe_3)_2$ – Synthesis and Characterization of Compounds Containing a rare Si=As double bond

3.1. Author contribution

Daniela Meyer: Synthesis and characterization of **3-2**, **3-3**, **3-4**, **3-5** and **3-6**

Gábor Balázs: DFT calculations

Michael Seidl: Solution and refinement of the solid state structure of **3-3**, support of the X-ray diffraction measurement of **3-2**

Manfred Scheer: Supervision of the research and revision of the manuscript

3.2. Abstract

Five novel compounds containing a rare silicon arsenic double bond were synthesized from the reaction of $[PhC(N^tBu)_2]SiCl$ (**3-1**) with $LiAs(SiMe_3)_2$. Thus it was possible to isolate $[PhC(N^tBu)_2]Si(SiMe_3)=AsSiMe_3$ (**3-2**) as well as $[PhC(N^tBu)_2]Si(H)=AsSiMe_3$ (**3-5**), both containing a polarized Si=As double bond. Furthermore, the compounds $\{[PhC(N^tBu)_2]Si\}_2=AsSiMe_3$ (**3**-3) and $\{[PhC(N^tBu)_2]Si=AsSiMe_3\}_2$ (**3-4**) could be obtained and their structure was determined by single crystal X-ray diffraction. The oxidation of **3-2** leads to $[PhC(N^tBu)_2]Si(OSiMe_3)=AsSiMe_3$ (**3-6**) in which an oxygen atom is inserted into the Si–Si bond of **3-2**. In addition to the X-ray structure analysis, compounds **3-2**, **3-5** and **3-6** were characterized by multinuclear NMR spectroscopy and mass spectrometry. Furthermore, DFT calculations show that all compounds possess a polarized a Si=As double bond.

3.3. Introduction

In the last few years, compounds with a silicon-phosphorus bond gained a lot of interest due the unusual bonding properties of the Si–P bond as well as the application potential as semiconducting materials.[1,2] Since the first synthesis of $[(Mes)_2Si=P(Mes^*)]$ (Mes^* = 2,4,6-$^tBu_3C_6H_2$) by Bickelhaupt *et al*. in 1984[3] and the first structural characterization by Nieger *et al*. in 1993[4] especially compounds with Si=P double bonds were intensely studied. Nowadays, a variety of phosphasilenes is known, which are stabilized by different sterically demanding and/or electron donating substituents. Examples are derivatives of Bickelhaupt's phosphasilene with residues like Si^tBu_3 or Tip (= 2,4,6-$^iPr_3C_6H_2$) (**3-A**, E = P), and compounds stabilized by β-diketiminato (**3-B**, **3-C**) or benzamidinato ligands (**3-D** – **3-G**) (Scheme 3 - 1).[5,6,7,8] Thereby, the use of sterically demanding ligands protects the Si=P bond from dimerization or polymerization while electron donating substituents are able to strongly polarize the double bond. As a consequence they raise the contribution of a zwitterionic mesomeric structure comprising a negative charge at the phosphorus (**3-B**, **3-D**) and improve the stability of the phosphasilene.[9,10] Thus, it is possible not only to enhance the polarization of the Si=P bond leading to an increased reactivity, but also even to reverse the polarization by carefully choosing suitable substituents ("push-pull" ligands), so that the normally negatively charged phosphorus atom is now

carrying the positive charge (**3-A**, E = P; R = $Tip_2N(Me)_2Si$, R' = Tip, R'' = NMe_2).[11] Also, the formation of larger compounds comprising an acyclic P=Si–Si=P chain is possible, as Roesky *et al*. were able to isolate $\{[PhC(N^tBu)_2]Si=P(Tip)\}_2$ (**3-E**) by the reaction of **3-1** with $TipPCl_2$ and the reducing agent KC_8.[12]

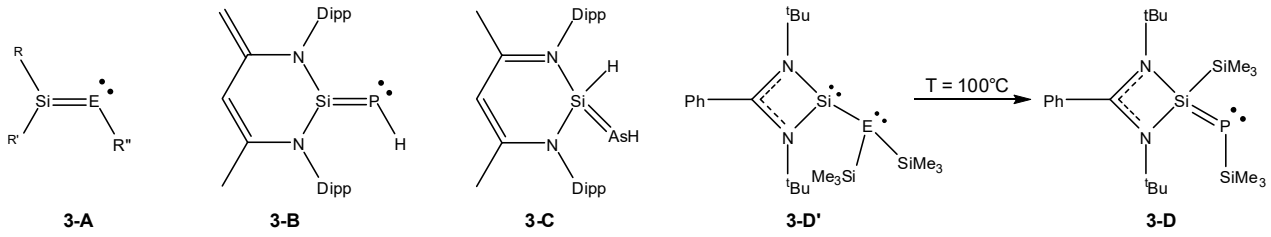

3-A **3-B** **3-C** **3-D'** **3-D**

E = P, As Dipp = 2,6-Diisopropyphenyl

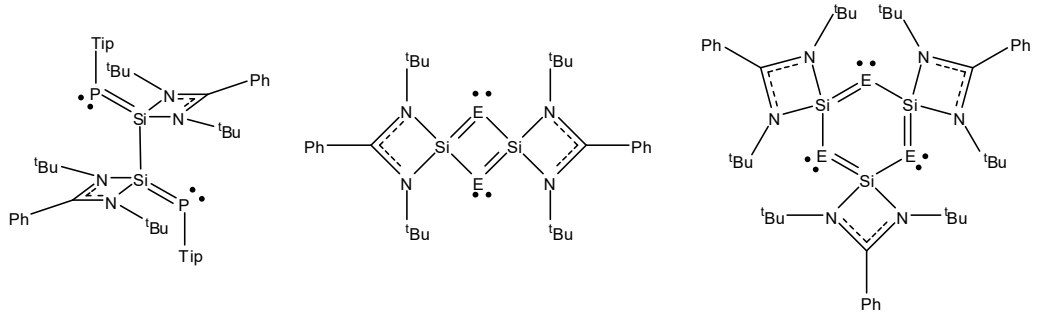

3-E **3-F** **3-G**

E = P, As E = P, As

Scheme 3 - 1: Selected examples of stable phospha- and arsasilenes. **3-D** is formed by heating the precursor **3-D'** to 100°C.[13]

While the chemistry of the phosphasilenes is well known,[10] only little is known about their heavier analogues, the arsasilenes, of which the first was reported with $Tip_2Si=As(Si^iPr_3)$ by Driess in 1992 followed by various representatives of type **3-A** (E = As, R = ^{t}Bu, R' = Tip, R'' = Si^iPr_3, $Si(Ph_2Me)$, $Si(Cy_2Me)$ (Cy = Cyclohexyl)) and type **3-C** some years later (Scheme 3 - 1).[14,15,16,17] Hereby, Driess *et al*. were able to show, that the arsenic derivatives **3-A** and **3-C** can be prepared in the same way as their phosphorus homologues. Recently, our group was investigating the usage of transfer reagents like $[Cp''_2Zr(\eta^2\text{-}E_4)]$ (E = P, As) for the synthesis of metastable compounds. Thus, we were successful in the preparation of the aromatic triphospha- and triarsasilabenzene derivatives **3-F** and **3-G**, respectively. Moreover, we also showed the different reactivity of silylenes and disilenes towards yellow arsenic, leading to compounds containing an As_{10} unit and an As_2 unit, respectively.[18] But still, merely few stable examples of arsasilenes can be found in literature due to their high reactivity, which is similar to the analogous phosphorus compounds as the polarization of the Si=As bond is akin to the polarization of the Si=P bond. Therefore, arsasilenes also need to be stabilized by substituents like β-diketiminato or benzamidinato. In the view of the rare existing examples of Si=As double bond compounds containing such a benzamidinato ligand we were interested in the isolation of other related species. So herein, we report on the reactivity of the chlorosilylene $[PhC(N^tBu)_2]SiCl$ (**3-1**)[19] towards

$LiAs(SiMe_3)_2$, leading to a series compounds containing Si=As double bonds stabilized by the benzamidinato ligand.

3.4. Results and Discussion

The reaction of **3-1** with one eq. of $LiAs(SiMe_3)_2$ in toluene at –80°C leads to the formation of $[PhC(N^tBu)_2]Si(SiMe_3)=AsSiMe_3$ (**3-2**), which can be isolated as yellow crystals in 78% yields (vide infra, Scheme 3 - 2). Compound **3-2** is stable under an inert atmosphere at room temperature in solution as well as in the solid state. It shows good solubility in thf, but is almost insoluble in non-polar solvents like n-hexane. As reaction pathway for the formation of **3-2** the initial generation of the intermediate $[PhC(N^tBu)_2]Si–As(SiMe_3)_2$ (**3-2'**) might be proposed followed by a Me_3Si shift from arsenic to silicon leading to **3-2**. This pathway was also suggested for the similar reaction of **3-1** with the phosphorus derivative $LiP(SiMe_3)_2$, reported by Driess *et al.*, which leads to **3-D'**, the phosphorus analogue of **3-2'**. **3-D'** is stable at room temperature and could be isolated. However, heating of **D'** to 100°C leads to the formation of **3-D** (Scheme 3 - 1).[13] Therefore, it is likely that the formation of **3-2** also proceeds via the migration of a $SiMe_3$ unit from the presumably formed intermediate **3-2'**. DFT calculations at the B3LYP/def2TZVP level of theory show that **3-2** is with 3.0 $kJ \cdot mol^{-1}$ more stable than **3-2'**, and both are connected via a transition state which is 125.5 $kJ \cdot mol^{-1}$ higher in energy than **3-2'** (Figure 3 - 1). Interestingly, **3-D'** is with 4.2 $kJ \cdot mol^{-1}$ more stable than **3-D**, however, the transition state connecting **3-D** with **3-D'** is with 135.2 $kJ \cdot mol^{-1}$ higher in energy than **3-D'**. Due to the similar thermodynamic parameters of **3-2**/**3-2'** and **3-D**/**3-D'** we would expect a higher stability of **3-2'**. Probably, the transformation of **3-2** into **3-2'** might be accelerated by intermolecular processes which might be the reason that all attempts to identify **3-2'** crystallographically or spectroscopically failed.

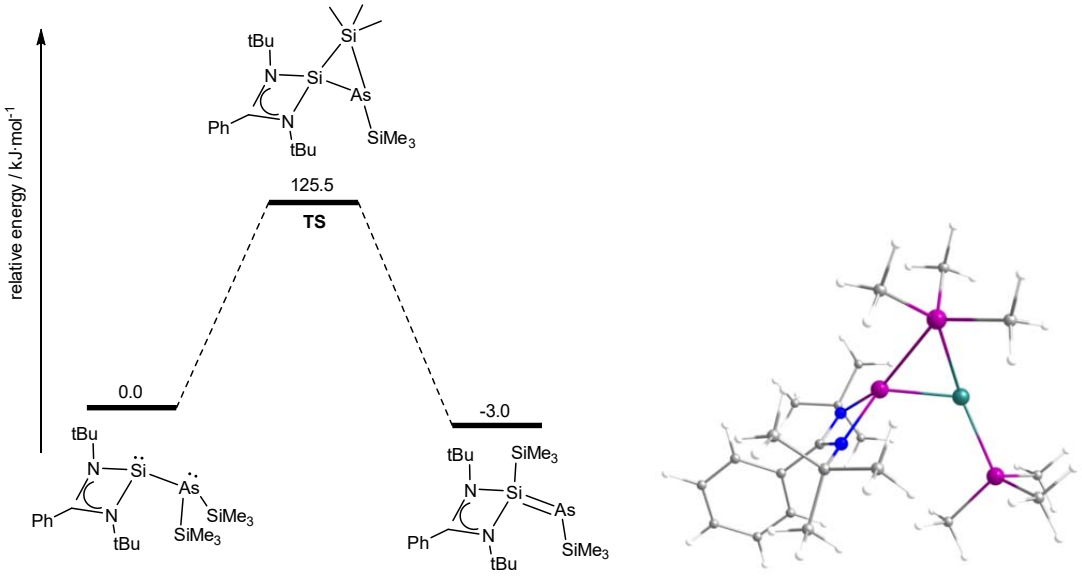

Figure 3 - 1: Energy diagram of the transformation of **3-2'** to **3-2** (left) and the structure of the transition state (right), calculated at the B3LYP/def2TZVP level of theory.

While we attempted to optimize the yields of **3-2**, we obtained in one case a very small amount of yellow platelets of the compound [{PhC(N^{t}Bu)$_2$}Si=AsSiMe$_3$]$_2$ (**3-3**) from the crude reaction mixture in toluene. Unfortunately, all attempts to reproduce **3-3** failed. However, it was detected several times by EI mass spectrometry in small amounts as a side product of the preparation of **3-2**. Probably, **3-3** is very unstable in solutions leading to a rapid decomposition. We speculate that **3-2'** is an intermediate in the formation of **3-3**, *i.e.* by the photochemical cleavage of a Me$_3$Si group in **3-2'** followed by dimerization of the formed radical species [PhC(N^{t}Bu)$_2$]Si–AsSiMe$_3$ leading to **3-3**. According to DFT calculations this process is strongly exothermic (−168.8 kJ·mol^{-1}). In one attempt to reproduce **3-2** using thf as solvent we were able to isolate the unique compound [PhC(N^{t}Bu)$_2$]Si([PhC(N^{t}Bu)$_2$]Si)=As(SiMe$_3$) (**3-4**) containing a second [PhC(N^{t}Bu)$_2$]Si fragment bound to [PhC(N^{t}Bu)$_2$]Si=As(SiMe$_3$) via a Si–Si bond. **3-4** exhibits a central structural motif which is the heavier homologue to the P=Si–Si=P chain of **3-E**, indicating a reaction pathway similar to the formation of **3-E** that involves a reduction step. This is quite surprising due to the fact that in the synthesis of **3-4** no reducing agent was used unlike in the preparation of **3-E** where KC$_8$ was added to the reaction mixture.[12] In principle, one could assume, that **3-4** is formed by the reaction of **3-2** with the starting material **3-1**. However, by carrying out such reactions, we could not yield **3-4**. Also other attempts to form **3-4** failed. In addition, we could observe, that if in the reaction of **3-1** with LiAs(SiMe$_3$)$_2$ not all traces of water are excluded, additionally to **3-2** the compound [PhC(N^{t}Bu)$_2$]Si(H)=AsSiMe$_3$ (**3-5**) is formed. **3-5** is stable at room temperature under inert atmosphere and also well soluble in polar organic solvents, such as thf or toluene. The rational synthesis of **3-5** was achieved by adding a controlled amount of water to a mixture of **3-1** and LiAs(SiMe$_3$)$_2$ in thf, whereby the best yield of **3-5** could be obtained by using a stoichiometry of **3-1**:LiAs(SiMe$_3$)$_2$:H$_2$O = 5:5:1. Interestingly, the hydrolysis of **3-2** does not lead to the formation of **3-5** indicating that **3-2** is not the intermediate for the formation of **3-5**. We speculate, that **3-5** is formed by the hydrolysis of the transient formed compound [PhC(N^{t}Bu)$_2$]Si–As(SiMe$_3$)$_2$ (**3-2'**). Support for this is given by DFT calculations, which shows that the reaction of **3-2'** with H$_2$O leading to **3-5** and Me$_3$SiOH is strongly exothermic (−134.5 kJ·mol^{-1}). Similarly, performing the reaction of **3-1** with LiAs(SiMe$_3$)$_2$ in the presence of tris(trimethylsilyl)peroxide results in the formation of [PhC(N^{t}Bu)$_2$]Si(OSiMe$_3$)=AsSiMe$_3$ (**3-6**), while the reaction of **3-2** with (Me$_3$Si)$_2$O$_2$ does not yield compound **3-6**.

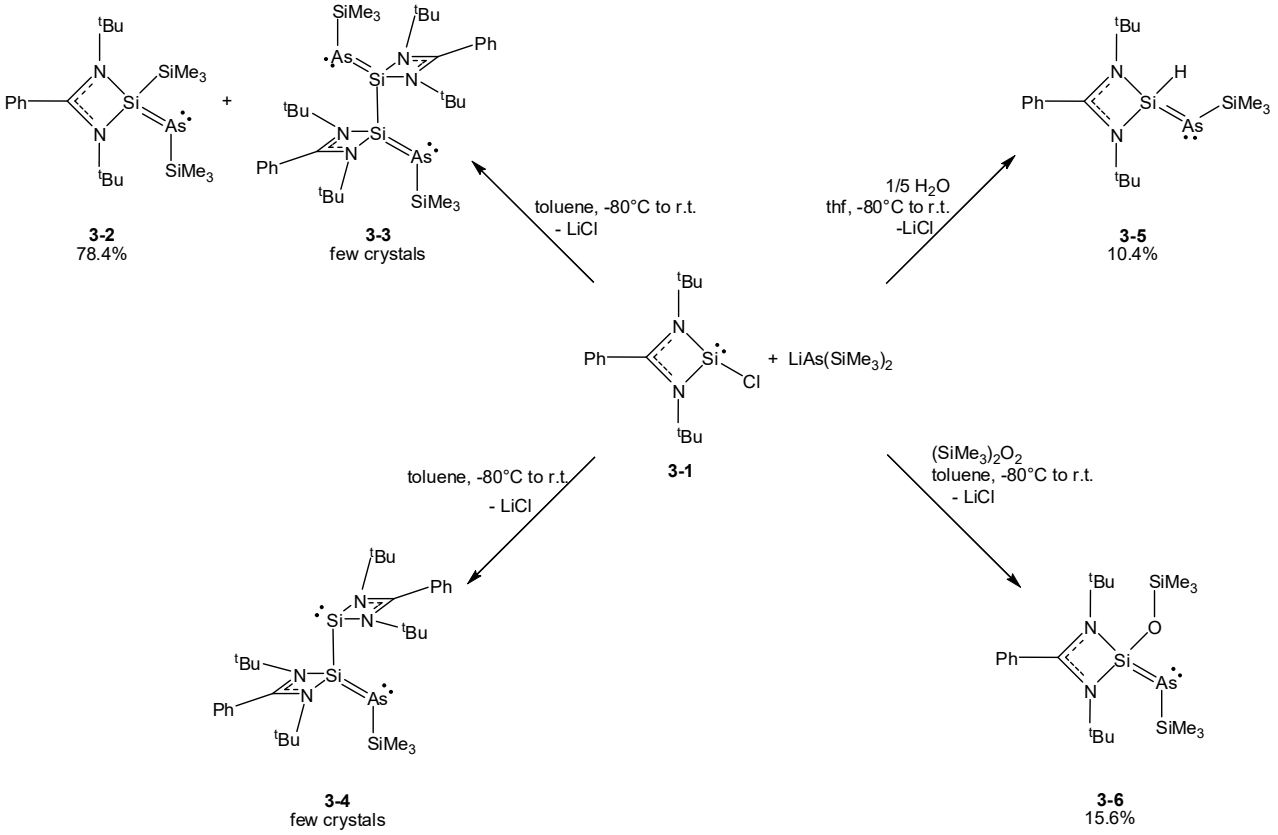

Scheme 3 - 2: The reaction of **3-1** with $LiAs(SiMe_3)_2$.

Compounds **3-2**, **3-5** and **3-6** were fully characterized by spectroscopic methods, i.e. ^{1}H, $^{13}C\{^{1}H\}$ and $^{29}Si\{^{1}H\}$DEPT NMR spectroscopy and mass spectrometry, whereas **3-3** was confirmed by solid state EI mass spectrometry.

The ^{1}H NMR spectrum of **3-2** shows the signals of the ^{t}Bu substituents and the phenyl group in the expected regions. The resonance signal of the $As(SiMe_3)$ residue can be found near the ^{t}Bu signals while the signal caused by the $SiMe_3$ substituent is located a little more in the high field (Table 3 - 1). The $^{29}Si\{^{1}H\}$ DEPT spectrum of **3-2** exhibits three singlets for its three Si atoms (Table 3 - 1). A comparison of the $^{29}Si\{^{1}H\}$DEPT NMR spectrum of **3-2** with the $^{29}Si\{^{1}H\}$ NMR spectrum of **3-D** clearly reveals the structural relation of both compounds as the signals of the silyl groups of **3-2** (δ[ppm] = –15.9, –2.1) and **3-D** (δ [ppm] = –17.5, –3.0)[13] are in good agreement, although the signals of the arsenic compound are slightly down-field shifted. For the Si atom of the double bond this shift is significantly larger as the signal of **3-D** occurs at 40.5 ppm,[13] while the corresponding signal of **3-2** appears at 46.5 ppm. Also the ^{1}H NMR spectra of **3-5** and **3-6** display the signals of the ^{t}Bu substituents and the phenyl group as well as the resonance signals of the $As(SiMe_3)$ residue. For **3-6** a singlet caused by the silicon bound $OSiMe_3$ substituent can be found, while in case of **3-5** a signal for the Si–H group is detected. As the $^{29}Si\{^{1}H\}$ DEPT NMR spectrum of **3-2**, the $^{29}Si\{^{1}H\}$ NMR spectrum of **3-6** exhibit three singlets. In contrast to this, the $^{29}Si\{^{1}H\}$ NMR spectrum of **3-5** shows two resonance signals. The ^{29}Si NMR spectrum of **3-5** reveals a splitting of the singlets into a doublet

($^1J(^{29}SiH)$ = 215.1 Hz), unequivocally indicating the Si–H bond, and a multiplet for the $SiMe_3$ signal ($^2J(^{29}SiH)$ = 6.4 Hz).

Table 3 - 1: ^{29}Si NMR chemical shifts of the compounds **3-2**, **3-5** and **3-6**. For **3-5** the $J(^{29}SiH)$ coupling constants are given as determined from the ^{29}Si NMR spectrum.

	As–*Si*Me$_3$ δ [ppm]	Si–*Si*Me$_3$ δ [ppm]	O–*Si*Me$_3$ δ [ppm]	*Si*=As δ [ppm]
3-2	2.1	–15.9	-	46.5
3-5	3.1 ($^2J(^{29}SiH)$ = 6.4 Hz)	-	-	25.7 ($^1J(^{29}SiH)$ = 215.1 Hz)
3-6	2.4	-	–6.6	10.0

Table 3 - 2: ^1H NMR chemical shifts of the compounds **3-2**, **3-5** and **3-6**. For **3-5** also the coupling constants of the ^{29}Si NMR spectrum are presented. (Table 3 - 1)

	As–Si*Me$_3$* δ [ppm]	Si–Si*Me$_3$* δ [ppm]	O–Si*Me$_3$* δ [ppm]	^{t}Bu δ [ppm]	Ph δ [ppm]	Si–H δ [ppm]
3-2	0.8	0.5	-	1.2	6.8 – 7.3	-
3-5	0.8 ($^2J(^{29}SiH)$ = 6.4 Hz)	-	-	1.1	6.7 – 6.9	7.2 ($^1J(^{29}SiH)$ = 215.1 Hz)
3-6	0.8	-	0.4	1.2	6.8 – 6.9	-

Comparing the $^{29}Si\{^1H\}$DEPT NMR spectrum of **3-2** to the $^{29}Si\{^1H\}$ NMR spectrum of **3-5** shows that the resonance signal of the central silicon of **3-5** is high field shifted compared to **3-2** (δ [ppm] = 46.5 (**3-2**); 25.7 (**3-5**)), while the resonance signals of the $SiMe_3$ groups are almost identical (δ [ppm] = 2.1 (**2**3-); 3.1 (**3-5**)). Both the $^{29}Si\{^1H\}$ NMR spectra of **3-2** and **3-6** show three signals, yet the signals of the As–*Si*Me$_3$ group and the O–*Si*Me$_3$ group of **3-6** are shifted to low field (**3-2**: δ [ppm] = –17.5 (As–*Si*Me$_3$), –2.19 (O–*Si*Me$_3$); **3-6**: δ [ppm] = –6.65 (As–*Si*Me$_3$), –2.41 (O–*Si*Me$_3$)). In contrast to the low field shifts of these two signals, the signal of the Si=As fragment is distinctly shifted to high field (Si=As: δ [ppm] = 46.5 (**3-2**); 9.96 (**3-6**)). Additionally to the $^{29}Si\{^1H\}$ DEPT and $^{29}Si\{^1H\}$ NMR spectra, also the ^1H NMR spectra show the similarity between the three compounds **3-2**, **3-5** and **3-6** as it can be seen in Table 3 - 2.

All of the isolated compounds **3-2** – **3-6** were characterised by X-ray structure analysis. **3-2** can be isolated as yellow platelets suitable for single crystal X-ray analysis by performing the reaction at –78°C and storing the toluene solution at the same temperature. **3-2** crystallizes in the space group $P2_1/n$. The asymmetric unit contains one molecule of $[PhC(N^tBu)_2]Si(SiMe_3)=AsSiMe_3$ and a disordered toluene molecule. Also **3-5** crystallizes in $P2_1/n$ with one molecule in its asymmetric unit. The yellow crystals suitable for X-ray analysis were obtained by storing a thf solution of **3-5** at –30°C. Last, but not least **3-6** crystallizes as yellow blocks from toluene at –30°C in the space group $P2_1/n$.

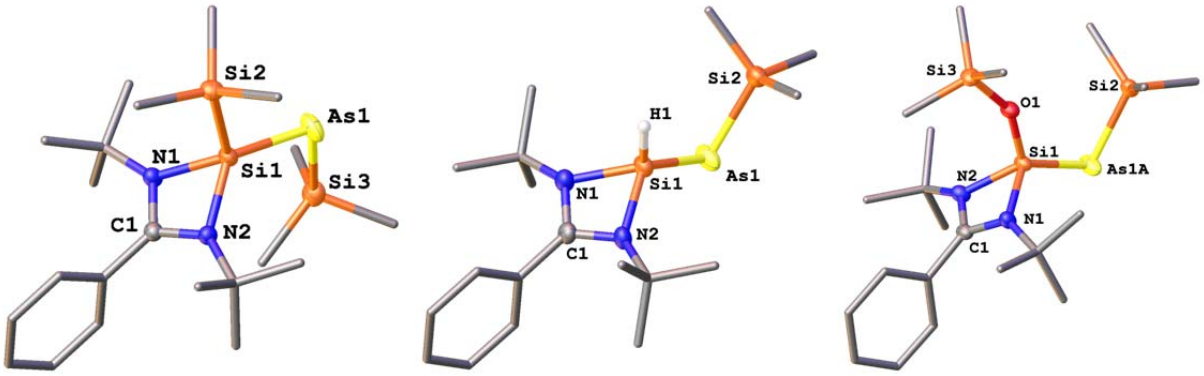

3-2 **3-5** **3-6**

Figure 3 - 2: Molecular structures of **3-2**, **3-5** and **3-6**. Thermal ellipsoids are shown with 50% probability level. H atoms and the toluene molecule are omitted for clarity. Selected lengths [Å] and angles [°]: **3-2**: Si1 – Si2 2.3451(7), Si1 – As1 2.2110(5), As1 – Si3 2.3175(6), Si1 – N1 1.8489(16), Si1 – N2 1.8462(16), N1 – C1 1.338(2), N2 – C1 1.337(2); Si2 – Si1 – As 108.97(2), Si1 – As1 – Si3 102.49(2), N1 – Si1 – N2 70.58(7). **3-5**: Si1 – H1 1.40(2), Si1 – As1 2.2069(5), As1 – Si2 2.3226(5), Si1 – N1 1.8371(15), Si1 – N2 1.8337(15), N1 – C1 1.338(2), N2 – C1 1.335(2); H1 – Si1 – As1 121.1(10), Si1 – As1 – Si2 94.803(19), N1 – Si1 – N2 71.13(6). **3-6:** Si1 – As1A 2.2124(19), Si1 –As1B 2.225(8), As1A – Si2 2.3253(19), As1B – Si2 2.302(8), Si1 – O1 1.6119(15), O1 – Si3 1.6491(15), Si1 – N1 1.8445(18), Si1 – N2 1.8282(17), N1 – C1 1.339(2), N2 – C1 1.335(3); Si1 – As1A – Si2 94.19(7), Si1 – As1B – Si2 94.5(3), Si1 – O1 – Si3 149.23(9), As1A – Si1 – O1 120.57(7), As1B – Si1 – O1 121.3(2), N1 – Si1 – N2 71.31(8). Disorder of the As1 atom: As1A : As1B = 81% : 19%.

The structures of **3-2**, **3-5** and **3-6** exhibit a four-membered ring consisting of a carbon atom, two nitrogen atoms and a silicon atom. In the case of **3-2** the Si1 is in a tetrahedrally distorted environment formed by a $SiMe_3$ group, the As1 atom and the benzamidinato ligand. The Si1–Si2 bond length of 2.3451(7) Å is in the range of a short Si–Si single bond (Si–Si: 2.3659(4) Å – 2.413(2) Å),[19,13,20] while the Si1–As1 bond of 2.2110(5) Å is consistent with a Si–As double bond (Si=As: 2.218 Å).[14] The geometric parameters of the derivative **3-D** are similar, except for the Si–P and the Si–As bond lengths, respectively. As depicted in Figure 3 - 2, the molecular structure of **3-5** is comparable to that of **3-2** apart from the orientation of the RSi=As($SiMe_3$) fragment (R = $SiMe_3$ (**3-2**), H(**3-5**)) which adopts a cis conformation in compound **3-5** (torsion angle: H1–Si1–As1–Si2 = 0.53°) and a trans conformation in **3-2** (torsion angle: Si2–Si1–As1–Si3 = –175.36°) due to sterical reasons. According to the DFT calculations the cis isomer of **3-5** is with 11.1 $kJ \cdot mol^{-1}$ more stable than the trans isomer, while in the case of **3-2** the trans isomer is with 2.15 $kJ \cdot mol^{-1}$ more stable than the cis isomer. The Si1–As1 bond in compound **3-5** of 2.2069 Å is in the range of a Si–As double bond (Si=As: 2.218 Å).[14] The Si1–H1 bond of 1.40 Å is a very short Si–H single bond (Si–H: 1.445 Å ($SiHF_3$)[21]) and is also in the range of the Si–H distance of the DFT optimised structure of **3-5** (Si–H: 1.488 Å).[22] The N1–Si1–N2 angle of **3-5** (71.13°) is slightly larger than it is in compound **3-2** (70.56°) which shows in combination with the H1–Si1–As1 angle (121.1°) the tetrahedrally distorted coordination sphere of the Si1 atom. Also **3-6** exhibits a structure akin to the one of **3-2** as the only differences are the oxygen atom formally inserted into the Si1–Si2 bond, the As–$SiMe_3$ group which is in cis conformation similar to **3-5** and the slightly elongated Si–As bond with an arsenic atom disordered over two positions (**3-6**: $Si1–As_{av.}$ 2.219(11) Å; **3-2**: Si1–As1 2.2108(6) Å). Due to this disorder the two Si1–As bond lengths are slightly different, but still in the range of a Si–As double bond (**3-6**: Si1–As1A: 2.2124(19) Å, Si1–As1B: 2.225(8) Å; Si=As: 2.218 Å[14]). The length of both Si–O bonds of 1.6119(15) Å (Si1–O1)

and 1.6491(15) Å (O1–Si3) are in good agreement of a slightly elongated Si–O single bond (Si–O: 1.610(9) Å[23]).

Yellow crystals of **3-3** suitable for single crystal X-ray structure analysis were isolated from a toluene solution at –30°C. Single crystals of **3-4** could be obtained by cooling a thf solution to –30°C. Like **3-3**, **3-4** crystallizes in the space group $P2_1/c$ with one molecule of **3-4** and one disordered thf molecule per asymmetric unit. The unique feature of the structure of **3-4** is the bis-benzamidinato silicon unit connected via a Si–Si bond. Additionally, one silicon binds to an $AsSiMe_3$ unit. The two $[PhC(N^tBu)_2Si$ fragments are rotated to each other by approximately 92.2(1)° as a consequence of the sterically enhanced residues, because of which the two benzamidinato ligands are in a distorted gauche conformation (torsion angle N2–Si1–Si2–N4 = 92.43°). The Si=As double bond (Si2–As1: 2.2419(6) Å) is slightly elongated compared to an average Si–As double bond (Si=As: 2.218 Å)[14] or the corresponding bonds in **3-2** (Si1–As1: 2.2110(5) Å) and **5** (Si1–As1: 2.2069 Å). Yet, it is similar to the one of **3-6** ($Si1–As_{av.}$ 2.219(11) Å).

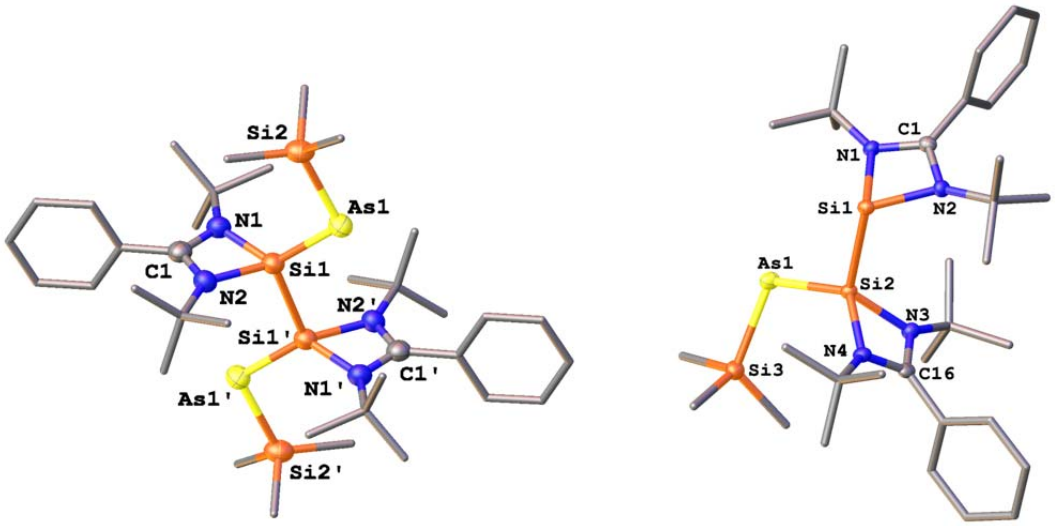

3-3 **3-4**

Figure 3 - 3: Molecular structures of **3-3** and **3-4**. Thermal ellipsoids are shown with 50% probability level. H atoms and the toluene molecule are omitted for clarity. Selected lengths [Å] and angles [°]: **3-3**: Si1–Si1' 2.4019(15), As1–Si1/As1'–Si1' 2.2141(8), Si2–As1/Si2'–As1' 2.3227(9), Si1–N1/Si1'–N1' 1.864(2), Si1–N2/Si1'–N2' 1.868(3); Si2–As1–Si1/Si2'–As1'–Si1' 103.43(3), As1–Si1–Si1'/As1'–Si1'–Si1 110.52(5), N1–Si1–N2/N1'–Si1'–N2' 70.03(11). **3-4**: Si1–Si2 2.4183(8), Si2–As1 2.2419(6), As1–Si3 2.3240(7), Si1–N1 1.873(2), Si1–N2 1.864(2), Si2–N3 1.856(2), Si2–N4 1.8590(19); Si1–Si2–As1 110.40(3), Si2–As1–Si3 108.99(2), N1–Si1–N2 69.39(8), N4–Si2–N3 70.37(9).

The structure of **3-3** is depicted in Figure 3 - 3 (left) and shows a centrosymmetric dimer in which two $[PhC(N^tBu)_2]Si=AsSiMe_3$ units are connected via a Si–Si bond with the two benzamidinato ligands in an antiperiplanar arrangement. The torsion angle between both $[PhC(N^tBu)_2]Si=AsSiMe_3$ fragments of **3-3** is 176.81°. The Si1–As1 bond length of 2.2141(8) Å is in the range of a silicon-arsenic double bond (Si=As: 2.218 Å).[14] The Si1–Si1' bond is an elongated single bond (2.4019(15) Å compared to Si–Si: 2.3659(4) Å – 2.413(2) Å[19,13,20]). The atoms Si1 and Si1' are in a distorted tetrahedral

environment (As–Si1–Si1': 110.52(5)°), while at the arsenic atom the substituents are arranged in an angled coordination (Si2–As1–Si1: 103.43(3)°).

As described above, Roesky *et al.* reported only recently on the synthesis of the phosphorus compound {[PhC(N^{t}Bu)$_2$]Si=PTip}$_2$ (**3-E**) displaying a similar structure as **3-3** (Scheme 3 - 1).[12] Both species show a trans-bent structure as described above. The Si–Si bond lengths do not differ considerably as the Si1–Si2 bond in **3-3** is only slightly longer than the one reported for **3-E** (**3-3**: Si1–Si2: 2.4005(8) Å, **3-E**: Si1–Si2: 2.3825(11) Å).

The Si1–Si2 bond length of 2.4183(8) Å in **3-4** is in the range of a rather long Si–Si single bond (Si–Si: 2.3659(4) Å – 2.413(2) Å),[19,13,20] whereby it is longer than the corresponding Si–Si bond of **3-3** (2.4019(15) Å). The Si2 atom is in a distorted tetrahedral environment, while Si1 shows a pyramidal geometry similar to that found for **3-D**.[24] The Si3–As1–Si2 angle of 108.99(2)° is larger than the corresponding angles in **3-2** (Si1–As1–Si3: 102.49(2)°), **3-5** (Si1–As1–Si2: 94.803(19)°) and **3-6** (Si1–As1A–Si2: 94.19(7)°). However, the As1–Si2–Si1 (110.40(3)°) and Si2–As1–Si3 (108.99(2)°) angles of **3-4** are similar to the one in **3-3** (As–Si1–Si1'/As'–Si1'–Si1: 110.52(5)°; Si2–As–Si1/Si2'–As'–Si1': 103.43(3)°) showing the analogy of both compounds.

In 2010 So *et al.* reported on the synthesis of monomeric silylsilylenes and their success in the preparation of [PhC(N^{t}Bu)$_2$]Si–Si{[PhC(H)(N^{t}Bu)$_2$]R} (R = Cl (**3-H**), H (**3-I**)) exhibiting a similar structure to the herein described compound **3-4**.[25] The Si–Si distances of both **3-H** (Si–Si: 2.381 Å) and **3-I** (Si–Si: 2.377 Å) are shorter than in **3-4** (Si1–Si2: 2.418 Å) due to the steric and electronic demand of the As(SiMe$_3$) group bound to Si2 in **3-4**. The most striking difference between the three species is the loss of the allylic system located at the NCN fragment of the Si2N3N4C16 ring in **3-H** and **3-I** due to the hydration of C16 which leads to structural changes as the phenyl rings are bent out of the SiN$_2$C ring plane. In **3-4** the allylic system of Si2N3N4C16 is still intact as the bond lengths show ([Å]: **3-4**: Si2–N3: 1.856(2), Si2–N4: 1.8590(19), N3–C16: 1.341(3), N4–C16: 1.340(3); **3-H**: Si2–N3: 1.730, Si2–N4: 1.735, N3–C16: 1.491, N4–C16: 1.489; **3-I**: Si2–N3: 1.753, Si2–N4: 1.759, N3–C16: 1.483, N4–C16: 1.487) and angles ([°]: **3-4**: N3–Si2–N4: 70.34(9), Si2–N3–C16: 91.92(15), Si2–N4–C16: 91.76(14), N3–C16–N4: 105.98(19); **3-H**: N3–Si2–N4: 78.2, Si2–N3–C16: 91.3, Si2–N4–C16: 91.1, N3–C16–N4: 94.2; **3-I**: N3–Si2–N4: 77.5, Si2–N3–C16: 91.0, Si2–N4–C16: 90.7, N3–C16–N4: 95.5). The Si1–Si2–R angles differ of course depending on the nature of R (**3-4**: Si1–Si2–As1: 110.40(3); **3-H**: Si1–Si2–Cl1: 101.1; **3-I**: Si1–Si2–H1: 104.7), revealing the high steric demand of the As(SiMe$_3$) residue.

In addition to the up to this point described crystal structures, we were able to isolate compound {[PhC(N^{t}Bu)$_2$]SiAs}$_2$ (**3-F**) (Scheme 3 - 1) from a VT NMR sample after the reaction mixture stood for two weeks at r.t.. **3-F** has been synthesized by our group by the reaction of **3-1** with [Cp''$_2$Zr($\eta^{1:1}$-As$_4$)]. Interestingly, species **3-F** prepared from [Cp''$_2$Zr($\eta^{1:1}$-As$_4$)] crystallizes in the triclinic $P\bar{1}$ instead of the monoclinic space group P2$_1$/c as it is the case for **3-F** obtained from a mixture of **3-1** with LiAs(SiMe$_3$)$_2$.[18,26]

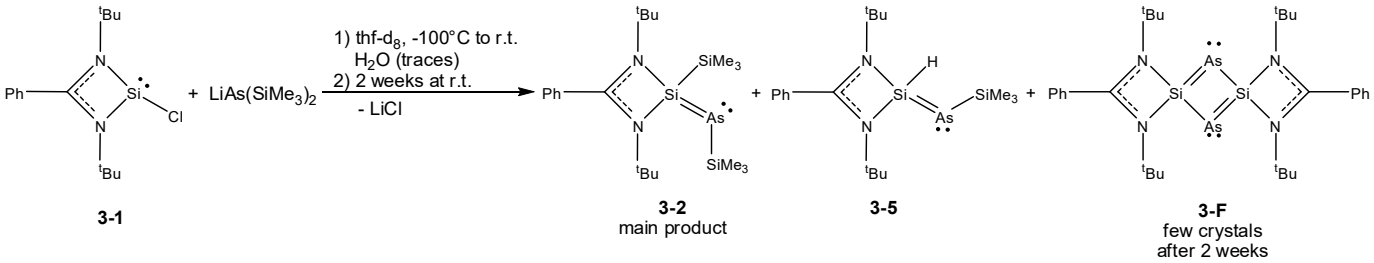

Scheme 3 - 3: Reaction of **3-1** with $LiAs(SiMe_3)_2$, in which **3-F** was obtained as a side product

3.5. Conclusion

As up to date, only a handful of compounds with Si=As bonds are known today, even less stabilized by a benzamidinato substituent, our group decided to study the promising one pot reaction of the monochlorosilylene **3-1** with $LiAs(siMe_3)_2$. Thus, we were able to synthesize five novel silicon arsenic products, which not only are stabilized by a benzamidinato ligand but represent especially rare examples of compounds containing Si=As double bonds. The main product $[PhC(N^tBu)_2]Si(SiMe_3)=AsSiMe_3$ (**3-2**) was confirmed to be the heavier homologue of $[PhC(N^tBu)_2]Si(SiMe_3)=PSiMe_3$ (**3-D**) by NMR spectroscopy and X-ray structure analysis. Furthermore, studies on the reactivity of the **3-1**/$LiAs(SiMe_3)_2$ system towards water and oxygen led to the successful preparation and characterization of the products $[PhC(N^tBu)_2]Si(H)=AsSiMe_3$ (**3-5**) and $[PhC(N^tBu)_2]Si(OSiMe_3)=AsSiMe_3$ (**3-6**). And last, but not least, we could obtain two larger silicon arsenic compounds, $\{[PhC(N^tBu)_2]Si\}_2=AsSiMe_3$ (**3-3**) and $\{[PhC(N^tBu)_2]Si=AsSiMe_3\}_2$ (**3-4**), showing very similar dimeric structures in comparison with the monomers being connected via Si–Si bonds. Moreover, **3-4** can be considered as the arsenic analogue of $\{[PhC(N^tBu)_2]Si=PTip\}_2$ (**3-E**).

3.6. Supporting Information

Experimental section

General procedures

All experiments were carried out under a dry nitrogen or argon atmosphere using standard Schlenk or drybox techniques. Solvents were dried by using an MBraun purification system followed by a distillation from sodium and stored over 3 Å mol sieve. The monochlorosilylene $[PhC(N^tBu)_2]SiCl$ [27,28], $As(SiMe_3)_3$ and $LiAs(SiMe_3)_2$[29] were prepared according to literature. The NMR spectra were recorded on a Bruker Avance 400 (^1H: 400.132 MHz, $^{13}C\{^1H\}$: 100.613 MHz, $^{29}Si\{^1H\}$DEPT/$^{29}Si\{^1H\}$/^{29}Si: 79.945 MHz) and an Avance 300 (^1H: 300.132 MHz) with δ referenced to external $SiMe_4$ (^1H, $^{13}C\{^1H\}$, $^{29}Si\{^1H\}$DEPT/$^{29}Si\{^1H\}$/^{29}Si). The EI- and LIFDI-MS studies were performed on a Jeol AccuTOF GCX.

Preparations

Preparation of $[PhC(N^tBu)_2]Si(SiMe_3)=As(SiMe_3)$ (3-2) and $[\{PhC(N^tBu)_2\}Si=AsSiMe_3]_2$ (3-3): $LiAs(SiMe_3)_2$ (516 mg, 1.29 mmol) in toluene (10 mL) was added to a stirred solution of $[PhC(N^tBu)_2]SiCl$ **3-1** (382.2 mg, 1.29 mmol) in toluene (5 mL) at –80°C. The reaction mixture was warmed to room temperature overnight. The yellow solution was filtered and concentrated. **3-2** was obtained as yellow platelets at –30°C (486.2 mg, 78.4%). **3-3** could be detected by solid state EI-MS in the solid resulting from the reaction mixture of **3-1** and $LiAs(SiMe_3)_2$.

^1H NMR (400.132 MHz, C_6D_6, 298K): δ[ppm] = 0.45 (s, 9 H, R-Si(Si(C*H*$_3$)-R'), 0.79 (s, 9 H, R-Si(SiMe$_3$)=AsSi(C*H*$_3$)); 1.16 (s, 18 H, ^{t}Bu), 6.82 – 7.03, 7.25 – 7.27 (m, 5 H, Ph); $^{13}C\{^1H\}$ NMR (100.613 MHz, C_6D_6, 298K): δ[ppm] = 0.21 (R-Si(Si(*C*H$_3$)-R'), 7.83 (R-Si(SiMe$_3$)=AsSi(*C*H$_3$)), 32.05 (NC(*C*H$_3$)), 55.23 (N*C*Me$_3$), 128.88, 130.26, 132.21 (Ar-*C*), 169.35 (N*C*N); $^{29}Si\{^1H\}$ DEPT NMR (79.945 MHz, C_6D_6, 298K): δ[ppm] = –15.86 (s, Si*Si*Me$_3$), 2.13 (s, As*Si*Me$_3$), 46.48 (s, *Si*=As(SiMe$_3$)). Solid state EI-MS calcd for $C_{21}H_{41}AsN_2Si_3$ (**3-2**), 480.1788, Found 480.1777; calcd for $C_{36}H_{64}As_2N_4Si_4$ (**3-3**), 814.2634, Found 814.2824. Elemental analysis was not performed due to the sensitivity to hydrolysis and the thermal instability of **3-2**.

Preparation of $[PhC(N^tBu)_2]Si([PhC(N^tBu)_2]Si)=As(SiMe_3)$ (3-4): $LiAs(SiMe_3)_2$ (171 mg, 0.51 mmol) in thf and $[PhC(N^tBu)_2]SiCl$ **3-1** (150 mg, 0.51 mmol) in thf (15 mL) were mixed at –80°C, followed by an immediate colour change to yellow. The reaction mixture was stirred and warmed to room temperature overnight. The solvent was concentrated to yield small yellow crystals of **3-4**.

Preparation of $[PhC(N^tBu)_2]Si(H)=As(SiMe_3)$ (3-5): A solution of $LiAs(SiMe_3)_2$ (171 mg, 0.51 mmol) in 10 mL thf and a solution of $[PhC(N^tBu)_2]SiCl$ **3-1** (150 mg, 0.51 mmol) in thf (15 mL) were mixed at –80°C, whereupon the solution turned immediately yellow. Subsequently 1.83 mL of a H_2O stock solution (0.1 mL H_2O in 100 mL thf) (0.1 mmol, $LiAs(SiMe_3)_2$:H_2O = 1:5) were added at –80°C. The reaction mixture was stirred and warmed to room temperature overnight. The solvent was removed and the yellow residue was extracted with n-hexane (30 mL). The filtrate was concentrated to yield small yellow crystals of **3-5** (50 mg, 10.4%).

^{1}H NMR (400.132 MHz, C_6D_6, 298K): δ[ppm] = 0.85 (s, 9 H, As(Si(CH_3)$_3$), 1.12 (s, 18 H, ^{t}Bu), 6.71 – 6.89 (m, 5 H, Ph), 7.22 (s, 1 H, ^{1}J = 215.1 Hz, R–Si–*H*); ^{13}C{^{1}H} NMR (100.613 MHz, C_6D_6, 298K): δ[ppm] = 7.28 (R-Si(H)=AsSi(*C*H$_3$)), 31.45 (NC(*C*H$_3$)), 55.21 (N*C*Me$_3$), 130.23, 131.71 (Ar-*C*), 173.13 (N*C*N); ^{29}Si{^{1}H} DEPT NMR (79.945 MHz, C_6D_6, 298K): δ[ppm] = 3.10 (s, R–Si(H)=As(*Si*Me$_3$)), 25.72 (s, R–*Si*(H)=As(SiMe$_3$)); ^{29}Si NMR (79.945 MHz, C_6D_6, 298K): δ[ppm] = 3.10 (m, ^{2}J = 6.36 Hz, R–Si(H)=As(*Si*Me$_3$)), 25.72 (d, ^{1}J = 215.1 Hz, R–*Si*(H)=As(SiMe$_3$)). LIFDI-MS calcd for $C_{18}H_{33}AsN_2Si_2$, 408.1393, Found 408.1396. Elemental analysis was not performed due to the sensitivity to hydrolysis and the thermal instability of **3-5**.

Preparation of [PhC(N^{t}Bu)$_2$]Si(OSiMe$_3$)=As(SiMe$_3$) (3-6): LiAs(SiMe$_3$)$_2$ (154 mg, 0.46 mmol) in thf was added to [PhC(N^{t}Bu)$_2$]SiCl **3-1** (135 mg, 0.46 mmol) in thf at –80°C, followed by the reaction mixture turning immediately yellow. Then 0.09 mL of TMS_2O_2 (0.46 mmol) were added at –80°C. The mixture was stirred and warmed to room temperature overnight, whereby the colour changed from yellow to light orange. The reaction mixture was filtered and concentrated to yield small yellow crystals of **3-6** (63 mg, 15.9%).

^{1}H NMR (400.132 MHz, C_6D_6, 298K): δ[ppm] = 0.36 (9 H, s, O(Si(CH_3)$_3$), 0.84 (9 H, s, As(Si(CH_3)$_3$), 1.21 (18 H, s, ^{t}Bu), 6.82 – 6.96 (5 H, m, Ph); ^{13}C{^{1}H} NMR (100.613 MHz, C_6D_6, 298K): δ[ppm] = 2.28 (R-Si(OSi(*C*H$_3$)$_3$)=AsSiMe$_3$), 7.88 (R-Si(OSiMe$_3$)=AsSi(*C*H$_3$)), 31.26 (NC(*C*H$_3$)), 55.07 (N*C*Me$_3$), 127.52, 130.27, 130.80 (Ar-*C*), 174.20 (N*C*N); ^{29}Si{^{1}H} DEPT NMR (79.945 MHz, C_6D_6, 298K): δ[ppm] = –6.64 (R–Si(O*Si*Me$_3$)=As(SiMe$_3$), 2.36 (R–Si(OSiMe$_3$)=As(*Si*Me$_3$), 9.96 (R–*Si*(OSiMe$_3$)=As(SiMe$_3$)). EI-MS calcd for C21H41AsN_2OSi_3, 496.1737, Found 496.2260. Elemental analysis was not performed due to the sensitivity to hydrolysis and the thermal instability of **3-6**.

Preparation of {[PhC(N^{t}Bu)$_2$]SiAs}$_2$ (3-F): THF-d_8 was added to a mixture of **3-1** (15 mg, 0.05 mmol) and LiAs(SiMe$_3$) (17.1 mg, 0.05 mmol) in a Young tube at –100°C. ^{1}H- and ^{29}Si{^{1}H} DEPT-NMR spectra were recorded at –100°C, –80°C, –60°C, –40°C, –20°C, 0°C and at room temperature using a Bruker Avance 400. Few crystals of compound {[PhC(N^{t}Bu)$_2$]SiAs}$_2$ (**3-F**) could be isolated after two weeks from this sample. **3-F** has already been reported by our group, but with a different space group and different unit cell parameters.[30]

NMR spectra

[PhC(N^{t}Bu)$_2$]Si(SiMe$_3$)=As(SiMe$_3$) (3-2):

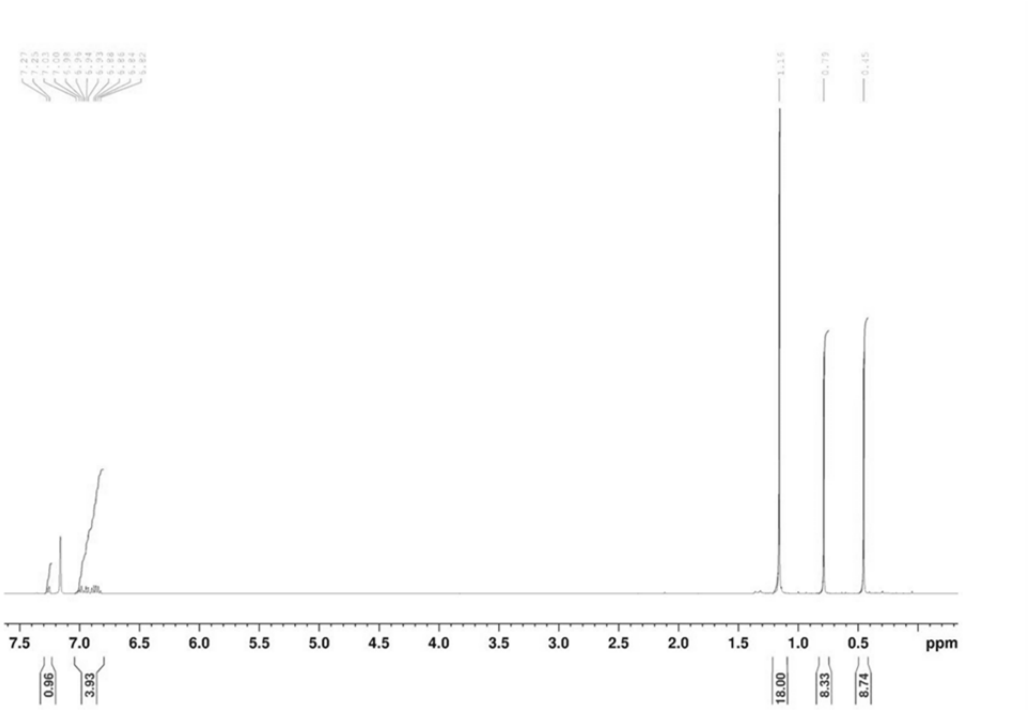

Figure 3 - 4: ^{1}H-NMR spectrum of the crystals of **3-2**.

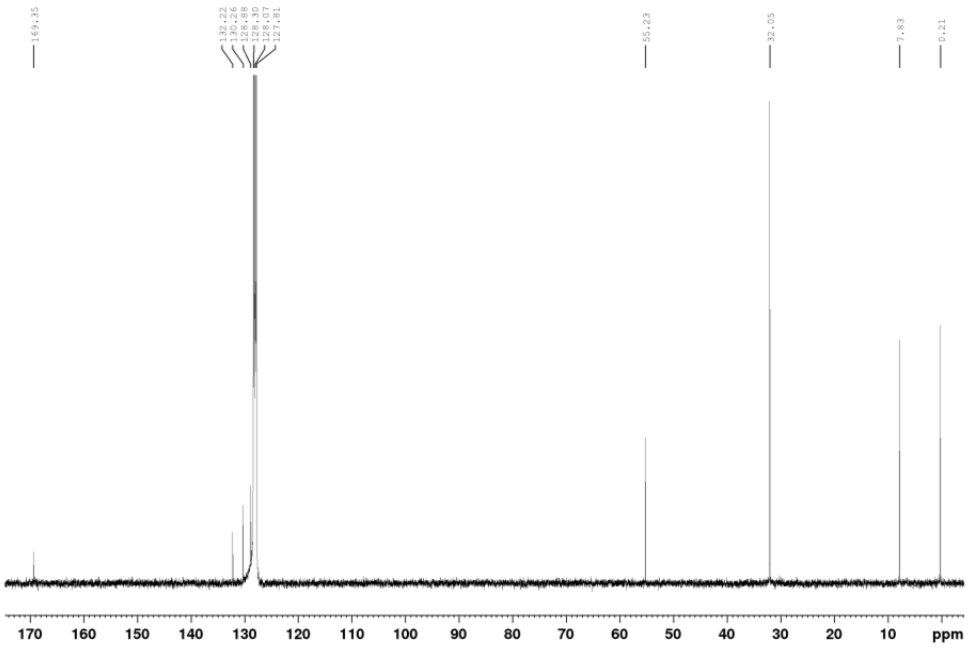

Figure 3 - 5: ^{13}C{^{1}H} NMR spectrum of the crystals of **3-2**.

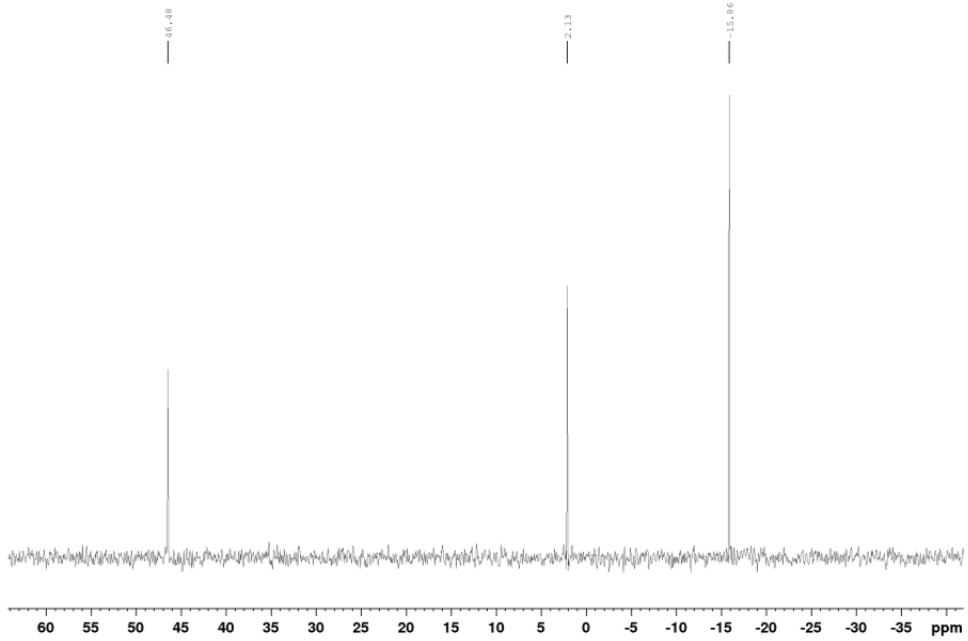

Figure 3 - 6: $^{29}Si\{^{1}H\}$ DEPT NMR spectrum of the crystals of **3-2**.

PhC(N^{t}Bu)$_2$]Si(H)=As(SiMe$_3$) (3-5):

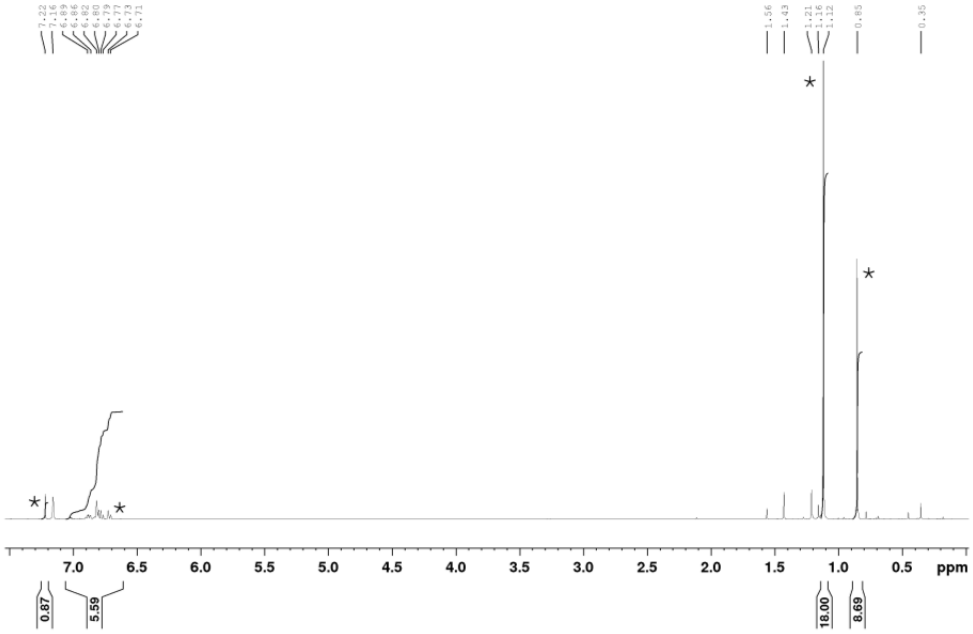

Figure 3 - 7: ^{1}H NMR spectrum of the crystals of **3-5**. The signals of **3-5** are labeled with *. The smaller signal sets belong to unidentified side products.

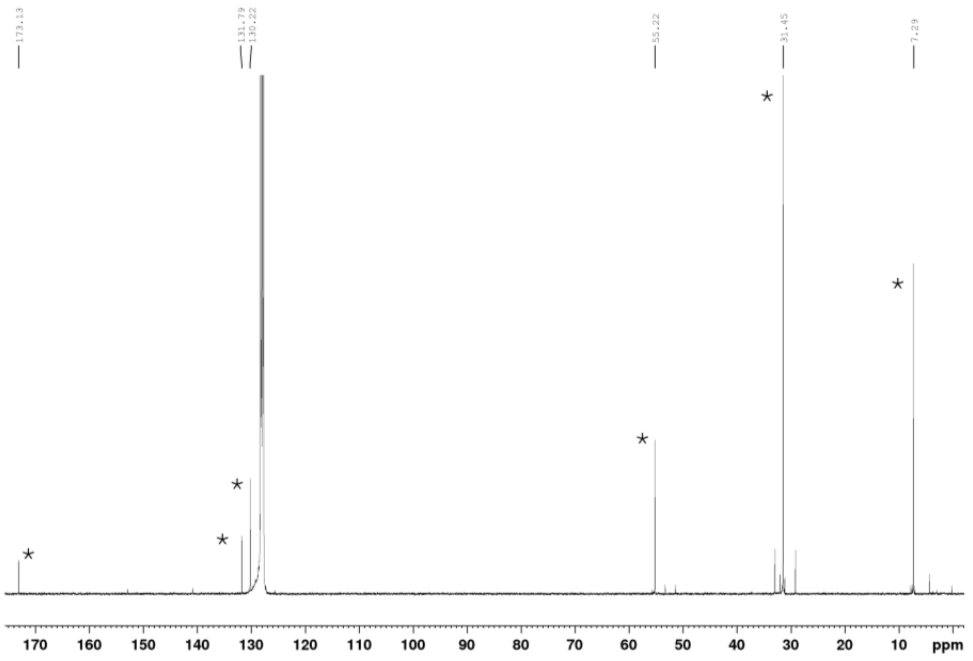

Figure 3 - 8: ^{13}C{^{1}H} NMR spectrum of the crystals of **3-5**. The signals of **3-5** are labeled with *. The remaining signals belong to unidentified side products.

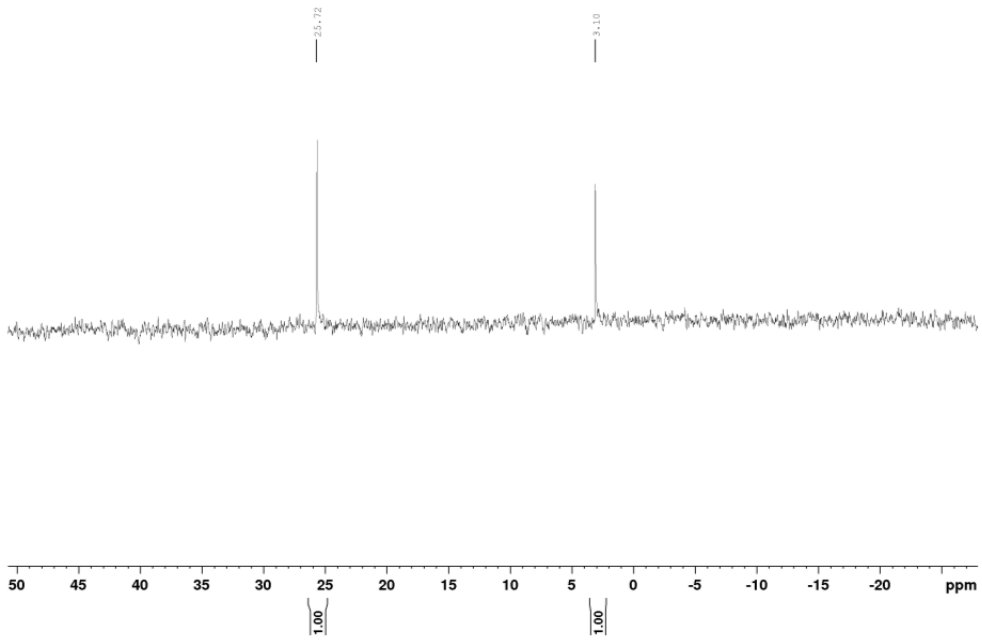

Figure 3 - 9: $^{29}Si\{^{1}H\}$ DEPT NMR spectrum of the crystals of **3-5**

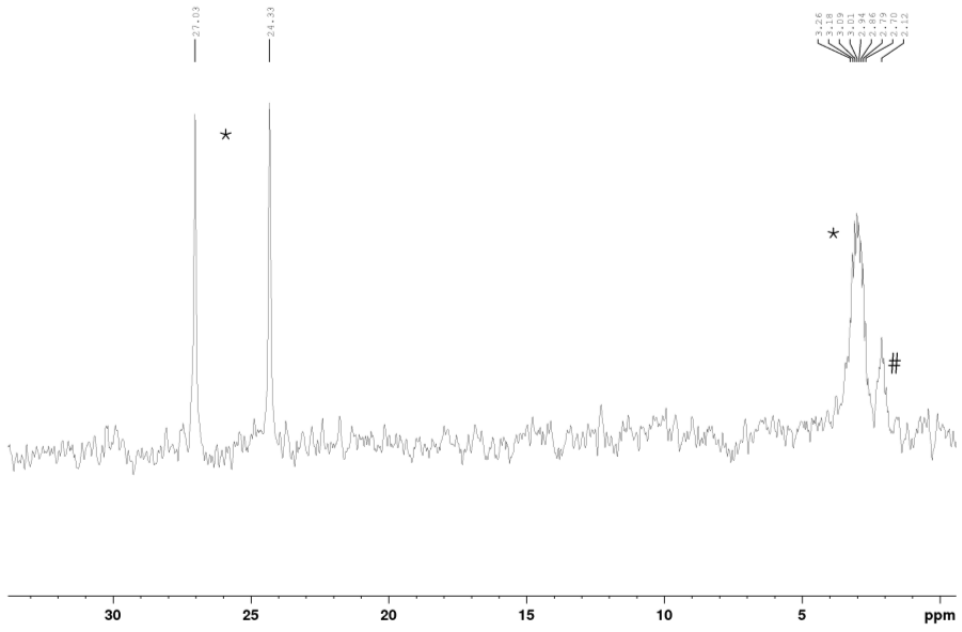

Figure 3 - 10: ^{29}Si NMR spectrum of the crystals of **3-5**. The signals of **3-5** are labeled with *, the signal labeled with # belongs to **3-2**, which crystallized as an impurity in the reaction of **3- 5**. Coupling constants: ^{1}J = 215.07 Hz at δ[ppm] = 24.33, 27.03 (d); ^{2}J = 6.3607 Hz at δ[ppm] = 2.70 – 3.26 (m)

[PhC(N^{t}Bu)$_2$]Si(OSiMe$_3$)=As(SiMe$_3$) (3-6):

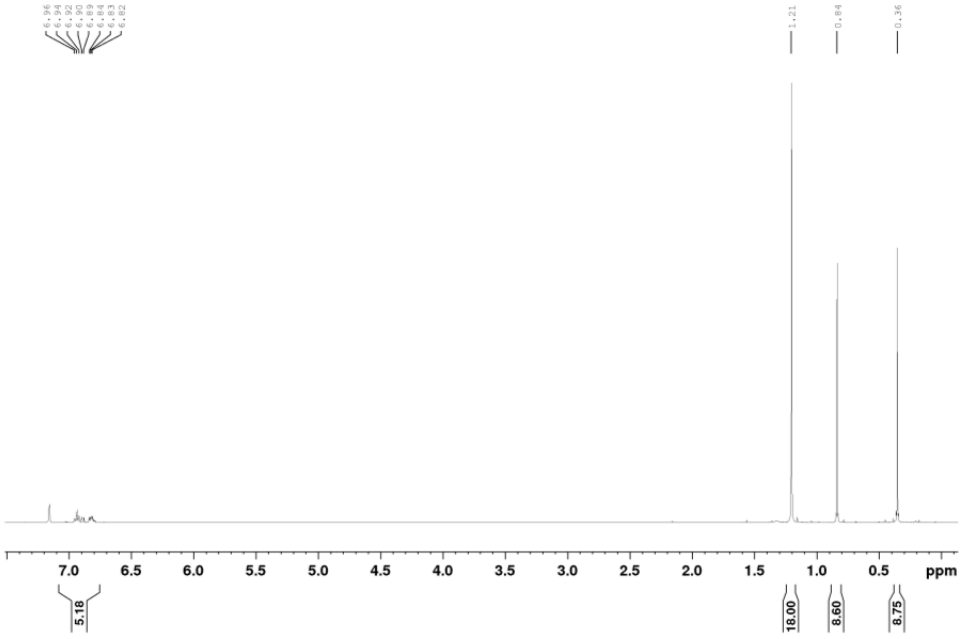

Figure 3 - 11: ^{1}H NMR spectrum of the crystals of **3-6**.

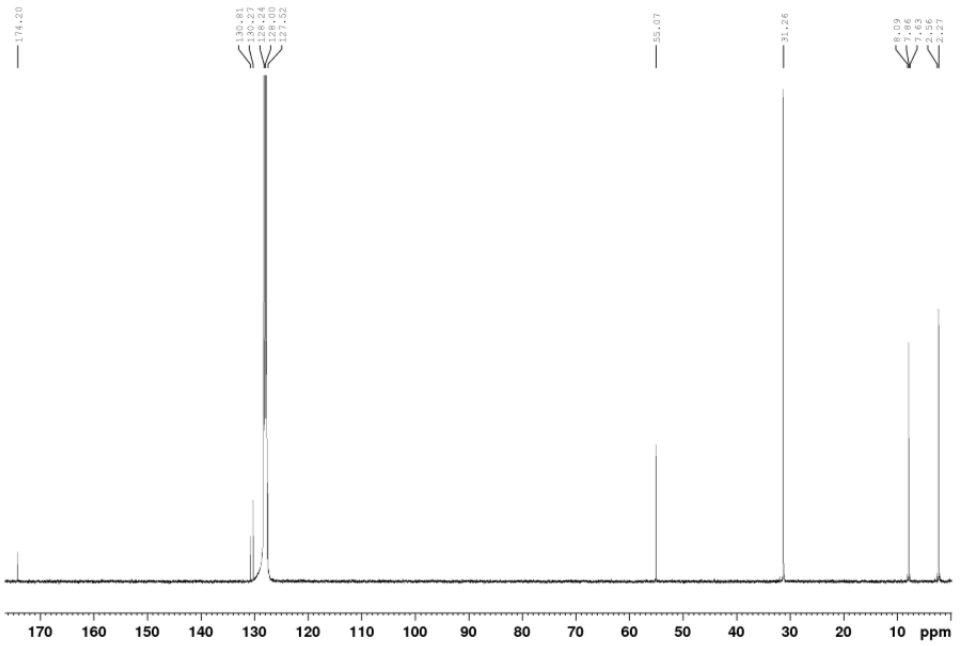

Figure 3 - 12: ^{13}C{^{1}H} NMR spectrum of the crystals of **6**.

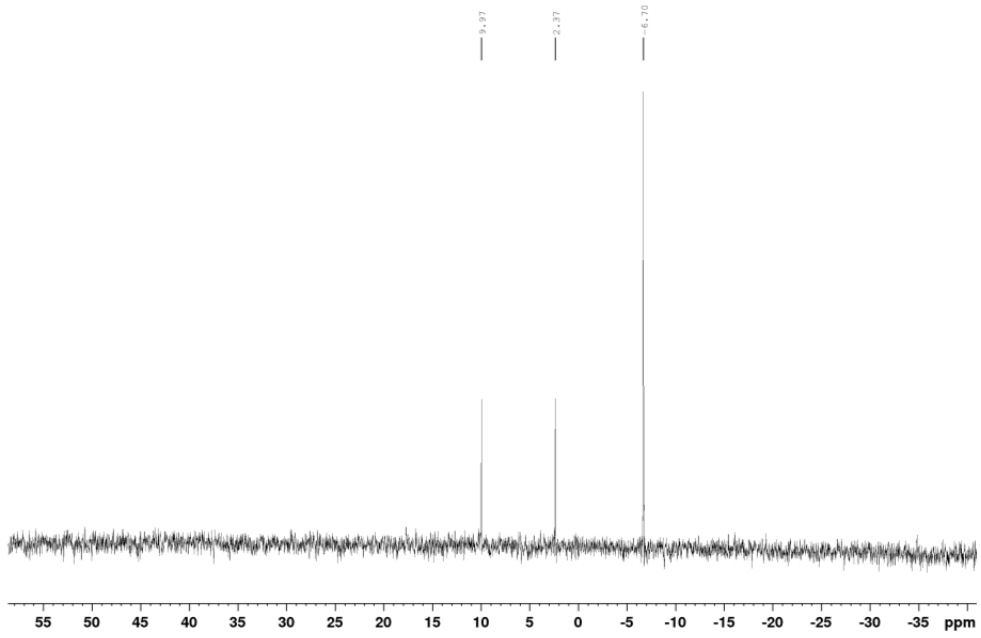

Figure 3 - 13: $^{29}Si\{^{1}H\}$ NMR spectrum of the crystals of **3-6**.

X-ray structure analysis:

The crystal samples were processed at a Gemini R Ultra with an Atlas S2 CCD detector (**3-2**, **3-3**, **3-4**) and a GV50 diffractometer with a Titan S2 CCD detector (**3-5**, **3-6**), respectively. Frames integration and data reduction were performed with CrysAlisPro ver. 171.38.41h.[31] Analytical absorption corrections from crystal faces[32] were applied to the data of **3-2**, **3-3** and **3-4**. A numerical absorption correction based on Gaussian integration over a multifaceted crystal model was applied to the data of **3-5** and **3-6**.[31] All structures were solved by SHELXT[33] using Olex2[34]. For all structures a least-square redinement on F^2 was carried out with SHELXL[35,36]. Hydrogen atoms at the carbon atoms were located in idealized positions and refined isotropically according to the riding model.

Crystallographic data

[PhC(N^{t}Bu)$_2$]Si(SiMe$_3$)=As(SiMe$_3$) (3-2):

3-2 crystallizes from toluene at –78°C as clear, yellow blocks with one molecule of toluene inserted into the unit cell. The toluene molecule shows a disorder over two positions (59:41). To describe the disorder the restrains SADI and RIGU were applied.

Sum formula	C_{28} H_{49} As N_2 Si_3
Molecular weight *M* [g/mol]	572.88
Crystal system	monoclinic
Space group	P 21/n
Unit cell dimensions [Å] or [°]	13.9496(2) 90
	12.76540(10) 108.977(2)
	19.1217(3) 90
Volume [Å^3]	3219.98(8)
Formula units *Z*	4
Temperature *T* [K]	123.15
Crystal size [mm^3]	0.3397 x 0.1728 x 0.0669
Crystal density ρ_{calc} [g · cm^{-3}]	1.182
F(000)	1224.0
Absorption coefficient $\mu_{Cu\text{-}K\alpha}$ [mm^{-1}]	2.621
Transmission T_{min} / T_{max}	0.887 /0.966
Absorption correction	analytical
Wavelength (λ) [Å]	1.54184 (CuK_α)
Measured / independent reflections (R_{int})	21355/ 5662 (0.0247)
Independent reflections [$I > 2\sigma(I)$]	5069
Index ranges *hkl*	$-16 \le h \le 16$
	$-15 \le k \le 14$
	$-22 \le l \le 22$
Measuring range θ_{min} / θ_{max} / θ_{full} [°]	4.239/66.395/66.395
Completeness (θ_{full})	0.997
Data / restraints / parameters	5662/105/384
R-indices (all data)	0.0357 /0.0801
R-indices [$I > 2\sigma(I)$]	0.0306 /0.0775
Goodness-of-fit for S (F^2)	1.099
Largest diff. peak and hole [e · Å^3]	0.55 /-0.28

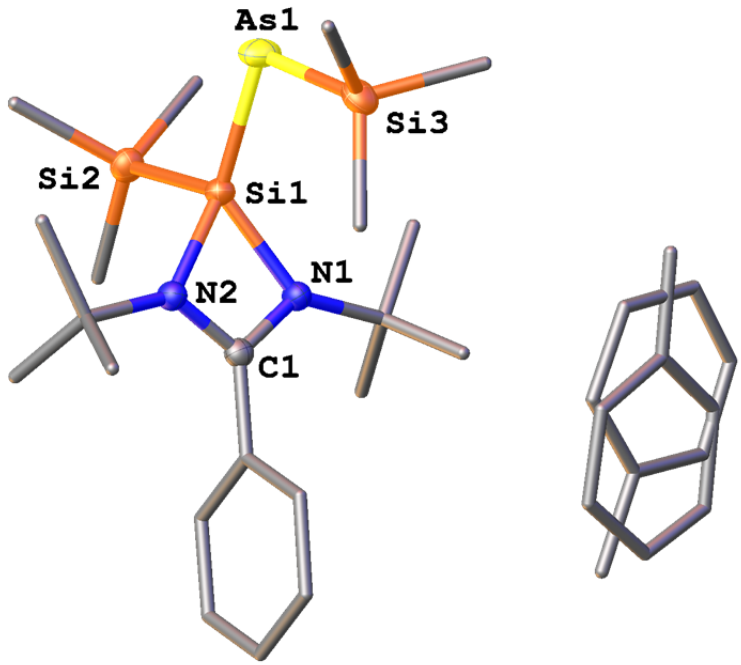

Figure 3 - 14: Molecular structure of **3-2**. Thermal ellipsoids are shown with 50% probability level. H atoms are omitted for clarity.

Distances [Å]		Angles [°]	
As1 – Si1	2.2110(5)	Si1 – As1 – Si3	102.49(2)
As1 – Si3	2.3175(6)	As1 – Si1 – Si2	108.97(2)
Si1 – Si2	2.3451(7)	N1 – Si1 – As1	126.64(5)
Si1 – N1	1.8489(16)	N1 – Si1 – Si2	108.62(5)
Si1 – N2	1.8462(16)	N1 – Si1 – N2	70.58(7)
Si2 – C16	1.876(2)	N2 – Si1 – As1	126.64(5)
Si2 – C17	1.874(2)	N2 – Si1 – Si2	108.65(5)
Si2 – C18	1.875(2)	C16 – Si2 – Si1	107.00(8)
Si3 – C19	1.875(3)	C17 – Si2 – Si1	109.32(8)
Si3 – C20	1.783(2)	C18 – Si2 – Si1	113.14(8)
Si3 – C21	1.872(3)	C16 – Si2 – C17	107.76(11)
N1 – C1	1.338(2)	C16 – Si2 – C18	109.86(12)
N2 – C1	1.337(2)	C17 – Si2 – C18	109.58(12)
N1 – C2	1.491(2)	C19 – Si3 – As1	109.31(9)
N2 – C6	1.488(2)	C20 – Si3 – As1	117.65(8)
C1 – C10	1.489(3)	C21 – Si3 – As1	109.00(10)
		C19 – Si3 – C20	107.76(13)
		C19 – Si3 – C21	106.45(13)
		C20 – Si3 – C21	106.10(13)
		N1 – C1 – N2	105.87(15)
		C1 – N1 – Si1	91.56(11)
		C1 – N2 – Si1	91.73(11)
		C1 – N1 – C2	130.82(15)
		C1 – N2 – C6	131.22(15)
		N1 – C1 – C10	126.98(16)
		N2 – C1 – C10	127.14(16)

{[PhC(N^{t}Bu)$_2$]Si=AsSiMe$_3$}$_2$ (3-3):

3-3 crystallizes as clear, yellow platelets from both thf and n-hexane at –18°C.

Sum formula	$C_{36}H_{64}As_2N_4Si_4$	
Molecular weight *M* [g/mol]	815.11	
Crystal system	monoclinic	
Space group	P 21/c	
Unit cell dimensions [Å] or [°]	9.7915(2)	90
	16.5189(3)	104.281(2)
	13.5174(3)	90
Volume [Å^3]	2118.81(8)	
Formula units *Z*	2	
Temperature *T* [K]	122.9(8)	
Crystal size [mm^3]	0.1321 x 0.1088 x 0.0845	
Crystal density ρ_{calc} [Mg · m^{-3}]	1.278	
F(000)	860	
Absorption coefficient $\mu_{Cu\text{-}K\alpha}$ [mm^{-1}]	3.250	
Transmission T_{min} / T_{max}	0.075/0.242	
Absorption correction	analytical	
Wavelength (λ) [Å]	1.54184 (CuK_α)	
Measured / independent reflections (R_{int})	12454/3728 (0.0471)	
Independent reflections [$I > 2\sigma(I)$]	3259	
Index ranges *hkl*	$-11 \le h \le 11$	
	$-16 \le k \le 19$	
	$-16 \le l \le 12$	
Measuring range θ_{min} / θ_{max} / θ_{full} [°]	4.307/66.779/66.779	
Completeness (θ_{full})	0.992	
Data / restraints / parameters	3728/0/217	
R-indices (all data)	0.0509/0.1209	
R-indices [$I > 2\sigma(I)$]	0.0444/0.1152	
Goodness-of-fit for S (F^2)	1.076	
Largest diff. peak and hole [e · Å^3]	0.913/-0.314	

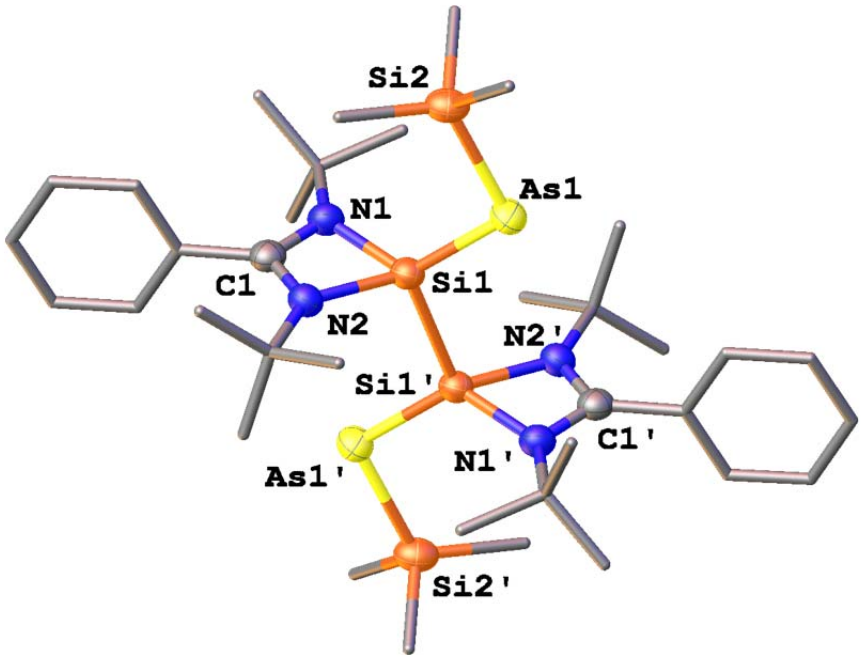

Figure 3 - 15: Molecular structure of compound **3-3**. Thermal ellipsoids are shown with 50% probability. H atoms are omitted for clarity

Distances [Å]		Angles [°]	
As1 – Si1	2.2141(8)	Si1 – As1 – Si2	103.436(3)
As1 – Si2	2.3227(9)	As1 – Si1 – Si1’	110.52(5)
Si1 – Si1’	2.4019(15)	N1 – Si1 – Si1‘	109.83(9)
Si1 – N1	1.864(2)	N1 – Si1 – As1	126.31(8)
Si1 – N2	1.868(3)	N1 – Si1 – N2	70.03(11)
Si2 – C16	1.869(4)	N2 – Si1 – Si1’	108.50(9)
Si2 – C17	1.870(4)	N2 – Si1 – As1	125.65(8)
Si2 – C18	1.870(4)	As1 – Si2 – C16	117.42(13)
N1 – C1	1.338(4)	As1 – Si2 – C17	105.33(14)
N1 – C2	1.488(4)	As1 – Si2 – C18	111.80(13)
N2 – C1	1.336(4)	C16 – Si2 – C17	107.3(2)
N2 – C6	1.488(4)	C16 – Si2 – C18	107.9(2)
C1 – C10	1.484(4)	C17 – Si2 – C18	106.5(2)
		N1 – C1 – N2	106.4(2)
		C1 – N1 – C2	129.2(2)
		C1 – N2 – C6	129.4(2)
		N1 – C1 – C10	127.5(3)
		N2 – C1 – C10	126.0(3)

{[PhC(N^{t}Bu)$_2$]Si}$_2$=AsSiMe$_3$ (3-4):

3-4 can be obtained as clear, yellow platelets from thf at –18°C. One molecule of thf is inserted into the unit cell and disordered over three positions (33% : 33% : 33%).

Sum formula	$C_{37}H_{63}AsN_4OSi_3$	
Molecular weight *M* [g/mol]	739.10	
Crystal system	monoclinic	
Space group	P 21/c	
Unit cell dimensions [Å] or [°]	11.3136(3)	90
	19.7185(4)	100.402(2)
	18.6791(5)	90
Volume [Å^3]	4098.58(16)	
Formula units *Z*	4	
Temperature *T* [K]	122.6(10)	
Crystal size [mm^3]	0.1491x 0.1248x 0.0552	
Crystal density ρ_{calc} [Mg · m^{-3}]	1.198	
F(000)	1584	
Absorption coefficient $\mu_{Cu\text{-}K\alpha}$ [mm^{-1}]	2.202	
Transmission T_{min} / T_{max}	0.950/0.978	
Absorption correction	analytical	
Wavelength (λ) [Å]	1.54184 (Cu)	
Measured / independent reflections (R_{int})	18270/7184 (0.0389)	
Independent reflections [$I > 2\sigma(I)$]	6009	
Index ranges *hkl*	$-13 \le h \le 12$	
	$-23 \le k \le 21$	
	$-21 \le l \le 22$	
Measuring range θ_{min} / θ_{max} / θ_{full} [°]	3.973/66.779/66.779	
Completeness (θ_{full})	0.987	
Data / restraints / parameters	7184/93/ 493	
R-indices (all data)	0.0503/0.0955	
R-indices [$I > 2\sigma(I)$]	0.0382/0.0896	
Goodness-of-fit for S (F^2)	1.024	
Largest diff. peak and hole [e · Å^3]	0.572/-0.392	

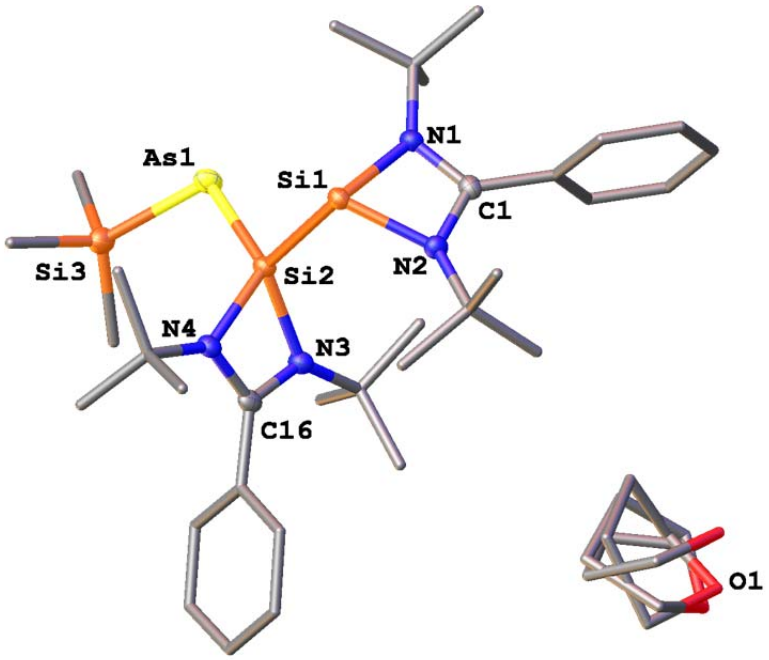

Figure 3 - 16: Molecular structure of compound **3-4**. Thermal ellipsoids are shown with 50% probability. H atoms are omitted for clarity.

Distances [Å]		Angles [°]	
Si1 – Si2	2.4181(8)	Si1 – Si2 – As1	110.40(3)
Si2 – As1	2.2419(6)	Si2 – As1 – Si3	109.00(2)
As1 – Si3	2.3245(7)	N1 – Si1 – N2	69.38(8)
Si1 – N1	1.8731(19)	Si2 – Si1 – N1	103.97(6)
Si1 – N2	1.865(2)	Si2 – Si1 – N2	105.38(7)
N1 – C1	1.336(3)	N1 – C1 – N2	105.30(19)
N2 – C1	1.340(3)	N1 – C1 – C10	127.4(2)
N1 – C2	1.480(3)	N2 – C1 – C10	127.3(2)
N2 – C6	1.480(3)	C1 – N1 – C2	130.24(19)
C1 – C10	1.492(3)	C1 – N2 – C6	130.40(19)
Si2 – N3	1.856(2)	Si1 – Si2 – N3	118.23(7)
Si2 – N4	1.8599(19)	Si1 – Si2 – N4	107.91(6)
N3 – C16	1.341(3)	Si2 – N3 – C16	91.92(15)
N4 – C16	1.340(3)	Si2 – N4 – C16	91.76(14)
N3 – C17	1.477(3)	N3 – Si2 – N4	70.34(9)
N4 – C21	1.4.81(3)	N3 – C16 – N4	105.98(19)
C16 – C25	1.496(3)	N3 – C16 – C25	125.9(2)
Si3 – C31	1.871(3)	N4 – C16 – C25	128.1(2)
Si3 – C32	1.884(3)	C16 – N3 – C17	132.4(2)
Si3 – C33	1.876(3)	C16 – N4 – C21	130.23(19)
		N3 – Si2 – As1	121.72(7)
		N4 – Si2 – As1	122.60(7)
		As1 – Si3 – C31	118.22(10)
		As1 – Si3 – C32	104.45(10)
		As1 – Si3 – C33	114.56(10)
		C31 – Si3 – C32	106.86(15)
		C31 – Si3 – C33	106.10(14)
		C32 – Si3 – C33	105.73(14)

[PhC(N^{t}Bu)$_2$]Si(H)=As(SiMe$_3$) (3-5):

3-5 crystallizes from n-hexane at –18°C as clear, yellow blocks.

Sum formula	C_{18} H_{33} As N_2 Si_2
Molecular weight *M* [g/mol]	408.56
Crystal system	monoclinic
Space group	P 21/n
Unit cell dimensions [Å] or [°]	13.89477(15) 90
	8.74288(12) 95.7478(10)
	18.4824(2) 90
Volume [Å^3]	2233.96(5)
Formula units *Z*	4
Temperature *T* [K]	123.00(10)
Crystal size [mm^3]	0.3209x 0.111x 0.0661
Crystal density ρ_{calc} [Mg · m^{-3}]	1.215
F(000)	864.0
Absorption coefficient $\mu_{Cu\text{-}K\alpha}$ [mm^{-1}]	3.083
Transmission T_{min} / T_{max}	0.836/0.959
Absorption correction	gaussian
Wavelength (λ) [Å]	1.54184 (CuK_α)
Measured / independent reflections (R_{int})	13066/ 4430 (0.0274)
Independent reflections [$I > 2\sigma(I)$]	4071
Index ranges *hkl*	$-17 \le h \le 15$
	$-10 \le k \le 7$
	$-23 \le l \le 19$
Measuring range θ_{min} / θ_{max} / θ_{full} [°]	3.803/73.740/67.684
Completeness (θ_{full})	1.000
Data / restraints / parameters	4430/0/221
R-indices (all data)	0.0376 /0.0998
R-indices [$I > 2\sigma(I)$]	0.0351 /0.0966
Goodness-of-fit for S (F^2)	1.028
Largest diff. peak and hole [e · Å^3]	0.66 /-0.84

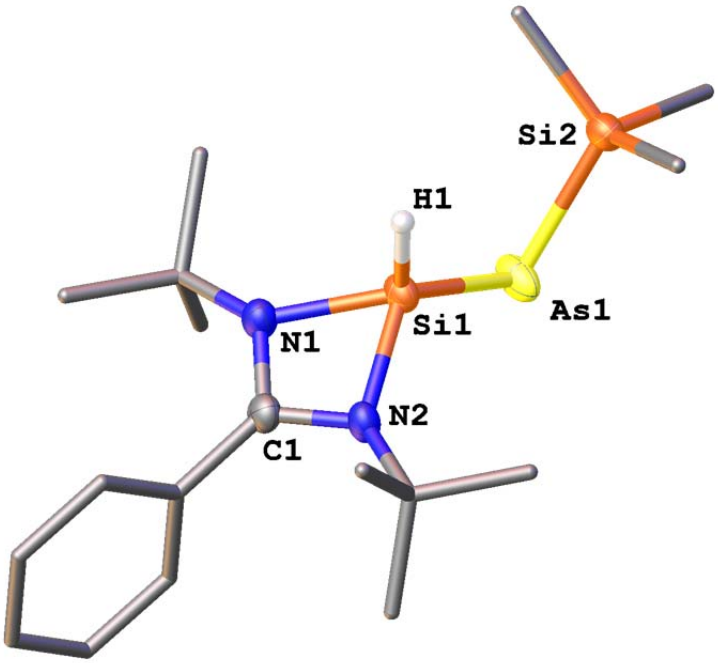

Figure 3 - 17: Molecular structure of compound **3-5**. Thermal ellipsoids are shown with 50% probability. H atoms are omitted for clarity.

Distances [Å]		Angles [°]	
As1 – Si1	2.2069(5)	Si1 – As1 – Si2	94.803(19)
As1 – Si2	2.3226(5)	As1 – Si1 – H1	121.1(10)
Si1 – N1	1.8371(15)	N1 – Si1 – As1	120.51(5)
Si1 – N2	1.8337(15)	N2 – Si1 – As1	122.67(5)
Si1 – H1	1.40(2)	N1 – Si1 – H1	105.9(10)
Si2 – C16	1.864(3)	N2 – Si1 – H1	104.5(10)
Si2 – C17	1.858(3)	N1 – Si1 – N2	71.13(6)
Si2 – C18	1.862(2)	As1 – Si2 – C16	105.02(10)
N1 – C1	1.338(2)	As1 – Si2 – C17	112.66(9)
N1 – C2	1.478(2)	As1 – Si2 – C18	114.99(9)
N2 – C1	1.335(2)	C16 – Si2 – C17	108.2(2)
N2 – C6	1.480(2)	C16 – Si2 – C18	107.46(14)
C1 – C10	1.487(2)	C17 – Si2 – C18	108.13(17)
		N1 – C1 – N2	106.02(14)
		C1 – N1 – C2	131.20(15)
		C1 – N2 – C6	130.48(14)
		N1 – C1 – C10	127.22(16)
		N2 – C1 – C10	126.75(15)

[PhC(N^{t}Bu)$_2$]Si(OSiMe$_3$)=As(SiMe$_3$) (3-6):

3-6 crystallizes from thf at –18°C as clear, yellow blocks. The arsenic atom of **3-6** is disordered over two positions (81% :19%).

Sum formula	C_{21} H_{419} As N_2 OSi_3
Molecular weight *M* [g/mol]	496.75
Crystal system	monoclinic
Space group	P 21/n
Unit cell dimensions [Å] or [°]	8.7496(2) 90
	17.0408(4) 99.993(2)
	18.5815(4) 90
Volume [Å^3]	2728.46(11)
Formula units *Z*	4
Temperature *T* [K]	123.00(10)
Crystal size [mm^3]	0.12117 x 0.0996 x 0.0545
Crystal density ρ_{calc} [g · cm^{-3}]	1.209
F(000)	1056.0
Absorption coefficient $\mu_{Cu\text{-}K\alpha}$ [mm^{-1}]	3.044
Transmission T_{min} / T_{max}	0.941 /0.970
Absorption correction	gaussian
Wavelength (λ) [Å]	1.54184 (CuK_α)
Measured / independent reflections (R_{int})	15446/ 5341 (0.0413)
Independent reflections [$I > 2\sigma(I)$]	4475
Index ranges *hkl*	$-10 \le h \le 10$
	$-14 \le k \le 20$
	$-23 \le l \le 22$
Measuring range θ_{min} / θ_{max} / θ_{full} [°]	3.544/73.967/67.684
Completeness (θ_{full})	0.994
Data / restraints / parameters	5341/0/274
R-indices (all data)	0.0452 /0.0863
R-indices [$I > 2\sigma(I)$]	0.0343 /0.0806
Goodness-of-fit for S (F^2)	1.037
Largest diff. peak and hole [e · Å^3]	0.35 /-0.30

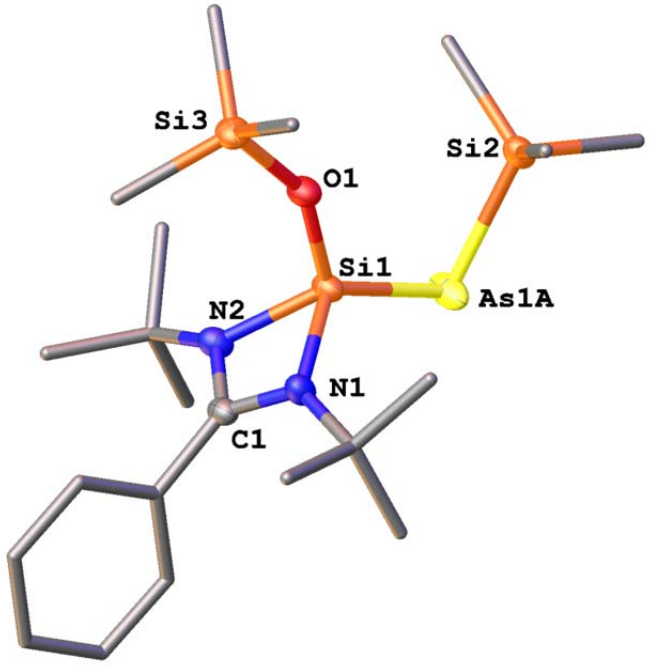

Figure 3 - 18: Molecular structure of **3-6**. Thermal ellipsoids are shown with 50% probability level. H atoms are omitted for clarity. Disorder of the As1 atom: As1A : As1B = 81% : 19%

Distances [Å]		Angles [°]	
As1A – Si1	2.2124(19)	Si1 – As1A – Si2	94.19(7)
As1A – Si2	2.3253(19)	Si1 – As1B – Si2	94.5(3)
As1B – Si1	2.225(8)	As1A – Si1 – O1	120.57(7)
As1B – Si2	2.302(8)	As1B – Si1 – O1	121.3(2)
Si1 – O1	1.6119(15)	Si1 – O1 – Si3	149.23(9)
O1 – Si3	1.6491(15)	N1 – Si1 – As1A	122.05(7)
Si1 – N1	1.8445(18)	N1 – Si1 – As1B	113.56(18)
Si1 – N2	1.8282(17)	N2 – Si1 – As1A	116.53(7)
Si2 – C16	1.872(3)	N2 – Si1 – As1B	122.91(19)
Si2 – C17	1.871(3)	N1 – Si1 – N2	71.31(8)
Si2 – C18	1.884(2)	As1A – Si2 – C16	112.90(9)
Si3 – C19	1.856(2)	As1A – Si2 – C17	116.26(9)
Si3 – C20	1.848(3)	As1A – Si2 – C18	105.74(10)
Si3 – C21	1.852(3)	As1B – Si2 – C16	122.60(15)
N1 – C1	1.339(2)	As1B – Si2 – C17	106.86(16)
N2 – C1	1.335(3)	As1B – Si2 – C18	105.1(2)
N1 – C2	1.480(3)	C16 – Si2 – C17	107.13(14)
N2 – C6	1.486(32)	C16 – Si2 – C18	107.07(11)
C1 – C10	1.492(3)	C17 – Si2 – C18	107.25(12)
		O1 – Si3 – C19	109.76(10)
		O1 – Si3 – C20	107.82(11)
		O1 – Si3 – C21	108.72(11)
		C19 – Si3 – C20	111.40(14)
		C19 – Si3 – C21	109.13(16)
		C20 – Si3 – C21	109.96(16)
		N1 – C1 – N2	106.38(16)
		C1 – N1 – C2	130.89(17)
		C1 – N2 – C6	131.29(17)
		N1 – C1 – C10	127.05(19)
		N2 – C1 – C10	126.54(18)

{[PhC(N^{t}Bu)$_2$]SiAs}$_2$ (3-F):[30]

3-F crystallizes from thf-d_8 at r.t. as clear, orange blocks.

Sum formula	$C_{30}H_{46}As_2N_4Si_2$
Molecular weight *M* [g/mol]	668.73
Crystal system	monoclinic
Space group	P 21/c
Unit cell dimensions [Å] or [°]	10.9979(3) 90
	8.9434(2) 105.572(3)
	17.5176(5) 90
Volume [Å^3]	1659.76(8)
Formula units *Z*	2
Temperature *T* [K]	123(1)
Crystal size [mm^3]	0.207 × 0.1396 × 0.0559
Crystal density ρ_{calc} [g · cm^{-3}]	1.338
F(000)	696.0
Absorption coefficient $\mu_{Cu\text{-}K\alpha}$ [mm^{-1}]	3.367
Transmission T_{min} / T_{max}	0.625/ 0.833
Absorption correction	analytical
Wavelength (λ) [Å]	1.54184 (CuK$_\alpha$)
Measured / independent reflections (R_{int})	8574/ 2903 (0.0242)
Independent reflections [$I > 2\sigma(I)$]	2670
Index ranges *hkl*	$-13 \le h \le 12$
	$-9 \le k \le 10$
	$-20 \le l \le 20$
Measuring range θ_{min} / θ_{max} / θ_{full} [°]	4.173/ 66.211/ 66.211
Completeness (θ_{full})	0.998
Data / restraints / parameters	2903/0/200
R-indices (all data)	0.0387/ 0.0872
R-indices [$I > 2\sigma(I)$]	0.0349/ 0.0858
Goodness-of-fit for S (F^2)	1.232
Largest diff. peak and hole [e · Å^3]	0.38/-0.32

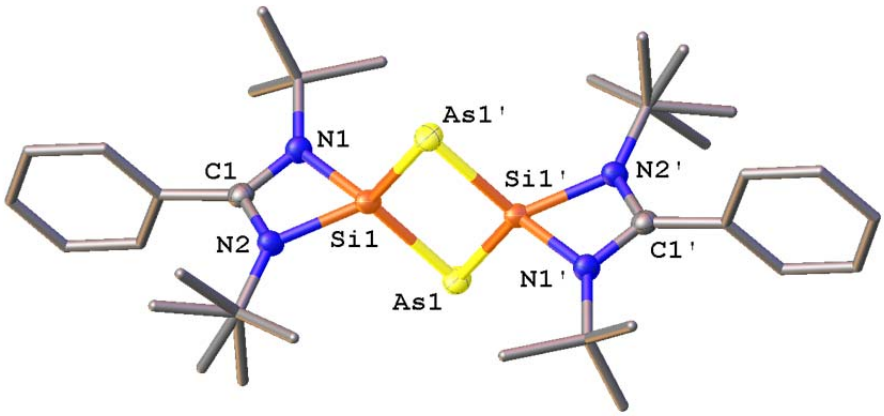

Figure 3 - 19: Molecular structure of **3-F**. Thermal ellipsoids are shown with 50% probability level. H atoms are omitted for clarity. Disorder of the N2-bond ^{t}Bu group: Part1 : Part2 = 60% : 40%.

Distances [Å]		**Angles [°]**	
As1 – Si1	2.2805(9)	Si1 – As1 – Si1’	71.83(3)
As1 – Si1’	2.2869(9)	As1 – Si1 – As1’	108.17(3)
As1’ – Si1	2.2869(9)	As1 – Si1 – Si1’	54.20(3)
Si1 – N1	1.854(3)	As1’ – Si1 – Si1’	53.98(3)
Si1 – N2	1.852(3)	N1 – Si1 – As1	119.96(9)
N1 – C1	1.339(4)	N1 – Si1 – As1’	117.19(9)
N2 – C1	1.340(4)	N2 – Si1 – As1	120.10(9)
N1 – C2	1.477(4)	N2 – Si1 – As1’	116.86(9)
N2 – C6	1.467(4)	N1 – Si1 – N2	70.94(12)
C1 – C12	1.494(4)	N1 – C1 – N2	106.8(3)
		C1 – N1 – Si1	91.06(19)
		C1 – N1 – C2	130.8(3)
		C1 – N2 – Si1	91.13(19)
		C1 – N2 – C6	130.6(3)
		N1 – C1 – C12	126.7(3)
		N2 – C1 – C12	126.4(3)

3.7. References

[1] Ch. Perrier, H. Vincent, P. Chaudouët, B. Chenevier, R. Madar, *Mater. Res. Bull.* **1995**, *30*, 357 – 364.
[2] A. Correia, B. Pichaud, A. Lhorte, J. B. Quoirin, *J. Appl. Phys.* **1996**, *79*, 2145 – 2147.
[3] C. N. Smit, F. M. Lock, F. Bickelhaupt, *Tetrahedron Lett.* **1984**, *25*, 3011 – 3014.
[4] H. R. G. Bender, E. Niecke, M. Nieger, *J. Am. Chem. Soc.* **1993**, *115*, 3314 – 3315.
[5] a) M. Driess, *Angew. Chem.* **1991**, *103*, 979 – 981; b) *Angew. Chem. Int. Ed.* **1991**, *30*, 1022 – 1024.
[6] H. Cui, J. Zhang, C. Cui, *Organometallics* **2013**, *32*, 1 – 4.
[7] K. Hansen, T. Szilvási, B. Blom, S. Inoue, J. Epping, M. Driess, *J. Am. Chem. Soc.* **2013**, *135*, 11795 – 11798.
[8] K. Hansen, T. Szilvási, B. Blom, E. Irran, M. Driess, *Chem. Eur. J.* **2014**, *20*, 1947 – 1956.
[9] M. Driess, *Coord. Chem. Rev.* **1995**, *145*, 1 – 25.
[10] V. Nesterov, N. C. Breit, S. Inoue, *Chem. Eur. J.* **2017**, *23*, 12014 – 12039.
[11] a) P. Willmes, M. J. Cowley, M. Hartmann, M. Zimmer, V. Huch, D. Scheschkewitz, *Angew. Chem. Int. Ed.* **2014**, *53*, 2216 – 2220; b) *Angew. Chem.* **2014**, *123*, 2248 – 2252.
[12] S. Kundu, C. Mohapatra, P. P. Samuel, J. Kretsch, M. G. Walawalkar, R. Herbst-Irmer, D. Stalke, S. De, D. Koley, H. W. Roesky, *Chem. Comm.* **2017**, *53*, 192 – 195.
[13] S. Inoue, W. Wenyuan, C. Präasang, M. Asay, E. Irran, M. Driess, *J. Am. Chem. Soc.* **2011**, *133*, 2868 – 2871.
[14] a) M. Driess, H. Pritzkow, *Angew. Chem. Int. Ed.* **1992**, *31*, 316 – 319; b) *Angew. Chem.* **1992**, *104*, 350 – 353.
[15] M. Driess, H. Pritzkow, *Phosphorus, Sulfur Silicon Relat. Elem.* **1993**, *76*, 57 – 90.
[16] C. Präsang, M. Stoelzel, S. Inoue, A. Meltzer, M. Driess, *Angew. Chem. Int. Ed.* **2010**, *49*, 10002 – 10005.
[17] S. Kundu, C. Mohapatra, P. P. Samuel, J. Kretsch, M. G. Walawalkar, R. Herbst-Irmer, D. Stalke, S. De, D. Koley, H. W. Roesky, *Chem. Comm.* **2017**, *53*, 192 – 195.
[18] A. E. Seitz, M. Eckhardt, A. Erlebach, E. V. Peresypkina, M. Sierka, M. Scheer, *J. Am. Chem. Soc.* **2016**, *138*, 10433 – 10436.
[19] S. S. Sen, H. W. Roesky, D. Stern, J. Henn, D. Stalke, *J. Am. Chem. Soc.* **2010**, *132*, 1132 – 1126.
[20] a) S. S. Sen, A. Jana, H. W. Roesky, C. Schulzke, *Angew. Chem*. **2009**, *121*, 8688 – 8690; b) *Angew. Chem. Int. Ed.* **2009**, *48*, 8536 – 8538.
[21] D. C. McKean, I. Torto, J. E. Boggs, K. Fan, *Journal of Molecular Structure (Theochem)* **1992**, *260*, 27 – 46.
[22] The hydrogen atom at the Si atom was located from the difference Fourier map and refined freely.
[23] L. Pauling, *American Mineralogist* **1980**, *65*, 321 – 323.
[24] a) C.-W. So, H. W. Roesky, J. Magull, R. B. Oswald, *Angew. Chem. Int. Ed.* **2006**, *45*, 3948 – 3950; b) *Angew. Chem.* **2006**, *118*, 4052 – 4054.
[25] S.-H. Zhang, H.-X. Yeong, H.-W. Xi, K. H. Lim, C.-W. So, *Chem. Eur. J.* **2010**, *16*, 10250 – 10254.
[26] Unit cell of **3-F**: monoclinic $P2_1/c$: a = 10.9979(3) Å, b = 8.9434(2) Å, c = 17.5176(5) Å; α = 90°, β = 105.572(3)°, γ = 90°; V = 1659.76(8) $Å^3$
[27] S.S. Sen, H. W. Roesky, D. Stern, J. Henn, D. Stalke, *J. Am. Chem. Soc.* **2009**, 1123 – 1126.
[28] S. S. Sen, A. Jana, H. W. Roesky, C. Schulzke, *Angew. Chem*. **2009**, 8688 – 8690.
[29] G. Becker, G. Gutekunst, H. J. Wessely, *Z. Anorg. Allg. Chem.* **1980**, 113 – 129.
[30] A. E. Seitz, M. Eckhardt, A. Erlebach, E. V. Peresypkina, M. Sierka, M. Scheer, *J. Am. Chem. Soc.* **2016**, *138*, 10433 – 10436.
[31] CrysAlisPro Software System, Rigaku Oxford Diffraction, (2015).
[32] R. C. Clark, J. S. Reid, *Acta Cryst*. **1995**, *A51*, 887 – 897.
[33] G. M. Sheldrick, *Acta Cryst*. **2015**, *A71*, 3 – 8.
[34] O.V. Dolomanov, L.J. Bourhis, R.J. Gildea, J. A. K. Howard, H. Puschmann, Olex2: A complete structure solution, refinement and analysis program, *J. Appl. Cryst.* **2009**, *42*, 339 – 341.
[35] G. M. Sheldrick, *Acta Cryst*. **2015**, C27, 3 – 8.
[36] G. M. Sheldrick, *Acta Cryst.* **2008**, *A64*, 112 – 122.

4. Synthesis of β-diketiminato-$MCH_2(SiMe_3)$ and β-diketiminato-$MAs(SiMe_3)_2$ (M = Ge, Sn) and studies on single source precursors for the preparation of M_xE_y nanoparticles (M = Ge, Sn; E = P, As)

4.1. Author contribution

Daniela Meyer: Synthesis and characterization of **4-1**, **4-2**, **4-3** and **4-4**, preparation and performance of the described nanoparticle studies

Edwin Baquero Valesco: Performance of the TEM and SEM/EDX analyses, supervision of the studies

Celine Nayral and Fabien Delpech: Supervision of the research

Manfred Scheer: Supervision of the research and revision of the manuscript

4.2. Abstract

Four novel complexes stabilized by the versatile β-diketiminato ligand were synthesized by salt metathesis reactions using $[CH(C(Me)N(dipp))_2]MCl$ (M = Ge (**4-A**), Sn (**4-B**)) and $LiCH_2(SiMe_3)$ or $LiAs(SiMe_3)_2$ as starting materials. As a result the compounds $[CH(C(Me)N(dipp))_2]MCH_2(SiMe_3)$ and $[CH(C(Me)N(dipp))_2]MAs(SiMe_3)_2$ (M = Ge (**4-1**, **4-3**), Sn (**4-2**, **4-4**)) were isolated and comprehensively characterized by single crystal X-ray analysis and multinuclear NMR spectroscopy. Furthermore, preliminary studies were performed in order to test the compounds $[CH(C(Me)N(dipp))_2]ME(SiMe_3)_2$ as single source precursors for the preparation of M_xE_y nanoparticles (M = Ge, Sn; E = P, As).

4.3. Introduction

In the past few decades, nanoparticles gained a lot of interest not only in the scientific community but also in industry due to their unique properties, which allow their use for various applications. Thus, e.g. TiO_2 nanoparticles can be found as protective component in suncream[1] or nanoscaled silver structures are used for antibacterial applications.[2] But not only transition metal based nanoparticles (NP) are utilized, also main group element ones are very interesting like i.e. carbon nanotubes are applied in batteries, transistors and composite materials,[3] while nano-Si is among others known as a material for solar cells.[4] Also NP of heavier homologue Ge are of great interest in areas like optoelectronics or energy conversion due to its size-dependent properties,[5] whereas tin NP are suitable as additive for silicon anodes[6] and interconnect material for on-chip and off-chip applications.[7] In addition to the nanoparticles of elements some nanoscaled mixed carbon and phosphorus containing compounds caught a lot attention, too, as group 14 carbide nanoparticles are imaginable as graphitic germanium carbide that might be promising as cathode for fuel cells and lithium-oxygen batteries[8] or as electro-optical devices.[9] Additionally, Cr-doped GeC and SnC might be useful in optical devices with large ranges of frequencies.[10] In the case of NP with phosphorus, i.e. GeP_3 forms a graphene-like film, which exhibits unique properties that might be applicable in photovoltaic technology.[11] Like their lighter analogues also Sn phosphides are attractive for industrial

use, as recently Oh *et al.* reported on the possibility to use Sn_3P_4 nanoparticles as electrode material for Na-ion batteries.[12]

In order to prepare nanoscale material a variety of physical and chemical methods can be used, of which the top down approaches like milling and photolithography are relatively easy to fabricate, but normally achieve nanoparticles with a great size distribution. In order to obtain homogenous particles the bottom up syntheses, as there are sol-gel processes or aerosol syntheses, are preferable.[13]

One method of the bottom up approach is the multi-source precursor synthesis, in which each component of the resulting particles originates from a different precursor. Though such a strategy is very favorable for commercially available reagents as well as it is suited for mass productions, it often lacks control of the obtained stoichiometry during the synthesis. Also the achievement of crystalline and monodispersive products is quite challenging.[14] Another technique is the single-source precursor method, where all components of the targeted nanoparticles are combined in one complex stabilized by ligands. Despite the advantages of monodispersive nanoscale material and the bonds, that are preformed between the components, the necessary synthesis of the single-source precursors is usually very challenging.

In order to stabilize such compounds the β-diketiminato ligand has proven to be very useful due to its steric and electronic tunabilities. These properties were first described by Collins *et al.*, who studied the synthesis of $[CH(C(Me)N(Ar))_2]Zr$ complexes (Ar = Ph, *p*-CF_3Ph) and were able to show that at least the variation of the aromatic residues leads to a change in the degree of σ and π binding modes.[15] In our group similar studies were performed, in which not only the aromatic flanking groups of the nacnac complex [LM(tol)] were varied, but also the aliphatic residues in the backbone (M = Fe, Co; L = L^0 = $CH[CHN(2,6\text{-}^iPr_2C_6H_3)]_2$, L^1 = $CH[C(Me)N(2,6\text{-}Me_2C_6H_3)]_2$, L^2 = $CH[CHN(2,6\text{-}Me_2C_6H_3)]_2$, L^3 = $CH[C(Me)N(2,6\text{-}^iPr_2C_6H_3)]_2$, L^4 = $CH[C(Me)N(2,6\text{-}Et_2C_6H_3)]_2$] (Scheme 4 - 1).[16,17]

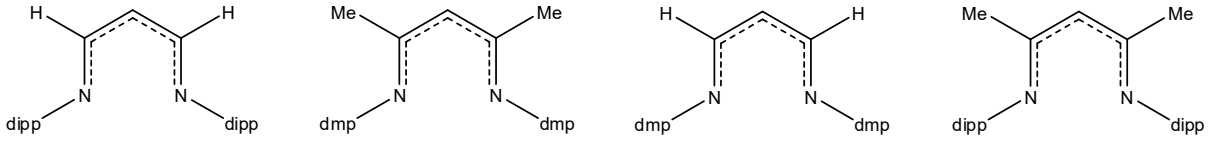

L^0 **L^1** **L^2** **L^3**

dipp = 2,6 - Diisopropylphenyl
dmp = 2,6 - Dimethylphenyl

Scheme 4 - 1: β-diketiminato ligands of β-diketiminato Fe(tol).[16]

Another, quite undesired property of the β-diketiminato ligand is its sensitivity towards hydrolysis. However, for precursors in nanoparticles synthesis this feature is useful as the ligand, though forming stable complexes, can easily be removed by the reaction with various acids or bases. Thus, the compounds are destabilized and the embedded components are released, whereby the formation of nanoparticles is enabled.

All these features make the β-diketiminato ligand a potentially very useful tool to synthesize single source precursors for nanoparticles synthesis. Due to this, the complexes $[CH(C(Me)N(dipp))_2]MCl$ (M = Ge (**4-A**), Sn (**4-B**))[18] caught our attention, as they can be reacted with different lithiated compounds, in particular with lithiated group 15 species. In 2006, Driess *et al.* reported on the reaction of **4-A** with $LiN(SiMe_3)_2$, which results in the germylene $[CH(C(Me)N(dipp))_2]Ge$ (**4-C**) instead of the

expected product $[CH(C(Me)N(dipp))_2]GeN(SiMe_3)_2$ due to the basic character of $LiN(SiMe_3)_2$.[19] Only two years later, Driess *et al.* showed that the reaction of $LiP(SiMe_3)_2$ with **4-A** leads to a different result since $[CH(C(Me)N(dipp))_2]GeP(SiMe_3)_2$ (**4-D**) was isolated.[20] In 2012, Fulton *et al.* synthesized the tin analogon $[CH(C(Me)N(dipp))_2]SnP(SiMe_3)_2$ (**4-E**) (Scheme 4 - 2).[21]

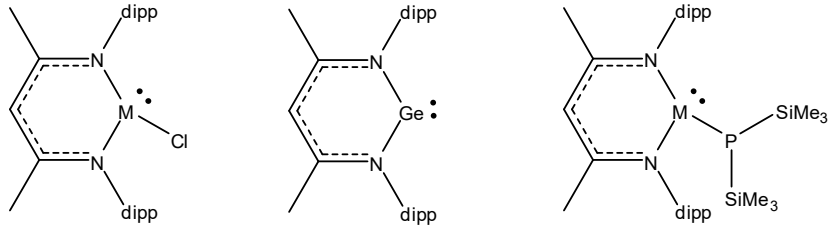

M = Ge (**4-A**), Sn (**4-B**) **4-C** M = Ge (**4-D**), Sn (**4-E**)

Scheme 4 - 2: Examples of different β-diketiminato germanium and tin complexes.

Both, **4-D** and **4-E** might be useful single source precursors in order to prepare nanoscale material like GeP_3 nanofilms,[11] Sn_4P_3 nanoparticles[12] or the unique tear-drop shaped SnP particles, which exhibit fascinating structural and electrochemical properties, e.g. for an application as anode material for high-capacity Li secondary batteries.[22]

Herein, we report on the reactions of **4-A** and **4-B** with the lithiated compounds $LiCH_2(SiMe_3)$ and $LiAs(SiMe_3)_2$ resulting in the hitherto unknown complexes $[CH(C(Me)N(dipp))_2]MCH_2(SiMe_3)$ (M = Ge (**1**), Sn (**2**)) and $[CH(C(Me)N(dipp))_2]MAs(SiMe_3)_2$ (M = Ge (**4-3**), Sn (**4-4**)). Furthermore, we performed preliminary studies, in which the compounds $[CH(C(Me)N(dipp))_2]MP(SiMe_3)_2$ (M = Ge (**4-D**), Sn (**4-E**)) and $[CH(C(Me)N(dipp))_2]SnAs(SiMe_3)_2$ (**4-4**) are tested for their suitability as single-source-precursor for germanium and tin phosphide and tin arsenide nanoparticles, respectively.

4.4. Results and Discussion

The reaction of L^3MCl (M = Ge (**4-A**), Sn (**4-B**)) with one eq. of $LiCH_2(SiMe_3)$ in toluene leads to the salt metatheisis products L^3 M–$CH(SiMe_3)_2$ (M = Ge (**4-1**), Sn (**4-2**)) as dark red crystals and as orange crystals, respectively. Analogously, the reaction of **4-A** and **4-B** with $LiAs(SiMe_3)_2$ results in the arsenic compounds L^3M–$As(SiMe_3)_2$ (M = Ge (**4-3**), Sn (**4-4**). While **4-3** appears orange to light red in solution, the solutions of **4-4** show a dark red to brown color, from which dark red block-shaped crystals can be isolated.

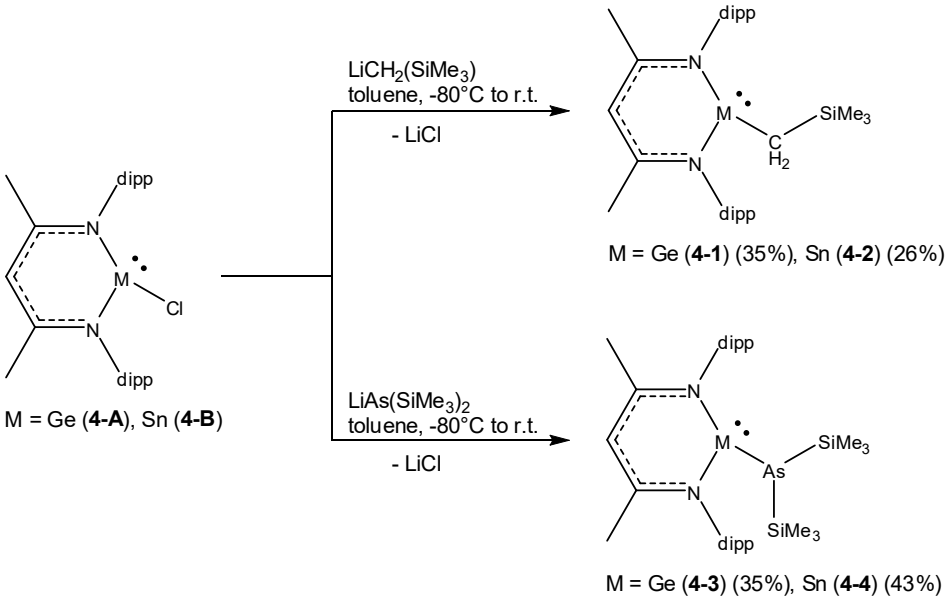

Scheme 4 - 3: Reactions of **4-A** and **4-B** with $LiCH_2(SiMe_3)$ and $LiAs(SiMe_3)_2$.

The ^1H NMR spectra of the four compounds show the typical resonance signals for the L^3 ligand as well as the signals of the $SiMe_3$ groups, which are shifted to low fields in the case of **4-1** and **4-2** (Table 4 - 1). The $^{29}Si\{^1H\}$ spectra display a singlet for each compound (Table 4 - 2) and the same is true for the $^{119}Sn\{^1H\}$ NMR spectrum of **4-2**. Surprisingly, no signals can be found in the $^{119}Sn\{^1H\}$ NMR spectrum of **4-4**, although the single crystal X-ray analysis of the concerned sample undoubtedly proofed the existence of the compound as described below and mass spectrometry revealed the presence of tin-containing fragments. This fact might be due to the interaction of the Sn nuclei with the quadrupolar As nuclei leading to a broadening of the ^{119}Sn NMR resonance signal and hence to the suppression of a detectable signal in the $^{119}Sn\{^1H\}$ NMR spectrum.

Table 4 - 1: ^1H NMR chemical shifts of the compounds **4-1** – **4-4**.

	Si*Me*$_3$ δ [ppm]	M–C*H*$_2$ δ [ppm]	^{i}Pr δ [ppm]	N*Me* δ [ppm]	^{i}P–*H* δ [ppm]	C*H*(C(Me)N$_2$ δ [ppm]	Ph δ [ppm]
1	–0.23 (s)	0.11 (s)	1.13 (d), 1.16 (d), 1.37 (d), 1.44 (d)	1.52 (s)	3.53 (sept), 3.78 (sept)	4.71 (s)	7.08 – 7.12 (m)
2	–0.16 (s)	–0.09 (s)	1.20 (d), 1.22 (d), 1.38 (d), 1.50 (d)	1.64 (s)	3.45 (sept), 3.82 (sept)	4.77 (s)	7.09 – 7.21 (m)
3	0.49 (s)	-	1.08 (d), 1.27 (“t”), 1.54 (d)	1.63 (s)	3.36 (sept), 3.85 (sept)	5.14 (s)	7.06 – 7.16 (m)
4	0.24 (s)	-	1.14 (d), 1.24 (d), 1.29 (d), 1.58 (d)	1.51 (s)	3.30 (sept), 3.98 (sept)	4.84 (s)	7.05 – 7.18 (m)

Table 4 - 2: $^{29}Si\{^1H\}$ NMR chemical shifts of the compounds **4-1** – **4-4**.

	*Si*Me$_3$ δ [ppm]
1	0.97 (s)
2	0.47 (s)
3	3.90 (s)
4	4.69 (s)

The ^{1}H NMR spectra of **4-1** and **4-2** suggest the structure depicted in Scheme 4 - 3. The most striking difference between the spectra is the shift of the C$\underline{H_2}$SiMe$_3$ signals at δ [ppm] = 0.11 (**4-1**) and δ [ppm] = –0.09 (**4-2**), which is due to the proximity of the H atoms to the ^{i}Pr$_2$C$_6$H$_3$-π-electrons and the resulting shielding. Between the ^{1}H NMR spectra of **4-3** and **4-4**, there are three major differences, starting with the distinct high field shift of the Si(C$\underline{H_3}$)$_3$ groups of **4-4** compared to its lighter homologue **4-3** and the starting materials **4-D** and **4-E** (δ [ppm] = 0.49 (s, **4-3**); 0.24(s, **4-4**); 0.43 (d, **4-D**); 0.46 (d, **4-E**)).[20,21] Furthermore, the ^{1}H NMR spectrum of **4-4** shows four doublets for its ^{i}Pr groups, while two of the four doublets of **4-3** are overlapping forming a pseudotriplet (Supporting Information Figure 3 and 11). At last, a severe low field shift of one ^{i}Pr signal of **4-4** can be observed as it is shifted to lower fields than the signals of the methyl groups in the backbone of the L^3 ligand. This is not the case for any of the three other compounds.

The ^{29}Si{^{1}H} spectra of **4-1** and **4-2** display the signals of the $\underline{Si}$Me$_3$ group (δ [ppm] = 0.97 (**4-1**); 0.47 (**4-2**)). In the ^{119}Sn{^{1}H} NMR spectrum of **4-2** one singlet at δ = 288 ppm can be found, which appears in a similar region as the signal of the starting material **4-B** (δ [ppm] = 224).[18] The signal of the $\underline{Si}$Me$_3$ groups in the ^{29}Si{^{1}H}DEPT NMR spectrum of **4-4** (δ = 4.69 ppm (s)) is only slightly downfield-shifted in comparison to **4-3** (δ = 3.90 ppm (s)). Both signals are in the same range as the corresponding signals of their lighter homologues ($\underline{Si}$Me$_3$:δ [ppm] =2.0 (**4-D**); 4.0 (**4-E**)).[20,21]

Crystals of **4-1** suitable for X-ray diffraction analysis were obtained by storing a solution of **4-1** in *n*-hexane at –30°C, leading to dark red blocks. It crystallizes in the space group P$\bar{1}$ with two molecules of L^{3}Ge–CH(SiMe$_3$)$_2$ in the asymmetric unit. Single crystals of **4-2** suitable for single crystal X-ray analysis were obtained by storing a *n*-hexane solution of **4-2** at –30°C. It crystallizes in the space group P2$_1$/n with one molecule of L^{3}Sn–CH$_2$(SiMe$_3$) per asymmetric unit. **4-3** can be obtained as orange crystals suitable for single crystal structure analysis by storing a solution of **4-3** in *n*-hexane at –30°C. It crystallizes in the orthorhombic space group Pbca. Suitable crystals of **4-4** for single crystal X-ray analysis can be obtained by storing a concentrated solution of **4-4** in *n*-hexane at –30°C. It crystallizes in the triclinic space group P$\bar{1}$ with two molecules of **4-4** in the asymmetric unit.

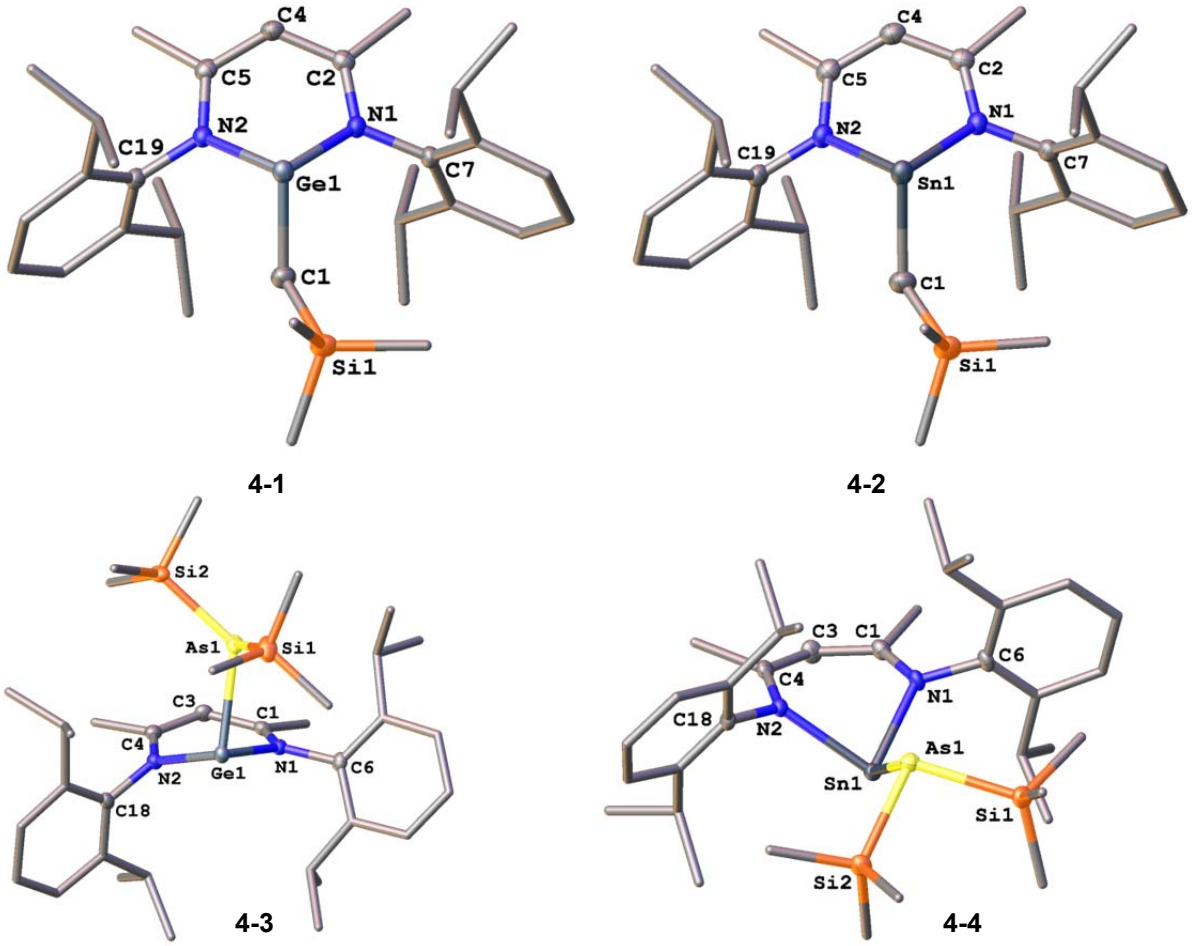

Figure 4 - 1: Molecular structures of **4-1**, **4-2**, **4-3** and **4-4** (top left, top right, bottom left, bottom right). Thermal ellipsoids are shown with 50% probability level. H atoms are omitted for clarity. Selected lengths [Å] and angles [°]: **4-1**: Ge1 – C1 2.020(3), C1 – Si1 1.856(3), Ge1 – N1 2.0190(2), Ge1 – N2 2.0239(2), N1 – C2 1.319(3), N2 – C5 1.317(3), C2 – C4 1.410(3), C4 – C5 1.408(3); Ge1 – C1 – Si1 116.58(1), N1 – Ge1 – N2 88.05(8), C1 – Ge1 – N1 100.86(9), C1 – Ge1 – N2 96.43(9), Ge1 – N1 – C2 118.92(2), Ge1 – N2 – C5 119.21(2), C2 – C4 – C5 125.8(2). **4-2**: Sn1 – C1 2.210(3), C1 – Si1 1.850(3), Sn1 – N1 2.208(2), Sn1 – N2 2.214(2), N1 – C2 1.331(3), N2 – C5 1.326(3), C2 – C4 1.407(4), C4 – C5 1.401(4); Sn1 – C1 – Si1 115.43(2), N1 – Sn1 – N2 83.23(8), C1 – Sn1 – N1 99.62(1), C1 – Sn1 – N2 93.58(9), Sn1 – N1 – C2 118.11(2), Sn1 – N2 – C5 118.52(2), C2 – C4 – C5 128.8(3). **4-3**: Ge1 – As1 2.5424(2), As1 – Si1 2.3388(5), As1 – Si2 2.3385(4), Ge1 – N1 2.0556(1), Ge1 – N2 1.9724(1), N1 – C1 1.3184(2), N2 – C4 1.4489(2), C1 – C3 1.415(2), C3 – C4 1.384(2); Ge1 – As1 – Si1 96.396(1), Ge1 – As1 – Si2 126.428(1), Si1 – As1 – Si2 103.321(2), N1 – Ge1 – N2 90.48(5), As1 – Ge1 – N1 86.91(3), As1 – Ge1 – N2 104.31(3), Ge1 – N1 – C1 122.62(9), Ge1 – N2 – C4 122.36(9), C1 – C3 – C4 127.13(1). **4-4**: Sn1 – As1 2.7256(3), As1 – Si1 2.3537(8), As1 – Si2 2.3618(8), Sn1 – N1 2.213(2), Sn1 – N2 2.251(2), N1 – C1 1.336(3), N2 – C4 1.325(3), C1 – C3 1.389(4), C3 – C4 1.404(4); Sn1 – As1 – Si1 109.47(2), Sn1 – As1 – Si2 94.98(2), Si1 – As1 – Si2 96.41(3), N1 – Sn1 – N2 83.22(8), As1 – Sn1 – N1 102.16(6), As1 – Sn1 – N2 97.20(5), Sn1 – N1 – C1 116.14(2), Sn1 – N2 – C4 116.98(2), C1 – C3 – C4 128.5(2).

4-1 exhibits a six-membered C_3N_2Ge ring with the N-bound dipp flanking groups located perpendicular to and slightly bent below the plane of the ring as the torsion angles prove (C4–C2–N1–C7: 4.25°, C4–C5–N2–C19: 7.073°). At the same time the Ge1 atom is lifted out of the C_3N_2-plane leading to a half-chair conformation of the ring (C4–C2–N1–Ge1: 23.6°), which is in contrast to the mostly planar C_3N_2Ge ring of **4-A**.[18] The $CH_2(SiMe_3)$ group is located below the C_3N_2Ge ring plane similar to the dipp substituents which is probably due to the stereochemically active lone pair of the germanium atom. The Ge1–N1 and Ge1–N2 bond lengths of 2.019(2) Å and 2.024(2) Å are in the range of rather long single bonds (Ge–N: 1.910 – 2.042 Å),[23] which is also true for the germanium carbon bond with a length of 2.020(3) Å (Ge–C: 1.950(2) – 2.04(2) Å).[24,25,26,27] In comparison to **4-A**, the Ge–N bonds are slightly elongated (**4-1**: Ge1–N1 2.019(2) Å, Ge1–N2 2.024(2) Å; **4-A**: Ge1–N1 1.988(2) Å, Ge1–N2 1.997(3) Å).[18]

The single crystal X-ray analysis proved **4-2** to be isostructural to **4-1** as not only the $CH_2(SiMe_3)$ group is oriented in the same way as it is in **4-1**. Also the half-chair conformation of the C_3N_2Sn ring and the bending of the dipp flanking groups are in a similar range (**4-1**: C4–C2–N1–C7: 4.25°, C4–C5–N2–C19: 7.073°, C4–C2–N1–Ge1: –23.6°; **4-2**: C4–C2–N1–C7: 8.075°, C4–C5–N2–C19: 6.842°, C4–C2–N1–Sn1: 26.0°). The Sn1–N1 (2.208(2) Å) and Sn1–N2 (2.214(2) Å) bond lengths are in the range of a single bond (Sn–N: 1.97 – 2.72 Å)[28,29,30] and slightly elongated compared to the Sn–N bond lengths of **4-B** (Sn1–N1: 2.185 Å, Sn1–N2: 2.180 Å).[18] The Sn1–C1 bond length is with 2.210(3) Å also in the range of a Sn–C single bond (2.12 – 2.451 Å).[30]

Compound **4-3** shows a slightly distorted six-membered C_3N_2Ge ring with one half of the ring being bent more than the other one (N1–C1–C3–C4: 23.56°, N2–C4–C3–C1: 12.08°). Furthermore the N2 bound dipp group (C18–N2–C4–C3: 26.072°) is pushed more below the plane of the C_3N_2Ge ring than the N1 bound one (C6–N1–C1–C3: 1.391°) which is likely caused by steric effects. The Ge1–As1 (2.5424(2) Å) as well as the As1–Si1 (2.3388(5) Å) and the As1–Si2 (2.3385(4) Å) bond lengths are in the range of rather long single bonds (Ge–As: 2.378 – 2.506 Å,[31,32] Si–As: 2.29 – 2.40 Å[33]). The slightly bent orientation of the $As(SiMe_3)_2$ group of **4-3** (N1–Ge1–As1: 86.91(3) Å, N2–Ge1–As1: 104.31(3) Å) is also observed for the $P(SiMe_3)_2$ substituent in **4-D** (N1–Ge1–P1: 103.46 Å, N2–Ge1–P1: 94.93 Å).[20] Also the bond lengths and angles of both species are in the same range, despite of course those involving the pnictogen atom.

The Sn1–As1 (2.7256(3) Å) and the As1–Si (As1–Si1: 2.3537(8) Å, As1–Si2: 2.3618(8) Å) bonds of **4-4** are in the range of single bonds (Sn–As: 2.54 – 3.03 Å,[34,35] Si–As: 2.29 – 2.40 Å).[33] Quite remarkable when comparing **4-3**, **4-4** and **4-E** is the half-chair conformation of the six-membered ring, which **4-4** adopts, while **4-3** and **4-E** exhibit a rather planar C_3N_2M ring (**4-4**: C3–C1–N1–Sn1: 29.1°, C3–C4–N2–Sn1: 20.1°; **4-3**: C3–C1–N1–Ge1: 1.5°, C3–C4–N2–Ge1: 22.9°; **4-E**: C2–C1–N1–Sn1: 14.8°, C2–C3–N2–Sn1: 7.1°). The orientation of the $As(SiMe_3)_2$ group of **4-4** therefore differs from the alignment of the $P(SiMe_3)_2$ substituent of **4-E** as the latter is almost perpendicular to the C_3N_2Sn ring,[21] while **4-4** adopts a larger angle between the $As(SiMe_3)_2$ group and the C_3N_2Sn ring (Figure 4 - 2). This leads to a conformation of **4-4**, that is more similar to the solid state structures of $L^3Pb–PPh_2$ (**4-F**) (C2–C1–N1–Pb1: 24.259°, C2–C3–N2–Pb1: 23.604°) and $L^3Pb–PCy_2$ (**G**) (C2–C1–N1–Pb1: 26.132°, C2–C3–N2–Pb1: 20.581°).[21]

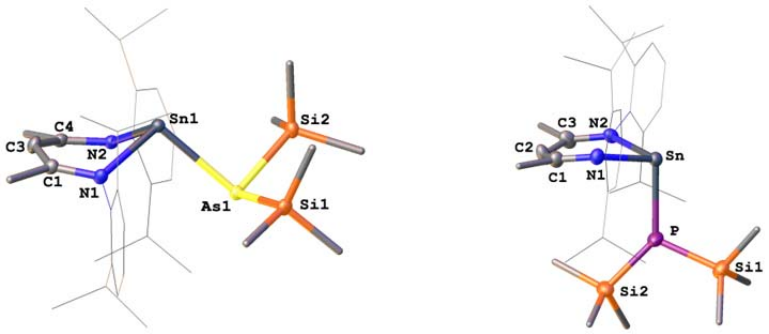

Figure 4 - 2: Comparison of the crystal structures of **4-4** (left) and **4-E** (right).[21]

Nanoparticles studies

Over the last few centuries, nanoparticles containing phosphorus and arsenic opened numerous applications in optoelectronics, solid-state technology or catalysis.[36-40] Especially InP, GaInP, InAs or GaAs exhibit different fields of usage in various branches of industry.[41-45] But not only the group 13 compounds are well-suited for high-tech applications, also nanoparticles of group 14 phosphides and arsenides might show unique properties for different applications, which can be seen, e.g. in the calculations of Li *et al.* concerning 2D films of SiP, SiAs and SiSb.[46] The reported results suggest promising features, that might also be true for nanoparticles of M_xE_y (M = Ge, Sn; E = P, As). Therefore, we did some preliminary studies for the use of **4-D**, **4-E** and **4-4** as single source precursors. Those complexes caught our attention because of their easy accessibility in moderately to high yields as well as their stable, yet simply detachable ligands. The bonds between the group 14 and group 15 atoms in the eventual nanoparticles are preformed in the complexes as well as the stochiometry might already be given. We also planned to test complex **3**, but unfortunately its yields were too small to use **3** as a suitable precursor.

In the experiments the ligands are removed by hydrolysis using palmitic acid (PA) or hexadecylamine (HDA), both containting long aliphatic residues that also act as stabilizers to inhibit the agglomeration of the nanoparticles. The experiments were performed by the use of the hot injection method in which all reagents are mixed in mesitylene and the reaction vessel (Fischer-Porter-Schlenk) is dipped into a hot oil or metal bath. Different heating times as well as different stabilizer stoichiometries were tested (Table 4 - 3). The reaction temperature was set to 150°C.

Table 4 - 3: Reaction conditions of the studies to use molecular precursors for the preparation of nanoparticles.

1 eq. precursor	1 eq. HDA	1 eq. PA	0.5 eq. HDA	0.5 eq. PA	0.5 eq. HDA + 0.5 eq. PA
24 h	**4-D**, **4-E**, **4-4**	**4-D**, **4-E**, **4-4**	**4-D**, **4-E**, **4-4**	**4-D**, **4-E**, **4-4**	**4-D**, **4-E**, **4-4**
1 h	**4-D**, **4-E**, **4-4**	**4-D**, **4-E**, **4-4**	**4-D**, **4-E**, **4-4**	**4-D**, **4-E**, **4-4**	**-**

In the experiments of **4-D** a significant change in color was observed from the initially light orange, clear reaction mixture to a dark reddish-brown solution with a brown precipitate. However, the TEM images of the grids prepared from reaction mixture did not show unequivocally, if the syntheses of nanoparticles were successful. Only the reaction of **4-D** with 1 eq. PA for 1 h led to the formation of nanoparticles with a large size distribution (Figure 4 - 3 b).

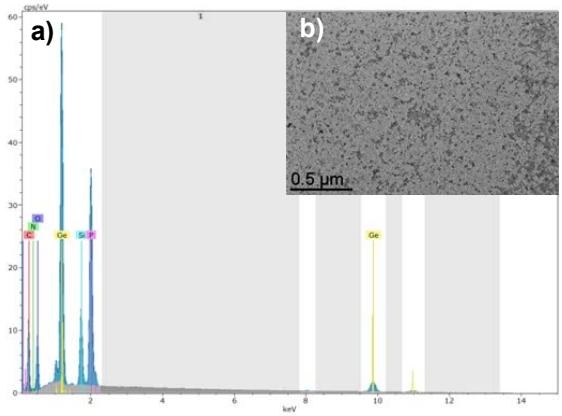

Figure 4 - 3: a) EDX spectrum of the reaction of **4-D** with 1 eq. PA after 1 h at 150°C. The integration reveals a composition of GeP; b) TEM picture of the reaction of **4-D** with 1 eq. PA after 1 h at 150°C.

Additionally to the TEM investigations, EDX and XRD studies were performed to determine the composition of the obtained precipitates. While the XRD analysis only showed that each experiment yielded amorphous product, the SEM coupled EDX revealed compositions of GeP and Ge_4P_3, which might depend on the reaction times. So, the reaction times of 1 h mainly led to a precipitate consisting of Ge_4P_3. GeP could be received by heating the mixtures for 24 h to 150°C.

The second tested compound was the tin phosphorus complex **4-E** that was treated with stabilizers in different stoichiometries (Table 4 - 3). In all experiments a change in color from clear yellow to cloudy black could be observed and in the 24 h tests a metallic precipitate was obtained. Yet, all of the experiments lead to the formation of monodisperse spheric nanoparticles exhibiting an average size of 10 to 22 nm, which are agglomerated to larger clusters (Figure 4 - 4 b).

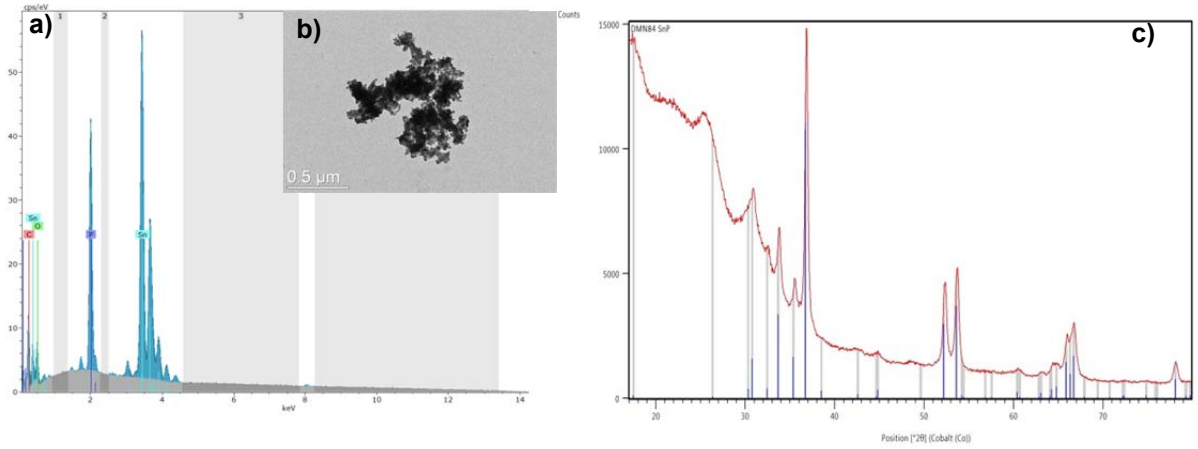

Figure 4 - 4: a) EDX spectrum of the reaction of **4-E** with 0.5 eq. HDA after 24 h at 150°C. The integration reveals a composition of Sn:P = 2:1; b) TEM picture of the reaction of **4-E** with 0.5 eq. HDA after 24 h at 150°C. c) XRD diffraction pattern of the reaction of **4-E** with 0.5 eq. HDA after 24 h at 150°C, the peaks show a composition of Sn_4P_3.

Again, XRD and EDX analyses were performed additionally to the very promising TEM studies that revealed in most cases a composition of Sn_4P_3 for the precipitated particles. Not for every experiment the results of EDX and XRD are consistent as the amount of tin detected by EDX is increased compared to the results of the XRD studies. This indicates an enrichment of tin on the particle surface. The TEM investigations showed that in case of HDA as stabilizer, a larger amount of nanoscaled

material is obtained as well as the material seems to be less blurry, hence, HDA might be considered as the preferred stabilizer for the use of **4-E** in nanoparticles synthesis. Surprisingly, the used amount of stabilizers does not have much influence on the received products, which is also true for the reaction time as in each test particles were obtained. As **4-E** could be proven to be a quite promising single source precursor, further experiments were performed in order to achieve separated particles. Therefore, higher amounts of stabilizers were chosen (Table 4 - 4). Unfortunately, it was not possible to inhibit the agglomeration as the following TEM pictures prove (Figure 4 - 5 b, d).

Table 4 - 4: Reaction conditions for the subsequent nanoparticles studies of **4-E**.

1 eq. precursor	5 eq. HDA	5 eq. PA	10 eq. HDA	10 eq. PA
24 h	**4-E**	-	**4-E**	**4-E**
1 h	**4-E**	-	**4-E**	**4-E**

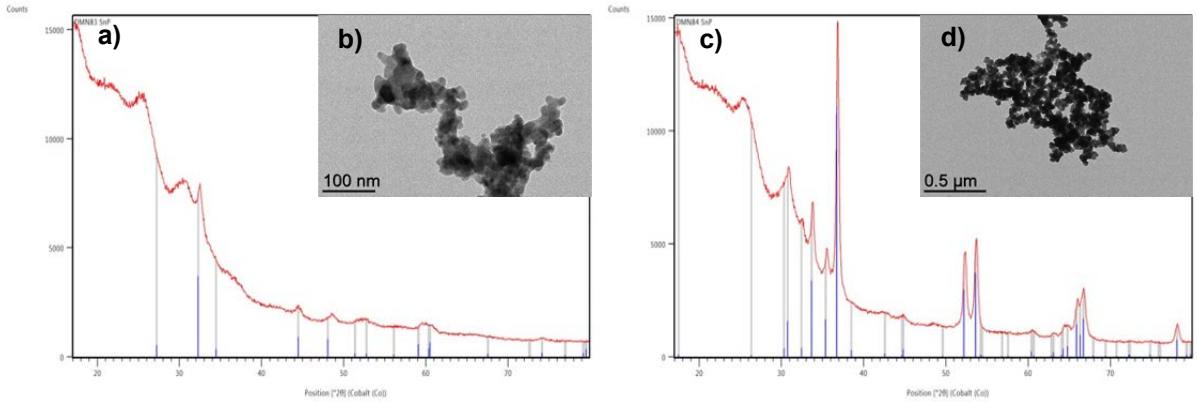

Figure 4 - 5: a) XRD diffractogram of the reaction of **4-E** with 5 eq. HDA after 1 h at 150°C. The composition is SnP; b) TEM picture of the reaction of **4-E** with 5 eq. HDA after 1 h at 150°C; c) XRD pattern of the reaction of **4-E** with 10 eq. HDA after 24 h at 150°C, the composition is Sn_4P_3; TEM picture of the reaction of **4-E** with 10 eq. HDA after 24 h at 150°C.

XRD analyses of the precipitated nanoparticles were performed which show a composition of metastable[47,48] SnP for the shorter reaction times and a composition of Sn_4P_3 for the 24 h experiments. Taking these results into account, it might be a possibility to control the stochiometry of the particles.

The previously reported experiments were also performed with $L^3SnAs(SiMe_3)_2$ in order to prepare tin arsenide nanoparticles (Table 4 - 3). Analogously to **4-E**, the thermolysis of **4-4** in mesitylene leads to a color change from clear, dark red to cloudy, black and the reaction mixtures, which were heated for 24 h formed a metallic precipitate. The TEM analysis shows, that for **4-4** the amount of used stabilizer and the reaction time have a lot more influence on the outcome than in case of **4-E**. While no particles could be received for the reactions of $L^3SnAs(SiMe_3)_2$ with the stabilizer HDA and PA in the stoichiometry 1:1 and reaction times of 24 h, monodisperse particles of average size of 10 to 14 nm could be obtained from the experiments with shorter heating times and lesser concentrations of used stabilizers (Figure 4 - 6 b).

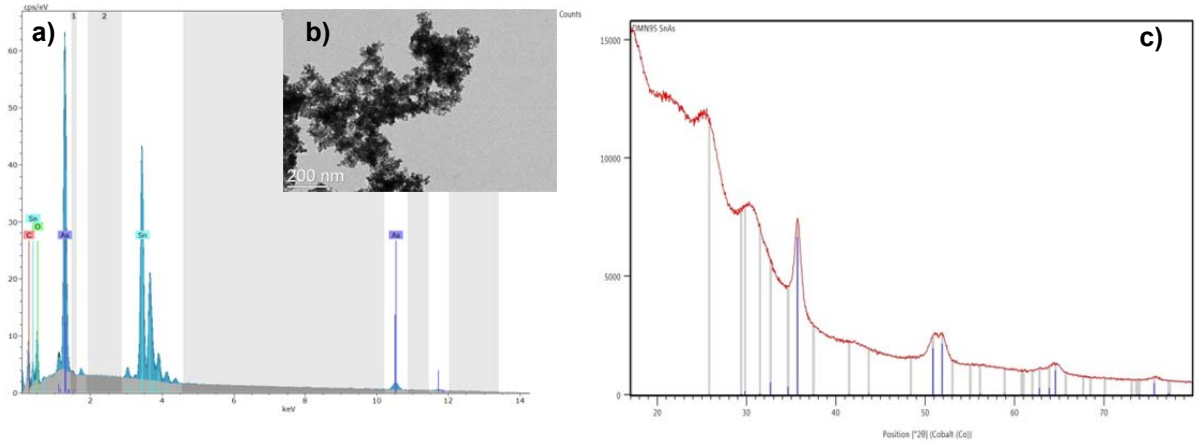

Figure 4 - 6: a) EDX spectrum of the reaction of **4-4** with 1 eq. PA after 1 h at 150°C. The integration reveals a composition of Sn_4As_3; b) TEM picture of the reaction of **4-4** with 1 eq. PA after 1 h at 150°C; c) XRD pattern of the reaction of **4-4** with 1 eq. PA after 1 h at 150°C, the peaks show a composition of Sn_4As_3.

The performed EDX and XRD studies reveal a composition of Sn_4As_3 in almost each experiment and are in almost all cases consistent, which might be taken as a hint that no surface enrichment of the particles takes place as it does in case of **4-E**. Considering the TEM images the PA stabilizer might be the reagent of choice for **4-4** as the resulting nanoparticles seem to be less agglomerated. Again, as the results of the tests were very promising, further experiments with quite large amounts of stabilizers were done to approach separated nanoparticles (Table 4 - 5), which was not successful (Figure 4 - 7).

Table 4 - 5: Reaction conditions for the subsequent nanoparticles experiments of **4-4**.

1 eq. precursor	5 eq. HDA	5 eq. PA	10 eq. HDA	10 eq. PA
24 h	**4-4**	-	**4-4**	**4-4**
1 h	**4-4**	-	**4-4**	**4-4**

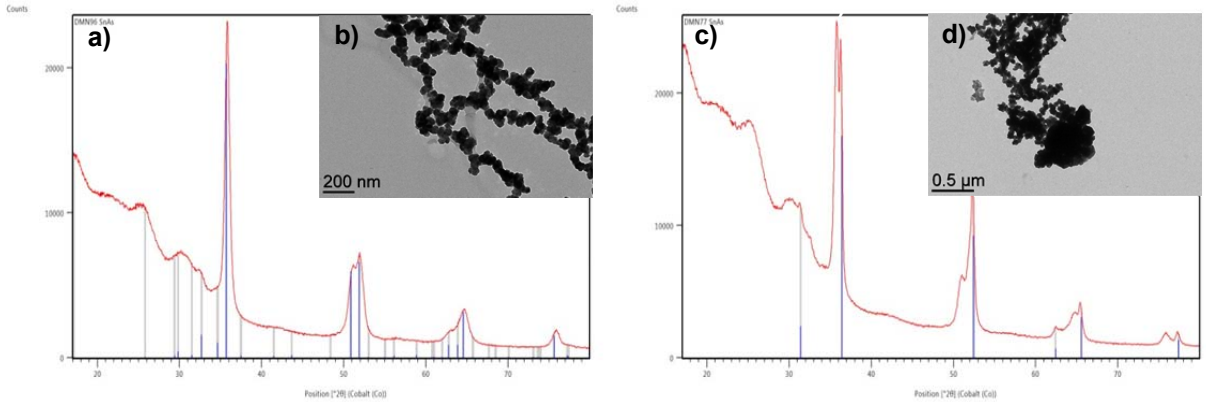

Figure 4 - 7: a) XRD diffractogram of the reaction of **4-4** with 10 eq. HDA after 1 h at 150°C. The composition is Sn_4As_3; b) TEM picture of the reaction of **4-4** with 10 eq. HDA after 1 h at 150°C; c) XRD diffractogram of the reaction of **4-4** with 10 eq. HDA after 24 h at 150°C, the composition is a mixture of Sn_4As_3 and SnAs; TEM picture of the reaction of **4-4** with 10 eq. HDA after 24 h at 150°C.

The XRD analyses of the particles obtained from these experiment show that the composition of the resulting particles doesn't change in case of **4-4** as significantly as for **4-E** as the precipitates of the

thermolysis of **4-4** leads to Sn_4As_3 for short reaction times and to a mixture of Sn_4As_3 and SnAs for 24 h (Figure 4 - 7). This indicates an opposite trend as it is described above for **4-E**.

4.5. Conclusion

Different studies in the last years have shown, that NP of group 14 and 15 elements have a great potential for application in electronics or semiconducting technology and the single source precursor approach might offer an improved control of the stoichiometry of the formed particles. Therefore, we synthesized the four potential single source precursors $[CH(C(Me)N(dipp))_2]MCH_2(SiMe_3)$ (M = Ge (**4-1**), Sn (**4-2**)) and $[CH(C(Me)N(dipp))_2]MAs(SiMe_3)_2$ (M = Ge (**4-3**), Sn (**4-4**)) bearing the β-diketiminato ligand as stabilizing substituent. The products could be obtained easily by a one pot synthesis of **4-A** and **4-B** with $LiCH_2(SiMe_3)$ and $LiAs(SiMe_3)_2$, respectively. Our main interest was the preparation of group 14 NP with phosphorus and arsenic, in which we were able to prove that the three compounds $[CH(C(Me)N(dipp))_2]GeP(SiMe_3)_2$ (**4-D**) and $[CH(C(Me)N(dipp))_2]SnE(SiMe_3)_2$ (E = P (**4-E**), As (**4-4**)) are indeed useful as single source precursors in the synthesis of Ge_4P_3 and Sn_4E_3 (E = P, As) NP.

4.6. Supporting Information

Experimental section

General procedures

All experiments were carried out under a dry nitrogen or argon atmosphere using standard Schlenk or drybox techniques. Solvents were dried by using an MBraun purification system followed by a distillation from sodium and stored over 3 Å mol sieve. The complexes $[CH(CNMe(dipp))_2]MCl$ (M = Ge (**4-A**), Sn (**4-B**))[49], $As(SiMe_3)_3$, $LiAs(SiMe_3)_2$[50] and $LiCH_2(SiMe_3)$[51] were prepared according to literature. The NMR spectra were recorded on a Bruker Avance 400 (^1H: 400.132 MHz, $^{13}C\{^1H\}$: 100.613 MHz, $^{29}Si\{^1H\}$DEPT/$^{29}Si\{^1H\}$/^{29}Si: 79.495 MHz, $^{119}Sn\{^1H\}$: 149.211 MHz) and an Avance 300 (^1H: 300.132 MHz) with δ referenced to external $SiMe_4$ (^1H, $^{13}C\{^1H\}$, $^{29}Si\{^1H\}$DEPT/$^{29}Si\{^1H\}$/^{29}Si, $^{119}Sn\{^1H\}$). The EI-MS studies were performed on a Jeol AccuTOF GCX.

Preparations

Preparation of $[CH(CNMe(dipp))_2]Ge–CH_2(SiMe_3)$ (4-1): A solution of $LiCH_2(SiMe_3)$ (54 mg, 0.57 mmol) in toluene (10 mL) were added to **4-A** (300.2 mg, 0.57 mmol) in toluene (10 mL) at –80°C while stirring. The reaction mixture was allowed to warm to room temperature overnight whereby the color changed from a light yellow to deep red. The solvent was removed *in vacuo* and the residue was extracted into *n*-hexane (30 mL). The concentrated red filtrate was stored at –30°C to yield dark red crystals of **4-1** (115.9 mg, 35% yield).

^1H NMR (400.132 MHz, C_6D_6, 298K): δ[ppm] = –0.23 (s, 9H, $Si(C\underline{H}_3)_3$), 0.11 (s, 2H, $Ge–C\underline{H}_2$), 1.13 (d, 6H, $^3J_{HH}$ = 6.9 Hz, $CH(C\underline{H}_3)Me$), 1.16 (d, 6H, $^3J_{HH}$ = 6.8 Hz, $CH(C\underline{H}_3)Me$), 1.37 (d, 6H, $^3J_{HH}$ = 6.8 Hz, $CH(C\underline{H}_3)Me$), 1.44 (d, 6H, $^3J_{HH}$ = 6.9 Hz, $CH(C\underline{H}_3)Me$), 1.52 (s, 6H, $NC(C\underline{H}_3)$), 3.53 (sept., 2H, $^3J_{HH}$ = 6.9 Hz, $C\underline{H}Me_2$), 3.78 (sept. 2H, $^3J_{HH}$ = 6.8 Hz, $C\underline{H}Me_2$), 4.71 (s, 1H, $^3J_{HH}$ = 6.9 Hz, $C\underline{H}(C(Me)N_2)$, 7.08 – 7.12 (m, 6H, Ph); $^{13}C\{^1H\}$ NMR (100.613 MHz, C_6D_6, 298K): δ[ppm] =0.8, 15.6, 22.9, 24.4, 24.6, 25.3, 26.9, 28.9, 96.1, 124.2, 125.2, 127.0, 140,1, 144,1, 146.0, 166.5; $^{29}Si\{^1H\}$ NMR (79.945 MHz, C_6D_6, 298K): δ[ppm] = 0.97 (s); EI-MS calcd for $C_{33}H_{52}GeN_2Si$ 491.2482, Found 491.2660 (100 %).

Preparation of $[CH(CNMe(dipp))_2]Sn–CH_2(SiMe_3)$ (4-2): To a solution of **4-B** (122.5 mg, 0.21 mmol) in toluene (5 mL) $LiCH_2Si(Me_3)$ (21 mg, 0.21 mmol) in toluene (10 mL) was added at –80°C and warmed to room temperature overnight while stirring. During the warming, the light yellow color of the mixture turned to a darker yellow. The solvent was evaporated and the remaining residue extracted with *n*-hexane. After storing the concentrated filtrate at –30°C, yellow crystals of **4-2** could be isolated (34.3 mg, 26% yield)

^1H NMR (400.132 MHz, C_6D_6, 298K): δ[ppm] = –0.16 (s, 9H, $Si(C\underline{H}_3)_3$), –0.09 (s, 2H, $Sn–C\underline{H}_2$), 1.20 (d, 6H, $^3J_{HH}$ = 6.8 Hz, $CH(C\underline{H}_3)Me$), 1.22 (d, 6H, $^3J_{HH}$ = 6.8 Hz, $CH(C\underline{H}_3)Me$), 1.38 (d, 6H, $^3J_{HH}$ = 6.8 Hz, $CH(C\underline{H}_3)Me$), 1.50 (d, 6H, $^3J_{HH}$ = 6.8 Hz, $CH(C\underline{H}_3)Me$), 1.64 (s, 6H, $NC(C\underline{H}_3)$), 3.45 (sept., 2H, , $^3J_{HH}$ = 6.8 Hz, $C\underline{H}Me_2$), 3.82 (sept., 2H, $^3J_{HH}$ = 6.8 Hz, $C\underline{H}Me_2$), 4.77 (s, 1H, $C\underline{H}(C(Me)N_2)$, 7.09 – 7.21 (m, 6H, Ph); $^{13}C\{^1H\}$ NMR (100.613 MHz, C_6D_6, 298K): δ[ppm] = 1.9, 20.7, 22.1, 23.4, 24.4, 24.7, 25.2, 27.0, 28.5, 28.6, 28.8, 96.6, 124.2, 125.0, 126.6, 141.6, 143.8, 144.4, 167.5; $^{29}Si\{^1H\}$ DEPT NMR

(79.945 MHz, C_6D_6, 298K): δ[ppm] = 0.47 (s); $^{119}Sn\{^1H\}$ NMR (149.211 MHz, C_6D_6, 298K): δ[ppm] = 288 (s).

Preparation of [CH(CNMe(dipp))$_2$]Ge–As(SiMe$_3$)$_2$ (4-3): $LiAs(SiMe_3)_2$ (128.3 mg, 0.38 mmol) in toluene (15 mL) were added to a stirred solution of **4-A** (199.9 mg, 0.38 mmol) at –80°C turning the initially yellow solution immediately red. The mixture was warmed to room temperature overnight, followed by evaporating the solvent. The red-orange residue was extracted into *n*-hexane (20 mL). The filtrate was concentrated to 3 mL and stored at –30°C. Orange-red crystals of **4-3** were obtained after 3 weeks (93.4 mg, 35% yield)

^1H NMR (400.132 MHz, C_6D_6, 298K): δ[ppm] = 0.49 (s, 18H, $Si(C\underline{H}_3)_3$), 1.08 (d, 6H, $^3J_{HH}$ = 6.8 Hz, $CH(C\underline{H}_3)Me$), 1.27 (“t”, 12H, $^3J_{HH}$ = 6.8 Hz, $CH(C\underline{H}_3)Me$), 1.54 (d, 6H, $^3J_{HH}$ = 6.6 Hz, $CH(C\underline{H}_3)Me$), 1.63 (s, 6H, $NC(C\underline{H}_3)$), 3.36 (sept. 2H, $^3J_{HH}$ = 6.6 Hz, $C\underline{H}Me_2$), 3.85 (sept. 2H, $^3J_{HH}$ = 6.6 Hz, $C\underline{H}Me_2$), 5.14 (s, 1H, $C\underline{H}(C(Me)N_2)$, 7.06 – 7.16 (m, 6H, Ph); $^{13}C\{^1H\}$ NMR (100.613 MHz, C_6D_6, 298K): δ[ppm] = 1.4, 5.8, 23.9, 24.4, 24.8, 25.1, 25.2, 28.2, 28.6, 29.1, 29.2, 102.6, 124.5, 125.5, 127.5, 141.3, 144.5, 147.0, 166.3; $^{29}Si\{^1H\}$ DEPT NMR (79.945 MHz, C_6D_6, 298K): δ[ppm] = 3.90 (s); EI-MS calcd for $C_{35}H_{59}AsGeN_2Si_2$ 712.2647, Found 711.2592 (0.01 %) $[M – H]^{+\cdot}$.

Preparation of [CH(CNMe(dipp))$_2$]Sn–As(SiMe$_3$)$_2$ (4-4): $LiAs(SiMe_3)_2$ (1.05 g, 2.81 mmol), dissolved in toluene, was added to a solution of **4-B** (1.51 g, 2.62 mmol) in toluene at –80°C. An immediate change of the yellow solution of **4-B** to dark red can be observed. The solution was warmed to room temperature over night while stirring. The solvent was removed under reduced pressure, the remaining solid was extracted with n-hexane. Dark red crystals of **4-4** were achieved from the concentrated dark brownish red solution after 2 days at –30°C (1.045 g, 43% yield).

^1H-NMR (C_6D_6, 300 MHz, r.t.): δ[ppm] = 0.24 (s, 18H, $Si(C\underline{H}_3)_3$), 1.14 (d, 6H, $^3J_{HH}$ = 6.9 Hz, $CH(C\underline{H}_3)Me$), 1.24 (d, 6H, $^3J_{HH}$ = 6.9 Hz, $CH(C\underline{H}_3)Me$), 1.29 (d, 6H, $^3J_{HH}$ = 6.9 Hz, $CH(C\underline{H}_3)Me$), 1.51 (s, 6H, $NC(C\underline{H}_3)$), 1.58 (d, 6H, $^3J_{HH}$ = 6.9 Hz, $CH(C\underline{H}_3)Me$), 3.30 (sept. 2H, $^3J_{HH}$ = 6.8 Hz, $C\underline{H}Me_2$), 3.98 (sept. 2H, $^3J_{HH}$ = 6.8 Hz, $C\underline{H}Me_2$), 4.84 (s, 1H, $C\underline{H}(C(Me)N_2)$, 7.05 – 7.18 (m, 6H, Ph); ^{13}C-NMR (C_6D_6, 75 MHz, r.t.): δ [ppm] = 6.1; 24.3, 24.4, 24.9, 26.1, 26.8, 28.5, 28.8, 99.1, 124.6, 125.3, 127.1, 143.6, 144.1, 144.7, 167.6; $^{29}Si\{^1H\}$ DEPT NMR (79.945 MHz, C_6D_6, 298K): δ[ppm] = 4.69 (s); $^{119}Sn\{^1H\}$ NMR (149.211 MHz, C_6D_6, 298K): no signal detected; EI-MS calcd for $C_{35}H_{59}AsSnN_2Si_2$ 758.2455, Found 757.2787 (0.12 %) $[M – H]^{+\cdot}$.

NMR spectra

[CH(CNMe(dipp))$_2$]Ge–CH$_2$(SiMe$_3$) (1):

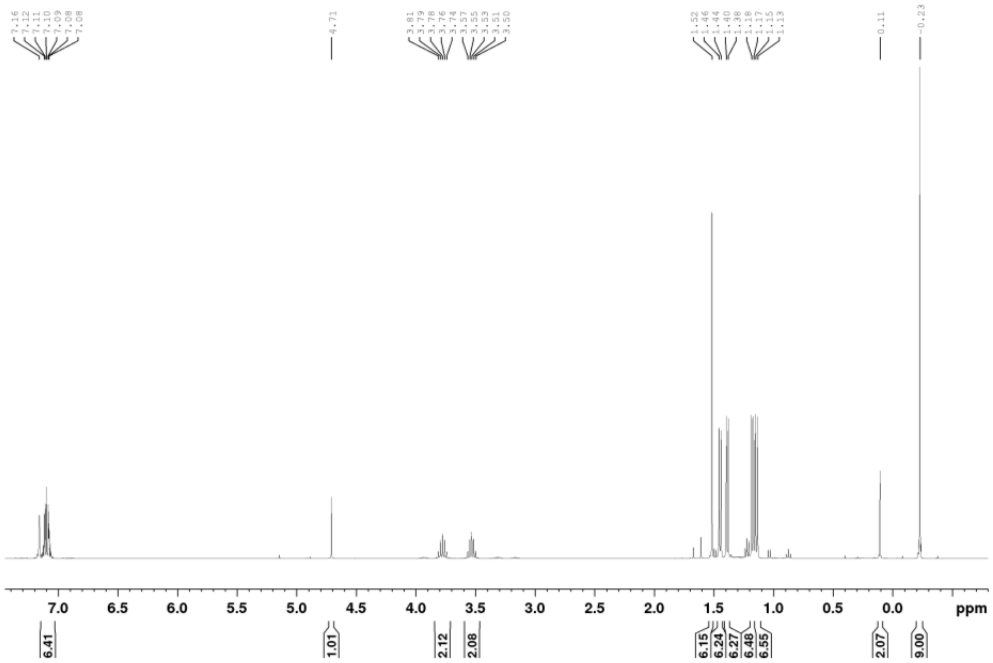

Figure 4 - 8: ^{1}H-NMR spectrum of the crystals of **4-1**.

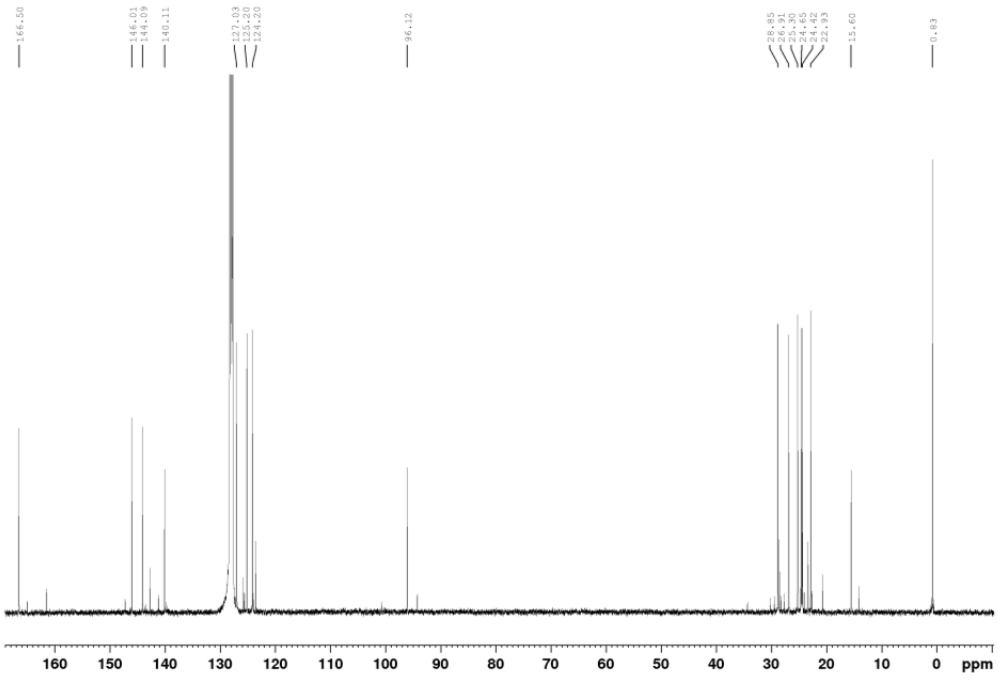

Figure 4 - 9: ^{13}C{^{1}H}-NMR spectrum of the crystals of **4-1**.

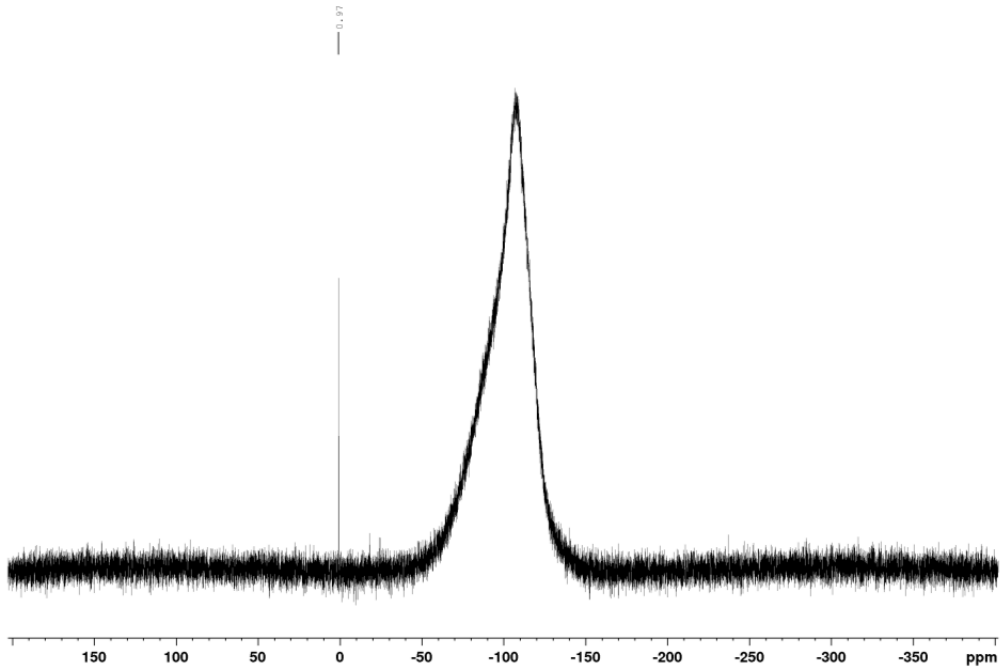

Figure 4 - 10: $^{29}Si\{^{1}H\}$-NMR spectrum of the crystals of **4-1**.

[CH(CNMe(dipp))$_2$]Sn–CH$_2$(SiMe$_3$) (4-2):

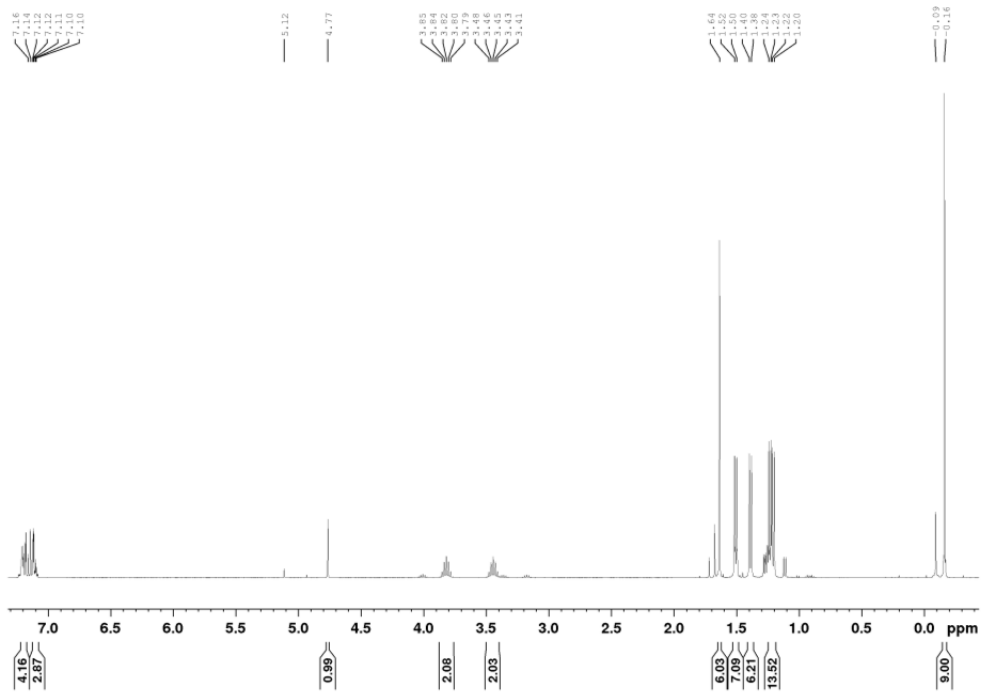

Figure 4 - 11: ^{1}H NMR spectrum of the crystals of **4-2**.

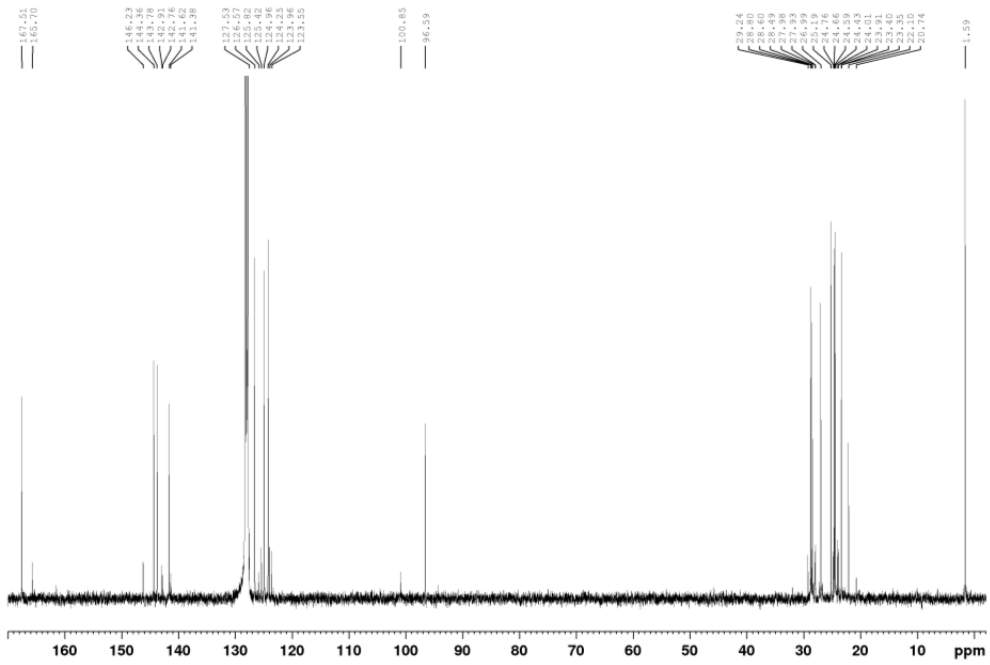

Figure 4 - 12: ^{13}C{^{1}H} NMR spectrum of the crystals of **4-2**.

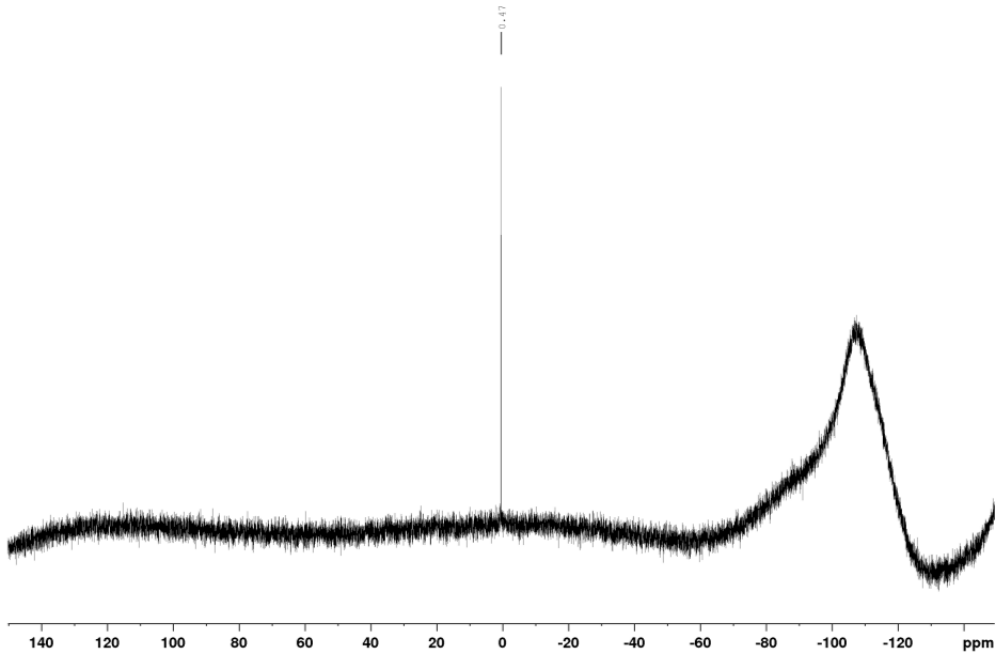

Figure 4 - 13: $^{29}Si\{^{1}H\}$ NMR spectrum of the crystals of **4-2**.

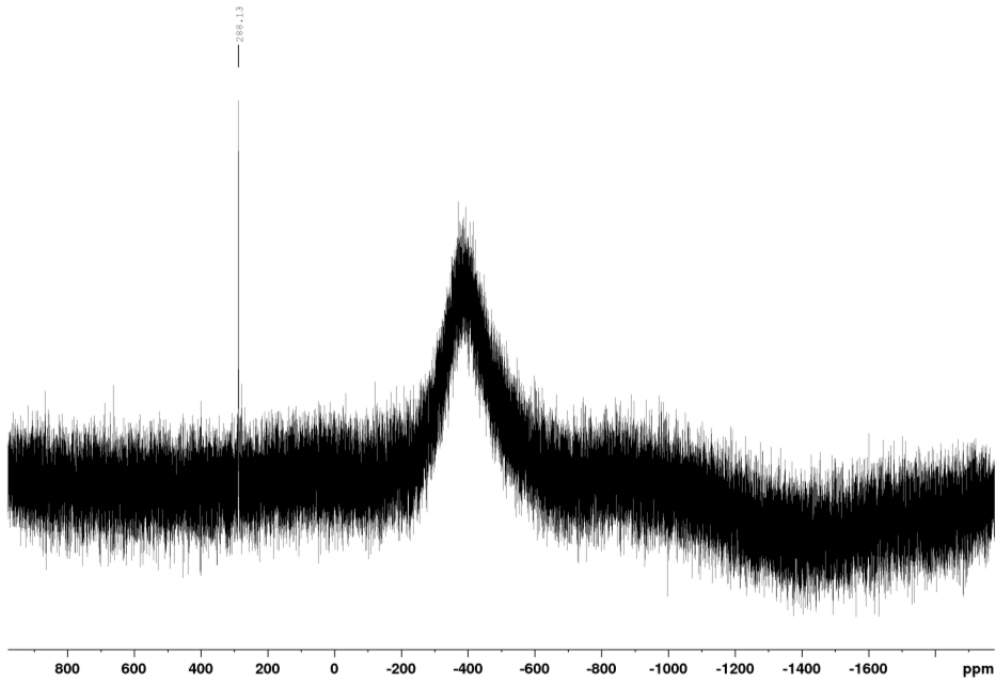

Figure 4 - 14: $^{119}Sn\{^{1}H\}$ NMR spectrum of the crystals of **4-2**.

[CH(CNMe(dipp))$_2$]Ge–As(SiMe$_3$)$_2$ (4-3):

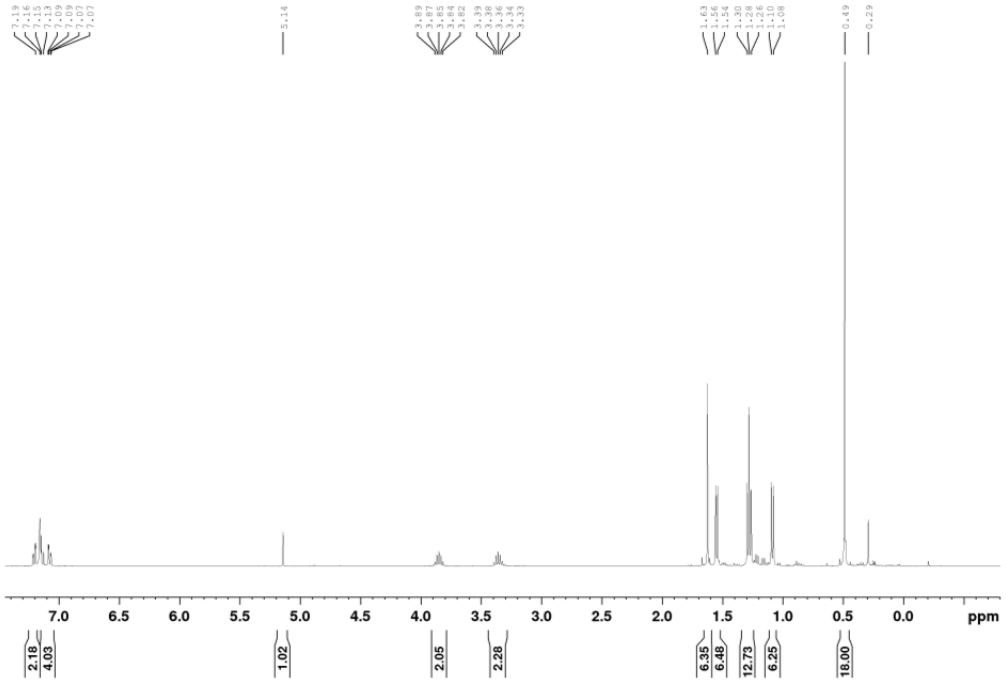

Figure 4 - 15: ^{1}H NMR spectrum of the crystals of **4-3**.

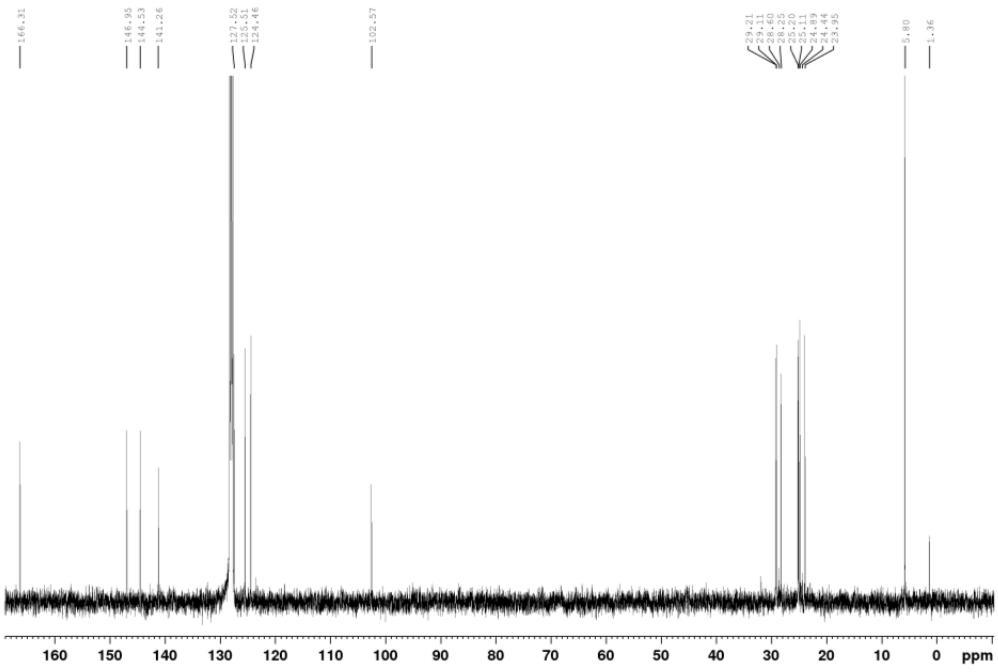

Figure 4 - 16: ^{13}C{^{1}H} NMR spectrum of the crystals of **4-3**.

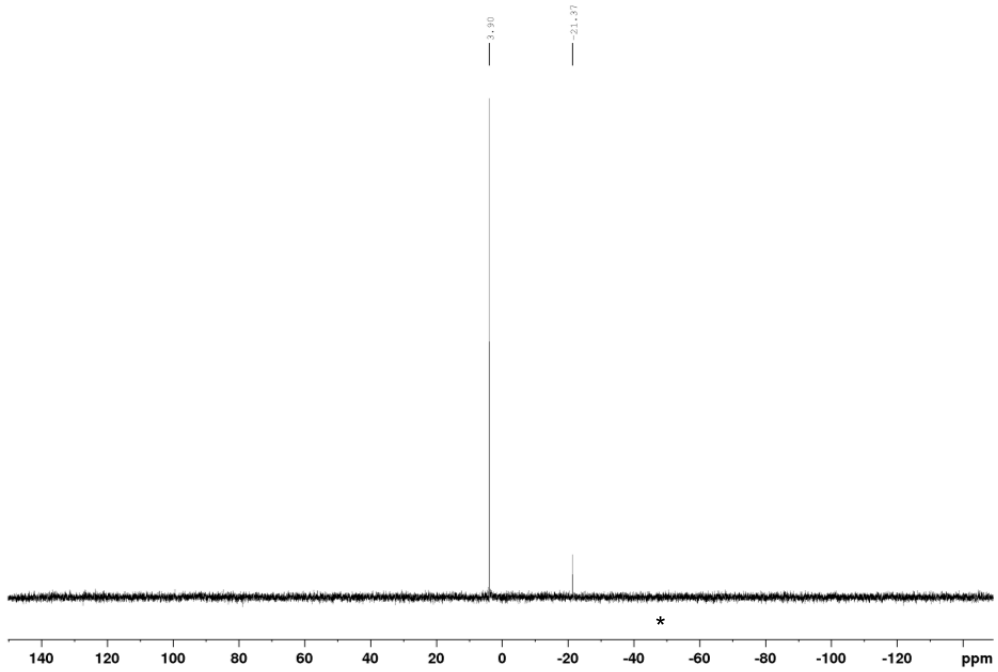

Figure 4 - 17: $^{29}Si\{^{1}H\}$ DEPT NMR spectrum of the crystals of **4-3**. * = impurity.

[CH(CNMe(dipp))$_2$]Sn–As(SiMe$_3$)$_2$ (4-4):

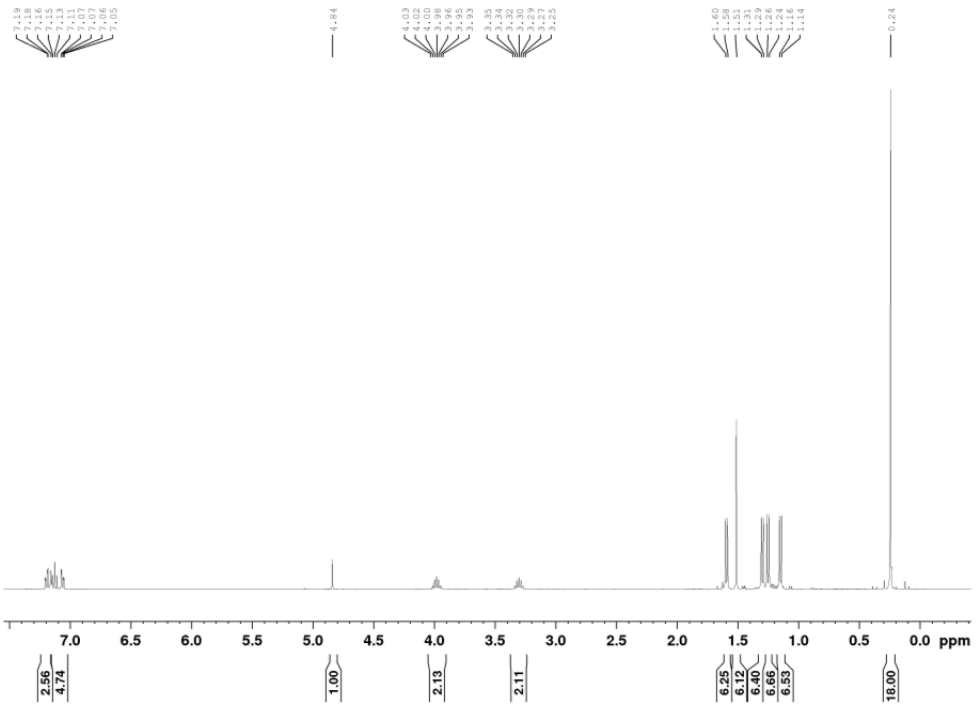

Figure 4 - 18: ^{1}H NMR spectrum of the crystals of **4-4**.

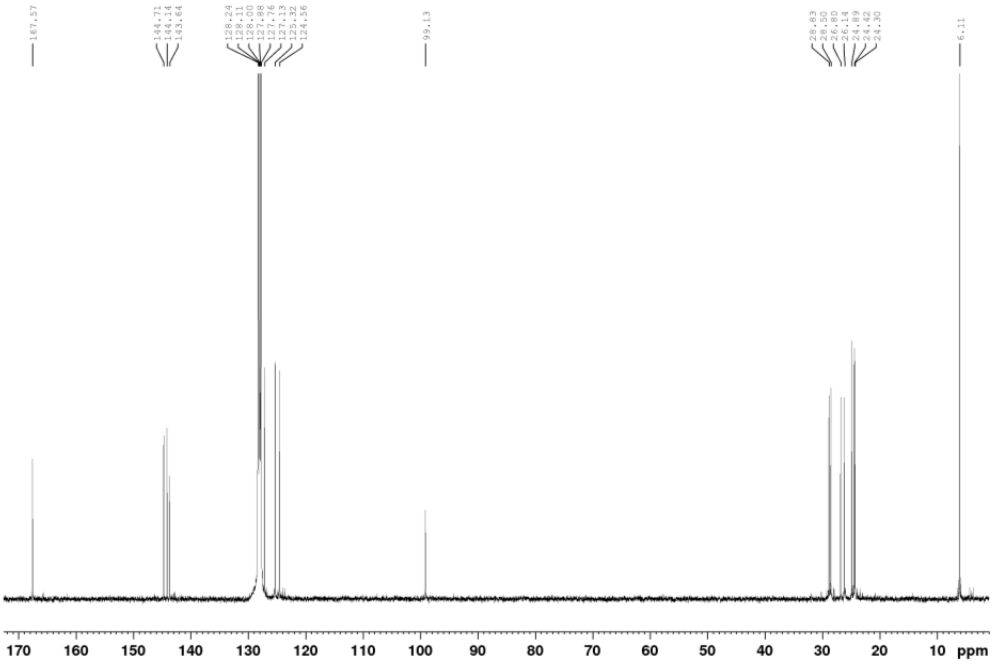

Figure 4 - 19: ^{13}C{^{1}H} NMR spectrum of the crystals of **4-4**.

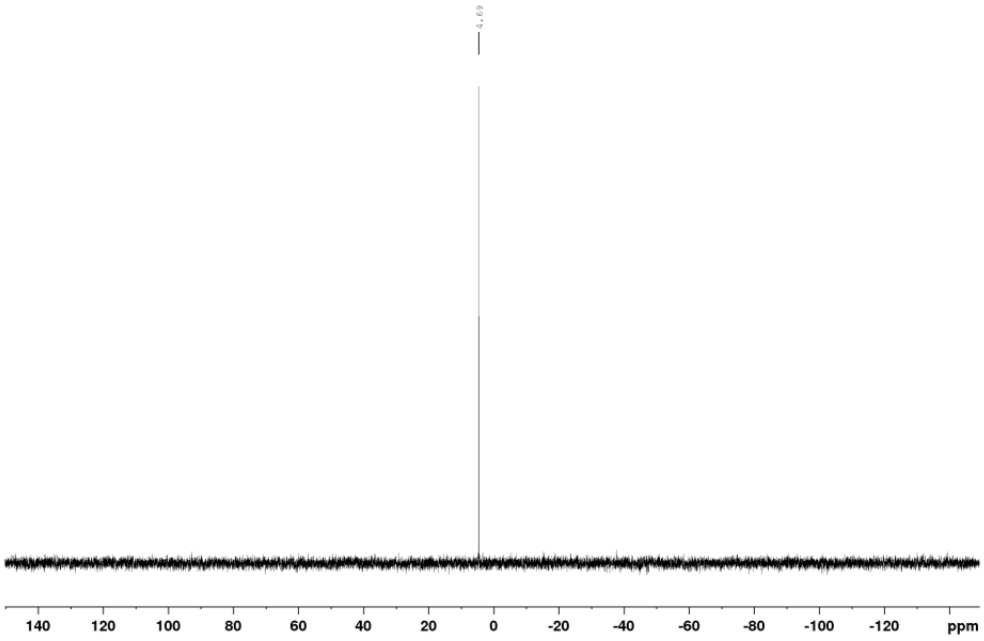

Figure 4 - 20: $^{29}Si\{^{1}H\}$ DEPT NMR spectrum of the crystals of **4-4**.

X-ray structure analysis:

The crystal samples were processed at a Supernova diffractometer with an Atlas CCD detector (**4-1**), a Gemini R Ultra with an Atlas S2 CCD detector (**4-2**, **4-3**) and a GV50 diffractometer with a Titan S2 CCD detector (**4-4**), respectively. Frames integration and data reduction were performed with CrysAlisPro ver. 171.38.41h.[52] Analytical absorption corrections from crystal faces[53] were applied to the data of **4-2** and **4-3**. A numerical absorption correction based on Gaussian integration over a multifaceted crystal model was applied to the data of **4-1** and **4-4**.[52] All structures were solved by SHELXT[54] using Olex2[55]. For all structures a least-square redinement on F^2 was carried out with SHELXL[56,57]. Hydrogen atoms at the carbon atoms were located in idealized positions and refined isotropically according to the riding model.

[CH(CNMe(dipp))$_2$]Ge–CH$_2$(SiMe$_3$) (4-1):

4-1 crystallizes from n-hexane at –30°C as clear, dark red blocks.

Sum formula	$C_{33}H_{52}GeN_2Si$
Molecular weight *M* [g/mol]	577.50
Crystal system	triclinic
Space group	P -1
Unit cell dimensions [Å] or [°]	8.9272(2) 91.3600(10)
	10.2432(2) 91.4300(10)
	19.8893(2) 113.304(2)
Volume [Å^3]	1668.72(6)
Formula units *Z*	2
Temperature *T* [K]	123(1)
Crystal size [mm^3]	0.113 × 0.086 × 0.026
Crystal density ρ_{calc} [Mg · m^{-3}]	1.149
F(000)	620
Absorption coefficient $\mu_{Cu\text{-}K\alpha}$ [mm^{-1}]	1.739
Transmission T_{min} / T_{max}	0.867/0.956
Absorption correction	gaussian
Wavelength (λ) [Å]	1.54184 (CuK_α)
Measured / independent reflections (R_{int})	12823/ 12823 (0.0486)
Independent reflections [$I > 2\sigma(I)$]	11421
Index ranges *hkl*	$-11 \le h \le 11$
	$-12 \le k \le 12$
	$-24 \le l \le 24$
Measuring range θ_{min} / θ_{max} / θ_{full} [°]	4.450/ 74.084/ 67.684
Completeness (θ_{full})	0.999
Data / restraints / parameters	12823/0/348
R-indices (all data)	0.0511/ 0.1581
R-indices [$I > 2\sigma(I)$]	0.0438/ 0.1354
Goodness-of-fit for S (F^2)	1.096
Largest diff. peak and hole [e · Å^3]	1.24 -0.47

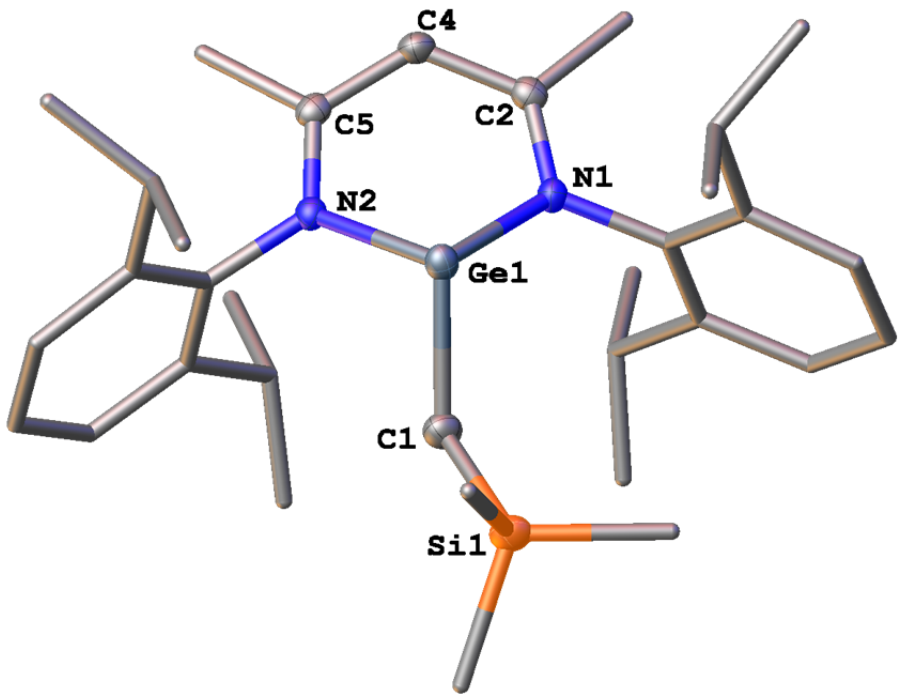

Figure 4 - 21: Molecular structure of compound **4-1**. Thermal ellipsoids are shown with 50% probability. H atoms are omitted for clarity.

Distances [Å]		Angles [°]	
Ge1 – C1	2.020(3)	Ge1 – C1 – Si1	116.58(13)
C1 – Si1	1.856(3)	N1 – Ge1 – N2	88.05(8)
Ge1 – N1	2.0190(19)	C1 – Ge1 – N1	100.86(9)
Ge1 – N2	2.0239(19)	C1 – Ge1 – N2	96.43(9)
Si1 – C31	1.874(3)	C1 – Si1 – C31	108.50(14)
Si1 – C32	1.864(3)	C1 – Si1 – C32	111.26(13)
Si1 – C33	1.875(3)	C1 – Si1 – C33	110.43(13)
N1 – C2	1.319(3)	Ge1 – N1 – C2	118.92(16)
N1 – C7	1.446(3)	Ge1 – N1 – C7	117.48(15)
N2 – C5	1.317(3)	Ge1 – N2 – C5	119.21(15)
N2 – C19	1.440(3)	Ge1 – N2 – C19	117.01(15)
C2 – C4	1.410(3)	N1 – C2 – C4	123.2(2)
C4 – C5	1.408(3)	N2 – C5 – C4	122.8(2)
		C2 – C4 – C5	125.8(2)
		C7 – N1 – C2	120.84(19)
		C5 – N2 – C19	121.82(19)

[CH(CNMe(dipp))$_2$]Sn–CH$_2$(SiMe$_3$) (4-2):

4-2 crystallizes from n-hexane at –30°C as clear, orange blocks.

Sum formula	$C_{33}H_{52}SnN_2Si$
Molecular weight *M* [g/mol]	623.54
Crystal system	monoclinic
Space group	$P2_1/n$
Unit cell dimensions [Å] or [°]	8.91450(10) 90
	19.8713(2) 92.6980(10)
	19.2539(3) 90
Volume [Å^3]	3406.91(7)
Formula units *Z*	4
Temperature *T* [K]	123(1)
Crystal size [mm^3]	0.233 × 0.114 × 0.09
Crystal density ρ_{calc} [Mg · m^{-3}]	1.216
F(000)	1312.0
Absorption coefficient $\mu_{Cu\text{-}K\alpha}$ [mm^{-1}]	6.448
Transmission T_{min} / T_{max}	0.486/ 0.687
Absorption correction	analytical
Wavelength (λ) [Å]	1.54184 (CuK_α)
Measured / independent reflections (R_{int})	17647/ 5951 (0.0311)
Independent reflections [$I > 2\sigma(I)$]	5459
Index ranges *hkl*	$-10 \le h \le 10$
	$-23 \le k \le 15$
	$-22 \le l \le 22$
Measuring range θ_{min} / θ_{max} / θ_{full} [°]	4.450/ 66.365/ 66.365
Completeness (θ_{full})	0.993
Data / restraints / parameters	5951/0/347
R-indices (all data)	0.0363/ 0.0835
R-indices [$I > 2\sigma(I)$]	0.0324/ 0.0835
Goodness-of-fit for S (F^2)	1.065
Largest diff. peak and hole [e · Å^3]	1.24 -0.65

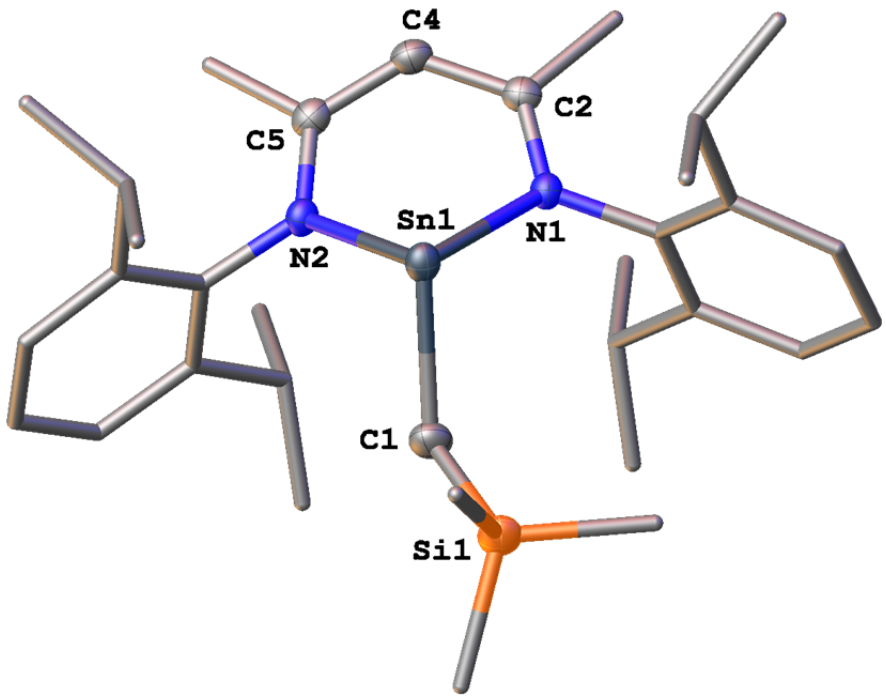

Figure 4 - 22: Molecular structure of compound **4-2**. Thermal ellipsoids are shown with 50% probability. H atoms are omitted for clarity.

Distances [Å]		Angles [°]	
Sn1 – C1	2.210(3)	Sn1 – C1 – Si1	115.43(15)
C1 – Si1	1.850(3)	N1 – Sn1 – N2	83.23(8)
Sn1 – N1	2.208(2)	C1 – Sn1 – N1	99.62(10)
Sn1 – N2	2.214(2)	C1 – Sn1 – N2	93.58(9)
Si1 – C31	1.860(3)	C1 – Si1 – C31	110.20(14)
Si1 – C32	1.870(4)	C1 – Si1 – C32	112.27(15)
Si1 – C33	1.872(4)	C1 – Si1 – C33	108.43(16)
N1 – C2	1.331(3)	Sn1 – N1 – C2	118.11(16)
N1 – C7	1.435(3)	Sn1 – N1 – C7	118.44(15)
N2 – C5	1.326(3)	Sn1 – N2 – C5	118.52(17)
N2 – C19	1.434(3)	Sn1 – N2 – C19	116.94(15)
C2 – C4	1.407(4)	N1 – C2 – C4	123.7(2)
C4 – C5	1.401(4)	N2 – C5 – C4	123.5(2)
		C2 – C4 – C5	128.8(3)
		C7 – N1 – C2	121.0(2)
		C5 – N2 – C19	122.2(2)

[CH(CNMe(dipp))$_2$]Ge–As(SiMe$_3$)$_2$ (4-3):

4-3 crystallizes from n-hexane at –30°C as clear orange plates.

Sum formula	$C_{35}H_{59}AsGeN_2Si_2$	
Molecular weight *M* [g/mol]	711.53	
Crystal system	orthorhombic	
Space group	Pbca	
Unit cell dimensions [Å] or [°]	11.05410(10)	90
	20.2900(2)	90
	33.9263(3)	90
Volume [Å^3]	7609.25(12)	
Formula units *Z*	8	
Temperature *T* [K]	123(2)	
Crystal size [mm^3]	0.2504 × 0.2085 × 0.1714	
Crystal density ρ_{calc} [Mg · m^{-3}]	1.242	
F(000)	3008.0	
Absorption coefficient $\mu_{Cu\text{-}K\alpha}$ [mm^{-1}]	2.834	
Transmission T_{min} / T_{max}	0.938/ 0.956	
Absorption correction	analytical	
Wavelength (λ) [Å]	1.54184 (CuK_α)	
Measured / independent reflections (R_{int})	54353/ 6722 (0.0273)	
Independent reflections [$I > 2\sigma(I)$]	6375	
Index ranges *hkl*	-13 ≤ *h* ≤ 13	
	-20 ≤ *k* ≤ 24	
	-40 ≤ *l* ≤ 40	
Measuring range θ_{min} / θ_{max} / θ_{full} [°]	4.358/ 66.747/ 66.747	
Completeness (θ_{full})	0.997	
Data / restraints / parameters	6722/0/ 386	
R-indices (all data)	0.0230/ 0.0545	
R-indices [$I > 2\sigma(I)$]	0.0213/ 0.0535	
Goodness-of-fit for S (F^2)	1.062	
Largest diff. peak and hole [e · Å^3]	0.316 -0.248	

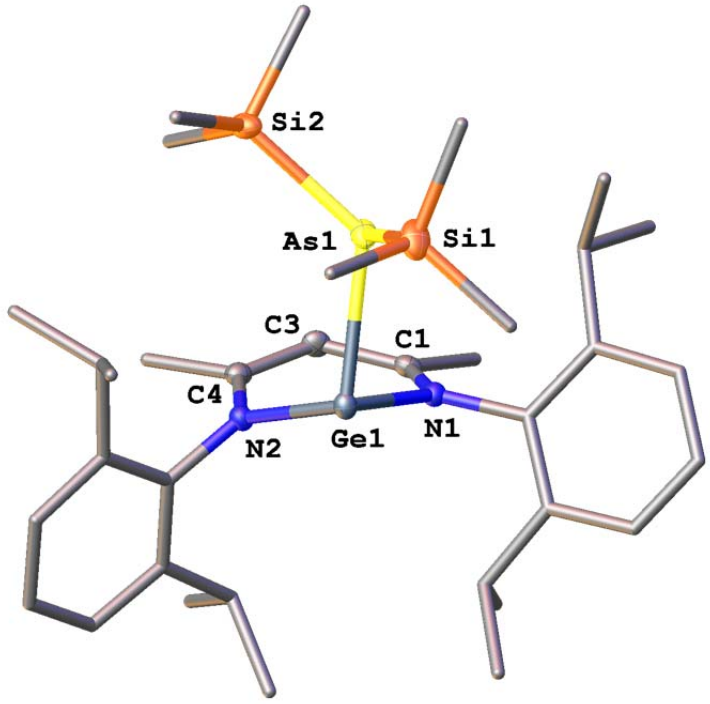

Figure 4 - 23: Molecular structure of compound **4-3**. Thermal ellipsoids are shown with 50% probability. H atoms are omitted for clarity

Distances [Å]		Angles [°]	
Ge1 – As1	2.5424(2)	Ge1 – As1 – Si1	96.396(13)
As1 – Si1	2.3388(5)	Ge1 – As1 – Si2	126.428(12)
As1 – Si2	2.3385(4)	Si1 – As1 – Si2	103.321(16)
Ge1 – N1	2.0556(11)	N1 – Ge1 – N2	90.48(5)
Ge1 – N2	1.9724(11)	As1 – Ge1 – N1	86.91(3)
N1 – C1	1.3184(18)	As1 – Ge1 – N2	104.31(3)
N1 – C6	1.4476(18)	As1 – Si1 – C30	108.16(6)
N2 – C4	1.4489(17)	As1 – Si1 – C31	107.92(7)
N2 – C18	1.3503(18)	As1 – Si1 – C32	117.60(6)
C1 – C3	1.415(2)	As1 – Si2 – C33	105.50(6)
C3 – C4	1.384(2)	As1 – Si2 – C34	118.21(5)
Si1 – C30	1.877(2)	As1 – Si2 – C35	109.36(6)
Si1 – C31	1.8733(19)	Ge1 – N1 – C1	122.62(9)
Si1 – C32	1.8668(19)	Ge1 – N1 – C6	113.48(8)
Si2 – C33	1.8767(16)	Ge1 – N2 – C4	122.36(9)
Si2 – C34	1.8750(16)	Ge1 – N2 – C18	118.57(9)
Si2 – C35	1.8699(17)	N1 – C1 – C3	122.86(12)
		N2 – C4 – C3	122.66(13)
		C1 – C3 – C4	127.13(13)
		C1 – N1 – C6	123.84(11)
		C4 – N2 – C18	119.00(11)

[CH(CNMe(dipp))$_2$]Sn–As(SiMe$_3$)$_2$ (4-4):

4-4 crystallizes from n-hexane at –30°C as dark red blocks.

Sum formula	$C_{39}H_{59}AsSnN_2Si_2$
Molecular weight *M* [g/mol]	757.63
Crystal system	triclinic
Space group	P-1
Unit cell dimensions [Å] or [°]	9.5581(2) 89.533(2)
	10.1755(2) 89.4200(10)
	21.0618(4) 70.134(2)
Volume [Å^3]	1926.41(7)
Formula units *Z*	2
Temperature *T* [K]	122.99(10)
Crystal size [mm^3]	0.0747 × 0.0955 × 0.147
Crystal density ρ_{calc} [Mg · m^{-3}]	1.306
F(000)	788.0
Absorption coefficient $\mu_{Cu\text{-}K\alpha}$ [mm^{-1}]	6.993
Transmission T_{min} / T_{max}	0.498/ 0.674
Absorption correction	gaussian
Wavelength (λ) [Å]	1.54184 (CuK_α)
Measured / independent reflections (R_{int})	52876/ 7740 (0.0858)
Independent reflections [$I > 2\sigma(I)$]	7479
Index ranges *hkl*	$-11 \le h \le 11$
	$-12 \le k \le 12$
	$-26 \le l \le 26$
Measuring range θ_{min} / θ_{max} / θ_{full} [°]	4.198/ 74.344/ 67.684
Completeness (θ_{full})	0.999
Data / restraints / parameters	7740/0/386
R-indices (all data)	0.0279/ 0.0676
R-indices [$I > 2\sigma(I)$]	0.0268/ 0.0671
Goodness-of-fit for S (F^2)	1.072
Largest diff. peak and hole [e · Å^3]	1.67 -1.07

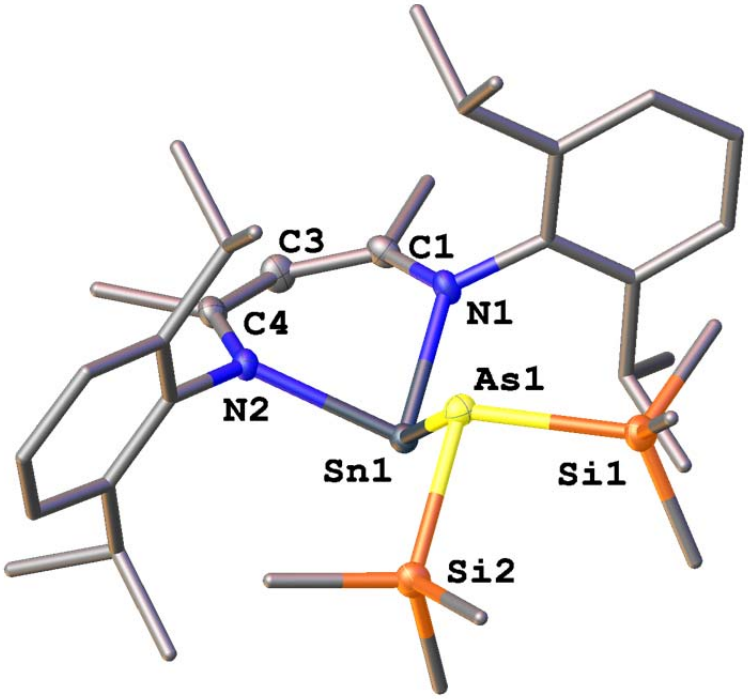

Figure 4 - 24: Molecular structure of compound **4-4**. Thermal ellipsoids are shown with 50% probability. H atoms are omitted for clarity.

Distances [Å]		Angles [°]	
Sn1 – As1	2.7256(3)	Sn1 – As1 – Si1	109.47(2)
As1 – Si1	2.3537(8)	Sn1 – As1 – Si2	94.98(2)
As1 – Si2	2.3618(8)	Si1 – As1 – Si2	96.41(3)
Sn1 – N1	2.213(2)	N1 – Sn1 – N2	83.22(8)
Sn1 – N2	2.251(2)	As1 – Sn1 – N1	102.16(6)
N1 – C1	1.336(3)	As1 – Sn1 – N2	97.20(5)
N1 – C6	1.438(3)	As1 – Si1 – C30	111.51(11)
N2 – C4	1.325(3)	As1 – Si1 – C31	116.50(11)
N2 – C18	1.442(3)	As1 – Si1 – C32	106.36(11)
C1 – C3	1.389(4)	As1 – Si2 – C33	115.61(10)
C3 – C4	1.404(4)	As1 – Si2 – C34	111.41(11)
Si1 – C30	1.868(3)	As1 – Si2 – C35	108.10(11)
Si1 – C31	1.874(3)	Sn1 – N1 – C1	116.14(18)
Si1 – C32	1.874(3)	Sn1 – N1 – C6	124.64(16)
Si2 – C33	1.884(3)	Sn1 – N2 – C4	116.98(16)
Si2 – C34	1.881(3)	Sn1 – N2 – C18	121.82(16)
Si2 – C35	1.866(3)	N1 – C1 – C3	124.1(2)
		N2 – C4 – C3	124.2(2)
		C1 – C3 – C4	128.5(2)
		C1 – N1 – C6	117.3(2)
		C4 – N2 – C18	118.6(2)

Nanoparticles studies

[CH(CNMe(dipp))$_2$]Ge–P(SiMe$_3$)$_2$ (4-D):

4-D and different stoichiometries of stabilizers were mixed in 3 mL of mesitylene. The mixtures were dipped into a 150°C oil bath and heated for either 24 h or 1 h. Grids for TEM analyses were prepared from the reaction solutions. The obtained particles were precipitated and washed twice with ethanol. Samples for EDX and XRD analyses were prepared from the washed and dried solid.

Table 4 - 6: Amounts of **4-D** and stabilizers used in the 24 h reactions as well as the achieved yields and the observed color changes.

24 h	**Ia**		**IIa**		**IIIa**		**IVa**		**V**		
	1 eq. HDA		0.5 eq. HDA		1 eq. PA		0.5 eq. PA		0.5 eq. HDA + 0.5 eq. PA		
	4-D	HDA	**4-D**	HDA	**4-D**	PA	**4-D**	PA	**4-D**	HDA	PA
m [mg]	69.9	24.9	70.1	13.2	70.1	27.1	69.9	14	69.9	13.9	14
n [mmol]	0.1	0.1	0.1	0.05	0.1	0.1	0.1	0.05	0.1	0.05	0.05
Yield [mg]	10.4		10.4		10.1		11.3		11.6		
Color (start)	Clear orange		Clear orange		Clear orange		Clear orange		Clear orange		
Color (end)	Dark brown Brown precipitate		Dark brown Brown precipitate		Dark brown Brown precipitate		Dark brown Brown precipitate		Dark red		

Table 4 - 7: Amounts of **4-D** and stabilizers used in the 1 h reactions as well as the achieved yields and the observed color changes.

1 h	**Ib**		**IIb**		**IIIb**		**IVb**	
	1 eq. HDA		0.5 eq. HDA		1 eq. PA		0.5 eq. PA	
	4-D	HDA	**4-D**	HDA	**4-D**	PA	**4-D**	PA
m [mg]	70.2	25.2	70.2	13.3	70.2	27.0	69.9	14
n [mmol]	0.1	0.1	0.1	0.05	0.1	0.1	0.1	0.05
Yield [mg]	4.0		2.8		2.9		–	
Color (start)	Clear orange		Clear orange		Clear orange		Clear orange	
Color (end)	Dark reddish brown		Dark reddish brown		Dark red		Dark red	

Ia

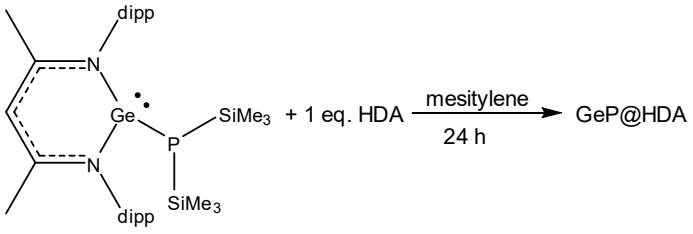

4-D

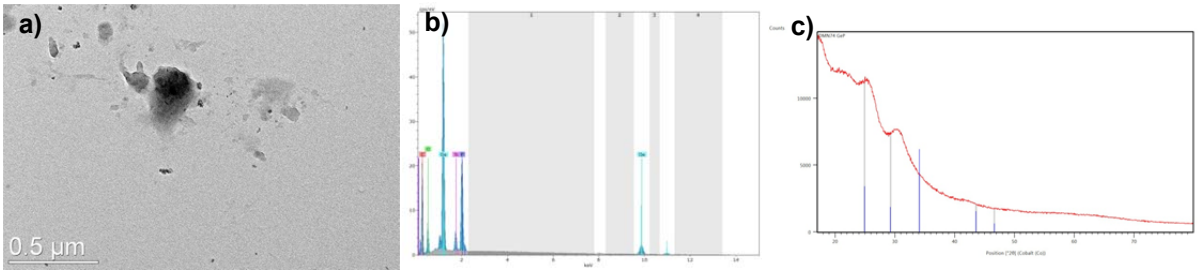

Figure 4 - 25: a) TEM image; b) EDX spectrum; c) XRD diffractogram of the reaction **Ia**.

Composition	
EDX	Ge_4P_3
XRD	amorphous

Ib

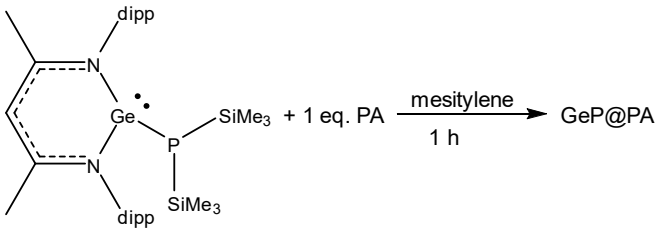

4-D

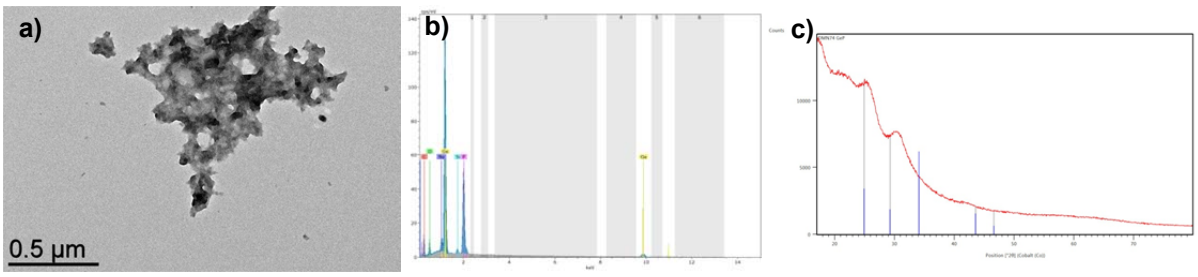

Figure 4 - 26: a) TEM image; b) EDX spectrum; c) XRD diffractogram of the reaction **Ib**.

Composition	
EDX	Ge_4P_3
XRD	amorphous

IIa

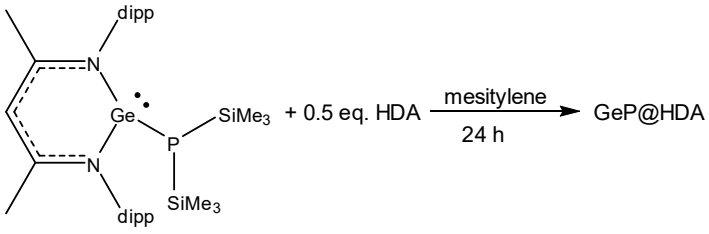

4-D

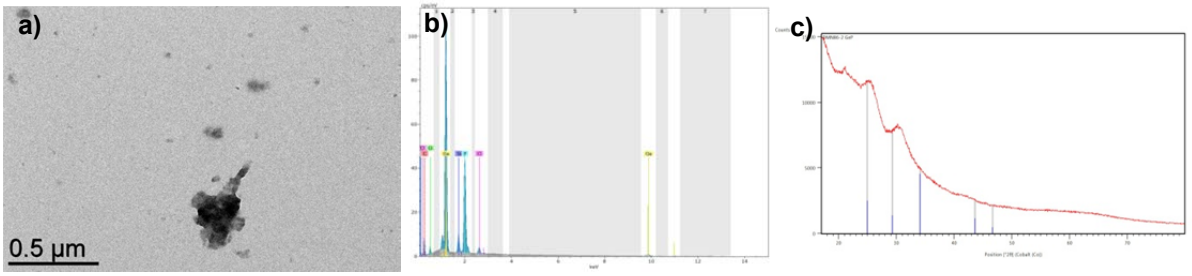

Figure 4 - 27: a) TEM image; b) EDX spectrum; c) XRD diffractogram of the reaction **IIa**. The EDX spectrum shows some slight impurities of chlorine, which are caused by traces of **4-A**.

Composition	
EDX	GeP
XRD	amorphous

IIb

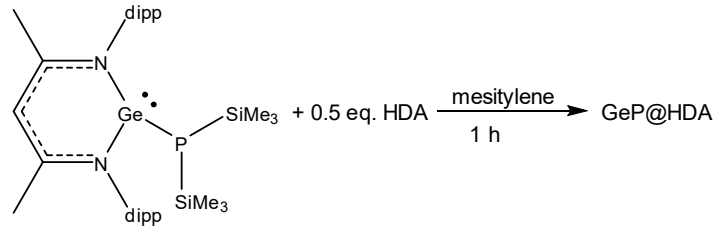

4-D

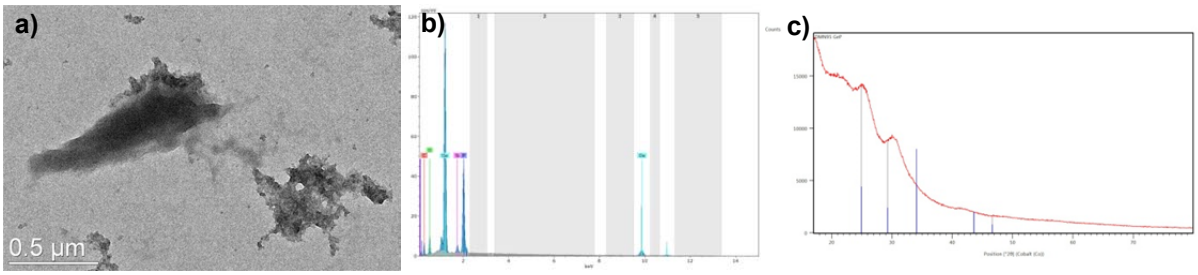

Figure 4 - 28: a) TEM image; b) EDX spectrum; c) XRD diffractogram of the reaction **IIb**.

Composition	
EDX	Ge_4P_3
XRD	amorphous

IIIa

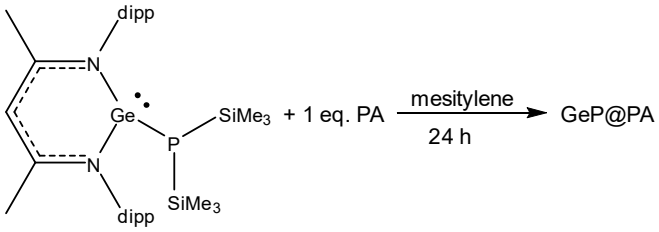

4-D

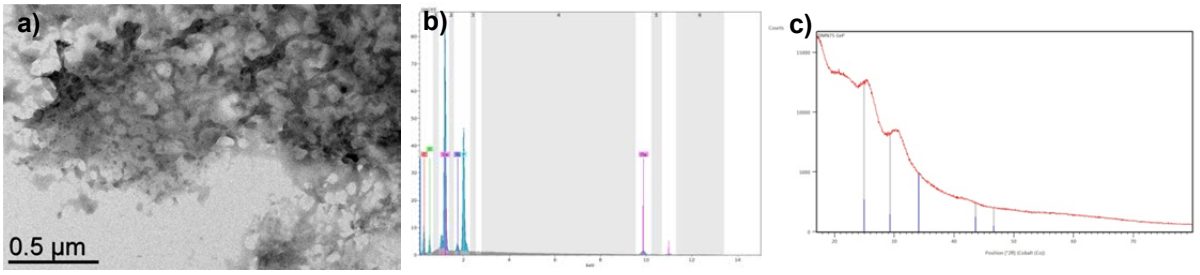

Figure 4 - 29: a) TEM image; b) EDX spectrum; c) XRD diffractogram of the reaction **IIIa**.

Composition	
EDX	GeP
XRD	amorphous

IIIb

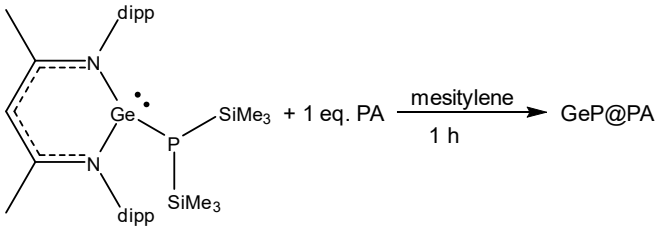

4-D

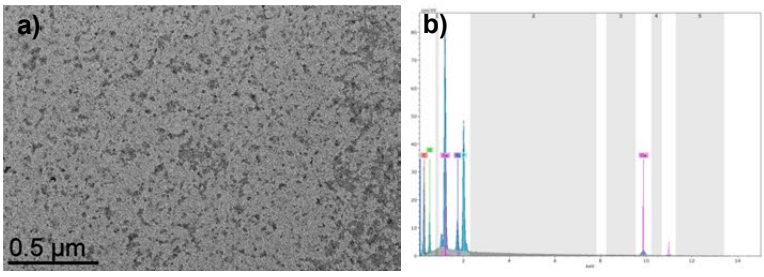

Figure 4 - 30: a) TEM image; b) EDX spectrum of the reaction **IIIb**. No XRD analysis was performed.

Composition	
EDX	GeP
XRD	–

IVa

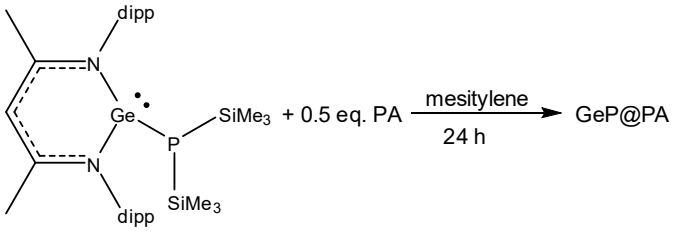

4-D

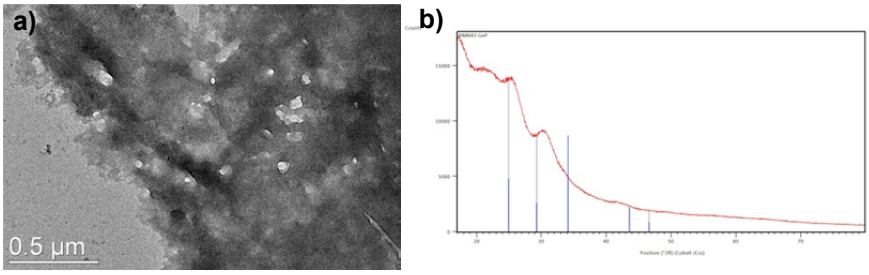

Figure 4 - 31: a) TEM image; b) XRD diffractogram of the reaction **IIIa**.

Composition	
EDX	GeP with an excess of Ge
XRD	amorphous

IVb

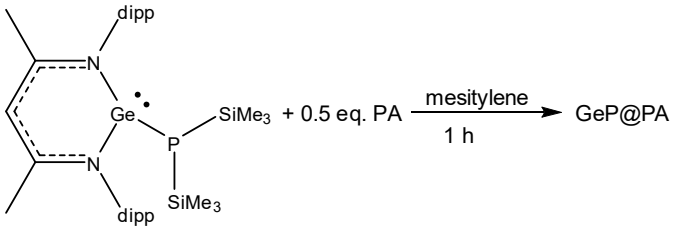

4-D

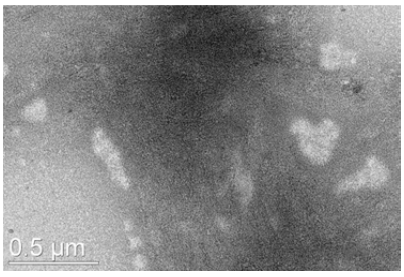

Figure 4 - 32: TEM image of the reaction **IVb**.

Composition	
EDX	GeP with an excess of Ge
XRD	–

Due to the very small yield, only a EDX analysis was carried out.

V

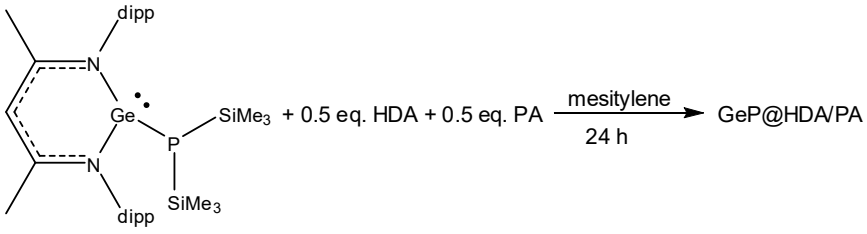

4-D

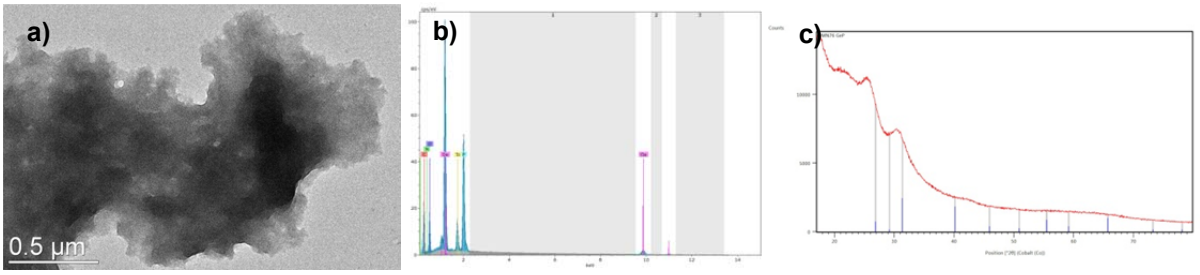

Figure 4 - 33: a) TEM image; b) EDX spectrum; c) XRD diffractogram of the reaction **V**.

Composition	
EDX	GeP
XRD	amorphous

[CH(CNMe(dipp))$_2$]Sn–P(SiMe$_3$)$_2$ (4-E):

As well as **4-D** also **4-E** was mixed with different stoichiometries of stabilizers in 3 mL of mesitylene, dipped into a 150°C oil bath and heated for either 24 h or 1 h. Grids for TEM analyses were prepared from the reaction solutions. The obtained particles were precipitated and washed twice with ethanol. Samples for EDX and XRD analyses were prepared from the washed and dried solid.

Table 4 - 8: Amounts of **4-E** and stabilizers used in the 24 h reactions as well as the achieved yields and the observed color changes.

24 h	**VIa**		**VIIa**		**VIIIa**		**IX**		**X**		
	1 eq. HDA		0.5 eq. HDA		1 eq. PA		0.5 eq. PA		0.5 eq. HDA + 0.5 eq. PA		
	4-E	HDA	**4-E**	HDA	**4-E**	PA	**4-E**	PA	**4-E**	HDA	PA
m [mg]	69.9	24.0	70.0	12.1	69.9	25.0	70.3	12.9	70.1	12.1	13.0
n [mmol]	0.1	0.1	0.1	0.05	0.1	0.1	0.1	0.05	0.1	0.05	0.05
Yield [mg]	–		8.5		5.8		7.8		4.0		
Color (start)	Clear yellow		Clear yellow		Clear yellow		Clear yellow		Clear yellow		
Color (end)	Colorless Black precipitate		Cloudy black		Colorless Black precipitate		Colorless Black precipitate		Cloudy black		

Table 4 - 9: Amounts of **4-E** and stabilizers used in the 1 h reactions as well as the achieved yields and the observed color changes.

1 h	**VIb**		**VIIb**		**VIIIb**	
	1 eq. HDA		0.5 eq. HDA		1 eq. PA	
	4-E	HDA	**4-E**	HDA	**4-E**	PA
m [mg]	69.9	23.9	69.8	12.1	70.1	24.9
n [mmol]	0.1	0.1	0.1	0.05	0.1	0.1
Yield [mg]	7.5		3.1		9.0	
Color (start)	Clear yellow		Clear yellow		Clear yellow	
Color (end)	Cloudy black		Cloudy black		Cloudy black	

VIa

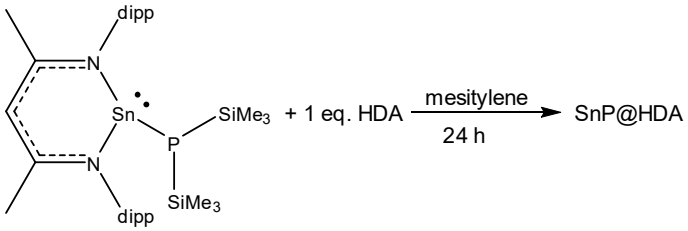

4-E

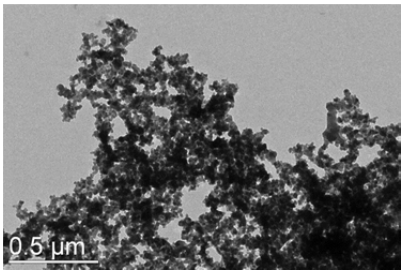

Figure 4 - 34: TEM image of the reaction **VIa**. No further analysis has been carried out. The particles show an average size of 14 nm.

VIb

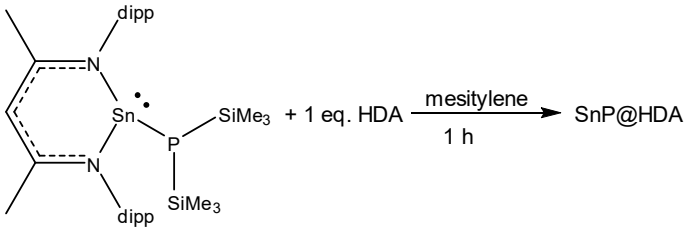

4-E

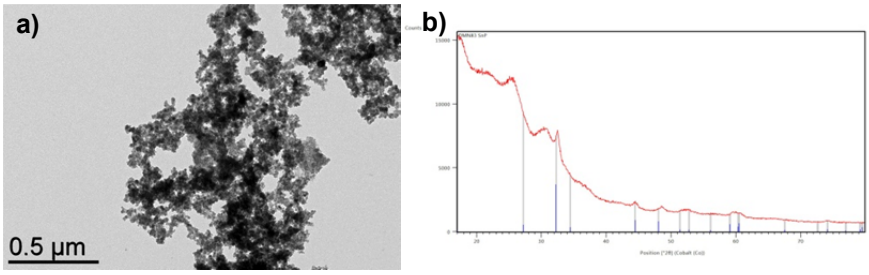

Figure 4 - 35: a) TEM image; b) XRD diffractogram of the reaction **VIb**. The particles show an average size of 22 nm.

Composition	
EDX	Sn:P = 12:1
XRD	SnP

VIIa

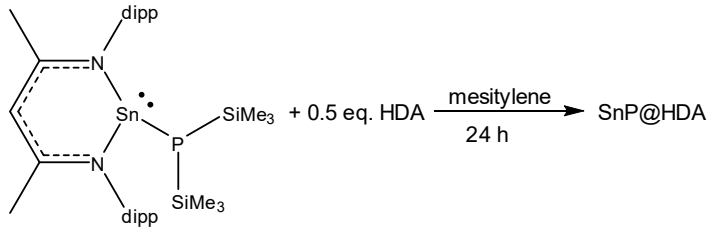

4-E

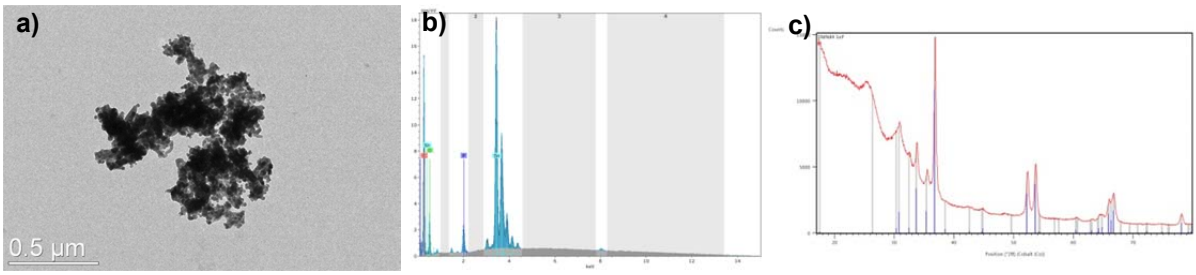

Figure 4 - 36: a) TEM image; b) EDX spectrum; c) XRD diffractogram of the reaction **VIIa**. The average size of the particles is about 19 nm.

Composition	
EDX	Sn_4P_3
XRD	Sn_4P_3

VIIb

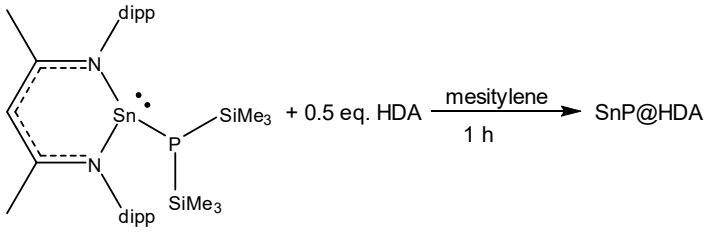

4-E

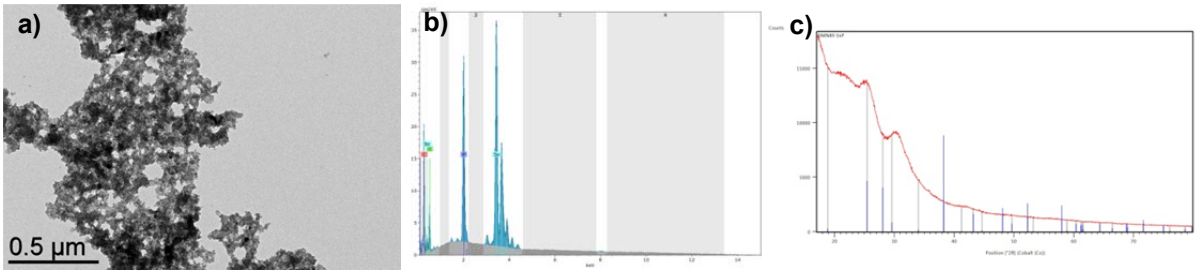

Figure 4 - 37: a) TEM image; b) EDX spectrum; c) XRD diffractogram of the reaction **VIIb**. The average size of the particles is about 22 nm.

Composition	
EDX	Sn_4P_3
XRD	amorphous

VIIIa

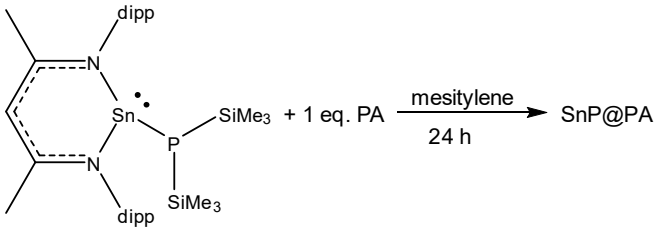

4-E

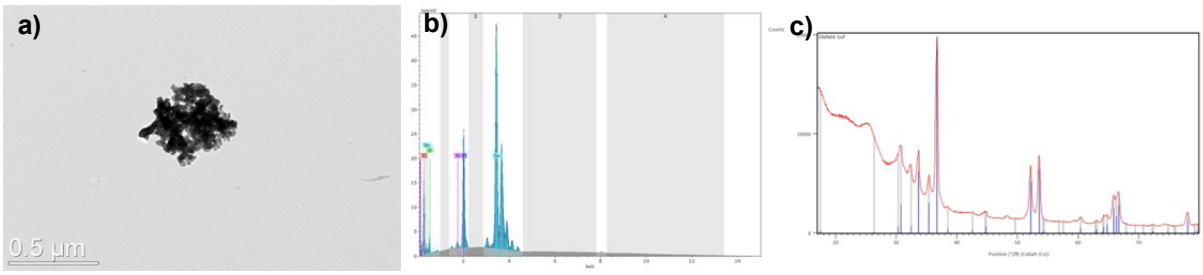

Figure 4 - 38: a) TEM image; b) EDX spectrum; c) XRD diffractogram of the reaction **VIIIa**. The average size of the particles is about 17 nm.

Composition	
EDX	Sn_4P_3
XRD	Sn_4P_3

VIIIb

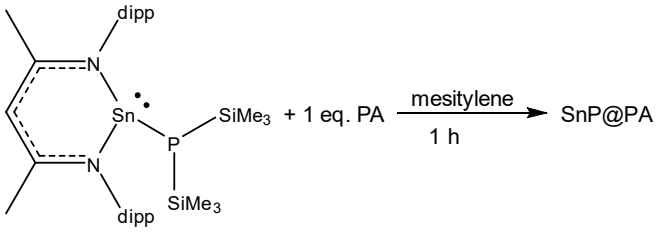

4-E

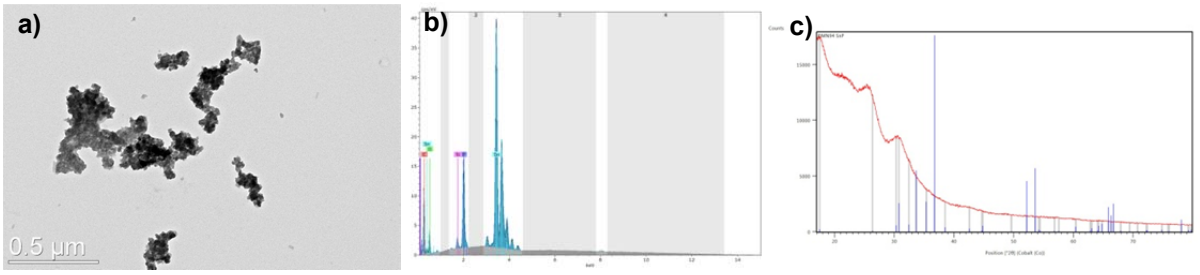

Figure 4 - 39: a) TEM image; b) EDX spectrum; c) XRD diffractogram of the reaction **VIIIb**. The particles display an average size of 10 nm.

Composition	
EDX	Sn_4P_3
XRD	amorphous

IX

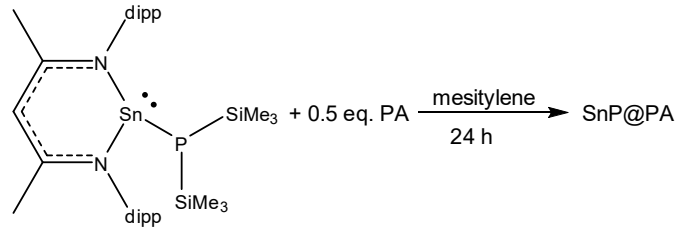

4-E

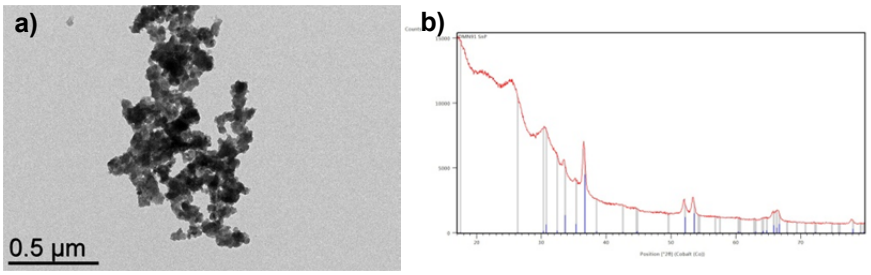

Figure 4 - 40: a) TEM image; b) XRD diffractogram of the reaction **IX**. The particles have an average size of 12 nm.

Composition	
EDX	Sn_4P_3
XRD	Sn_4P_3

X

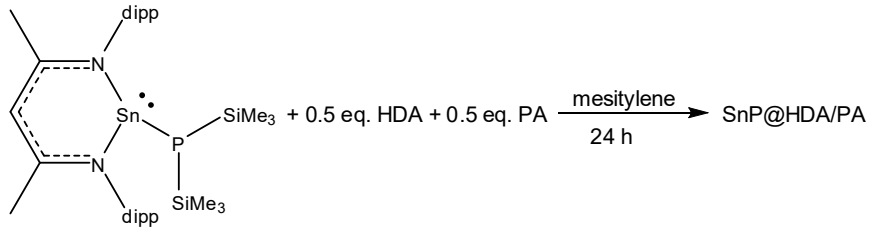

4-E

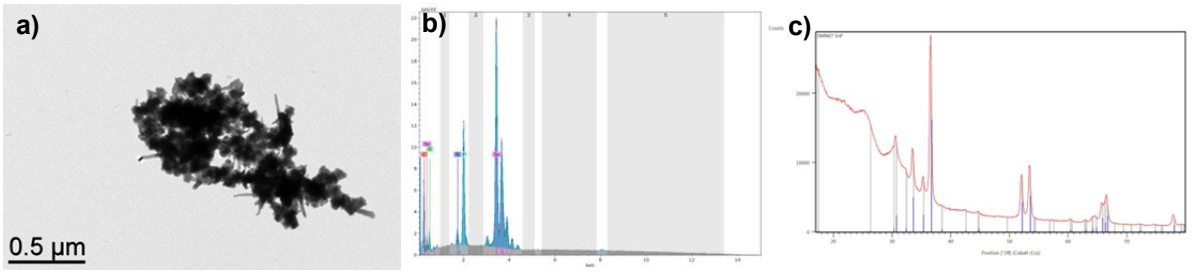

Figure 4 - 41: a) TEM image; b) EDX spectrum; c) XRD diffractogram of the reaction **X**. The average particle size is about 30 nm.

Composition	
EDX	Sn_4P_3
XRD	Sn_4P_3

Due to the promising results of the first orienting studies of **4-E**, further experiments with higher amounts of stabilizers were done in order to separate the agglomerated particles. These reactions were carried out in the same way as the previously described studies.

Table 4 - 10: Amounts of **4-E** and stabilizers used in the 24 h reactions as well as the observed color changes.

24 h	**XIa**		**XIIa**		**XIIIa**	
	5 eq. HDA		10 eq. HDA		10 eq. PA	
	4-E	HDA	**4-E**	HDA	**4-E**	PA
m [mg]	70.1	118.7	70.1	237.0	70.0	251.4
n [mmol]	0.1	0.5	0.1	1.0	0.1	1.0
Color (start)	Clear yellow		Clear yellow		Clear yellow	
Color (end)	Colorless Black precipitate		Colorless Black precipitate		Colorless Black precipitate	

Table 4 - 11: Amounts of **4-E** and stabilizers used in the 1 h reactions as well as the observed color changes.

1 h	**XIb**		**XIIb**		**XIIIb**	
	5 eq. HDA		10 eq. HDA		10 eq. PA	
	4-E	HDA	**4-E**	HDA	**4-E**	PA
m [mg]	70.3	118.5	69.9	236.5	70.1	251.7
n [mmol]	0.1	0.5	0.1	1.0	0.1	1.0
Color (start)	Clear yellow		Clear yellow		Clear yellow	
Color (end)	Cloudy black		Cloudy black		Cloudy black	

XIa

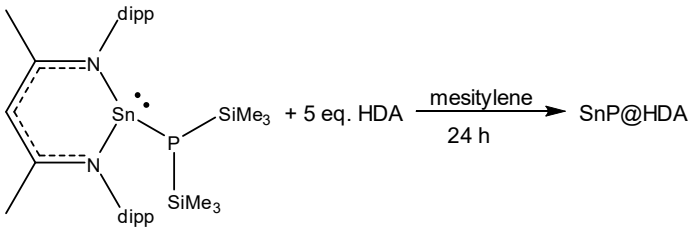

4-E

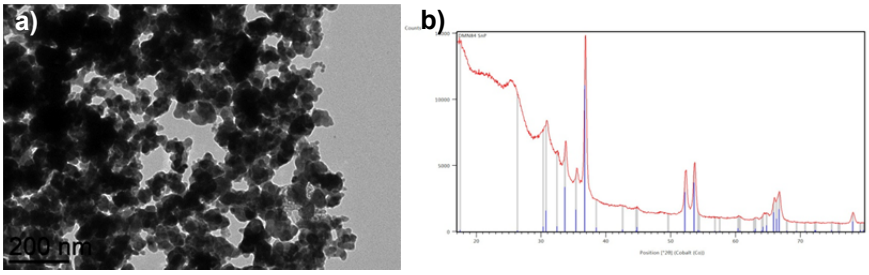

Figure 4 - 42: a) TEM image; b) XRD diffractogram of the reaction **XIa**. The average size of the particles is about 20 nm.

Composition	
EDX	–
XRD	Sn_4P_3

XIb

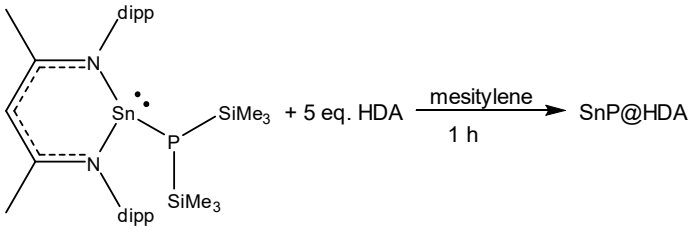

4-E

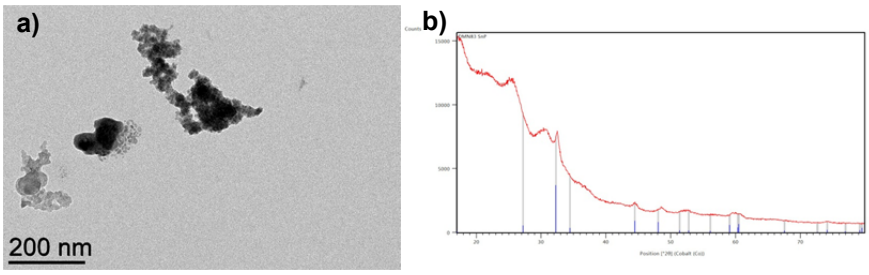

Figure 4 - 43: a) TEM image; b) XRD diffractogram of the reaction **XIb**. The particles have an average size of 13 nm.

Composition	
EDX	–
XRD	SnP

XIIa

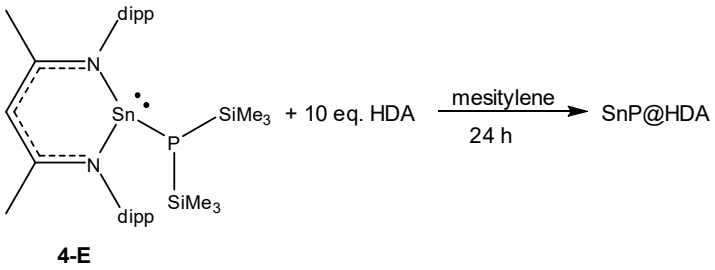

4-E

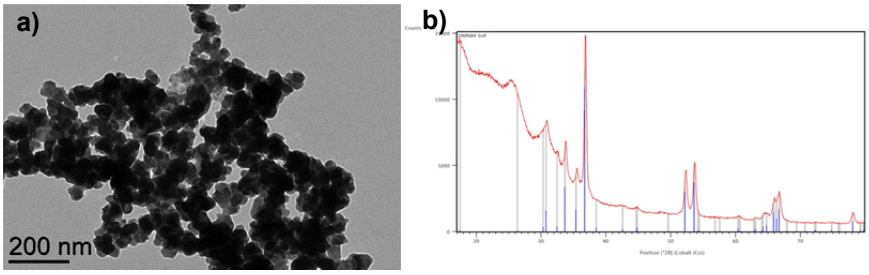

Figure 4 - 44: a) TEM image; b) XRD diffractogram of the reaction **XIIa**. The particles show an average size of 35 nm.

Composition	
EDX	–
XRD	Sn_4P_3

XIIb

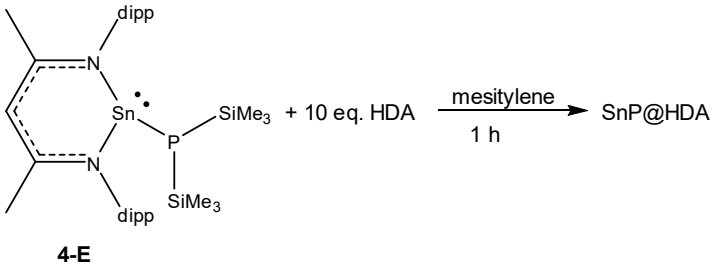

4-E

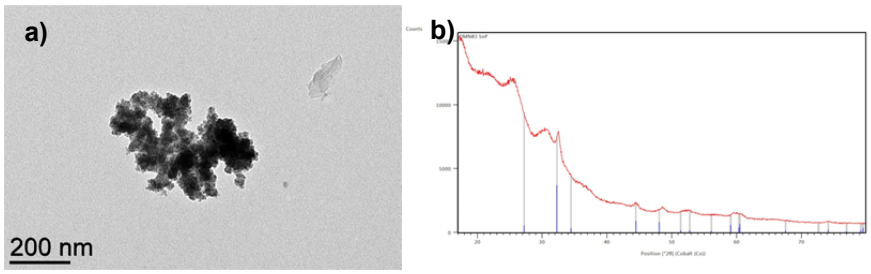

Figure 4 - 45: a) TEM image; b) XRD diffractogram of the reaction **XIIb**. The particles exhibit an average size of 18 nm.

Composition	
EDX	–
XRD	SnP

XIIIa

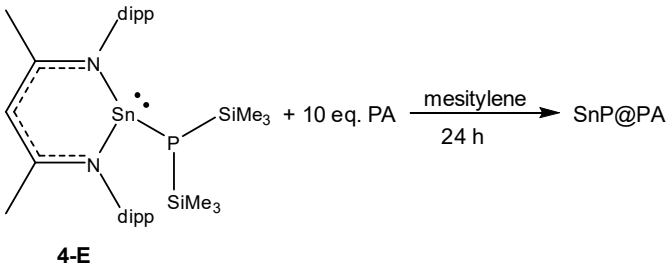

4-E

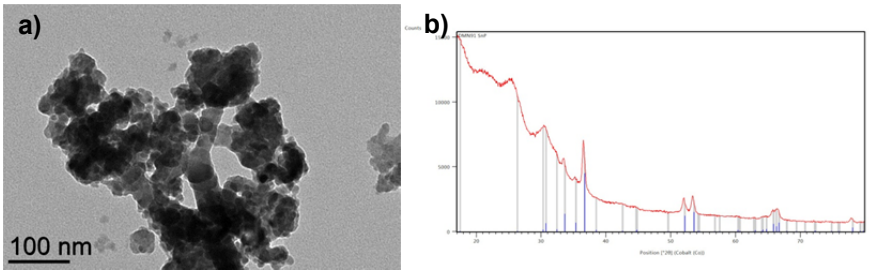

Figure 4 - 46: a) TEM image; b) XRD diffractogram of the reaction **XIIIa**. The particles exhibit an average size of 12 nm.

Composition	
EDX	–
XRD	Sn_4P_3

XIIIb

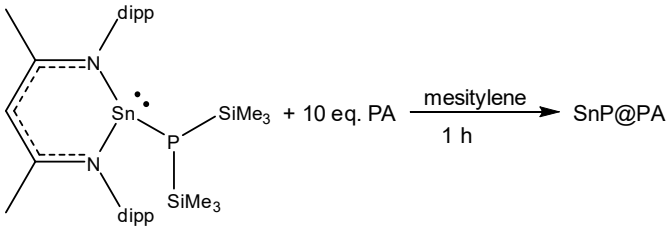

4-E

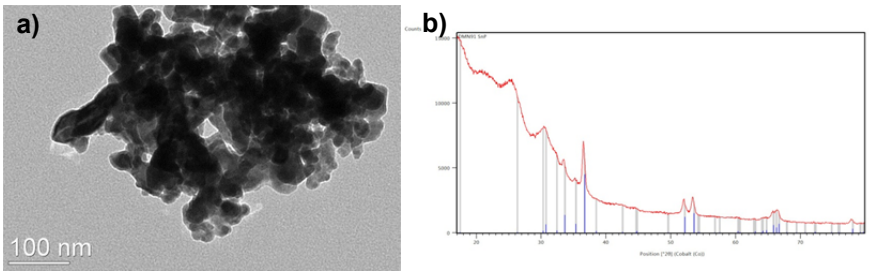

Figure 4 - 47: a) TEM image; b) XRD diffractogram of the reaction **XIIIb**. The average size of the particles is about 18 nm.

Composition	
EDX	–
XRD	Sn_4P_3

[CH(CNMe(dipp))$_2$]Sn–As(SiMe$_3$)$_2$ (4-4):

Also in case of **4-4** reaction mixtures of compound **4-4** and different stoichiometries of stabilizers were dissolved in 3 mL of mesitylene, dipped into a 150°C oil bath and heated for either 24 h or 1 h. Grids for TEM analyses were prepared from the reaction solutions. The obtained particles were precipitated and washed twice with ethanol. Samples for EDX and XRD analyses were prepared from the washed and dried solids.

Table 4 - 12: Amounts of **4-4** and stabilizers used in the 24 h reactions as well as the achieved yields and the observed color changes.

24 h	**IVXa**		**XVa**		**XVIa**		**XVII**		**XVIII**		
	1 eq. HDA		0.5 eq. HDA		1 eq. PA		0.5 eq. PA		0.5 eq. HDA + 0.5 eq. PA		
	4-4	HDA	**4-4**	HDA	**4-4**	PA	**4-4**	PA	**4-4**	HDA	PA
m [mg]	70.0	21.9	70.2	11.1	70.1	23.8	70.1	11.9	70.1	11.0	12.1
n [mmol]	0.1	0.1	0.1	0.05	0.1	0.1	0.1	0.05	0.1	0.05	0.05
Yield [mg]	6.0		–		–		–		–		
Color (start)	Clear red		Clear red		Clear red		Clear red		Clear red		
Color (end)	Colorless Black precipitate		Colorless Tin mirror Metallic precipitate		Colorless Tin mirror Metallic precipitate		Colorless Tin mirror Metallic precipitate		Colorless Tin mirror Metallic precipitate		

If a tin mirror or a spherical metallic precipitate was obtained from the experiments, only a TEM analysis has been carried out.

Table 4 - 13: Amounts of **4-4** and stabilizers used in the 1 h reactions as well as the achieved yields and the observed color changes.

1 h	**IVXb**		**XVb**		**XVIb**	
	1 eq. HDA		0.5 eq. HDA		1 eq. PA	
	4-4	HDA	**4-4**	HDA	**4-4**	PA
m [mg]	69.9	22.0	70.3	11.0	70.0	24.0
n [mmol]	0.1	0.1	0.1	0.05	0.1	0.1
Yield [mg]	5.8		13.4		19.8	
Color (start)	Clear red		Clear red		Clear red	
Color (end)	Cloudy black		Cloudy black		Cloudy black	

IVXa

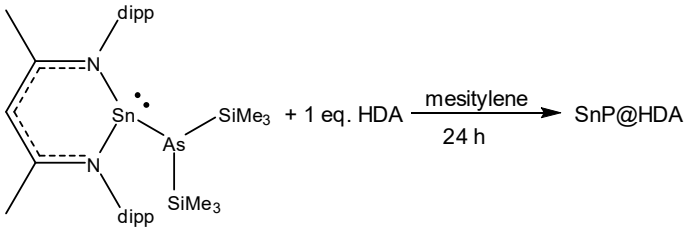

4-4

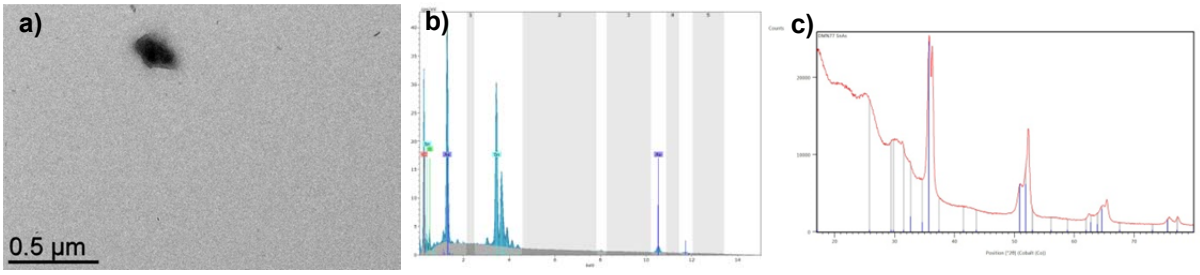

Figure 4 - 48: a) TEM image; b) EDX spectrum; c) XRD diffractogram of the reaction **IVXa**.

Composition	
EDX	Sn_4As_3
XRD	Sn_4As_3/SnAs

IVXb

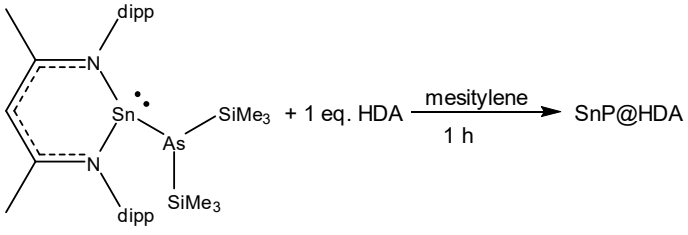

4-4

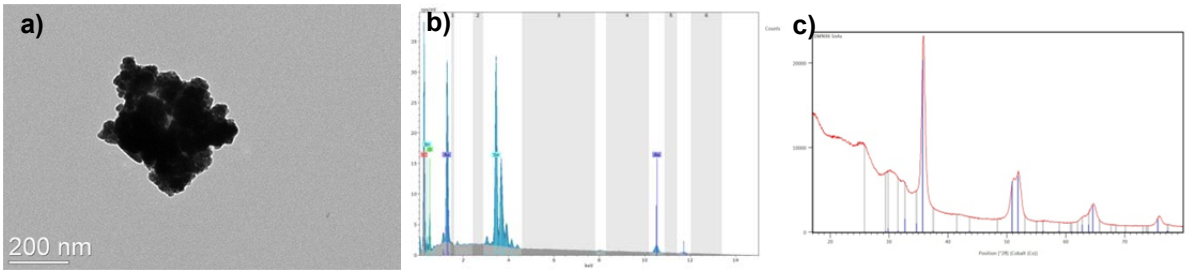

Figure 4 - 49: a) TEM image; b) EDX spectrum; c) XRD diffractogram of the reaction **IVXb**. The average size of the particles is about 10 nm.

Composition	
EDX	Sn_4As_3
XRD	Sn_4As_3

XVa

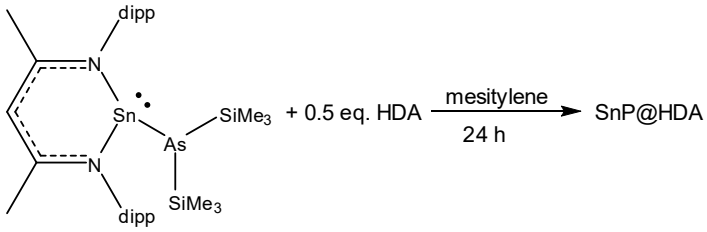

4-4

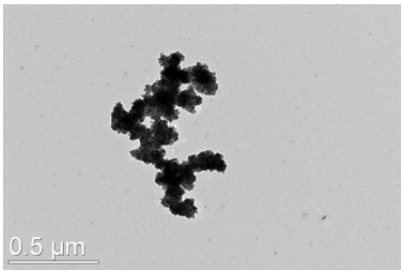

Figure 4 - 50: TEM image of the reaction **XVa**. The size of the particles is about 6 nm.

XVb

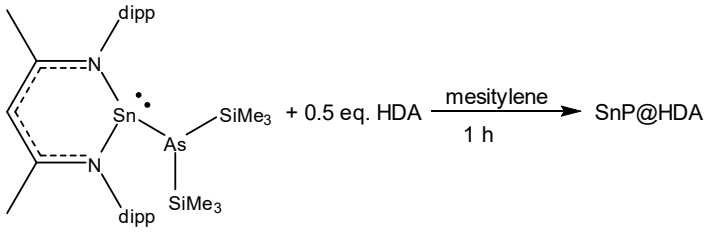

4-4

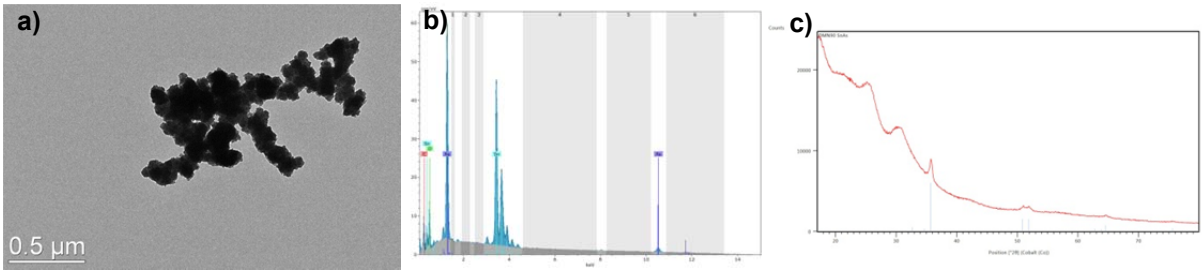

Figure 4 - 51: a) TEM image; b) EDX spectrum; c) XRD diffractogram of the reaction **IVXb**. The average size of the particles is about 10 nm.

Composition	
EDX	Sn_4As_3
XRD	SnAs

XVIa

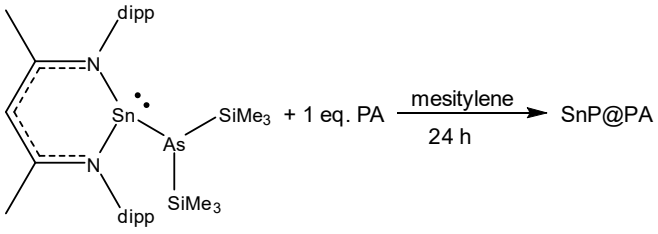

4-4

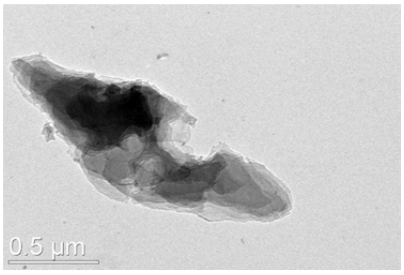

Figure 4 - 52: TEM image of the reaction **XVIa**.

XVIb

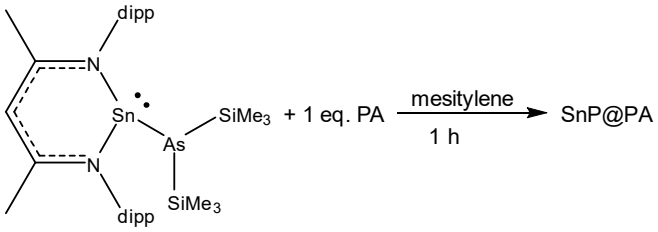

4-4

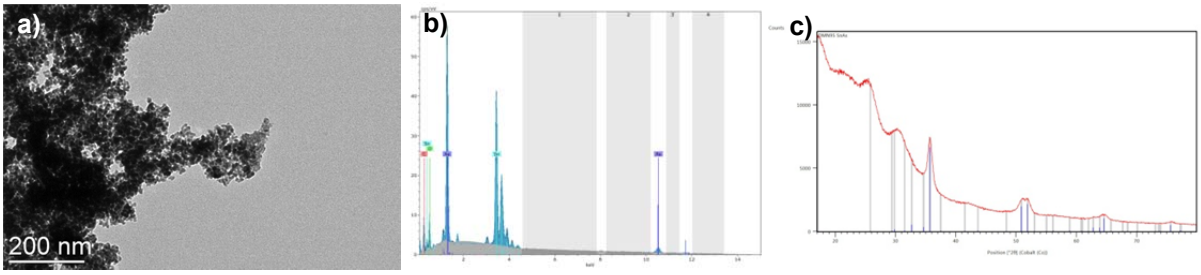

Figure 4 - 53: a) TEM image; b) EDX spectrum; c) XRD diffractogram of the reaction **XVIb**. The average size of the particles is about 10 nm.

Composition	
EDX	Sn_4As_3
XRD	Sn_4As_3

XVII

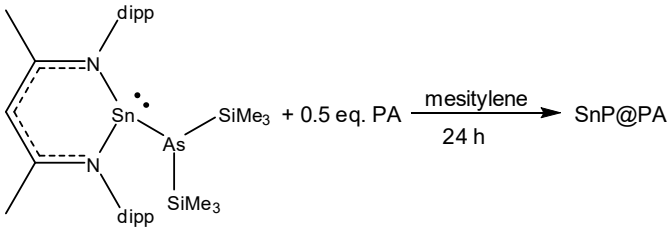

4-4

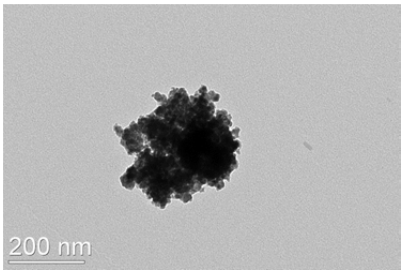

Figure 4 - 54: TEM image of the reaction **XVII**. The particles display an average size of 14 nm.

XVIII

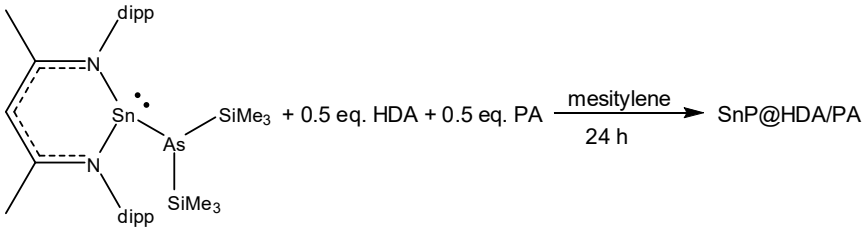

4-4

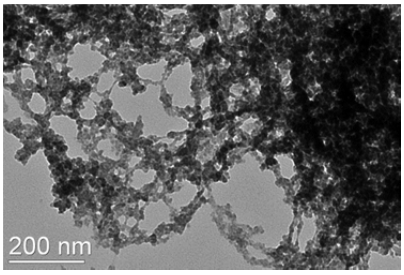

Figure 4 - 55: TEM image of the reaction **XVIII**. The particles display an average size of 10 nm.

Analogous to **4-E** also for **4-4** further experiments with higher amounts of stabilizers were performed to separate the agglomerated particles. Again the reactions were done like the previously described studies.

Table 4 - 14: Amounts of **4-4** and stabilizers used in the 24 h reactions as well as the observed color changes.

24 h	**IXXa**		**XXa**		**XXIa**	
	5 eq. HDA		10 eq. HDA		10 eq. PA	
	4-4	HDA	**4-4**	HDA	**4-4**	PA
m [mg]	70.3	111.2	70.2	223.3	69.8	237.0
n [mmol]	0.1	0.5	0.1	1.0	0.1	1.0
Color (start)	Clear red		Clear red		Clear red	
Color (end)	Colorless Black precipitate		Colorless Black precipitate		Colorless Black precipitate	

Table 4 - 15: Amounts of **4-4** and stabilizers used in the 1 h reactions as well as the observed color changes.

1 h	**IXXb**		**XXb**		**XXIb**	
	5 eq. HDA		10 eq. HDA		10 eq. PA	
	4-4	HDA	**4-4**	HDA	**4-4**	PA
m [mg]	69.8	111.5	70.0	222.9	70.1	237.2
n [mmol]	0.1	0.5	0.1	1.0	0.1	1.0
Color (start)	Clear red		Clear red		Clear red	
Color (end)	Cloudy black		Cloudy black		Cloudy black	

XXa

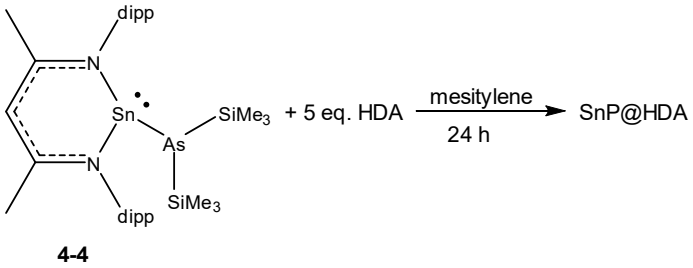

4-4

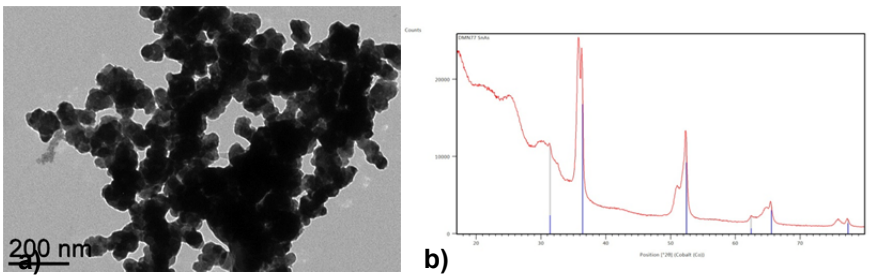

Figure 4 - 56: a) TEM image; b) XRD diffractogram of the reaction **IXXa**. The average size of the particles is about 35 nm.

Composition	
EDX	–
XRD	Sn_4As_3/SnAs

IXXb

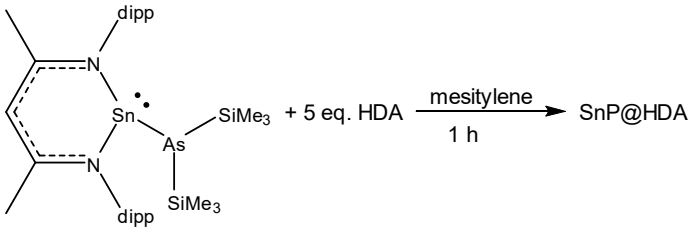

4-4

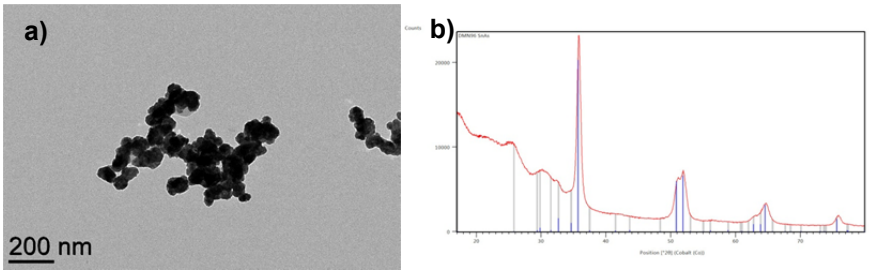

Figure 4 - 57: a) TEM image; b) XRD diffractogram of the reaction **IXXb**. The average size of the particles is about 24 nm.

Composition	
EDX	–
XRD	Sn_4As_3

XXa

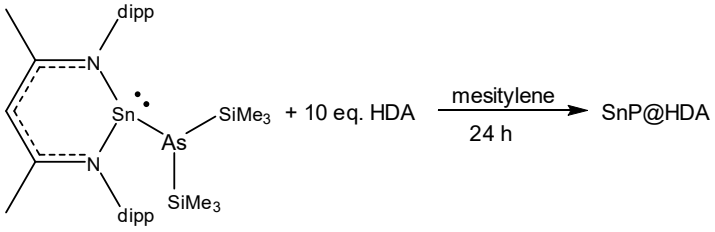

4

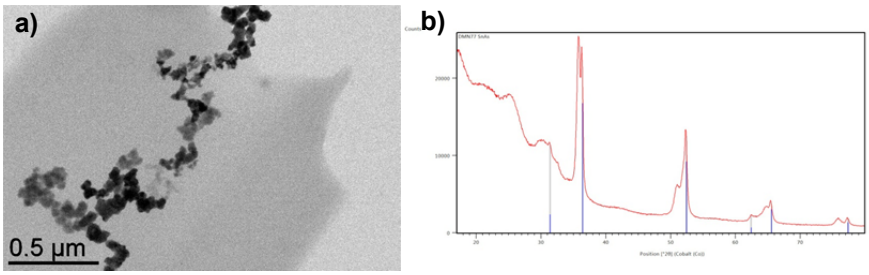

Figure 1: a) TEM image; b) XRD diffractogram of the reaction **IXXb**. The average size of the particles is about 33 nm.

Composition	
EDX	–
XRD	Sn_4As_3/SnAs

XXb

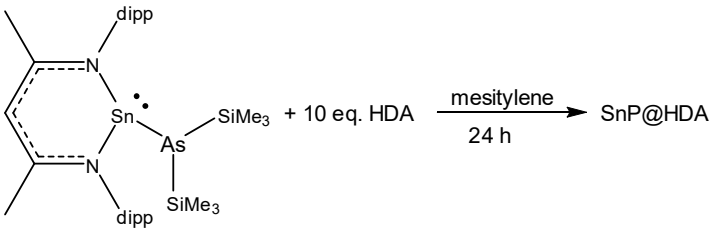

4-4

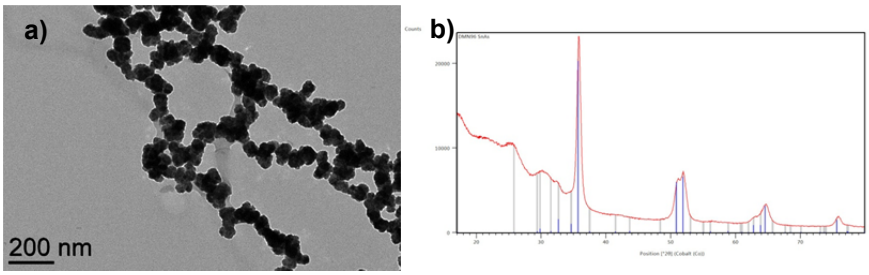

Figure 4 - 58: a) TEM image; b) XRD diffractogram of the reaction **XXb**. The average size of the particles is about 38 nm.

Composition	
EDX	–
XRD	Sn_4As_3

XXIa

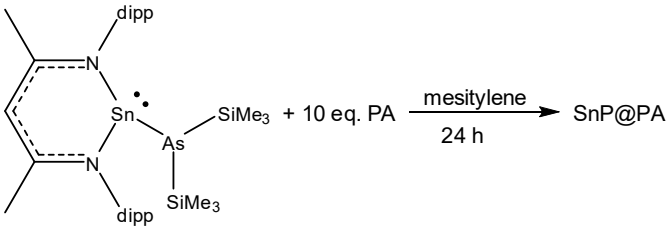

4-4

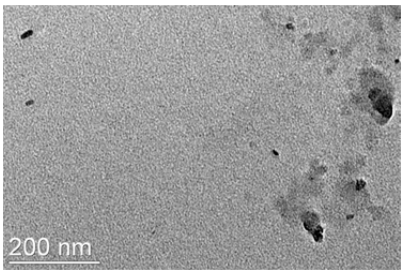

Figure 4 - 59: TEM image of the reaction **XXIa**.

XXIb

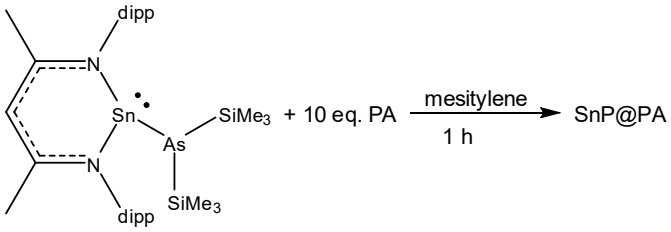

4-4

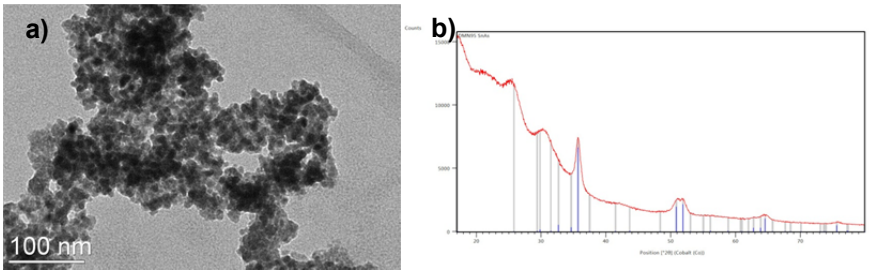

Figure 4 - 60: a) TEM image; b) XRD diffractogram of the reaction **XXIb**. The average size of the particles is about 10 nm.

Composition	
EDX	–
XRD	Sn_4As_3

4.7. References

[1] A. P. Popov, A. V. Priezzhev, J. Lademann, R. Myllylä, *J. Phys. D: Appl. Phys.* **2005**, *38*, 2564 – 2570.
[2] H. Koga, T. Kitaoka, D. Pozo Perez (Ed.), *Silver Nanoparticles (InTech)* **2010**, 277 – 294.
https://www.intechopen.com/books/silver-nanoparticles/on-paper-synthesis-of-silver-nanoparticles-for-antibacterial-applications.
[3] M. F. L. De Volder, S. H. Tawfick, R. H. Baughman, A. J. Hart, *Science* **2013**, *339*, 535 – 539.
[4] D. Moore, S. Krishnamurthy, Y. Chao, Q. Wang, D. Brabazon, P. J. McNally, *Phys. Status Solidi A* **2011**, *208*, 604 – 607.
[5] D. D. Vaughn, R. E. Schaak, *Chem. Soc. Rev.* **2013**, *42*, 2861 – 2879.
[6] L. Zhong, C. Beaudette, J. Guo, K. Bozhilov, L. Mangolini, *Sci. Rep.* **2016**, *6*, 30952 – 30960.
[7] H. Jiang, K.-s. Moon, H. Dong, F. Hua, C. P. Wong, *Chem. Phys. Lett.* **2006**, *429*, 492 – 496.
[8] Y. Ji, H. Dong, T. Hou, Y. Li, *Journal of Materials Chemistry A* **2018**, Advance Article.
[9] L. Hu, D. Wei, *PCCP* **2017**, *19*, 2235 – 2244.
[10] M. Rostami, M. Moradi, Z. Javdani, H. Salehi, *Materials Science in Semiconductor Processing* **2015**, 218 – 227.
[11] Y. Jing, Y. Ma, Y. Li, T. Heine, *Nano Lett.* **2017**, *17*, 1833 – 1838.
[12] Y. Kim, Y. Kim, A. Choi, S. Woo, D. Mok, N.-S. Choi, Y. S. Jung, J. H. Ryu, S. M. Oh, K. T. Lee, *Adv. Mater.* **2014**, *26*, 4139 – 4144.
[13] D. Mijatovic, J. C. T. Eijkel, A. van den Berg, *Lab Chip* **2005**, *5*, 492 – 500.
[14] S. Mathur, C. Cavelius, K. Moh, H. Shen, J. Bauer, *Z. Anorg. Allg. Chem.* **2009**, *635*, 898 – 902.
[15] M. Rahim, N. J. Taylor, S. Xin, S. Collins, *Organometallics* **1998**, *17*, 1315 – 1323.
[16] F. Spitzer, C. Graßl, G. Balázs, E. M. Zolnhofer, K. Meyer, M. Scheer, *Angew. Chem.* **2016**, *128*, 4412 – 4416; *Angew. Chem. Int. Ed.* **2016**, *55*, 4340 – 4344.
[17] F. Spitzer, C. Graßl, G. Balázs, E. Mädl, M. Keilwerth, E. M. Zolnhofer, K. Meyer, M. Scheer, *Chem. Eur. J.* **2017**, *23*, 2716 – 2721.
[18] Y. Ding, H. W. Roesky, M. Noltemeyer, H.-G. Schmidt, P. P. Power, *Organometallics* **2001**, *20*, 1190 – 1194.
[19] M. Driess, S. Yao, M. Brym, C. v. Wüllen, , *Angew. Chem.* **2006**, *118*, 4455 – 4458*; Angew. Chem. Int. Ed.* **2006**, *45*, 4349 – 4352.
[20] S. Yao, M. Brym, K. Merz, M. Driess, *Organometallics* **2008**, *27*, 3601 – 3607.
[21] E. C. Y. Tam, N. A. Maynard, D. C. Apperley, J. D. Smith, M. P. Coles, J. R. Fulton, *Inorg. Chem.* **2012**, *51*, 9403 – 9415.
[22] Y. Kim, H. Hwang, C. S. Yoon, M. G. Kim, J. Cho, *Adv. Mater.* **2007**, *19*, 92 – 96.
[23] S. R. Foley, Y. Zhou, G. P. A. Yap, D. S. Richeson, *Inorg. Chem.* **2000**, *39*, 924 – 929.
[24] B. E. Eichler, D. R. Powell, R. West, *Organometallics* **1998**, *17*, 2147 – 2148.
[25] E. Csákvári, B. Rozsondai, I. Hargittai, *J. Mol. Struct.* **1991**, *245*, 349 – 355.
[26] M. Rivière-Baudet, A. Morère, J. F. Britten, M. Onyszchuk, *J. Organomet. Chem.* **1992**, *423*, C5 – C8.
[27] T. Fjeldberg, A. Haaland, B. E. R. Schilling, H. V. Volden, M. F. Lappert, A. J. Thorne, *J. Organomet. Chem.* **1985**, *280*, C43 – C46.
[28] M. Veith, V. Huch, *J. Organomet. Chem.* **1985**, *293*, 161 – 176.
[29] A. M. Domingos, G. M. Sheldrick, *J. Organomet. Chem.* **1974**, *69*, 207 – 212.
[30] K. M. Lo, S. Selvaratnam, S. W. Ng, C. Wei, V. G. K. Das, *J. Organomet. Chem.* **1992**, *430*, 149 – 166.
[31] J. L. Shreeve-Keyer, R. C. Haushalter, Y.-S. Lee, S. Li, C. J. O'Connor, D.-K. Seo, M.-H. Whangbo, *J. Solid State Chem.* **1997**, *130*, 234 – 249.
[32] J. H. Bryden, *Acta Crystallographica* **1962**, *15*, 167 – 171.
[33] M. Driess, H. Pritzkow, *Angew. Chem.* **1992**, *104*, 350 – 353.
[34] K. A. Kovnir, A. V. Sobolev, I. A. Presniakov, O. I. Lebedev, G. V. Tendeloo, W. Schnelle, Y. Grin, A. V. Shevelkov, *Inorganic Chemistry* **2005**, *44*, 8786 – 8793.
[35] K. Kovnir, Y. V. Kolen'ko, A. I. Baranov, I. S. Neira, A. V. Sobolev, M. Yoshimura, I. A. Presniakov, A. V. Shevelkov, *J. Solid State Chem.* **2009**, *182*, 630 – 639.
[36] Q. Gao, H. J. Joyce, S. Paiman, J. H. Kang, H. H. Tan, Y. Kim, L. M. Smith, H. E. Jackson, J. M. Yarrison-Rice, X. Zhang, J. Zou, C. Jagadish, *Phys. Status Solidi C* **2009**, *6*, 2678 – 2682.
[37] M.-H. Bae, B.-K. Kim, D.-H. Ha, S. J. Lee, R. Sharma, K. J. Choi, J.-J. Kim, W. J. Choi, J. C. Shin, *Cryst. Growth Des.* **2014**, *14*, 1510 – 1515.
[38] A. Krasnok, M. Caldarola, N. Bonod, A. Alú, *Adv. Opt. Mater.* **2018**, *6*, 1701094-1 – 1701094-22.
[39] F. E. Kruisa, H. Fissana, A. Peleda, *J. Aerosol Sci* **1998**, *29*, 511 – 535.
[40] S. L. Brock, K. Senevirathne, *J. Solid State Chem.* **2008**, *181*, 1552 – 1559.

[41] A. A. Guzelian, J. E. B. Katari, A. V. Kadavanich, U. Banin, K. Hamad, E. Juban, A. P. Alivisatos, *J. Phys. Chem.* **1996**, *100*, 7212 – 7219.
[42] S. Koh, T. Eom, W. D. Kim, K. Lee, D. Lee, Y. K. Lee, H. Kim, W. K. Bae, D. C. Lee, *Chem. Mater.* **2017**, *29*, 6346 – 6355.
[43] S. Prucnal, S. Zhou, X. Ou, H. Reuther, M. O. Liedke, A. Mücklich, M. Helm, J. Zuk, M. Turek, K. Pyszniak, W. Skorupa, *Nanotechnology* **2012**, *23*, 485204-1 – 485204-8.
[44] A. K. Nowak, M. D. Martín, H. P. v. d. Meulen, J. M. Ripalda, L. González, Y. González, L. Viña, J. M. Calleja, *Europhys. Lett.* **2014**, *108*, 17002-1 – 17002-5.
[45] A. A. Guzelian, U. Banin, A. V. Kadavanich, X. Peng, A. P. Alivisatos, *Appl. Phys. Lett.* **1996**, *69*, 1432 - 1434.
[46] S. Lin, J. Gu, Y. Wang, Y. Wang, S. Zhang, X. Liu, H. Zeng, Z. Chen, *J. Mater. Chem. A* **2018**, *6*, 3738 – 3746.
[47] T. P. Sushkova, E. Yu. Kononova, Yu. A. Savinova, E. S. Dorokhina, G. V. Semenova, *Kondensirovannye Sredy i Mezhfaznye Granitsy* **2014**, *16*, 210 – 214.
[48] V. Tallapally, R. J. A. Esteves, L. Nahar, I. U. Arachchige, *Chem. Mater.* **2016**, *28*, 5406 – 5414.
[49] Y. Ding, H. W. Roesky, M. Noltemeyer, H.-G. Schmidt, P. P. Power, *Organometallics* **2001**, *20*, 1190 – 1194.
[50] G. Becker, G. Gutekunst, H. J. Wessely, *Z. Anorg. Allg. Chem.* **1980**, 113 – 129.
[51] J. W. Connolly, G. Urry, *Inorg. Chem.* **1963**, *2*, 645 – 646.
[52] CrysAlisPro Software System, Rigaku Oxford Diffraction, (2015).
[53] R. C. Clark, J. S. Reid, *Acta Cryst.* **1995**, *A51*, 887 – 897.
[54] G. M. Sheldrick, *Acta Cryst.* **2015**, *A71*, 3 – 8.
[55] O.V. Dolomanov, L.J. Bourhis, R.J. Gildea, J. A. K. Howard, H. Puschmann, Olex2: A complete structure solution, refinement and analysis program, *J. Appl. Cryst.* **2009**, *42*, 339 – 341.
[56] G. M. Sheldrick, *Acta Cryst.* **2015**, C27, 3 – 8.
[57] G. M. Sheldrick, *Acta Cryst.* **2008**, *A64*, 112 – 122.

5. Thesis Treasury

5.1. Synthesis of new single-source-precursors for zinc phosphide nanoparticles

5.1.1. Author contribution

Daniela Meyer: Synthesis and analytics of the described compounds

Michael Seidl: Solution and refinement of the solid state structures of **5-1-2** and **5-1-3**

5.1.2. Introduction

With the theoretical invention of the transistor in 1925 by Lilienfeld[1] followed by its practical realization by the physicist Oskar Heil[2] in 1934 the golden times of solid-state technology began and with it the rise of semiconducting materials application. The most famous semiconductor is likely silicon due to its wide-spread use in solar cells in which it is the prime constituent. Si is well-suited as it is not only abundant in earth's crust, therefore cheap, and nontoxic, it is also very easy to prepare in a highly pure form. However, its efficiency of 18 to 25%, depending on the crystallinity of the electricity generating layers,[3] is unfavourable so that scientists all over the world are searching for an alternative which on the one hand includes all the advantages of silicon, while on the other hand offers a higher effectiveness. Such alternatives are for example FeS_2, CuO or Zn_3P_2.[4] For decades, zinc phosphide has only been a rodenticide, the toxic part of poisoned wheat, releasing PH_3 when it gets in contact with gastric acid.[5,6] But after the discovery of its semiconducting features it was focussed as new photovoltaic material because of its elements' availability and its broad direct band gap due to which the compound is able to absorb a large range of the light of the solar spectrum. Its electronic properties even surpass the ones of Si.[7] Furthermore, studies of bulk-Zn_3P_2 as well as tests with nanoparticles of zinc phosphide revealed quantum effects occurring in the nanoscale material leading to an increase of the band gap.[8-10] The emission of those nanocorpuscles could be determined to 424 – 535 nm for spherical quantum dots,[11] while the unique trumpet-shaped nanoparticles exhibit an emission of about 585 nm at room temperature.[12] Additionally to their mainly temperature-independent luminescence,[13,14] it could also be shown that thin films of nanocrystalline Zn_3P_2 display a transmittance of about 87% with a simultaneously decreased reflectance so that the substance might also be useful as solar cell coating.[15] Beside the hitherto described application in photovoltaics Zn_3P_2 is promising in optoelectronics as well as in combination with ZnO in photon detectors,[16] or as nano-wires in water which show disinfecting properties when being irradiated solely with visible light.[17]

Bulk-Zn_3P_2 exists in a black, tetragonal form and at elevated temperatures in a cubic form.[18-20] Yet, there is another zinc phosphide of the composition ZnP_2 that shows not only a red, tetragonal crystal structure, but also a black monoclinic one which is transformed to a pseudo-cubic form at pressures higher than 15 kbar.[21,19] Even ZnP_4 can be prepared, either from the elements at pressures of about 4 GPa[22] or from ZnP_2 and P_{black} at 500°C and 40 kbar.[19] Monoclinic ZnP_2 was also thought to be a promising material for Li ion batteries due to its electronic properties, but during the charge/discharge cycles a decomposition of the LiP and ZnP_2 phases accompanied by a capacity fade of the cell was observed.[23]

For the preparation of nanoscale Zn_3P_2 the top down approach of laser ablation[16] is as useful as the bottom up synthesis utilizing multi source precursors. Like the bulk material, nano-Zn_3P_2 can be prepared from the elements, but also from a whole variety of molecular compounds like ZnS, $ZnMe_2$, zinc perchlorate or zinc alkoxide in combination with PH_3, $P(SiMe_3)_3$ or trioctylphosphine (TOP).[13,14,4] All these syntheses have in common that for zinc and phosphorus separate starting materials are used in order to achieve the nanoscopic product. But so far there is no example for a single source precursor approach in which complexes of zinc with P containing substituents are decomposed to form the desired nanoparticles (chapter 1.3.3.2). Nevertheless, potential reagents can be found as there is compound **5-1-A**, showing a central cage-like structural motif of 6 Zn and 4 P atoms,[24] along with **5-1-B** and **5-1-C** with a Zn_3P_3 or a Zn_2P_2 core.[25,26] In contrast to these complexes with more than one Zn and P atom, species **5-1-D** displays a zinc centre with a PHPh substituent and a stabilizing *β*-diketiminato ligand (Scheme 5-1 - 1).[27]

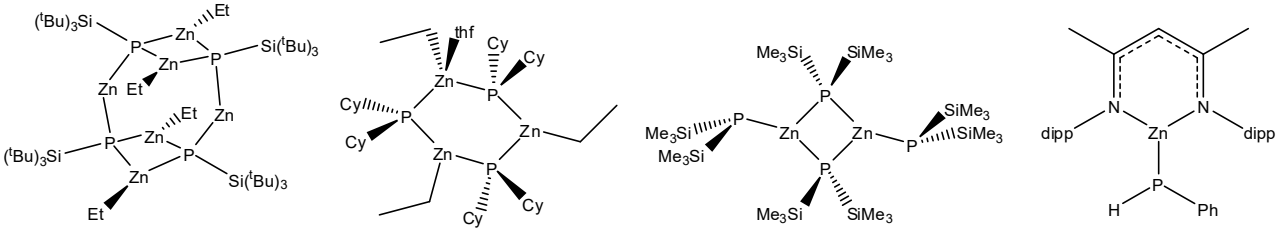

dipp = 2,6 - Diisoproylphenyl
Cy = Cyclohexyl

Scheme 5-1 - 1: Examples for different Zn–P complexes.

Beside the highly tunable *β*-diketiminato ligand also the smaller amidinato substituent is very useful in order to stabilize a compound although a tense four-membered ring instead of a six-membered ring is formed if the amidinato residue acts as a η^2-ligand. Still, this type of ligands is also very variable as its flanking groups and the backbone substituent can be changed as easily as it is the case for the *β*-diketiminato residue.[28] But although the class of amidinates is wellknown,[29,30] it took some time, until the amidinato ligand was found in many different complexes of main group elements just like in compounds containing transition metals.[31-40]

In the following the three new complexes $[PhC(N^tBu)_2]_2Zn$ (**5-1-1**), $\{[PhC(N^tBu)_2]Zn_2Br_3\}_n$ (**5-1-2**) and $[PhC(NtBu)_2]H \cdot ZnBr_2$ (**5-1-3**) bearing a Zn metal centre that is coordinated by the benzamidinato ligand $[PhC(N^tBu)_2]$ will be presented as well as the reactivity of **5-1-3** towards the lithiated compounds $LiP(SiMe_3)_2$ and $LiAs(SiMe_3)_2$.

5.1.3. Results and Discussion

The reaction of one eq. of $[PhC(NtBu)_2]Li$ (**5-1-E**) prepared *in situ* and one eq. $ZnBr_2$ in toluene at –80°C led to the formation of $[PhC(NtBu)_2]_2Zn$ (**5-1-1**) where both bromine atoms are replaced by a benzamidinato ligand, instead of the expected compound $[PhC(NtBu)_2]ZnBr$. **5-1-1** shows a good solubility in toluene. As the stoichiometric reaction of *in situ* prepared **5-1-E** with one eq. $ZnBr_2$ led to the substitution of both halogen atoms, the same experiment was performed using two eq. of zinc

bromide, leading to the formation of the polymeric compound $\{[PhC(N^tBu)_2]Zn_2Br_3\}_n$ (**5-1-2**) as colourless crystals, that are only poorly soluble in toluene or C_6D_6. In another attempt to synthesize the monomeric analogue of **5-1-2**, **5-1-E** was isolated[41] before the stoichiometric reaction with $ZnBr_2$. Regardless of several attempts, only the product of hydrolysis $[PhC(NtBu)_2]H \cdot ZnBr_2$ (**5-1-3**) could be isolated. The compound displays a good solubility in polar solvents like toluene.

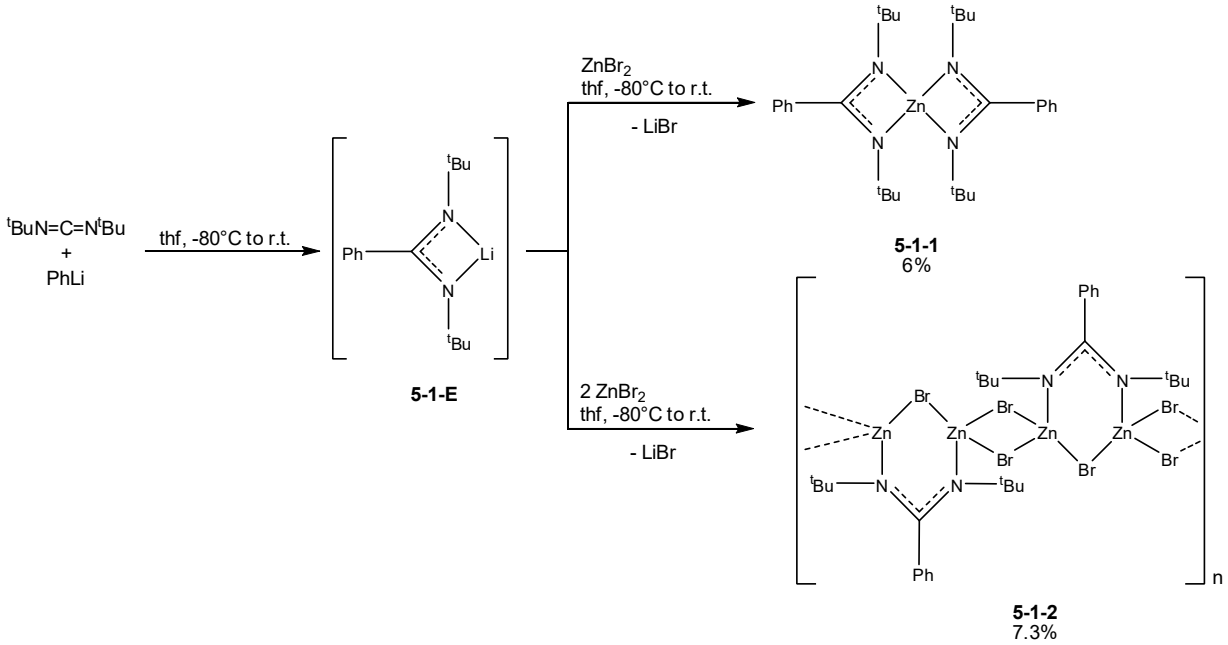

Scheme 5-1 - 2: Preparation of **5-1-1** and **5-1-2** via the *in situ* formation of **5-1-E**.

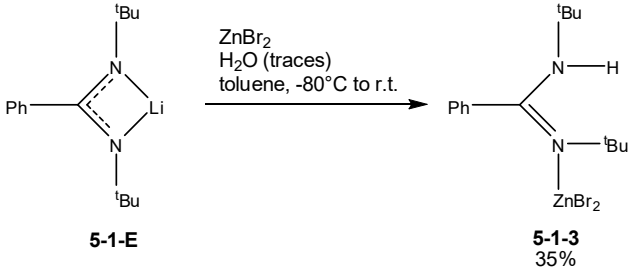

Scheme 5-1 - 3: Synthesis of **5-1-3** starting from **5-1-E**.

The compounds **5-1-1** and **5-1-3** were fully characterized by ^1H and $^{13}C\{^1H\}$ NMR spectroscopy, showing the expected sets of signals, while the NMR spectroscopic studies of the polymeric **5-1-2** did not lead to an informative spectrum.

The ^1H NMR spectrum of **5-1-1** exhibits a signal for the ^{t}Bu groups at 1.21 ppm and the signal for its aromatic phenyl groups appears at 7.01 – 7.38 ppm which are both in the typical region for this type of ligand. Similar to the ^1H NMR spectrum of **5-1-1**, also the ^1H NMR spectrum of compound **5-1-3** shows signals of the ligand (δ [ppm] = 1.21 (s, 18H, ^{t}Bu), 7.02 – 7.04 (m, 3H, Ph), 7.23 – 7.25 (m, 2H, Ph)) although one signal for each ^{t}Bu group should exist. Also, the signal of the NH residue of **5-1-3** (δ [ppm] = 3.27 ppm) displays an integral of only 0.4 H atoms instead of 1 H atom which might be caused by the lower relaxation time of the N bound hydrogen in comparison to the other relaxation times

leading to an apparently smaller integral. These two facts lead to the conclusion, that the molecular structure in solid state (Scheme 5-1 - 3) and in solution might differ from each other or both ^{t}Bu residues happen to be chemically equivalent.

Colourless crystals suitable for single crystal X-ray analysis could be obtained by storing the thf solution of **5-1-1** and **5-1-2** at –30°C. **5-1-1** crystallizes in the space group C2/c with four molecules per unit cell. The single crystal X-ray structure analysis of **5-1-2** revealed a monoclinic space group of I2/a with four fomula units per unit cell. Colourless crystals of **5-1-3** suitable for X-ray analysis could be obtained from a toluene solution stored at –30°C. $[PhC(NtBu)_2]H \cdot ZnBr_2$ crystallizes in the orthorhombic space group $P2_12_12_1$ and was refined as a 2-component inversion twin (Flack parameter 0.43(5)).

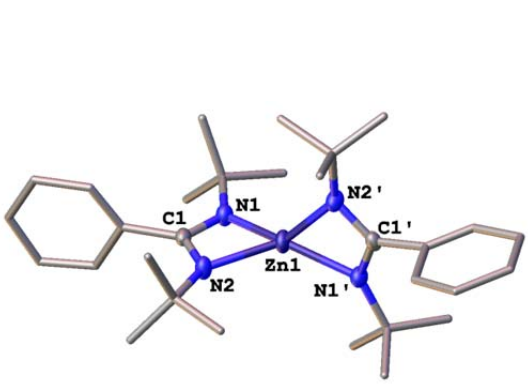

5-1-1

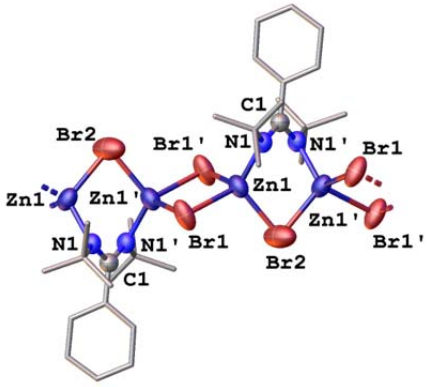

5-1-2

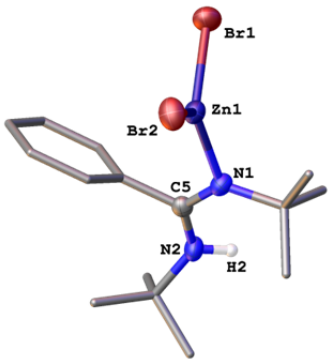

5-1-3

Figure 5-1 - 1: Molecular structures of **5-1-1**, **5-1-2** and **5-1-3**. Thermal ellipsoids are shown with 50% probability. H atoms are omitted for clarity. Selected lengths [Å] and angles [°]: **5-1-1**: Zn1 – N1 2.0009(13), Zn1 – N1‘ 2.0010(13), Zn1 – N2 2.0343(13), Zn1 – N2‘ 2.0342(13), N1/N1‘ – C1/C1‘ 1.332(2), N2/N2‘ – C1/C1‘ 1.331(2), C1/C1‘ – C10/C10‘ 1.499(2); N1/N1‘ – Zn1 – N2/N2‘ 66.04(5), N1/N1‘ – C1/C1‘ – N2/N2‘ 111.37(13). **5-1-2**: Zn1/Zn1‘ – N1/N1‘ 1.960(3), Zn1/Zn1‘ – Br1/Br1‘ 2.4796(7), Zn1 – Br1‘/Zn1‘ – Br1 2.4597(5), Zn1/ Zn1‘ – Br2 2.3957(8), N1/N1‘ – C1 1.337(3); N1/N1‘ – Zn1/Zn1‘ – Br2 112.37(7), Zn1 – N1 – C1/Zn1‘ – N1‘ – C1 113.83(19), Zn1 – Br2 – Zn1‘ 80.14(3), Zn1 – Br1/Br1‘ – Zn1 86.879(19); N1/N1‘ – Zn1/Zn1‘ – Br1/Br1‘ 109.16(8), N1 – Zn1 – Br1‘/N1‘ – Zn1‘ – Br1 124.22(7), N1 – C1 – N1‘ 116.3(4), Br1 – Zn1/Zn1‘ – Br1‘ 93.122(19), Br1/Br1‘ – Zn1/ZN1‘ – Br2 113.02(2), Br1‘ – Zn1 – Br2/Br1 – Zn1‘ – Br2 103.60(3). **5-1-3**: Zn1 – Br1 2.3162(12), Zn1 – Br2 2.3221(12), Zn1 – N1 1.998(6), N1 – C5 1.306(10), N2 – H2 0.8600, N2 – C5 1.327(9); Br1 – Zn1 – Br2 118.01(5), Br1 – Zn1 – N1 117.11(18), Br2 – Zn1 – N1 123.55(18), H2 – N2 – C5 114.1, N1 – C5 – N2 125.2(7).

Typically for benzamidinato complexes compound **5-1-1** shows two four-membered rings as main structural motif, which are twisted against each other with a torsion angle of 84.5°. Therefore, the Zn centre is coordinated by its substituents in a distorted tetrahedral way as it can be seen by comparing

the concerned angles (N1/N1'–Zn1–N2/N2' 66.04(5)°, N1–Zn1–N2'/N2–Zn1–N1' 133.55(5)°) with the tetrahedral angle of 109.5°. The Zn1–N bond lengths of **5-1-1** are in the range of rather short single bonds (**5-1-1**: Zn1–N1 2.0009(13) Å, Zn1–N2 2.0010(13) Å; Zn–N: 1.97 – 2.28 Å[42,43]). All remaining bond lengths and angles are in the typical range of the ligand.

The X-ray analysis of crystals of **5-1-2** reveals a quite unexpected solid state structure as the product of the reaction of *in situ* generated **E** with 2 eq. of $ZnBr_2$ turns out to be polymeric in the solid state. Also the bridging binding mode of the benzamidinato ligand is rather uncommon compared to the frequently observed coordination to one metal centre. Here, each $[PhC(NtBu)_2]$ fragment binds to a Zn_2Br_3 unit leading to a one-dimensional strand. This results in a distorted tetrahedral environment around the zinc atoms (N1/N1'–Zn1/Zn1'–Br2 112.37(7)°, Br1–Zn1/Zn1'–Br1' 93.122(19)°) although the distortion is not as accentuated as it is in case of **5-1-1** due to the benzamidinato substituent which is not coordinating to one metal centre as in compound **5-1-2**. Another remarkable feature are the Zn1–N1/Zn1 – N1' bond lengths of 1.960(3) Å, which are short compared to the Zn–N bond lengths of **5-1-1** and those reported in literature (**5-1-1**: Zn1–N1 2.0009(13) Å, Zn1–N2 2.0010(13) Å; Zn–N: 1.97 – 2.28 Å[42,43]). In contrast to the short Zn–N bonds, the Zn1/Zn1'–Br1/Br1' bonds of 2.4796(7) Å are exceptionally long compared to the Zn1/Zn1'–Br2 bonds of 2.3957(8) Å which are in the range of a Zn–Br single bond (Zn–Br: 2.37 – 2.42 Å [44,45]). Apart from these deviations the bond lengths and angles are in the range of the typical values of the ligand.

The zinc atom of **5-1-3** is not coordinated by the ligand in an η^1:η^1 fashion but only binds to the nitrogen atom N1, which is similar to **5-1-2**. Additionally, due to steric reasons the N1 bound ^{t}Bu group is adjusted parallel to the phenyl ring which is in contrast to the N2 bound ^{t}Bu residue or the ^{t}Bu substituents of the compounds **5-1-1** and **5-1-2**. Another conspicuousness is the N1–C5 bond length of 1.306 Å which is significantly shorter than the length of N2–C5 (1.328 Å) or the average N–C bond length of the $[PhC(NtBu)_2]$ ligand (**5-1-1**: N1–C1 1.332(2) Å, N2–C2 1.331(2) Å; **5-1-2**: N1–C1 1.337(3) Å, Chapter 3.4: **5-1-1**: N1–C1 1.338(2) Å, N2–C1 1.337(2) Å; **5-1-2**: N1–C1 1.338(2) Å, N2–C1 1.335(2) Å). This shows a partial localisation of the N–C double bond between the atoms N1 and C5 although both C–N bonds of **5-1-3** are still in the range of a C–N double bond and a C–N(sp^2) single bond[46]. The Zn1–N1 bond length of 1.998(6) Å is an average Zn–N single bond (Zn–N: 1.97 – 2.28 Å[42,43]), the same is true for the Zn–Br bonds (Zn1–Br1 2.3162, Zn1–Br2 2.3221, Zn–Br: 2.37 – 2.42 Å[44,45]), which are due to the coordination of the ligand significantly longer than the Zn–Br bonds of free $ZnBr_2$ ($Zn–Br_{gaseous}$ 2.204 Å[47]). Due to the η^1 coordination behaviour of the benzamidinato ligand in **5-1-3**, the N1–C1–N2 angle is quite large (125.3°).

As **5-1-3** might be a suitable starting material to synthesize a molecular precursor complex for the preparation of zinc phosphide nanoparticles, it was reacted with the lithiated compounds $LiE(SiMe_3)_2$ (E = P, As). Here, the conversion of **5-1-3** with $LiAs(SiMe_3)_2$ only led to the decomposition of both

compounds. Nevertheless, the reaction of **5-1-3** with the lighter homologue $LiP(SiMe_3)_2$ resulted in the formation of **5-1-C**, which is also formed by the reaction of $ZnBr_2$ and $LiP(SiMe_3)_2$, that has been done at our workgroup.[48]

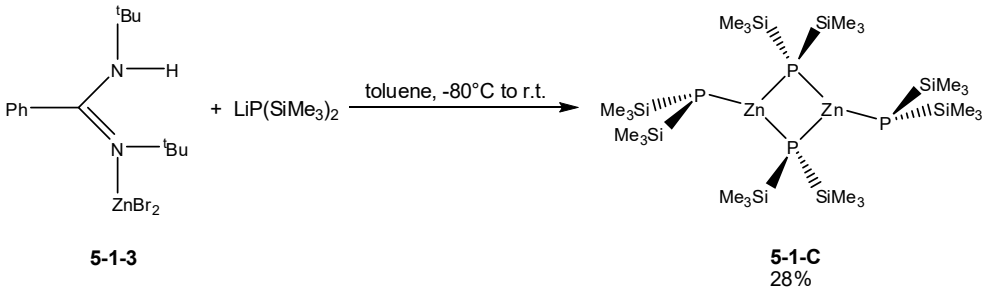

5-1-3 **5-1-C** 28%

Scheme 5-1 - 4: Reaction of **5-1-3** with $LiP(SiMe_3)_2$.

5-1-C has already been synthesized in 1990 by Goel *et al.* with $Zn[N(SiMe_3)_2]_2$ and $HP(SiMe_3)_2$ as starting material.[25] As described, the formation of **5-1-C** can be clearly identified by ^{31}P and $^{31}P\{^1H\}$ NMR spectroscopy where two sets of broad multiplets at –184.9 ppm and –239.7 ppm can be found (literature: δ [ppm] = –183.0 (br, s); –237.3 (br, s)).[25]

Suitable crystals for the X-ray analysis of **5-1-C** could be obtained from the toluene solution which was stored at –30°C. Again, the received data didn't differ much from literature, but here the measurement was performed at 183 K and not at room temperature like by Goel *et al.*[25] Due to the fact that the X-ray experiment was initially planned at 123 K, a phase transition of **5-1-C** accompanied by a loss in crystallinity could be observed at 137.5 K.

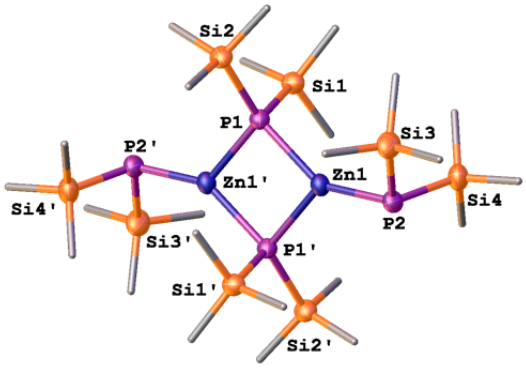

Figure 5-1 - 2: Molecular structure of **5-1-C**. Thermal ellipsoids are shown with 50% probability. H atoms are omitted for clarity. Selected lengths [Å] and angles [°]: Zn1/Zn1‘ – P1/P1‘ 2.4139(6), Zn1 – P1‘/Zn1‘ – P1 2.4145(7), Zn1/Zn1‘ – P2/P2‘ 2.2921(7), P1/P1‘ – Si1/Si1‘ 2.2542(9), P1/P1‘ – Si2/Si2‘ 2.2513(9), P2/P2‘ – Si3/Si3‘ 2.2238(10), P2/P2‘ – Si4/Si4‘ 2.2337(10); P1 – Zn1/Zn1‘ – P1‘ 90.46(2), Zn1 – P1/P1‘ – Zn1‘ 89.54(2), P1/P1‘ – Zn1/Zn1‘ – P2/P2‘ 125.14(3), P1 – Zn1‘ – P2‘/P1‘ – Zn1 – P2 143.97(3).

5.1.4. Conclusion

In summary, it was possible to synthesize the three novel zinc complexes $[PhC(NtBu)_2]_2Zn$ (**5-1-1**), $\{[PhC(NtBu)_2]Zn_2Br_3\}_n$ (**5-1-2**) and $[PhC(NtBu)_2]H \cdot ZnBr_2$ (**5-1-3**) with a stabilizing benzamidinato ligand, that has not been used for the coordination to this metal yet. Moreover, studies regarding the reactivity of **5-1-3** towards the lithiated compounds $LiE(SiMe_3)_2$ (E = P, As) have been performed, of

which the phosphorus analogue led to the formation of compound **5-1-C** reported by Goel *et al.* For **5-1-C**, a hitherto unknown phase transition was observed. Goel *et al*. additionally showed a thermal decomposition study of their compound **5-1-C** which forms the polymeric product $[ZnP(SiMe_3)]_n$ in refluxing toluene instead of the desired Zn_3P_2.[49] These results induced us to no longer consider **5-1-C** as a suitable single source precursor of Zn/P containing nanoparticles.

5.1.5. Supporting Information

Experimental section

General procedures

All experiments were carried out under a dry nitrogen or argon atmosphere using standard Schlenk or drybox techniques. Solvents were dried by using an MBraun purification system and stored over a dried 3 Å mol sieve. Fine powder of $ZnBr_2$ was dried at 350°C before use. The starting materials i.e. $[PhC(NtBu)_2]Li$[50,51] (prepared *in situ*), $As(SiMe_3)_3$ and $LiAs(SiMe_3)_2$[52] were synthesized according to the literature procedures. The NMR spectra were recorded on a Bruker Avance 400 (^1H: 400.132 MHz, ^{13}C: 100.613 MHz) with δ referenced to external $SiMe_4$ (^1H, ^{13}C). The EI- and LIFDI-MS studies were performed on a Jeol AccuTOF GCX.

Preparations

Preparation of $[PhC(N^tBu)_2]_2Zn$ (5-1-1): According to literature, PhLi (3.6 mL, 7.2 mmol, 1.8 M in dibutyl ether) was added to $^tBuN=C=N^tBu$ (1.06 mL, 6.86 mmol) in toluene (20 mL) at –80°C. The reaction mixture was allowed to warm to room temperature over 5 h. Then it was added to a suspension of $ZnBr_2$ (1.79 g, 7.9 mmol) in toluene (10 mL) at –80°C. The resulting white suspension was stirred and warmed to room temperature over night. The mixture was filtrated and the slightly yellow solution was concentrated and stored at –30°C to yield colourless crystals of **5-1-1** (yield: 1.58 g, 6%).

^1H NMR (400.132 MHz, C_6D_6, 298K): δ[ppm] = 1.21 (s, 36 H, ^tBu), 7.01 – 7.05, 7.22 – 7.8 (m, 10 H, Ph); $^{13}C\{^1H\}$ NMR (100.613 MHz, C_6D_6, 298K): δ[ppm] = 25.5, 33.5, 51.1, 68.5, 127.2, 129.8, 138.9. Elemental analysis was not performed due to the sensitivity to hydrolysis of **5-1-1**.

Preparation of $\{[PhC(N^tBu)_2]Zn_2Br_3\}_n$ (5-1-2): Similar to **5-1-1**, **5-1-2** was synthesized by preparing $[PhC(N^tBu)_2]Li$ with PhLi (3.6 mL, 7.2 mmol, 1.8 M in dibutyl ether) and $^tBuN=C=N^tBu$ (1.06 mL, 6.86 mmol) in toluene and adding it to $ZnBr_2$ (3.0 g, 13.3 mmol) in toluene at –80°C. The work-up procedure is the same as for **5-1-1**. The storage of the concentrated solution at – 30°C led to the formation of colourless crystals of **5-1-2** (yield: 314.3 mg, 7.3%).

Preparation of $[PhC(NtBu)_2]H \cdot ZnBr_2$ (5-1-3): For the preparation of **5-1-3**, **E** (199.8 mg, 0.8 mmol) was dissolved in toluene (10 mL) and added to a suspension of $ZnBr_2$ (189.1 mg, 0.8 mmol) in toluene (5 mL) at –80°C. The reaction mixture was allowed to warm to room temperature while stirring over night. Subsequently, the white solid was separated from the colourless solution by filtration. Colourless crystals could be obtained from the solution after concentration (yield: 113.3 mg, 35%).

^1H NMR (400.132 MHz, C_6D_6, 298K): δ[ppm] = 1.21 (s, 18 H, ^tBu), 3.27 (br. s, 0.4 H, N*H*), 7.02 – 7.04, 7.23 – 7.25 (m, 5 H, Ph); $^{13}C\{^1H\}$ NMR (100.613 MHz, C_6D_6, 298K): δ[ppm] = 29.1, 33.3, 33.6, 51.1, 127.2, 129.8, 173.3. EI-MS was performed but only led to peaks of the ligand.

Reaction of 5-1-3 with $LiP(SiMe_3)_2$: $LiP(SiMe_3)_2$ (140.7 mg, 0.48 mmol) in toluene (5 mL) was added to **5-1-3** (110.3 mg, 0.24 mmol) in toluene (5 mL) at –80°C. The mixture was stirred and warmed to room temperature over night. The white suspension was filtrated to yield a colourless solution from which colourless crystals of **5-1-C** were obtained after concentration (yield: 56.6 mg, 28%).

Reaction of 5-1-3 with $LiAs(SiMe_3)_2$: $LiAs(SiMe_3)_2$ (244 mg, 0.71 mmol) in toluene (5 mL) was added to **5-1-3** (164.1 mg, 0.36 mmol) in toluene (5 mL) at –80°C. The mixture was stirred and warmed to room temperature over night. The brown suspension was filtrated to yield a yellow solution. Unfortunately, NMR spectrometric studies revealed the decomposition of the reagents.

NMR spectroscopy

[PhC(N^{t}Bu)$_2$]$_2$Zn (5-1-1):

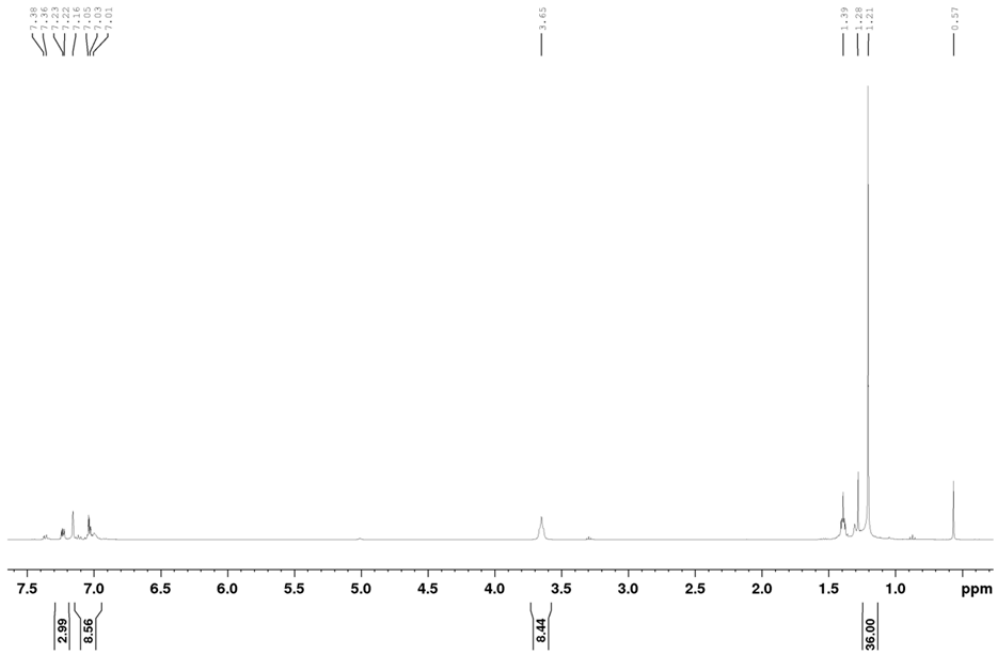

Figure 5-1 - 3: ^{1}H NMR spectrum of **5-1-1**.

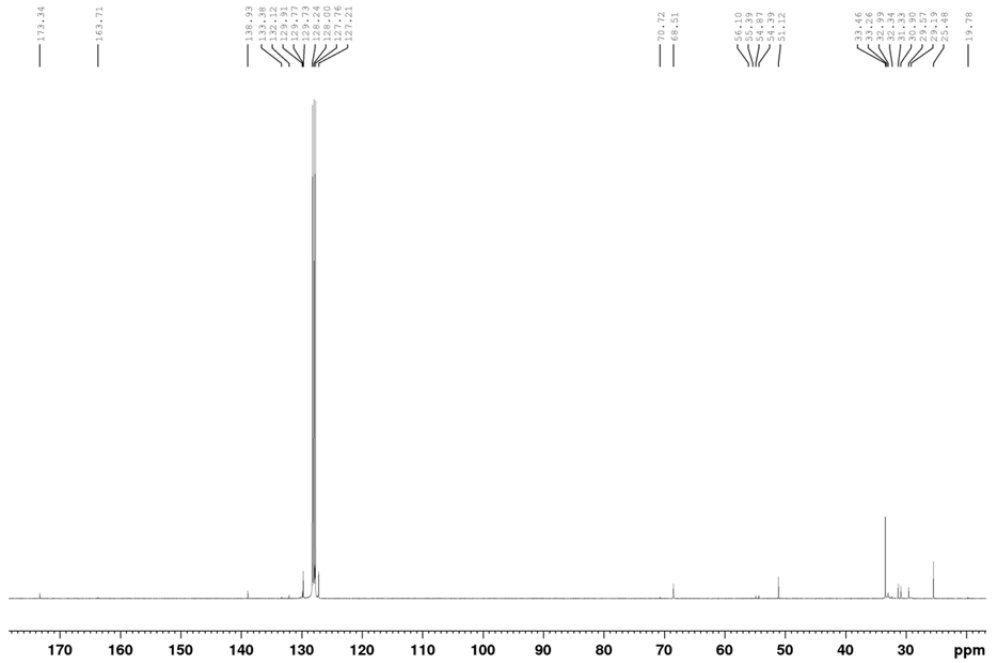

Figure 5-1 - 4: ^{13}C{^{1}H} NMR spectrum of compound **5-1-1**.

[PhC(NtBu)$_2$]H · ZnBr$_2$ (5-1-3):

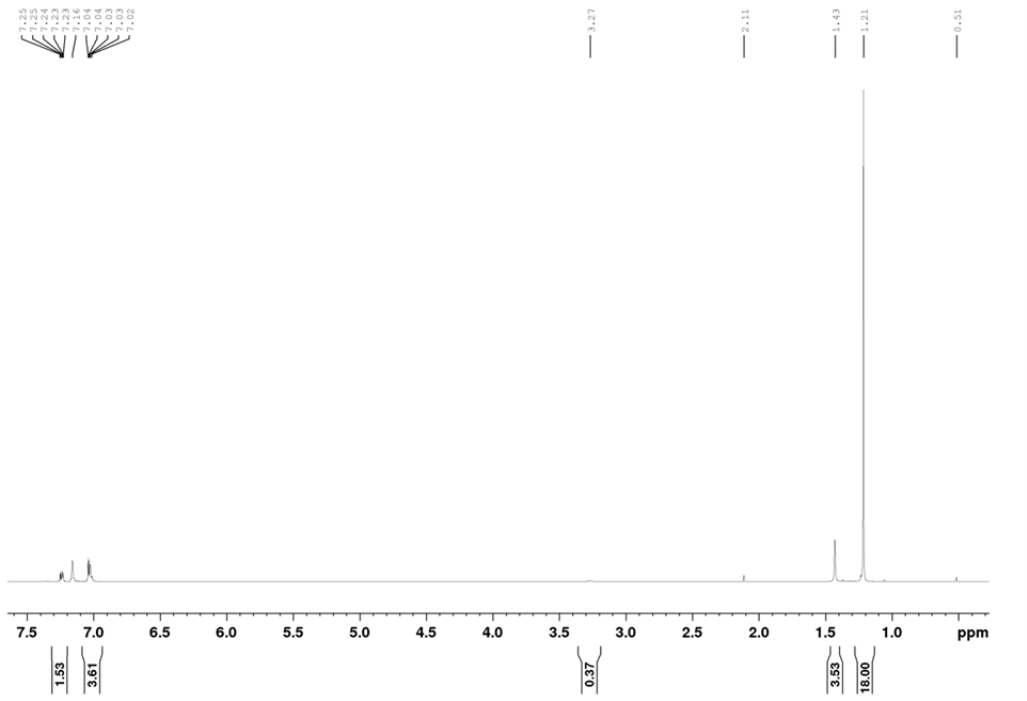

Figure 5-1 - 5: ^{1}H NMR spectrum of the crystals of **5-1-3**.

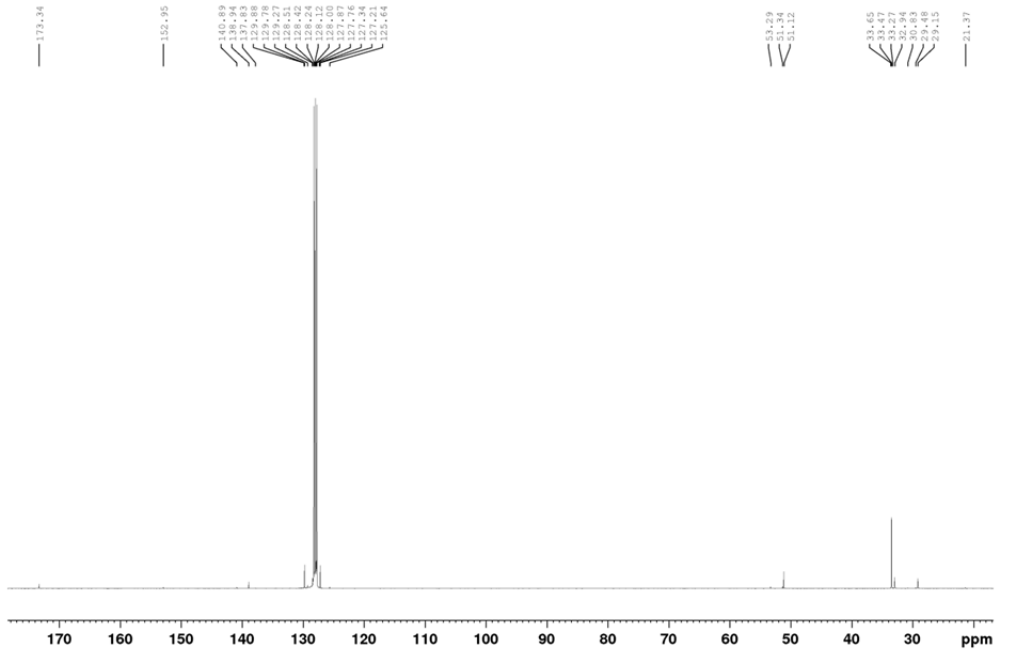

Figure 5-1 - 6: ^{13}C {^{1}H} NMR spectrum of **5-1-3**.

X-ray structure analysis

The crystal samples were processed at a Supernova diffractometer with an Atlas CCD detector (**5-1-3**) and a GV1000 diffractometer with a Titan S2 CCD detector (**5-1-1**, **5-1-2**, **5-1-C**), respectively. Frames integration and data reduction were performed with CrysAlisPro ver. 171.38.41h.[53] Analytical absorption corrections from crystal faces[54] were applied to the data of **5-1-2**. A numerical absorption correction based on Gaussian integration over a multifaceted crystal model was applied to the data of **5-1-1**, **5-1-3** and **5-1-C**.[52] All structures were solved by SHELXT[55] using Olex2[56]. For all structures a least-square redinement on F^2 was carried out with SHELXL[57,58]. Hydrogen atoms at the carbon atoms were located in idealized positions and refined isotropically according to the riding model.

$[PhC(N^tBu)_2]_2Zn$ (5-1-1):

5-1-1 crystallizes from toluene at –30°C as clear, colourless blocks.

Sum formula	$C_{30}H_{46}N_4Zn$	
Molecular weight *M* [g/mol]	528.08	
Crystal system	monoclinic	
Space group	C2/c	
Unit cell dimensions [Å] or [°]	24.6589(12)	90
	8.5217(2)	128.813(7)
	18.2174(8)	90
Volume [$Å^3$]	2982.9(3)	
Formula units *Z*	4	
Temperature *T* [K]	123	
Crystal size [mm^3]	0.468 x 0.193 x 0.149	
Crystal density ρ_{calc} [$g \cdot cm^{-3}$]	1.176	
F(000)	1136.0	
Absorption coefficient $\mu_{Cu\text{-}K\alpha}$ [mm^{-1}]	1.302	
Transmission T_{min} / T_{max}	0.833 /0.923	
Absorption correction	gaussian	
Wavelength (λ) [Å]	1.54184 (CuK_α)	
Measured / independent reflections (R_{int})	8354/ 2924 (0.0362)	
Independent reflections [$I > 2\sigma(I)$]	2760	
Index ranges *hkl*	$-30 \le h \le 30$	
	$-10 \le k \le 8$	
	$-22 \le l \le 22$	
Measuring range θ_{min} / θ_{max} / θ_{full} [°]	4.603/74.134/67.684	
Completeness (θ_{full})	0.991	
Data / restraints / parameters	2924/0/215	
R-indices (all data)	0.0382/0.1024	
R-indices [$I > 2\sigma(I)$]	0.0366/0.1004	
Goodness-of-fit for S (F^2)	1.044	
Largest diff. peak and hole [$e \cdot Å^3$]	0.421/-0.465	

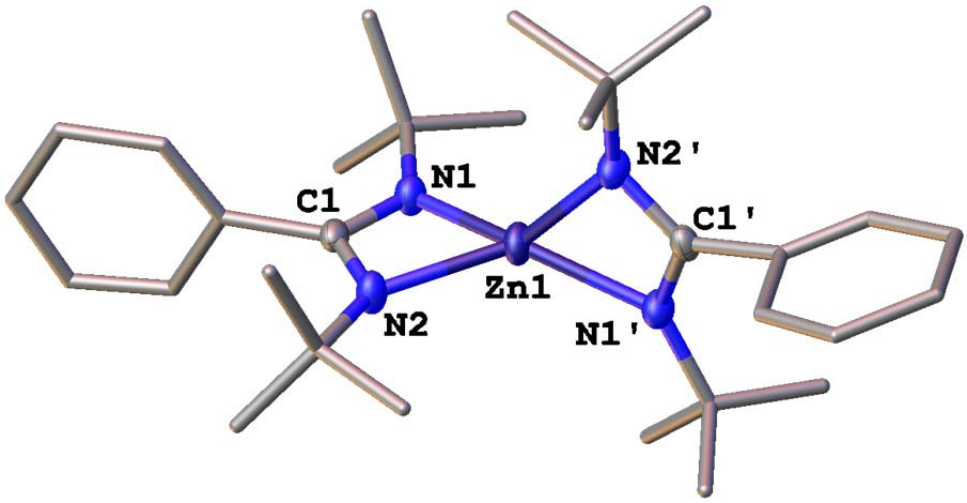

Figure 5-1 - 7: Molecular structure of **5-1-1**. Thermal ellipsoids are shown with 50% probability level. H atoms are omitted for clarity.

Distances [Å]		Angles [°]	
Zn1 – N1	2.0009(13)	N1 – Zn1 – N1‘	144.47(8)
Zn1 – N1‘	2.0010(13)	N1 – Zn1 – N2	66.04(5)
Zn1 – N2	2.0343(13)	N1 – Zn1 – N2‘	133.55(5)
Zn1 – N2‘	2.0342(13)	N2 – Zn1 – N2‘	124.75(8)
N1/N1‘ – C1/C1‘	1.332(2)	N2 – Zn1 – N1‘	133.55(5)
N2/N2‘ – C1/C1‘	1.331(2)	N1‘ – Zn1 – N2‘	66.04(5)
N1/N1‘ – C2/C2‘	1.471(2)	Zn1 – N1/N1‘ – C1/C1‘	91.65(9)
N2/N2‘ – C6/C6‘	1.466(2)	Zn1 – N1/N1‘ – C2/C2‘	136.89(10)
C1/C1‘ – C10/C10‘	1.499(2)	Zn1 – N2/N2‘ – C1/C1‘	90.23(9)
		Zn1 – N2/N2‘ – C6/C6‘	138.26(10
		N1/N1‘ – C1/C1‘ – N2/N2‘	111.37(13)
		N1/N1‘ – C1/C1‘ – C10/C10‘	123.78(14)
		N2/N2‘ – C1/C1‘ – C10/C10‘	124.84(14)

{[PhC(N^{t}Bu)$_2$]Zn$_2$Br$_3$}$_n$ (5-1-2):

5-1-2 crystallizes from toluene at –18°C as clear, colourless blocks.

Sum formula	$C_{15}H_{23}Br_3N_2Zn_2$	
Molecular weight *M* [g/mol]	601.82	
Crystal system	monoclinic	
Space group	I2/a	
Unit cell dimensions [Å] or [°]	12.5113(3)	90
	19.5824(4)	102.335(2)
	13.6821(2)	90
Volume [Å^3]	3274.75(11)	
Formula units *Z*	4	
Temperature *T* [K]	123	
Crystal size [mm^3]	0.158 x 0.12 x 0.10	
Crystal density ρ_{calc} [g · cm^{-3}]	1.221	
F(000)	1168.0	
Absorption coefficient $\mu_{Cu\text{-}K\alpha}$ [mm^{-1}]	6.069	
Transmission T_{min} / T_{max}	0.319/0.490	
Absorption correction	analytical	
Wavelength (λ) [Å]	1.54184 (CuK_α)	
Measured / independent reflections (R_{int})	9430/ 3246 (0.0190)	
Independent reflections [$I > 2\sigma(I)$]	2818	
Index ranges *hkl*	$-15 \le h \le 11$	
	$-23 \le k \le 23$	
	$-16 \le l \le 16$	
Measuring range θ_{min} / θ_{max} / θ_{full} [°]	4.004/73.513/67.684	
Completeness (θ_{full})	0.999	
Data / restraints / parameters	3246/50/131	
R-indices (all data)	0.0838/0.2723	
R-indices [$I > 2\sigma(I)$]	0.0782/0.2723	
Goodness-of-fit for S (F^2)	1.303	
Largest diff. peak and hole [e · Å^3]	1.890/-1.005	

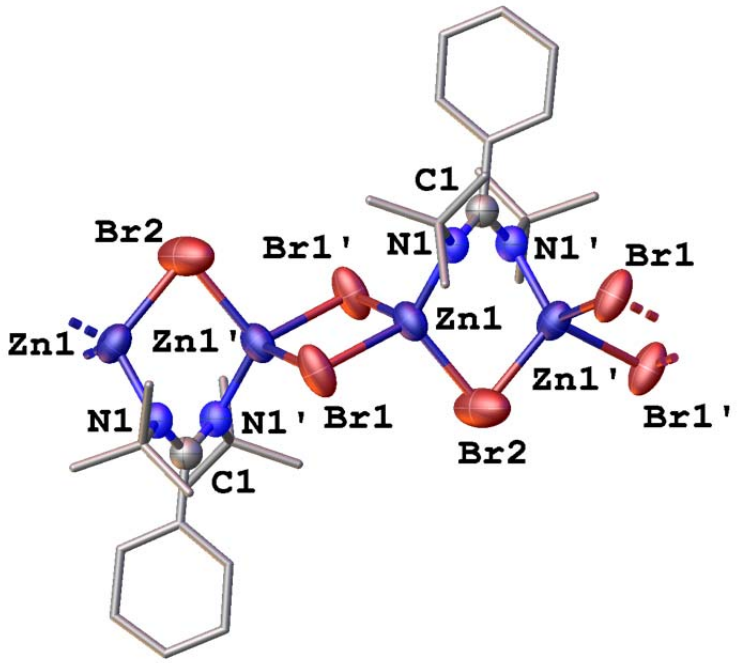

Figure 5-1 - 8: Molecular structure of **5-1-2**. Thermal ellipsoids are shown with 50% probability level. H atoms are omitted for clarity.

Distances [Å]		Angles [°]	
Zn1/Zn1‘ – N1/N1‘	1.960(3)	N1 – Zn1 – Br2/N1‘ – Zn1‘ – Br2	112.37(7)
Zn1/Zn1‘ – Br1/Br1‘	2.4796(7)	Zn1 – N1 – C1/Zn1‘ – N1‘ – C1	113.83(19)
Zn1 – Br1‘/Zn1‘ – Br1	2.4597(5)	Zn1 – Br2 – Zn1‘	80.14(3)
Zn1/ Zn1‘ – Br2	2.3957(8)	Zn1 – N1 – C8/Zn1‘ – N1‘ – C8‘	119.00(18)
N1 – C1/ N1‘ – C1	1.337(3)	Zn1 – Br1 – Zn1‘/Zn1 – Br1‘ – Zn1‘	86.879(19)
N1 – C8/ N1‘ – C8‘	1.514(3)	N1 – Zn1 – Br1/N1‘ – Zn1‘ – Br1‘	109.16(8)
C1 – C2	1.470(7)	N1 – Zn1 – Br1‘/N1‘ – Zn1‘ – Br1	124.22(7)
		N1 – C1 – N1‘	116.3(4)
		N1 – C1 – C2	123.3(10)
		N1‘ – C1 – C2	120.3(10)
		C1 – N1 – C8/C1 – N1‘ – C8‘	125.8(3)
		Br1 – Zn1 – Br1‘/B1 – Zn1‘ – Br1‘	93.122(19)
		Br1 – Zn1 – Br2/Br1‘ – Zn1‘ – Br2	113.02(2)
		Br1‘ – Zn1 – Br2/Br1 – Zn1‘ – Br2	103.60(3)

[PhC(NtBu)$_2$]H · ZnBr$_2$ (5-1-3):

5-1-3 crystallizes from toluene at –30°C as clear, colourless blocks.

Sum formula	$C_{15}H_{24}Br_2N_2Zn$	
Molecular weight *M* [g/mol]	457.55	
Crystal system	orthorhombic	
Space group	$P2_12_12_1$	
Unit cell dimensions [Å] or [°]	11.0391(6)	90
	11.5844(8)	90
	14.2911(8)	90
Volume [Å^3]	1827.57(19)	
Formula units *Z*	4	
Temperature *T* [K]	123	
Crystal size [mm^3]	0.249 x 0.055 x 0.041	
Crystal density ρ_{calc} [g · cm^{-3}]	1.663	
F(000)	912.0	
Absorption coefficient $\mu_{Cu\text{-}K\alpha}$ [mm^{-1}]	6.916	
Transmission T_{min} / T_{max}	0.431/1.000	
Absorption correction	gaussian	
Wavelength (λ) [Å]	1.54184 (CuK_α)	
Measured / independent reflections (R_{int})	5907/ 3528 (0.0386)	
Independent reflections [$I > 2\sigma(I)$]	3317	
Index ranges *hkl*	$-13 \le h \le 13$	
	$-13 \le k \le 14$	
	$-17 \le l \le 17$	
Measuring range θ_{min} / θ_{max} / θ_{full} [°]	4.914/74.046/67.684	
Completeness (θ_{full})	0.997	
Data / restraints / parameters	3528/0/188	
R-indices (all data)	0.0585/0.1487	
R-indices [$I > 2\sigma(I)$]	0.0562/0.1461	
Goodness-of-fit for S (F^2)	1.036	
Largest diff. peak and hole [e · Å^3]	1.56/-0.84	
Flack parameter	0.43(5)	

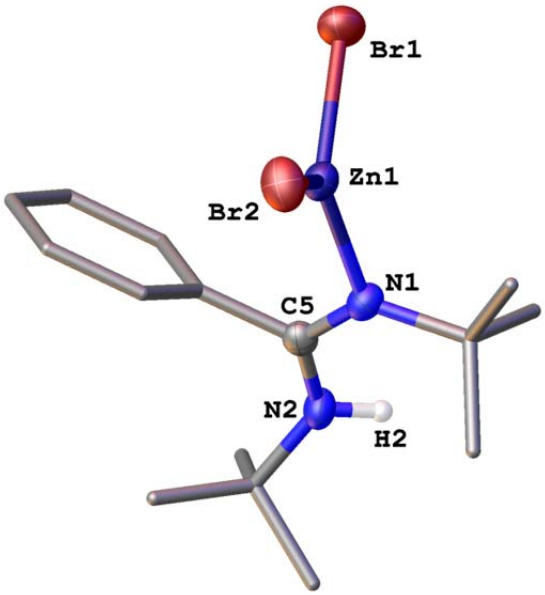

Figure 5-1 - 9: Molecular structure of **5-1-3**. Thermal ellipsoids are shown with 50% probability level. H atoms are omitted for clarity.

Distances [Å]		Angles [°]	
Zn1 – Br1	2.3162(12)	Br1 – Zn1 – Br2	118.01(5)
Zn1 – Br2	2.3221(12)	Br1 – Zn1 – N1	117.11(18)
Zn1 – N1	1.998(6)	Br2 – Zn1 – N1	123.55(18)
N1 – C1	1.488(9)	Zn1 – N1 – C2	118.1(5)
N1 – C5	1.306(10)	Zn1 – N1 – C5	116.1(5)
N2 – H2	0.8600	H2 – N2 – C5	114.1
N2 – C5	1.327(9)	H2 – N2 – C12	114.1
N2 – C12	1.501(9)	N1 – C5 – N2	125.2(7)
C5 – C6	1.496(10)	N1 – C5 – C6	115.1(6)
		N2 – C5 – C6	119.6(6)

{Zn[P(SiMe$_3$)$_2$]$_2$}$_2$ (5-1-C):

5-1-C crystallizes from toluene at –30°C as clear, colourless blocks.

7	$C_{24}H_{72}P_4Si_8Zn_2$	
Molecular weight *M* [g/mol]	840.15	
Crystal system	triclinic	
Space group	P-1	
Unit cell dimensions [Å] or [°]	9.7559(4)	81.627(3)
	10.6338(4)	67.874(3)
	12.6143(4)	81.605(3)
Volume [Å^3]	1193.40(8)	
Formula units *Z*	1	
Temperature *T* [K]	182.96(18)	
Crystal size [mm^3]	0.336 x 0.105 x 0.075	
Crystal density ρ_{calc} [g · cm^{-3}]	1.169	
F(000)	448.0	
Absorption coefficient $\mu_{Cu\text{-}K\alpha}$ [mm^{-1}]	4.530	
Transmission T_{min} / T_{max}	0.425/0.757	
Absorption correction	gaussian	
Wavelength (λ) [Å]	1.54184 (CuK_α)	
Measured / independent reflections (R_{int})	7093/ 4611 (0.0267)	
Independent reflections [$I > 2\sigma(I)$]	4030	
Index ranges *hkl*	$-12 \le h \le 9$	
	$-13 \le k \le 12$	
	$-15 \le l \le 12$	
Measuring range θ_{min} / θ_{max} / θ_{full} [°]	3.801/74.804/67.684	
Completeness (θ_{full})	0.982	
Data / restraints / parameters	4611/0/184	
R-indices (all data)	0.0418/0.0980	
R-indices [$I > 2\sigma(I)$]	0.0359/0.0934	
Goodness-of-fit for S (F^2)	0.941	
Largest diff. peak and hole [e · Å^3]	0.434/-0.597	

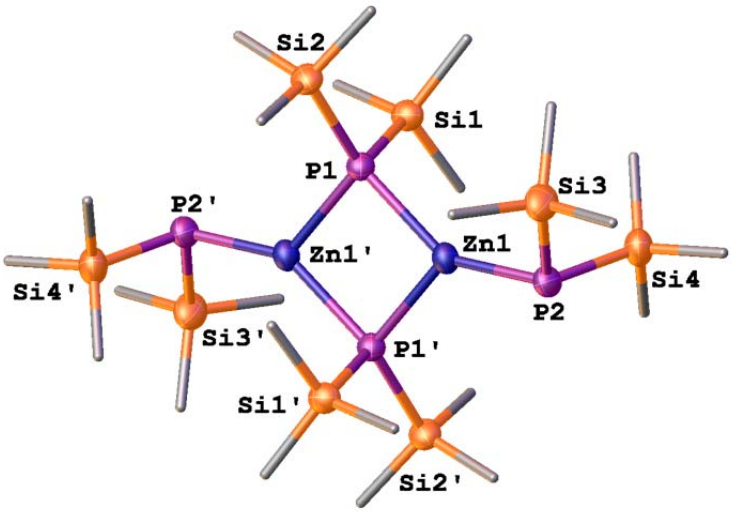

Figure 5-1 - 10: Molecular structure of **5-1-C**. Thermal ellipsoids are shown with 50% probability level. H atoms are omitted for clarity.

Distances [Å]		Angles [°]	
Zn1/Zn1‘ – P1/P1‘	2.4139(6)	P1 – Zn1/Zn1‘ – P1‘	90.46(2)
Zn1 – P1‘/Zn1‘ – P1	2.4145(7)	Zn1 – P1/P1‘ – Zn1‘	89.54(2)
Zn1/Zn1‘ – P2/P2‘	2.2921(7)	P1/P1‘ – Zn1/Zn1‘ – P2/P2‘	125.14(3)
P1/P1‘ – Si1/Si1‘	2.2542(9)	P1 – Zn1‘ – P2‘/P1‘ – Zn1 – P2	143.97(3)
P1/P1‘ – Si2/Si2‘	2.2513(9)	Zn1/Zn1‘ – P1/P1‘ – Si1/Si1‘	99.26(3)
P2/P2‘ – Si3/Si3‘	2.2238(10)	Zn1/Zn1‘ – P1/P1‘ – Si2/Si2‘	118.08(3)
P2/P2‘ – Si4/Si4‘	2.2337(10)	Zn1 – P1‘ – Si1‘/Zn1‘ – P1 – Si1	103.83(3)
		Zn1 – P1‘ – Si2‘/Zn1‘ – P1 – Si2	133.54(3)
		Zn1/Zn1‘ – P2/P2‘ – Si3/Si3‘	102.60(3)
		Zn1/Zn1‘ – P2/P2‘ – Si4/Si4‘	106.70(4)
		Si1/Si1‘ – P1/P1‘ – Si2/Si2‘	107.09(4)
		Si3/Si3‘ – P2/P2‘ – Si4/Si4‘	105.94(4)

The cooling of **5-1-C** to 137.5 K leads to a phase transition during which the total loss of crystallinity was observed.

5.1.6. References

[1] J. E. Lilienfeld, *Vol. CA 272437*, USA, **1925**, pp. 1 – 9.
[2] O. Heil, *Vol. GB439457*, Germany, **1934**, pp. 1 – 4.
[3] M. A. Green, K. Emery, Y. Hishikawa, W. Warta, *Prog. Photov.* **2011**, *19*, 84 – 92.
[4] C. Wadia, A. P. Alivisatos, D. M. Kammen, *Environ. Sci. Technol.* **2009**, *43*, 2072 – 2077.
[5] G. A. Hood, *Proceedings of the 5th Vertebrate Pest Conference* **1972**, *16*, 85 – 92.
[6] N. Yogendranathan, H. M. M. T. B. Herath, T. Sivasundaram, R. Constantine, A. Kulatunga, *BMC Pharmacol. Toxicol.* **2017**, *18*, 18:37-1 – 18:37-6.
[7] E. A. Fagen, *J. Appl. Phys.* **1979**, *50*, 6505 – 6515
[8] E. J. Luber, M. H. Mobarok, J. M. Buriak, *ACS Nano* **2013**, *7*, 8136 – 8146.
[9] M. H. Mobarok, E. J. Luber, G. M. Bernard, L. Peng, R. E. Wasylishen, J. M. Buriak, *Chem. Mater.* **2014**, *26*, 1925 – 1935.
[10] M. Q. Ho, R. J. A. Esteves, G. Kedarnath, I. U. Arachchige, *J. Phys. Chem. C* **2015**, *119*, 10576 – 10584.
[11] B. A. Glassy, B. M. Cossairt, *Chem. Commun.* **2014**, *51*, 5283 – 5286.
[12] G. Z. Shen, Y. Bando, J. Q. Hu, D. Golberg, *Appl. Phys. Lett.* **2006**, *88*, 143105-1 – 143105-3.
[13] L. Huldt, N. G. Nilsson, B. O. Sundström, W. Ždanowicz, *Phys. Status Solidi A* **1979**, *53*, K15 – K18.
[14] J. Misiewicz, Z. Gumienny, R. Cywiński, E. Mugeński, *Phys. Status Solidi A* **1989**, *111*, K249 – K252.
[15] C. Bouzara, S. Kaci, A. Boukezzata, F. Kezzoula, I. Bozetine, A. Keffous, M. Trari, A. Manseri, H. Menari, R. Azzouz, M. Leitgeb, M.-A. Ouadfel, L. Talbi, K. Benfadel, Y. Ouadah, *Silicon* **2018**, *ahead of print*.
[16] R. Yang, Y.-L. Chueh, J. R. Morber, R. Snyder, L.-J. Chou, Z. L. Wang, *Nano Lett.* **2007**, *7*, 269 – 275.
[17] C. C. Vancea, S. Vaddirajub, R. Karthikeyana, *J. Environ. Chem. Eng.* **2018**, *6*, 568 – 573.
[18] V. B. Link, C. O. Mohr, *Bull. World Health Organ.* **1953**, *9*, 585 – 596.
[19] Y. Tanaka, *Rev. Phys. Chem. Jpn* **1968**, *38*, 137 – 150.
[20] H. Okamoto, *J. Phase Equilib. Diff.* **2011**, *32*, 79.
[21] I. J. Hegyi, E. E. Loebner, E. W. Poor Jr., J. G. White, *J. Phys. Chem. Solids* **1963**, *24*, 333 – 337.
[22] X. Li, F. Peng, X. Zhou, P. Wang, *Solid State Sci.* **2013**, *21*, 51 – 53.
[23] H. Hwang, M. G. Kim, Y. Kim, S. W. Martin, J. Cho, *J. Mater. Chem.* **2007**, *17*, 3161 – 3166.
[24] M. Westerhausen, G. Sapelza, M. Zabel, A. Pfitzner, *Z. Naturforsch. B* **2004**, *59b*, 1548 – 1550.
[25] S. C. Goel, M. Y. Chiang, W. E. Buhro, *J. Am. Chem. Soc.* **1990**, *112*, 5636 – 5637.
[26] A. J. Edwards, M. A. Paver, P. R. Raithby, C. A. Russell, D. S. Wright, *Organometallics* **1993**, *12*, 4687 – 4690.
[27] B. A. Vaughan, E. M. Arsenault, S. M. Chan, R. Waterman, *J. Organomet. Chem.* **2012**, *696*, 4327 – 4331.
[28] R. Tacke, C. Kobelt, J. A. Baus, R. Bertermann, C. Burschka, *Dalton Trans.* **2015**, *44*, 14959 – 14974.
[29] A. R. Sanger, *Inorg. Nucl. Chem. Lett.* **1973**, *9*, 351 – 354.
[30] R. T. Boeré, R. T. Oakley, R. W. Reed, *J. Organomet. Chem.* **1987**, *331*, 161 – 167.
[31] E. Hey, C. Ergezinger, K. Dehnicke, *Z. Naturforsch. B* **1988**, *43*, 1679 – 1682.
[32] M. Wedler, F. Knösel, U. Pieper, D. Stalke, F. T. Edelmann, H. D. Amberger, *Chem. Ber.* **1992**, *125*, 2171 – 2181.
[33] F. T. Edelmann, *Coord. Chem. Rev.* **1994**, *137*, 403 – 481.
[34] R. Duchateau, C. T. v. Wee, A. Meetsma, P. T. v. Duijnen, J. H. Teuben, *Organometallics* **1996**, *15*, 2279 – 2290.
[35] J. R. Hagadorn, J. Arnold, *Organometallics* **1996**, *15*, 984 – 991.
[36] J. R. Hagadorn, J. Arnold, *J. Chem. Soc. Dalton Trans.* **1997**, *0*, 3087 – 3096.
[37] D. Walther, P. Gebhardt, R. Fischer, U. Kreher, H. Görls, *Inorg. Chim. Acta* **1998**, *281*, 181 – 189.
[38] A. J. Gallant, K. M. Smith, B. O. Patrick, *Chem. Commun.* **2002**, 2914 – 2915.
[39] G.-L. Xu, R. J. Crutchley, M. C. DeRosa, Q.-J. Pan, H.-X. Zhang, X. Wang, T. Ren, *J. Am. Chem. Soc.* **2005**, *127*, 13354 – 13363.
[40] S. Tanaka, K. Mashima, *Inorg. Chem.* **2011**, *50*, 11384 – 11393.
[41] Y. Yamaguchi, H. Nagashima, *Organometallics* **2000**, *19*, 725 – 727.
[42] C. Kirchner, B. Krebs, *Inorg. Chem.* **1987**, *36*, 3569 – 3576.
[43] E. Cavero, S. Uriel, P. Romero, J. L. Serrano, R. Giménez, *J. Am. Chem. Soc.* **2007**, *129*, 11608 – 11618.
[44] P. L. Goggin, G. Johansson, M. Maeda, H. Wakita, *Acta Chem. Scand.* **1984**, *A 38*, 625 – 639.
[45] H. Kasano, M. Takesada, H. Mashiyama, *J. Phys. Soc. Jpn.* **1992**, *61*, 1580 – 1584.
[46] C. W. S. Dr., H. W. R. P. Dr., J. M. P. Dr., R. B. O. Dr., *Angew. Chem. Int. Ed.* **2006**, *45*, 3948 – 3950; *Angew. Chem.*. **2006**, *118*, 4052 – 4054.
[47] M. Hargittai, J. Tremmel, I. Hargittai, *Inorg. Chem.* **1986**, *25*, 3163 – 3166.
[48] D. Meyer **2013**, „Synthese von molekularen Precursoren zur Darstellung von EP-Nanopartikeln (E = Ge, Sn, Zn)" *Master thesis*, Universität Regensburg.
[49] S. G. Goel, M. Y. Chiang, D. J. Rauscher, W. E. Buhro, *J. Am. Chem. Soc.* **1993**, *115*, 160 – 169.
[50] S. S. Sen, H. W. Roesky, D. Stern, J. Henn, D. Stalke, *J. Am. Chem. Soc.* **2010**, *132*, 1132 – 1126.

[51] S. S. Sen, A. Jana, H. W. Roesky, C. Schulzke, *Angew. Chem*. **2009**, 8688 – 8690.
[52] G. Becker, G. Gutekunst, H. J. Wessely, *Z. Anorg. Allg. Chem.* **1980**, 113 – 129.
[53] CrysAlisPro Software System, Rigaku Oxford Diffraction, (2015).
[54] R. C. Clark, J. S. Reid, *Acta Cryst*. **1995**, *A51*, 887 – 897.
[55] G. M. Sheldrick, *Acta Cryst*. **2015**, *A71*, 3 – 8.
[56] O.V. Dolomanov, L.J. Bourhis, R.J. Gildea, J. A. K. Howard, H. Puschmann, Olex2: A complete structure solution, refinement and analysis program, *J. Appl. Cryst*. **2009**, *42*, 339 – 341.
[57] G. M. Sheldrick, *Acta Cryst*. **2015**, C27, 3 – 8.
[58] G. M. Sheldrick, *Acta Cryst.* **2008**, *A64*, 112 – 122.

5.2. Studies on the preparation of Ga_xP_y nanoparticles

5.2.1. Author contribution

Daniela Meyer: Preparation and performance of the described studies

Edwin Baquero Valesco: Performance of the TEM and SEM/EDX analyses, supervision of the studies

Susanne Bauer: Synthesis and analytics of **5-2-B**

5.2.2. Introduction

A special branch of the above mentioned transistor technique, which started with the use of semiconductors like Ge or Si, each owning an indirect band gap, is the field of light emitting diodes (LED) utilizing materials with direct band gaps. The main component of a LED is the semiconducting crystal often doped with electron donating or electron accepting substances in order to enhance the electric generation of free charge carriers electrons e^- and holes h^+. In the course of recombination of those charge carriers over a direct band gap, radiation of light occurs matching the energy difference between the conduction band and the valence band (Figure 5-2 - 1). Therefore, LEDs emit a defined wavelength specific to the element or compound.[1,2]

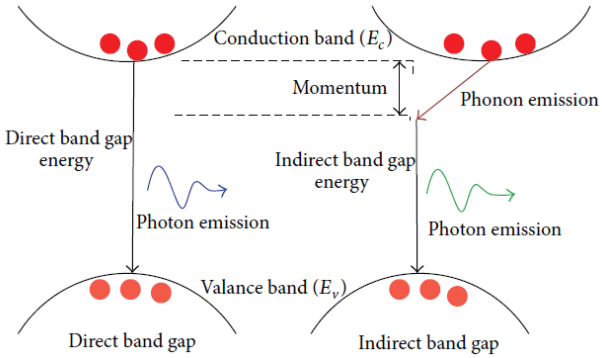

Figure 5-2 - 1: Comparison between two models of a direct and an indirect band gap. Image from Journal of Materials Research, "MATLAB User Interface for Simulation of Silicon Germanium Solar Cell", A. K. Singh, J. Tiwari, A. Yadav, R. K. Jha, 2015, CC BY 3.0.

The first compound to exhibit the phenomenon of electroluminescence was carborundum SiC discovered by Henry Joseph Round in 1907, who observed that the material began to glow yellow when a power of about 10 V was applied. At higher currents colours of orange, green and blue occurred.[2] Further investigations about this fascinating topic were done by the young Russian scientist Oleg Losev by studying SiC and also ZnO_2,[3] but it was Georges Destriau who tested different inorganic substances in alternating electric fields and who introduced the term *electroluminescence* for the first time.[4] Nevertheless, these properties of some inorganic elements and compounds remained a part of fundamental research until in 1948 Bardeen and Brattain invented the bipolar junction transistor[5] which became the basis of a laser diode developed in 1962.[6-10] Only six years later, the commercial production of LEDs began although they were limited by effectivity and colour as the mainly used semiconductors GaAs and GaAsP only emitted a red colour.[11] In the next decades, the gaps in the visible spectrum were closed[11,12] at what the synthesis of defect-free GaN for the preparation of blue LEDs in 1989 was the biggest obstacle to overcome.[13-16] Henceforth, the production of white light LED setups was possible and with them a replacement for the inefficient, yet

still indispensable light bulbs. Today, the improvement of LED technique[11,17] still goes on so that the current-saving, cold light sources rose from the use as little signal lamps to the application in illumination systems for whole cities.

During this process, gallium has always been one of the most important elements as it forms compounds with interesting optical features in combination with arsenic, phosphorus or nitrogen leading to substances suitable for substituting the semiconductors diamond, silicon or tin.[18] In this course, GaP is not only applicable for nonlinear optics due to its high nonlinear second order coefficient, the transparency or the large refractive index.[19] Its nanoparticles, exhibiting a variety of shapes like columns or wires, may be used in photonics, sensors and other optical usages,[20,21,19] while layers of porous GaP were found to show an emission in the blue and ultraviolet range of the light spectrum.[22] Doping gallium phosphide with different elements as there are Eu, N, Cu, C, Li, Zn, Te or Nd enhances the photoluminescence of the material or leads to changes in the radiated wavelength because of the new light emitting centres.[23-30]

In order to prepare gallium phosphide usable in LEDs setups be it bulk-GaP or nanostructures, different approaches can be used. While for the synthesis of bulk GaP the elements are reacted at high temperatures,[31] the nanoscopic material is prepared by multi-source-precursor methods with $P(SiMe_3)_3$ and $^tBu_3Ga$[32] or Ga, Ga_2O_3 and P_{red}.[33,34] But in contrast to the previous chapter (chapter 5.1) the single-source precursor approach has been taken into account. Complex **5-2-A** has been synthesized from $GaCl_3$ and $P(SiMe_3)$ and was subsequently thermally decomposed which leads to the formation of GaP and Me_3SiCl.[35]

But not only compound **5-2-A** became apparent to be a suitable precursor for the preparation of GaP, also $[CH(C(Me)N(2,6\text{-}^iPr_2C_6H_3))_2]Ga(PH_2)_2$ (**5-2-B**)[36] stabilized by a *β*-diketiminato ligand might be a promising candidate for the preparation gallium phosphide nanoparticles.

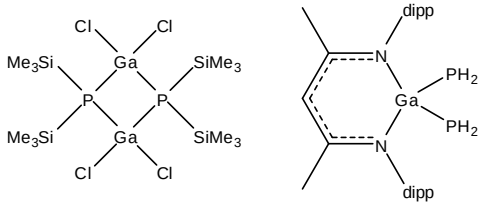

5-2-A

5-2-B

dipp = 2,6 - Diisopropylphenyl

Scheme 5-2 - 1: Examples for single source precursors probably suitable for the GaP synthesis.

5.2.3. Results and Discussion

As the *β*-diketiminato ligand forms stable complexes with various metal centres and it can also be removed very easily due to its sensitivity towards moisture it was the ligand of choice for a potential single source precursor for GaP nanoparticles. Another advantage of **5-2-B** is its straightforward synthesis by the reaction of 1 eq. $[CH(C(Me)N(2,6\text{-}^iPr_2C_6H_3))_2]GaCl_2$ (**5-2-C**) with 2 eq. of $NaPH_2$ from which **5-2-B** can be isolated in reasonable yields.[36]

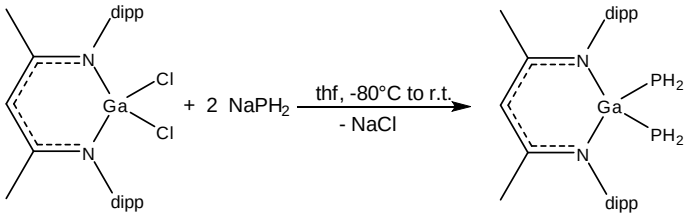

5-2-C **5-2-B**

Scheme 5-2 - 2: Preparation of **5-2-B**.[36]

Due to the reasons that were already discussed above, different amounts of the stabilizers HDA and PA were used for the nanoparticles tests of **5-2-B** (**5-2-B**:HDA = 1:1, **5-2-B**:PA = 1:1, **5-2-B**:HDA:PA = 1:0.5:0.5). The reaction conditions are similar to the previously described experiments using mesitylene as solvent and the hot injection method. In contrast to the reactions of $[CH(C(Me)N(2,6\text{-}^{i}Pr_2C_6H_3))_2]MP(SiMe_3)_2$ (M = Ge, Sn) and $[CH(C(Me)N(2,6\text{-}^{i}Pr_2C_6H_3))_2]SnAs(SiMe_3)_2$ only very small changes in the colour of the mixtures of **5-2-B** could be observed at 150°C for 24 h. Therefore, the temperature was increased to 180°C for 24 h. As a result, in all cases the reaction mixtures turned from colourless to orange, but only for **5-2-B**:HDA = 1:1 and for **5-2-B**:HDA:PA = 1:0.5:0.5 an additional precipitate was formed. This suggests that HDA is a more suitable stabilizer for the reactions of **5-2-B**. The precipitate of the reaction of **5-2-B**:HDA = 1:1 was further studied by TEM, EDX and XRD. The TEM samples, that were taken from the crude reaction mixture, show the presence of solids with different shapes and sizes but the formation of nanoparticles could be ruled out unequivocally.

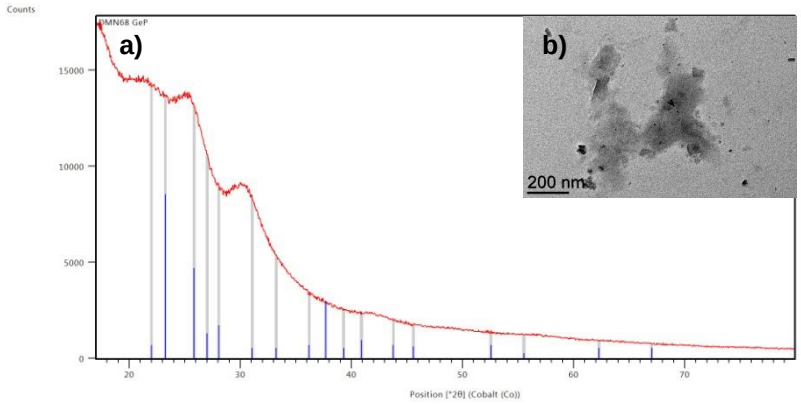

Figure 5-2 - 2: a) XRD diffractogram of the reaction of **5-2-B** with 1 eq. of HDA (180°C, 24 h) revealing an amorphous composition of the precipitate; b) TEM picture of the reaction.

While the XRD investigations only proved the solids of the reaction of **5-2-B** with 1 eq. of HDA to be amorphous, the EDX studies clearly showed a composition of GaP with a small excess of Ga (Ga:P = 1.33:1).

5.2.4. Conclusion

The experiments of **5-2-B** in order to prepare GaP exhibit that although the precipitate formed during the reactions has the fitting composition (Ga:P = 1.3:1) no nanoparticles could be obtained. Thus, **5-2-B** does not represent a suitable single source precursor for the synthesis of GaP nanoparticles.

5.2.5. Supporting Information

Experimental Section

General Prodecures

All experiments were carried out under a dry nitrogen or argon atmosphere using standard Schlenk or drybox techniques. Solvents were dried by using an MBraun purification system followed by a distillation from sodium and stored over 3 Å mol sieve. The complexes $[CH(C(Me)N(2,6\text{-}{}^{i}Pr_2C_6H_3))_2]Ga(PH_2)_2$ (**5-2-B**), $[CH(CNMe(dipp))_2]GaCl_2$ (**5-2-C**)[36] and $NaPH_2$[37] were prepared according to literature. The NMR spectra were recorded on a Bruker an Avance 300 (^1H: 300.132 MHz, $^{31}P\{^1H\}$:121.5 MHz, ^{31}P: 121.5 MHz) with δ referenced to external $SiMe_4$ (^1H) and H_3PO_4 ($^{31}P\{^1H\}$, ^{31}P).

Nanoparticles studies

5-2-B and different stoichiometries of stabilizers were mixed in 3 mL of mesitylene. The mixtures were dipped into an oil bath at 180°C and heated for 24 h, except for reaction **II** which was heated for 72 h. The grid for the TEM analysis was prepared from the reaction solutions. The obtained particles were precipitated and washed twice with ethanol. Samples for EDX and XRD analyses were prepared from the washed and dried solid.

Table 5-2 - 1: Amounts of **5-2-B** and stabilizers used in the 24 h reactions as well as the achieved yields and the observed color changes.

24 h	**I**		**II** (72 h)		**III**		
	1 eq. HDA		1 eq. PA		0.5 eq. HDA + 0.5 eq. PA		
	5-2-B	HDA	**5-2-B**	PA	**5-2-B**	HDA	PA
m [mg]	70.5	31.5	70.2	32.1	69.3	15	16.1
n [mmol]	0.12	0.12	0.12	0.12	0.12	0.06	0.06
Yield [mg]	16.6		-		-		
Color (start)	Clear colourless		Clear colourless		Clear colourless		
Color (end)	Orange Orange precipitate		Orange		Orange Orange precipitate		

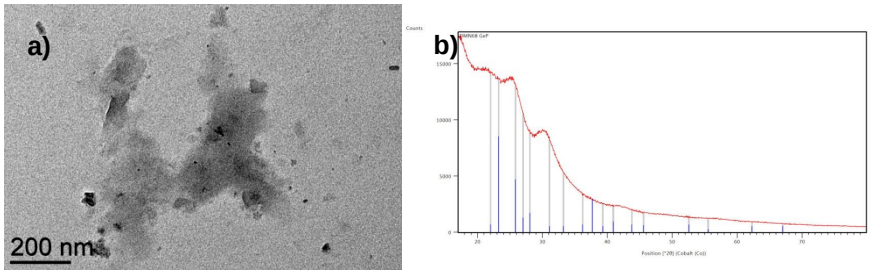

Figure 5-2 - 3: a) TEM image; b) XRD diffractogram of the reaction **I**.

Composition	
EDX	GaP (Ga:P = 1.33:1)
XRD	-

5.2.6. References

[1] I. I. Bayneva, *Int. J. Pharm. Technol.* **2016**, *8*, 15304 – 15309.
[2] E. F. Schubert **2018**, „Light-Emitting Diodes" 3rd Edition: E. Fred Schubert.
[3] N. Zheludev, *Nat. Photonics* **2007**, *1*, 198 – 192.
[4] G. Destriau, *The London, Edinburgh, and Dublin Philosophical Magazine and Journal of Science* **1947**, *38*, 700 – 739.
[5] J. Bardeen, W. H. Brattain, *Phys. Rev.* **1948**, *74*, 230 – 231.
[6] N. Holonyak, S. F. Bevacqua, *Appl. Phys. Lett.* **1962**, *1*, 82 – 83.
[7] R. N. Hall, G. E. Fenner, J. D. Kingsley, T. J. Soltys, R. O. Carlson, *Phys. Rev. Lett.* **1962**, *9*, 366 – 368.
[8] M. I. Nathan, W. P. Dumke, G. Burns, F. H. Dill, G. Lasher, *Appl. Phys. Lett.* **1962**, *1*, 62 – 64.
[9] T. M. Quist, R. H. Rediker, R. J. Keyes, W. E. Krag, B. Lax, A. L. McWhorter, H. J. Zeigler, *Appl. Phys. Lett.* **1962**, *1*, 91 – 92.
[10] M. Feng, N. H. Jr., W. Hafez, *Appl. Phys. Lett.* **2004**, *84*, 151 – 153.
[11] R. Haitz, J. Y. Tsao, *Optik & Photonik* **2011**, *6*, 26 – 30.
[12] S. Keller, S. P. Denbaars, *Curr. Opin. Solid State Mater. Sci.* **1998**, *3*, 45 – 50.
[13] H. Amano, I. Akasaki, K. Hiramatsu, N. Koide, N. Sawaki, *Thin Solid Films* **1988**, *163*, 415 – 420.
[14] H. Amano, I. Akasaki, T. Kozawa, K. Hiramatsu, N. Sawaki, K. Ikedaa, Y. Ishiia, *J. Lumin.* **1988**, *40 - 41*, 121 – 122.
[15] H. Amano, K. Hiramatsu, I. Akasaki, *Jpn. J. Appl. Phys., Part 2* **1988**, *27*, L1384 – L1386.
[16] S. Nakamura, T. Mukai, M. Senoh, *Jpn. J. Appl. Phys., Part 2* **1991**, *30*, L1998 – L2001.
[17] X. Dai, Y. Deng, X. Peng, Y. Jin, *Adv. Mater.* **2017**, *29*, 1607022-1 – 1607022-22.
[18] H. Welker, *Z. Naturforsch. A* **1952**, *7*, 744 – 749.
[19] E. D. Luca, R. Sanatinia, S. Anand, M. Swillo, *Opt. Mater. Express* **2016**, *6*, 587 – 596.
[20] R. Sanatinia, M. Swillo, S. Anand, *Nano Lett.* **2012**, *12*, 820 – 826.
[21] A. Dobrovolsky, P. O. Å. Persson, S. Sukrittanon, Y. Kuang, C. W. Tu, W. M. Chen, I. A. Buyanova, *Nano Lett.* **2015**, *15*, 4052 – 4058.
[22] A. Anedda, A. Serpi, V. A. Karavanskii, I. M. Tiginyanu, V. M. Ichizli, *Appl. Phys. Lett.* **1995**, *67*, 3316 – 3318.
[23] G. A. Wolff, R. A. Hebert, J. D. Broder, *Phys. Rev.* **1955**, *100*, 1144 – 1145
[24] D. R. Wight, *J. Phys. D: Appl. Phys.* **1977**, *10*, 431 – 454.
[25] K. Moser, W. Eisfeld, W. Penzenstadler, W. Prettl, *J. Phys. D: Appl. Phys.* **1985**, *18*, 2303 – 2308.
[26] P. Bergman, B. Monemar, *J. Lumin.* **1987**, *38*, 87 – 89.
[27] H. P. Gislason, B. Monemar, P. Bergman, M. E. Pistol, *Phys. Rev. B* **1988**, *38*, 5466 – 5473.
[28] K. Takahei, H. Nakagome, *J. Appl. Phys.* **1992**, *72*, 3674 – 3678.
[29] S. L. Pyshkin, A. Anedda, F. Congiu, A. Mura, *Pure Appl. Opt.* **1993**, *2*, 499 – 503.
[30] H. Elhouichet, S. Daboussi, H. Ajlani, A. Najar, A. Moadhen, M. Oueslati, I. M. Tiginyanu, S. Langa, H. Föll, *J. Lumin.* **2005**, *113*, 329 – 337.
[31] N. Wiberg, A. F. Hollemann **2007**, „Hollemann, Wiberg – Lehrbuch der Anorganischen Chemie" 102nd Edition: de Gruyter Berlin.
[32] F. M. Davidson, R. Wiacek, B. A. Korgel, *Chem. Mater.* **2005**, *17*, 230 – 233.
[33] C. Tang, S. Fan, M. L. d. l. Chapelle, H. Dang, P. Li, *Adv. Mater.* **2000**, *12*, 1346 – 1348.
[34] Q. Wu, Z. Hu, C. Liu, X. Wang, Y. Chen, *J. Phys. Chem. B* **2005**, *109*, 19719 – 19722.
[35] R. L. Wells, M. F. Self, A. T. McPhail, S. R. Aubuchon, *Organometallics* **1993**, *12*, 2832 – 2834.
[36] S. Bauer **2014**, „Synthese und Charakterisierung von potentiellen Einkomponentenvorstufen für Übergangsmetall- und Hauptgruppenelementpnictogenid-Nanopartikel" *Dissertation*, Universität Regensburg.
[37] R. Klement, G. Bauer (Editor) **1987** „Handbuch der Präparativen Anorganischen Chemie" Vol. 2, Ferdinand Enke Verlag, Stuttgart.

6. Conclusion

6.1. English version

In summary, the present work provides a variety of potential single source precursors for the synthesis of group 14 element pnictogenide nanoparticles (M_xE_y with M = Ge, Sn; E = P, As), which are stabilized by a *β*-diketiminato ligand that can easily be removed by acidic or basic reagents under mild conditions. Furthermore, five novel compounds exhibiting a rare silicon arsenic double bond with a coordinating benzamidinato ligand could be synthesized and characterized and also studies on the preparation and the reactivity of hitherto unknown benzamidinato zinc complexes were successfully performed.

6.1.1. Five novel arsasilene complexes

Following the reaction of [PhC(N^{t}Bu)$_2$]SiCl and LiP(SiMe$_3$)$_2$ reported by Driess *et al.* in 2011, it could be shown that a simple one-pot synthesis using [PhC(N^{t}Bu)$_2$]SiCl and the arsenic compound LiAs(SiMe$_3$)$_2$ leads to the formation of [PhC(N^{t}Bu)$_2$]Si(SiMe$_3$)=As(SiMe$_3$) (**3-1**) (Figure 6-1 - 1 top left). Studies on the reactivity of the reaction mixture of the starting materials towards water and oxygen revealed the formation of a hydrolysis product [PhC(N^{t}Bu)$_2$]Si(H)=As(SiMe$_3$) (**3-2**) and an oxidation product [PhC(N^{t}Bu)$_2$]Si(OSiMe$_3$)=As(SiMe$_3$) (**3-5**) (Figure 6-1 - 1 top middle and right). Additionally, the species {[PhC(N^{t}Bu)$_2$]Si}$_2$=AsSiMe$_3$ (**3-3**) and {[PhC(N^{t}Bu)$_2$]Si=AsSiMe$_3$}$_2$ (**3-4**) could be obtained in reactions which were performed to reproduce **3-1** (Figure 6-1 - 1 bottom). Yet, all attempts to synthesize **3-3** and **3-4** selectively failed.

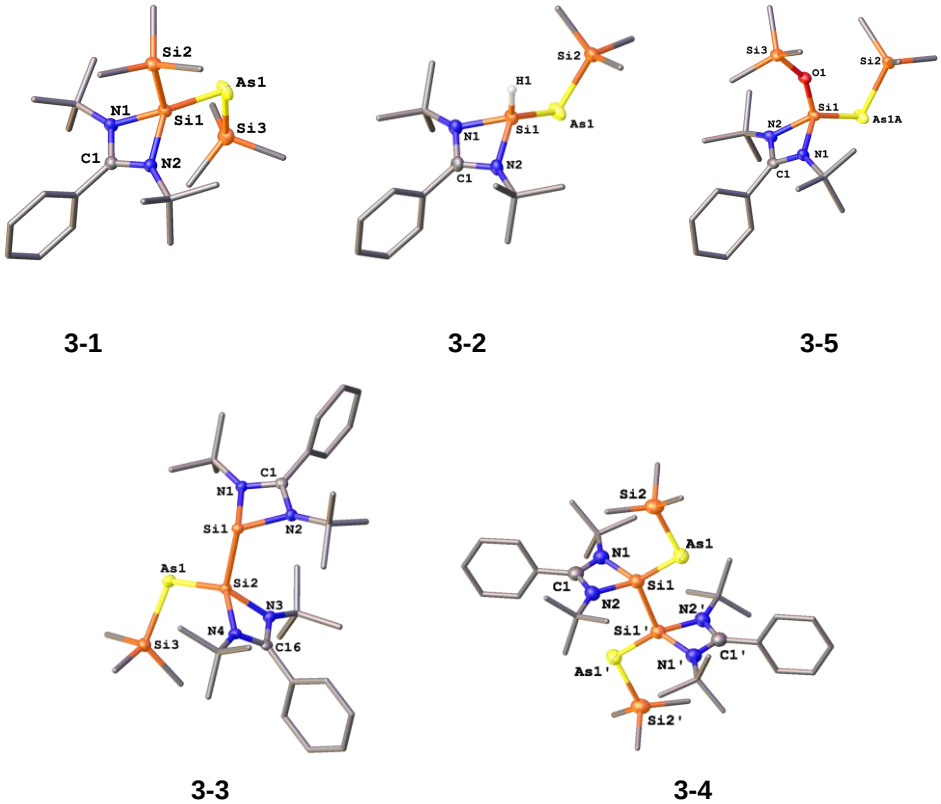

3-1 **3-2** **3-5**

3-3 **3-4**

Figure 6-1 - 1: The solid state structures of the compounds **3-1**, **3-2**, **3-3**, **3-4** and **3-5**.

3-1 was prepared from the reaction of [PhC(N^{t}Bu)$_2$]SiCl with LiAs(SiMe$_3$)$_2$, it was fully characterized by NMR spectroscopy, EI mass spectrometry and X-ray structure analysis whereby it was necessary for the latter to permanently cool the reaction mixtures to –80°C to grow suitable crystals. **3-2** could be obtained by adding a defined amount of water to the thf solutions (H$_2$O:[PhC(N^{t}Bu)$_2$]SiCl:LiAs(SiMe$_3$)$_2$ = 1:5:5), which may not be exceeded to avoid decomposition. It was also fully characterized by the typical spectroscopic methods but in addition by ^{29}Si NMR spectroscopy to unequivocally detect the Si–H coupling. In a similar way to **3-2**, a stoichiometric quantity of (SiMe$_3$)$_2$O$_2$ mixed with [PhC(N^{t}Bu)$_2$]SiCl and LiAs(SiMe$_3$)$_2$ leads to the formation of compound **3-5** (Scheme 6-1 - 1). In the case of **3-3** and **3-4**, just a few crystals appeared as side products of the synthesis of **3-1**. It was also possible to detect the molecular peak of **3-4** by solid state EI mass spectrometry.

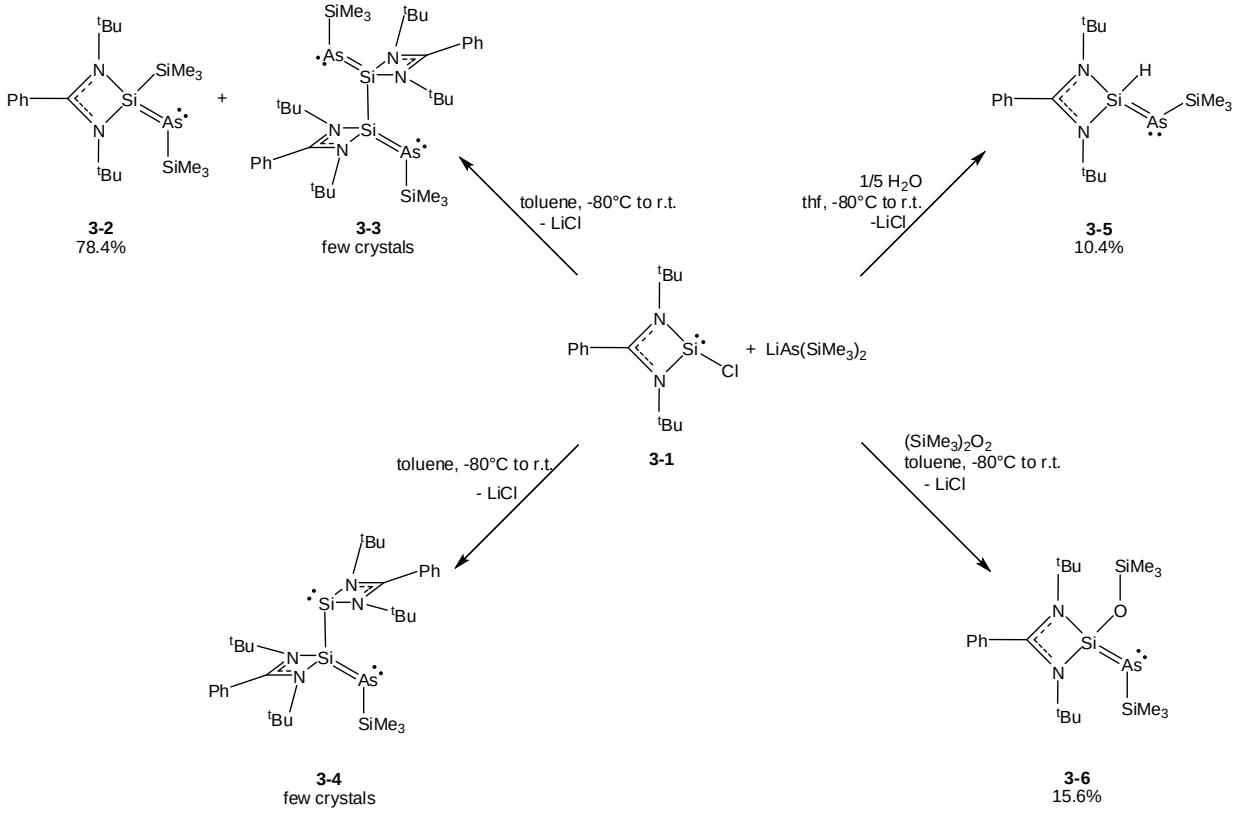

Scheme 6-1 - 1: Overview of the preparation of the arsasilenes **3-1** to **3-5**.

Also, some studies concerning the reactivity of **3-1** were performed, especially investigations in order to transform **3-1** into **3-2** and **3-5**, but these attempts were not conclusive as **3-2** and **3-5** can only be obtained from the reaction of the monochlorosilylene with LiAs(SiMe$_3$)$_2$ and water or (SiMe$_3$)$_2$O$_2$, respectivley. Additionally, VT NMR investigations were done to elucidate the mechanistic details of the formation of **3-1** and possibly to gain hints on the formation of the arsenic analogue of Driess' [PhC(N^{t}Bu)$_2$]SiP(SiMe$_3$)$_2$, which was not successful. But instead, crystals of the literature known compound {[PhC(N^{t}Bu)$_2$]SiAs}$_2$ **3-F** with a yet unknown unit cell were isolated from the thf-d$_8$ mixture.

6.1.2. Nanoparticles from $[CH(C(Me)N(2,6\text{-}^{i}Pr_2C_6H_3))_2]ME(SiMe_3)_2$ (M = Ge, Sn; E = P, As)

As it has already been described in the chapters 1.3.7 and 4.2, numerous possibilities exist to utilize nanoparticles and especially the still scarcely explored nanoscale material containing elements of group 14 and 15 might show interesting properties. In general, nanoparticles can be synthesized by various methods, starting either from bulk material (top down approaches like milling) or from atoms and molecules (bottom up method). The bottom up approach of hot injections starts with the solution of the precursors in a high boiling, sometimes coordinating solvent, followed by a fast heating step, that leads to the decomposition of the starting material and the formation of the nanoscopic material. If a separate starting material for each component of the resulting nanoparticles is used, the method is called multi source precursor approach. In contrast to this is the single source precursor method, in which all components of the nanoparticles are combined in one molecule. As this approach shows important advantages like mild reaction conditions and the avoidance of volatile and/or pyrophoric substances, the single source precursor approach was the method of choice to prepare M_xE_y nanoparticles (M = Ge, Sn; E = P, As). As the most promising complexes to decompose in order to achieve the desired nanoscopic matter, the two literature known compounds $[CH(C(Me)N(2,6\text{-}^{i}Pr_2C_6H_3))_2]MP(SiMe_3)_2$ (M = Ge (**4-D**), Sn(**4-E**)) and the novel $[CH(C(Me)N(2,6\text{-}^{i}Pr_2C_6H_3))_2]SnAs(SiMe_3)_2$ (**4-4**) were studied. Previously, the heavier homologues of **4-D** and **4-E** $[CH(C(Me)N(2,6\text{-}^{i}Pr_2C_6H_3))_2]MAs(SiMe_3)_2$ (M = Ge (**4-3**), Sn(**4-4**)) were successfully synthesized and fully characterized (Figure 6-1 - 2).

4-3 and **4-4** are prepared by the reaction of $[CH(C(Me)N(2,6\text{-}^{i}Pr_2C_6H_3))_2]MCl$ (M = Ge, Sn) with $LiAs(SiMe_3)_2$, whereby **4-4** is achieved in good yields, while **4-3** can only be isolated in minor quantities amounts because of which **4-3** is discarded as single source precursor.

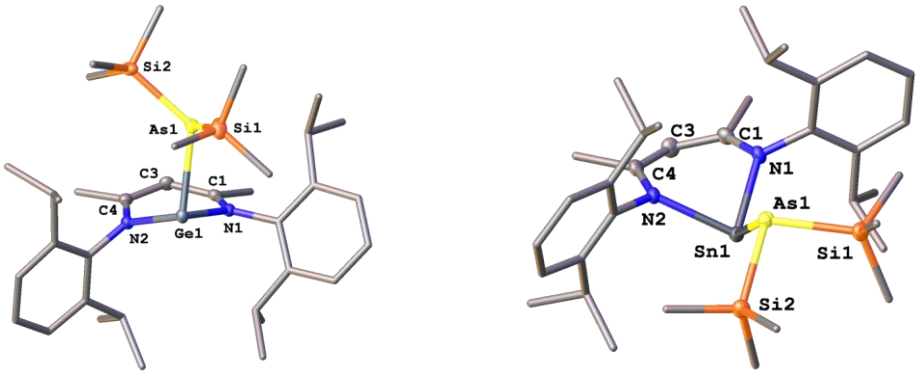

Figure 6-1 - 2: Left: Solid state structure of **4-3**. Right: Solid state structure of **4-4**.

Therefore, only the tin analogon **4-4** was used in the hot injection nanoparticles tests with PA as starting material, leading to the formation of agglomerated spherical particles, which could not be separated. Nevertheless, the particles show an average size of 10 to 14 nm and a composition of mostly Sn_4As_3, proving the applicability of **4-4** for the synthesis of tin arsenide nanoscale material (Figure 6-1 - 3).

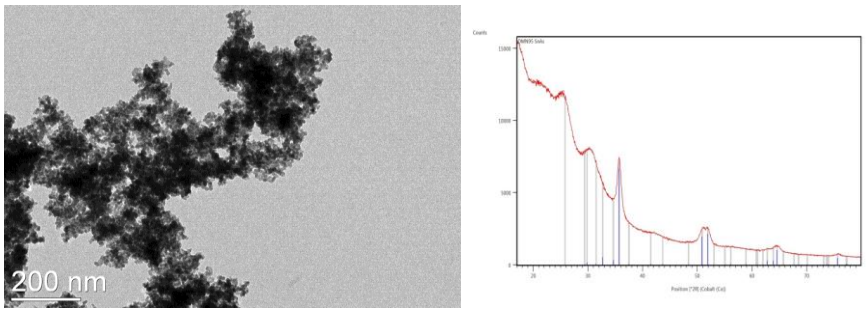

Figure 6-1 - 3: Left: TEM images of the nanoparticles formed during the decomposition of **4-4** with 1 eq. PA. Right: XRD diffractogram of the nanoparticles revealing a composition of Sn_4As_3.

Beside **4-4**, also the phosphorus compounds **4-D** and **4-E** were studied for their potential use in the synthesis of nanoparticles, which showed that the Ge compound **4-D** is not a suitable precursor. Despite decomposing to the desired germanium phosphide Ge_4P_3 which could be proven by EDX, investigations using TEM analysis clearly displayed the absence of regular shaped and similar sized nanoparticles leading to the discard of **4-D** (Figure 6-1 - 4).

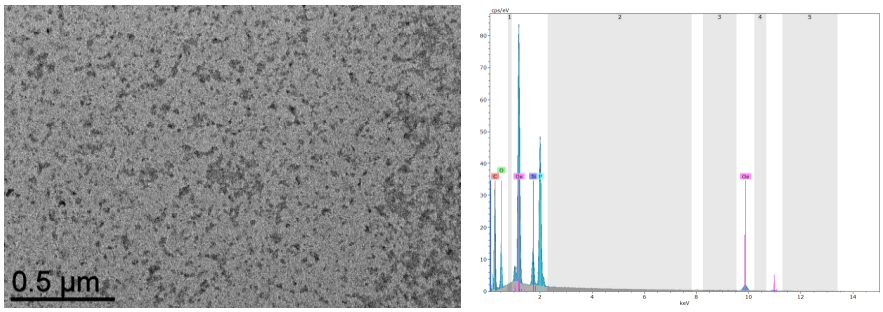

Figure 6-1 - 4: Left: TEM images of the decomposition of **4-D** with 1 eq. PA (1 h). Right: EDX spectrum of the precipitate obtained from the decomposition of **4-D** consisting of Ge_4P_3.

On the other hand, its heavier homologue **4-E** provided in the reactions with HDA very satisfactory results as the complex not only decomposes to Sn_4P_3 as required, but also forms agglomerated spherical nanoparticles with an average size of about 10 to 22 nm (Figure 6-1 - 5).

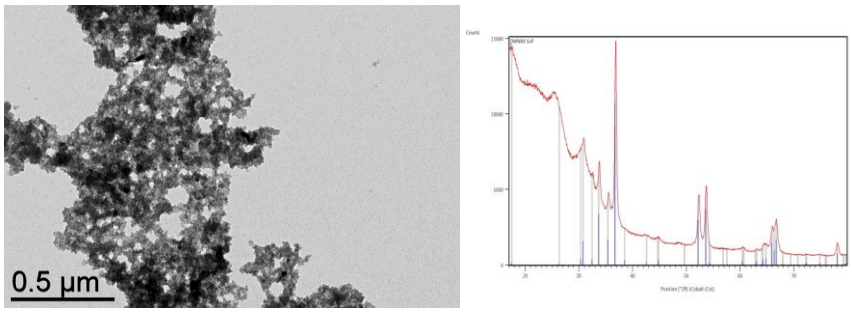

Figure 6-1 - 5: Left: Nanoparticles from the reaction of **4-E** with 0.5 eq. HDA (1 h). Right: XRD diffractogram of the reaction products of **4-E** with a composition of Sn_4P_3.

In summary, the analyses performed in the course of the experiments show that both tin compounds $[CH(C(Me)N(2,6\text{-}^{i}Pr_2C_6H_3))_2]SnE(SiMe_3)_2$ (E = P (**4-E**), As (**4-4**)) are suitable and promising single source precursors for the synthesis of nanoparticles.

Additionally to the synthesis of **4-3** and **4-4** which were especially prepared for their use as single source precursors, also basic reactivity studies were done using $[CH(C(Me)N(2,6\text{-}^{i}Pr_2C_6H_3))_2]MCl$ (M = Ge, Sn) and the lithiated compound $LiCH_2SiMe_3$ as starting material. Those approaches led to the formation of $[CH(C(Me)N(2,6\text{-}^{i}Pr_2C_6H_3))_2]MCH_2SiMe_3$ (M = Ge (**4-1**), Sn (**4-2**)), that were fully characterized by NMR spectroscopy, mass spectrometry, elemental analysis and X-ray structure analysis (Figure 6-1 - 6).

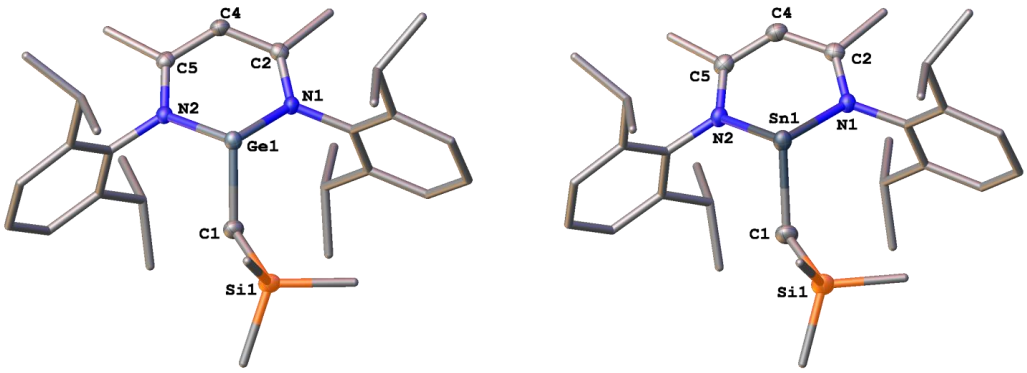

Figure 6-1 - 6: Left: Crystal structure of **4-1**. Right: Solid state structure of **4-2**.

6.1.3. Single source precursors containing phosphorus, zinc and gallium

Zinc phosphide precursors

As nanoscale Zn_2P_3 is thought to be a promising material for future photovoltaic application easy and non-toxic synthetic methods like the single source precursor approach are very attractive raising the interest in the preparation novel zinc phosphorus compounds useful for the decomposition to nanoparticles. Here, the focus is on the synthesis of a new family of zinc complexes stabilized by a variable benzamidinato ligand which might be convertible into P containing precursors. Thus, the isolation of three different Zn compounds $[PhC(N^{t}Bu)_2]_2Zn$ (**5-1-1**), $\{[PhC(N^{t}Bu)_2]Zn_2Br_3\}_n$ (**5-1-2**) and $[PhC(NtBu)_2]H \cdot ZnBr_2$ (**5-1-3**) was successful, of which the reaction of the latter with $LiP(SiMe_3)_2$ results in $\{Zn[P(SiMe_3)_2]_2\}_2$ (**5-1-C**).

While **5-1-1** can be obtained by mixing one eq. $^{t}BuN{=}C{=}N^{t}Bu$, one eq. PhLi and one eq. $ZnBr_2$, the polymeric **5-1-2** is the unexpected product of the reaction of one eq. $^{t}BuN{=}C{=}N^{t}Bu$ with one eq. PhLi and two eq. $ZnBr_2$ (Figure 6-1 - 7 top). Because both of the more obvious approaches didn't lead to a monomeric zinc bromine complex, $[PhC(N^{t}Bu)_2]Li$, the product of the reaction of $^{t}BuN{=}C{=}N^{t}Bu$ and PhLi, was isolated and then reacted in a 1:1 stoichiometry with $ZnBr_2$. However, due to traces of water that could not be avoided, the reaction resulted in compound **5-1-3** (Figure 6-1 - 7 bottom left) which was then mixed with $LiP(SiMe_3)_2$ in order to obtain a precursor for zinc phosphide nanoparticles. The

achieved product is the literature known species **5-1-C**, that was already thermally decomposed by the authors of the corresponding publication who did not get the desired Zn_2P_3. As the crystal structure of **5-1-C** was previously determined at room temperature, it was now possible to detect a phase transition at 137 K while performing the X-ray analysis at low temperatures (Figure 6-1 - 7 bottom right).

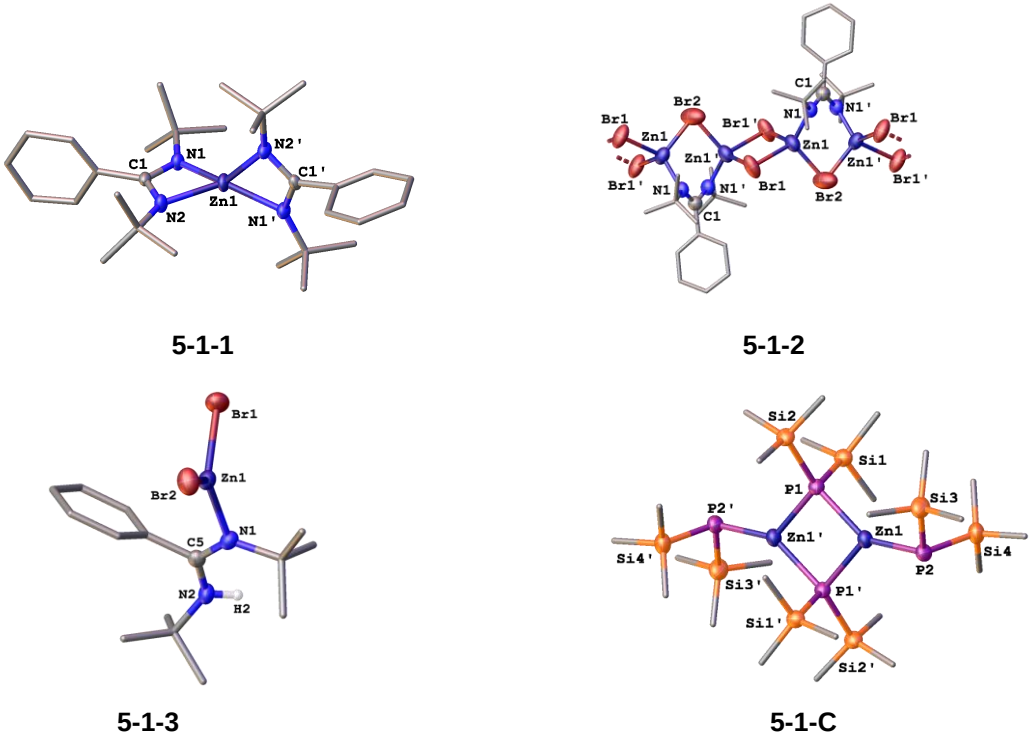

5-1-1 **5-1-2**

5-1-3 **5-1-C**

Figure 6-1 - 7: Crystal structure of **5-1-1**, **5-1-2**, **5-1-3** and **5-1-C**.

Preliminary investigations for the usage of $[CH(C(Me)N(2,6\text{-}^{i}Pr_2C_6H_3))_2]Ga(PH_2)_2$ in nanoparticle synthesis

Also, studies concerning the preparation of GaP nanoparticles were realized using the gallium compound $[CH(C(Me)N(2,6\text{-}^{i}Pr_2C_6H_3))_2]Ga(PH_2)_2$ (**5-2-B**) which was initially synthesized and characterized by Susanne Bauer. The experiments were performed similar to those described in chapter 4.4 with HDA and PA as decomposing and stabilizing agents.

Unfortunately, it was not possible to obtain any nanocorpuscles (Figure 6-1 - 8), yet, the EDX analyses of the precipitate revealed the desired composition of GaP with a slight excess of Ga.

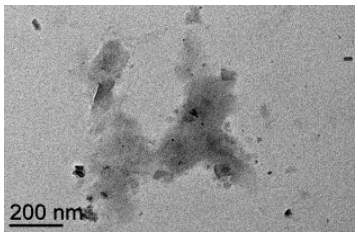

Figure 6-1 - 8: TEM image of the precipitate of reaction of **5-2-B** with 1 eq. HDA.

6.2. German version – Zusammenfassung

Zusammenfassend stellt die vorliegende Arbeit eine Reihe von möglichen single-source-Precursoren zur Synthese von Pnictogenid-Nanopartikeln der Gruppe 14 (M_xE_y mit M = Ge, Sn; E = P, As) vor, die von einem *β*-Diketiminato-Liganden stabilisiert werden, welche leicht durch saure oder basische Reagenzien unter milden Bedingungen entfernt werden können. Darüber hinaus konnten fünf neue Verbindungen charakterisiert werden, die eine seltene Silicium-Arsen-Doppelbindung mit einem koordinierenden Benzamidinatoliganden aufweisen. Außerdem wurden erfolgreich Untersuchungen zur Herstellung und Reaktivität bisher unbekannter Benzamidinato-Zinkkomplexe durchgeführt.

6.2.1. Fünf neuartige Arsasilen-Komplexe

Gemäß der von Driess *et al.* berichteten Reaktion von [PhC(N^{t}Bu)$_2$]SiCl und LiP(SiMe$_3$)$_2$ ergab die Durchführung einer einfachen Eintopfsynthese von [PhC(N^{t}Bu)$_2$]SiCl mit LiAs(SiMe$_3$)$_2$ die Bildung von [PhC(N^{t}Bu)$_2$]Si(SiMe$_3$)=As(SiMe$_3$) (**3-1**) (Abbildung 6-2 - 1 oben links). Studien über das Reaktionsverhalten der beiden Ausgangsmaterialen gegenüber Wasser und Sauerstoff führten zur Isolierung des Hydrolyseprodukts [PhC(N^{t}Bu)$_2$]Si(H)=As(SiMe$_3$) (**3-2**) sowie des Oxidationsprodukts [PhC(N^{t}Bu)$_2$]Si(OSiMe$_3$)=As(SiMe$_3$) (**3-5**) (Abbildung 6-2 - 1 oben Mitte und rechts). Hingegen war es nicht möglich, die Bildung der Spezies {[PhC(N^{t}Bu)$_2$]Si}$_2$=AsSiMe$_3$ (**3-3**) und {[PhC(N^{t}Bu)$_2$]Si=AsSiMe$_3$}$_2$ (**3-4**) zu reproduzieren, die in Reaktionen zur Verbesserung der Ausbeute von **3-1** als Nebenprodukte erhalten wurden (Abbildung 6-2 - 1 unten).

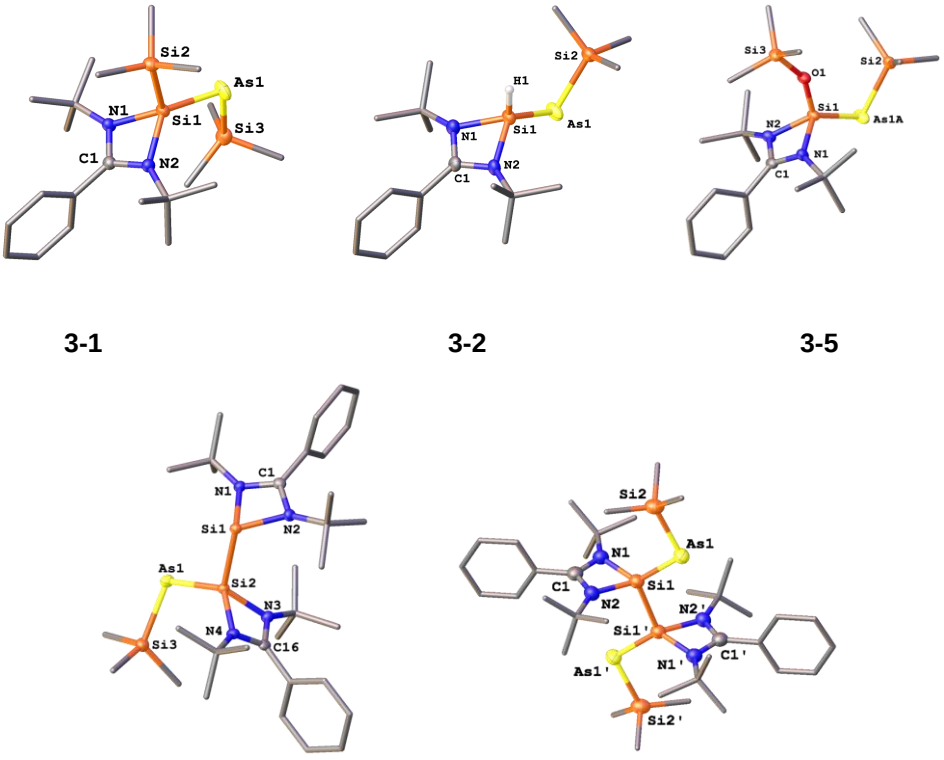

3-1 **3-2** **3-5**

3-3 **3-4**

Abbildung 6-2 - 1: Kristallstrukturen von **3-1**, **3-2**, **3-3**, **3-4** und **3-5**.

3-1 wurde aus der Reaktion von [PhC(N^{t}Bu)$_2$]SiCl mit LiAs(SiMe$_3$)$_2$ dargestellt und durch NMR-Spektroskopie, EI-Massenspektrometrie und Röntgenanalyse vollständig charakterisiert, wobei die Reaktionsmischungen im Falle von letzterem permanent auf –80°C gekühlt werden mussten, um geeignete Kristalle zu erhalten. **3-2** konnte durch Zugabe einer genau definierten Menge Wasser zu den Reaktionslösungen (H$_2$O:[PhC(N^{t}Bu)$_2$]SiCl:LiAs(SiMe$_3$)$_2$ = 1:5:5) erhalten werden, welche allerdings nicht überschritten werden darf, um eine Zersetzung zu vermeiden. **3-2** wurde ebenfalls vollständig charakterisiert, wobei zusätzlich die Si-H-Kopplung im ^{1}H-NMR-Spektrum ebenso wie im ^{29}Si-NMR-Spektrum eindeutig nachgewiesen wurde. Ähnlich wie bei **3-2** muss eine stöchiometrische Menge an (SiMe$_3$)$_2$O$_2$ zu einer Lösung von [PhC(N^{t}Bu)$_2$]SiCl und LiAs(SiMe$_3$)$_2$ zugegeben werden, um die Verbindung **3-5** zu erhalten (Schema 6-2 - 1). Im Falle von **3-3** und **3-4** wurden nur wenige Kristalle als Nebenprodukte bei der Synthese von **3-1** erhalten. Nur **3-4** konnte durch Festkörper-EI-Massenspektrometrie zusätzlich charakterisiert werden.

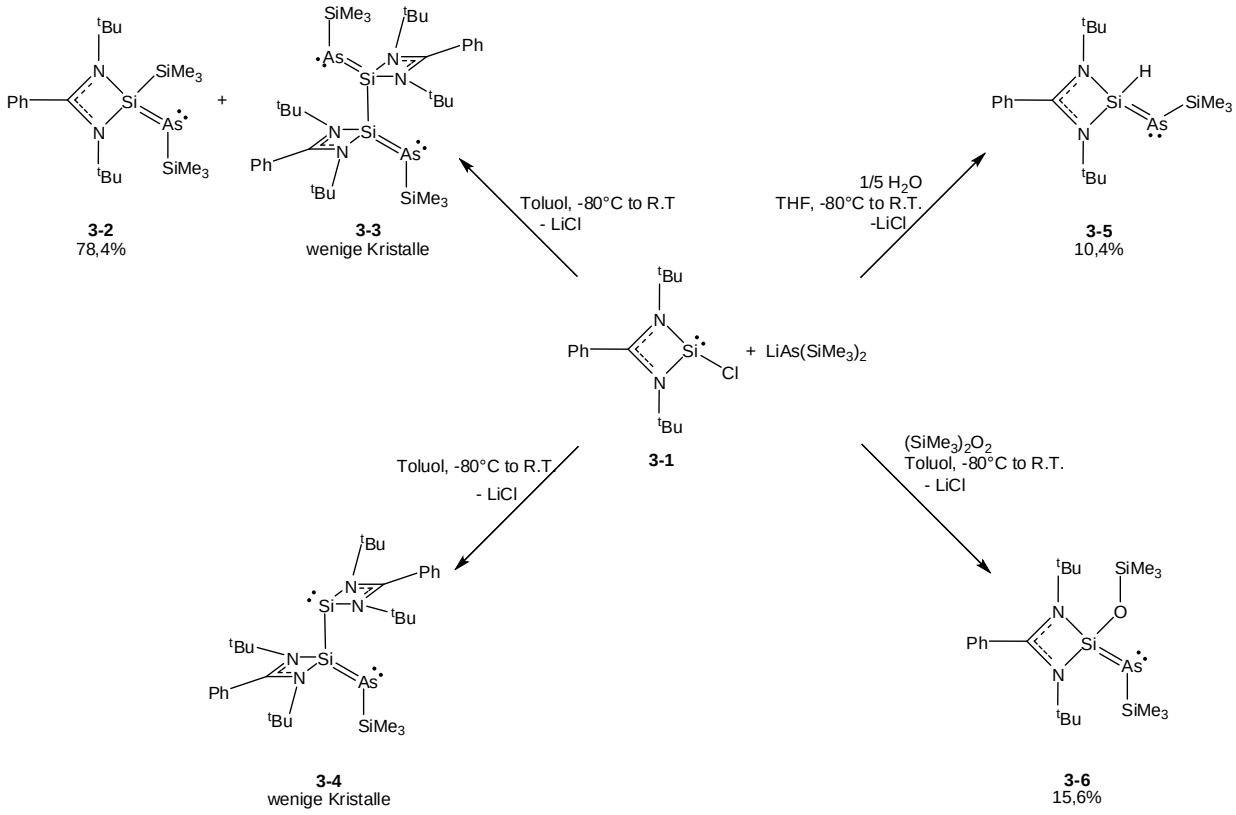

Schema 6-2 - 1: Überblick über die Darstellung der Arsasilene **3-1** bis **3-5**.

Es wurden zudem einige Untersuchungen zur Reaktivität von **3-1** unternommen, insbesondere Experimente, ob sich **3-1** in **3-2** und **3-5** überführen lässt. Es war jedoch nicht möglich, die beiden letzteren auf einem anderen Weg darzustellen als in Schema 6-2 - 1 gezeigt. Zusätzlich wurden VT-NMR-Untersuchungen durchgeführt, um mechanistische Details der Bildung von **3-1** aufzuklären und möglicherweise Hinweise auf die Bildung des Arsenanalogons des von Driess *et al.* berichteten [PhC(N^{t}Bu)$_2$]SiP(SiMe$_3$)$_2$ zu erhalten, was nicht jedoch erfolgreich war. Stattdessen wurden Kristalle des von Scheer *et al.* beschriebenen {{PhC(N^{t}Bu)$_2$]SiAs}$_2$ **3-F** mit einer bis dato unbekannten Elementarzelle aus der thf-d$_8$-Lösung isoliert.

6.2.2. Nanopartikeldarstellung unter der Verwendung der *β*-Diketiminato-Komplexe $[CH(C(Me)N(2,6\text{-}^{i}Pr_2C_6H_3))_2]ME(SiMe_3)_2$ (M = Ge, Sn; E = P, As)

Wie bereits in den Kapiteln 1.3.7 und 4.2 beschrieben, bestehen zahlreiche Möglichkeiten zur Verwendung von Nanopartikeln und insbesondere das noch kaum erforschte nanoskalige Material mit Elementen der Gruppen 14 und 15 könnte interessante Eigenschaften aufweisen. Ganz allgemein lassen sich Nanopartikel auf verschiede Weisen darstellen, wobei entweder von einem bulk-Material (Top-down-Methoden wie etwa Mahlen in Kugelmühlen) oder von Atomen und Molekülen (Bottom-Up-Herangehensweise) ausgegangen wird. Im Falle von letzterem nutzt die Hot-injection-Methode das Lösen des Ausgangsmaterials in hochsiedenden und manchmal koordinierenden Lösungsmitteln, gefolgt von schnellem Aufheizen, um die Precursoren zu zersetzen und dadurch Nanopartikel zu bilden. Wird dabei für jede Komponente der entstehenden Nanopartikel eine eigene Ausgangsverbindung verwendet, spricht man vom Multi-source-precursor-Ansatz. Im Gegensatz dazu nutzt die Single-source-precursor-Methode Moleküle, in denen alle Komponenten des späteren Partikels bereits vorliegen. Dadurch ergeben sich einige Vorteile, wie etwa milde Reaktionsbedingungen und die Vermeidung von flüchtigen und/oder pyrophoren Substanzen, sodass die Synthese der single-source-Precursor und deren Nutzung als Ausgangsprodukte zur Herstellung von M_xE_y-Nanokpartikeln (M = Ge, Sn; E = P, As) die Methode der Wahl war. Dabei schienen die beiden literaturbekannten Verbindungen $[CH(C(Me)(2,6\text{-}^{i}Pr_2C_6H_3))_2]MP(SiMe_3)_2$ (M = Ge (**4-D**), Sn (**4-E**)) sowie das neuartige $[CH(C(Me)N\text{-}(2,6\text{-}^{i}Pr_2C_6H_3))_2]SnAs(SiMe_3)_2$ (**4-4**) äußerst vielversprechend für die Zersetzung in die gewünschten nanoskopischen Substanzen zu sein. Zuvor wurden jedoch die schwereren Homologen von **4-D** und **4-E** $[CH(C(Me)N(2,6\text{-}^{i}Pr_2C_6H_3))_2]MAs(SiMe_3)_2$ (M = Ge (**4-3**), Sn (**4-4**)) erfolgreich synthetisiert und vollständig charakterisiert (Abbildung 6-2 - 2).

4-3 und **4-4** wurden dabei durch die Reaktion von $[CH(C(Me)N(2,6\text{-}^{i}Pr_2C_6H_3))]MCl$ (M = Ge, Sn) mit $LiAs(SiMe_3)_2$ dargestellt, wobei **4-4** in guten Ausbeuten erhalten werden konnte, während **4-3** in nicht ausreichenden Mengen isolierbar war, weshalb **4-3** als möglicher single-source-Precursor nicht in Betracht gezogen wurde.

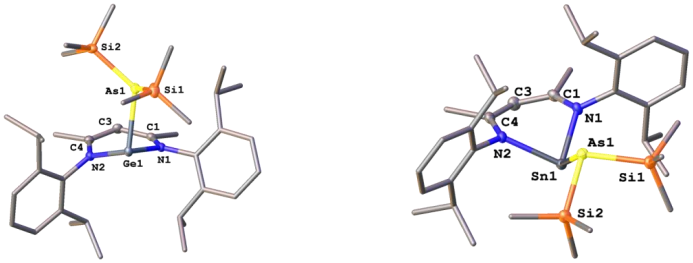

Abbildung 6-2 - 2: Links: Kristallstruktur von **4-3**. Rechts: Molekülstruktur von **4-4**.

Daher wurde nur das Zinn-Analogon **4-4** in den Nanopartikel-Tests verwendet. Dabei wurden alle Experimente gemäß der hot-injection-Methode in Mesitylen bei einer Gesamtreaktionszeit von 1 h oder 24 h und einer Temperatur von 150 ° C durchgeführt. Im Fall von **4-4** führten diese Ansätze zur Bildung agglomerierter, sphärischer Teilchen, die allerdings nicht separierbar waren. Nichtsdestotrotz zeigen die Partikel eine durchschnittliche Größe von 10 bis 14 nm und eine Zusammensetzung von hauptsächlich Sn_4As_3 (Abbildung 6-2 - 3), was zeigt, dass **4-4** gut geeignet ist, um Zinnarsenid-Nanopartikel darzustellen.

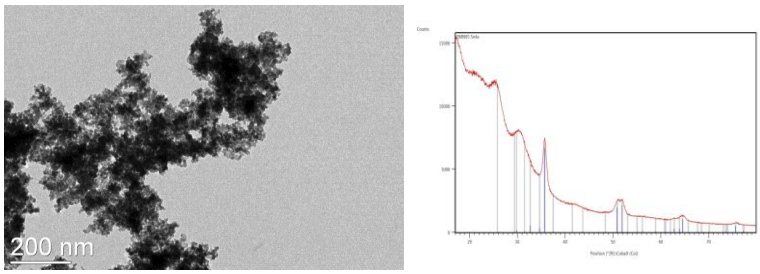

Abbildung 6-2 - 3: Links: TEM-Aufnahmen der aus der Zersetzung von **4-4** mit 1 äq. PA erhaltenen Nanopartikel. Rechts: XRD-Diffraktogramm der Partikel mit einer Zusammensetzung von Sn_4As_3.

Neben **4-4** wurden auch die Phosphorverbindungen **4-D** von Driess und **4-E** von Fulton auf ihre Eignung für die Synthese von Nanopartikeln hin untersucht, wobei sich ergab, dass die Ge-Verbindung **4-D** kein geeigneter Precursor ist. Trotz der Zersetzung zum gewünschten Germaniumphosphid Ge_4P_3, welches durch EDX-Analyse nachgewiesen werden konnte, zeigten Untersuchungen mit TEM-Analyse deutlich, dass keine regelmäßig geformten Nanopartikel von ähnlicher Größe vorhanden waren (Abbildung 6-2 - 4), was dazu führte, dass **4-D** als potentieller single-source-Precursor verworfen wurde.

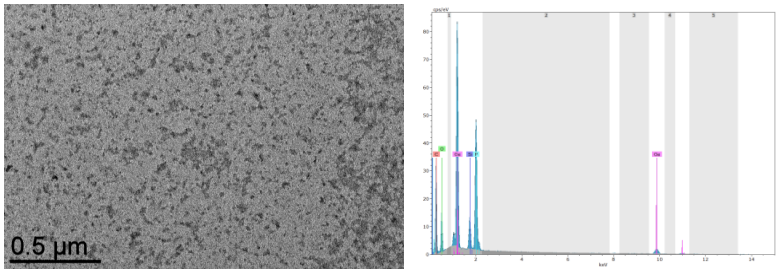

Abbildung 6-2 - 4: Links: TEM-Aufnahmen der Zersetzung von **4-D** mit 1 äq. PA (1 h). Rechts: EDX-Spektrum des aus der Zersetzung von **4-D** erhaltenen Niederschlags mit einer Zusammensetzung von Ge_4P_3. Die durchgeführten XRD-Analysen ergaben einen amorphen Feststoff.

Das schwerere Homologe **4-E** lieferte dagegen in den Reaktionen mit HDA sehr zufriedenstellende Ergebnisse, da der Komplex nicht nur wie erforderlich agglomerierte sphärische Nanopartikel mit einer durchschnittlichen Größe von etwa 10 bis 22 nm bildet, sondern auch zu Sn_4P_3 zerfällt (Abbildung 6-2 - 5).

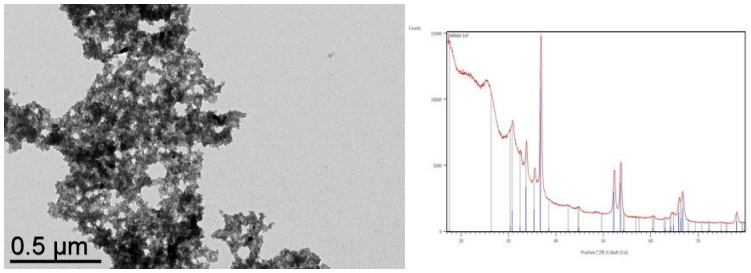

Abbildung 6-2 - 5: Links: TEM-Bild der Nanopartikel aus der Umsetzung von **4-E** mit 0,5 äq. HDA (24 h). Rechts: XRD-Diffraktogramm der Produkte der Reaktion von **4-E** mit einer Zusammensetzung von Sn_4P_3.

Zusammengefasst zeigen die im Verlauf der Experimente durchgeführten Analysen, dass die beiden Zinnverbindungen $[CH(C(Me)N(2,6\text{-}^{i}Pr_2C_6H_3))_2]SnE(SiMe_3)_2$ (E = P (**4-E**), As (**4-4**)) geeignete und vielversprechende molekulare Vorstufen für die Synthese von Nanopartikeln sind.

Zusätzlich zu den Synthesen von **4-3** und **4-4**, die speziell für ihre Verwendung als Precursor hergestellt wurden, wurden auch grundlegende Untersuchungen zur Reaktivität von $[CH(C(Me)N(2,6\text{-}^{i}Pr_2C_6H_3)_2]MCl$ (M = Ge, Sn) mit der lithierten Verbindung $LiCH_2SiMe_3$ durchgeführt. Diese Ansätze resultierten in der erwarteten Bildung von $[CH(C(Me)N(2,6\text{-}^{i}Pr_2C_6H_3))]MCH_2SiMe_3$ (M = Ge (**4-1**), Sn (**4-2**)), die vollständig durch NMR-Spektroskopie, Massenspektrometrie, Elementar- und Röntgenstrukturanalyse charakterisiert wurden (Abbildung 6-2 - 6).

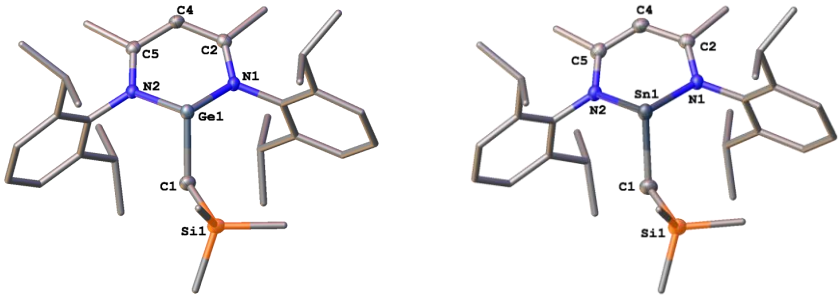

Abbildung 6-2 - 6: Links: Festkörperstruktur von **4-1**. Rechts: Molekülstruktur von **4-2**.

6.2.3. Phosphor, Zink und Gallium enthaltende molekulare Vorstufen

Zinkphosphid-Precursor

Nanoskaliges Zn_2P_3 verspricht ein geeignetes Material für zukünftige photovoltaische Anwendungen zu sein, sodass einfache und ungiftige Synthesemethoden wie die der single-source-Precursor-Methode sehr attraktiv scheinen und somit das Interesse an der Herstellung neuer Zinkphosphorverbindungen für die Zersetzung zu Nanopartikeln geweckt wird. In dieser Arbeit liegt nun der Fokus auf der Synthese einer neuen Familie von Zinkkomplexen, stabilisiert durch einen vielseitigen Benzamidinatoliganden, die in P-haltige Vorstufen umgewandelt werden können. So war es möglich, die drei Zn-Verbindungen $[PhC(N^{t}Bu)_2]_2Zn$ (**5-1-1**), $\{[PhC(N^{t}Bu)_2]Zn_2Br_3\}_n$ (**5-1-2**) und $[PhC(N^{t}Bu)_2]H \cdot ZnBr_2$ (**5-1-3**) erfolgreich darzustellen, wobei letzteres in der Reaktion mit $LiP(SiMe_3)_2$ zur Bildung von $\{Zn[P(SiMe_3)_2]_2\}_2$ (**5-1-C**) führt.

Während **5-1-1** erhalten werden kann, indem ein äq. $^{t}BuN=C=N^{t}Bu$, ein äq. PhLi und ein äq. $ZnBr_2$ zur Reaktion gebracht werden, ist das polymere **5-1-2** das unerwartete Produkt der Reaktion von einem äq. $^{t}BuN=C=N^{t}Bu$ und einem äq. PhLi mit zwei äq. $ZnBr_2$ (Abbildung 6-2 - 7 oben). Da diese beiden naheliegenden Ansätze nicht zu einem monomeren Zinkbromidkomplex führten, wurde das Intermediat der Umwandlung von $^{t}BuN=C=N^{t}Bu$ und PhLi $[PhC(N^{t}Bu)_2]Li$ zunächst isoliert und dann 1:1 mit $ZnBr_2$ umgesetzt. Die Reaktion ergab allerdings durch Spuren von Wasser, die sich nicht vermeiden ließen, die Verbindung **5-1-3** (Abbildung 6-2 - 7 unten links), welche dann mit $LiP(SiMe_3)_2$ zu einem potentiellen Vorläufer für Zinkphosphid-Nanopartikel reagierte. Das erzielte Produkt ist die

literaturbekannte Spezies **5-1-C**, die von den Autoren der entsprechenden Publikation bereits thermisch zersetzt wurde, wobei aber nicht das gewünschte Zn_2P_3 erhalten werden konnte. Da die Kristallstruktur von **5-1-C** zuvor bei Raumtemperatur bestimmt wurde, war es nun möglich, bei der Durchführung der Röntgenstrukturanalyse bei tiefen Temperaturen einen Phasenübergang bei 137 K zu beobachten (Abbildung 6-2 - 7 unten rechts).

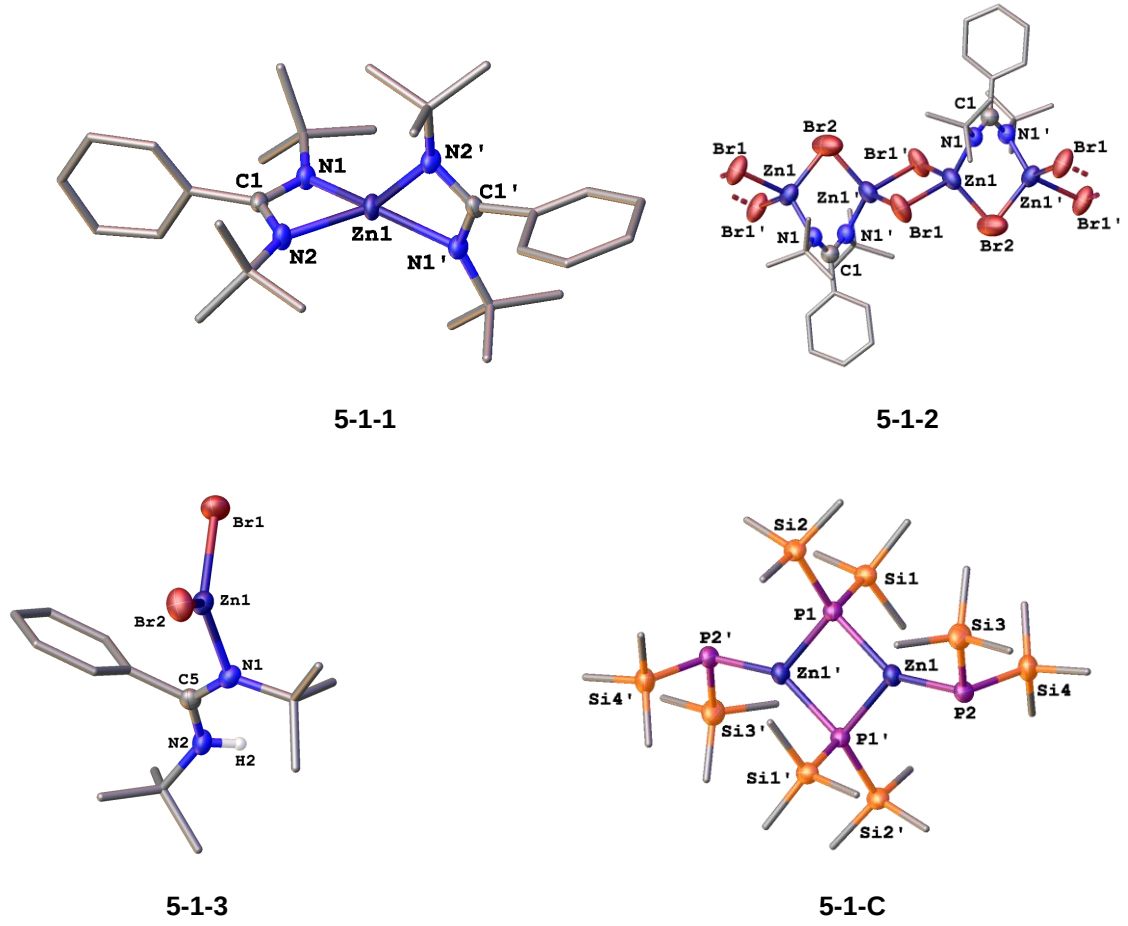

Abbildung 6-2 - 7: Kristallstrukturen von **5-1-1**, **5-1-2**, **5-1-3** und **5-1-C**.

Voruntersuchungen zur Verwendung von $[CH(C(Me)N(2,6\text{-}^{i}Pr_2C_6H_3))_2]Ga(PH_2)_2$ in der Nanopartikelsynthese

Abschließend wurde eine Studie zur Herstellung von GaP-Nanopartikeln unter Verwendung der von Susanne Bauer erstmals synthetisierten und charakterisierten Galliumverbindung $[CH(C(Me)N(2,6\text{-}^{i}Pr_2C_6H_3))_2]Ga(PH_2)_2$ (**5-2-B**) durchgeführt. Die Experimente wurden dabei analog zu der in Kapitel 4.4 beschriebenen Vorgehensweise mit HDA und PA als Zersetzungs- und Stabilisierungsmittel durchgeführt.

Obwohl es im Zuge dieser Experimente nicht möglich war, Nanopartikel zu erhalten (Abbildung 6-2 - 8), zeigten die EDX-Analysen des gebildeten Niederschlags die gewünschte Zusammensetzung von GaP mit einem leichten Galliumüberschuss.

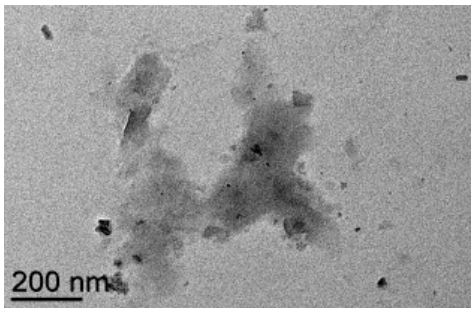

Abbildung 6-2 - 8: TEM-Aufnahme des Niederschlags aus der Reaktion von **5-2-B** mit 1 äq. HDA.

7. Appendix

7.1. List of numbered compounds

Numbered compound	Structural formula	Crystal structure
Starting material		
3-1	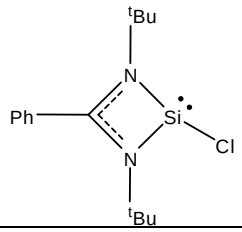	-
Synthesized during this thesis		
3-2	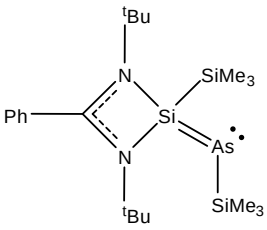	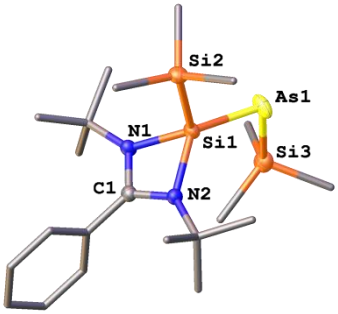
3-3	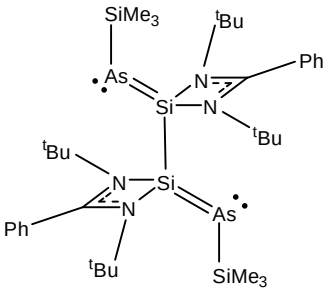	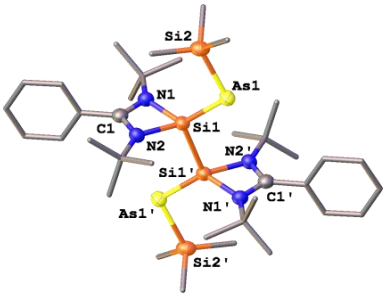
3-4	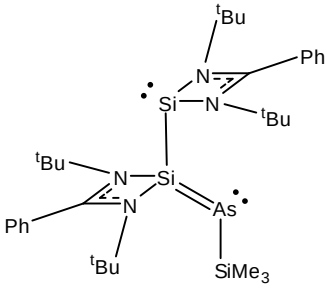	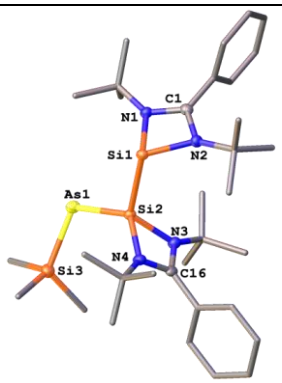
3-5	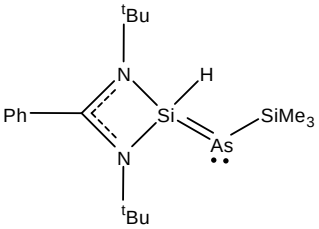	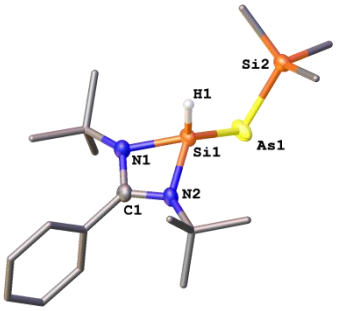

3-6	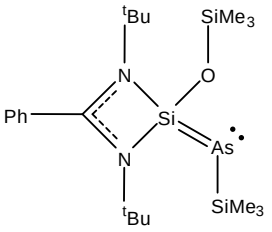	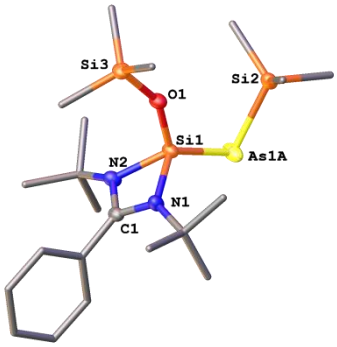
3-F Already known in literature	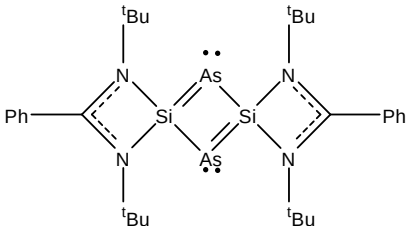	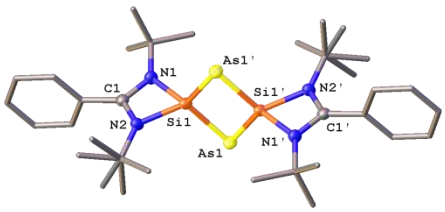
Starting material		
4-A	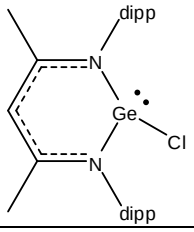	-
4-B	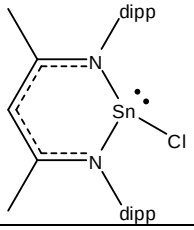	-
Ligand used		
L^3	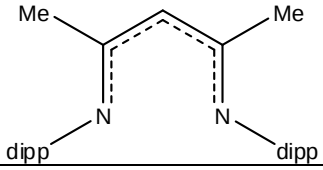	-
Synthesized during this thesis		
4-1	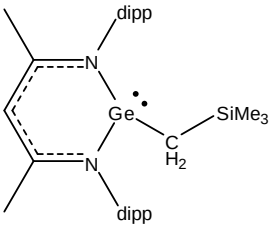	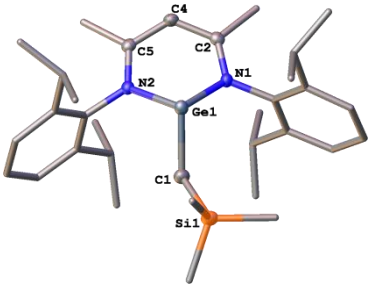

4-2	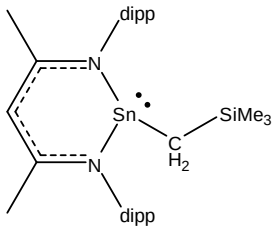	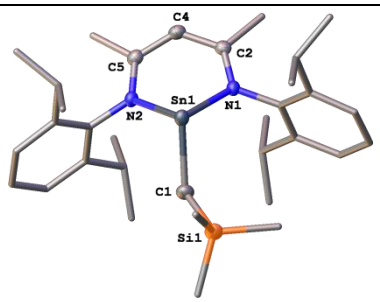
4-3	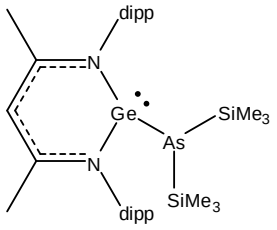	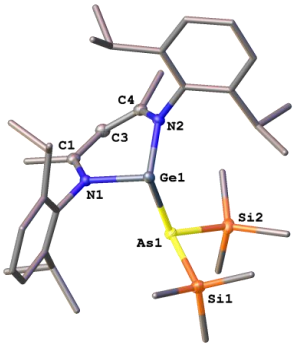
4-4	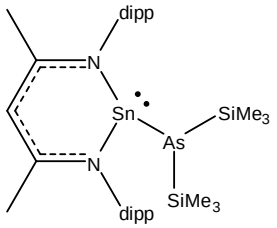	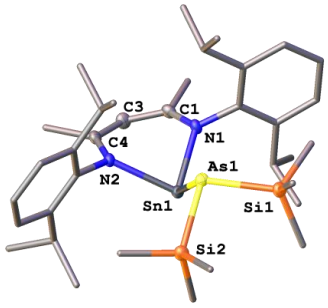
Starting material		
5-1-E	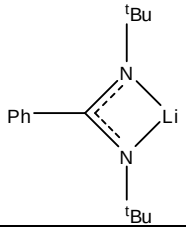	-
Synthesized during this thesis		
5-1-1	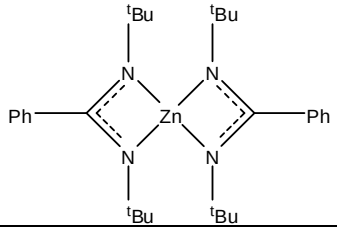	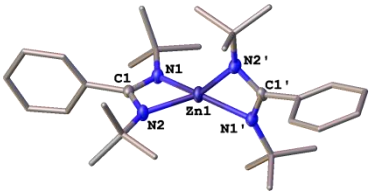
5-1-2	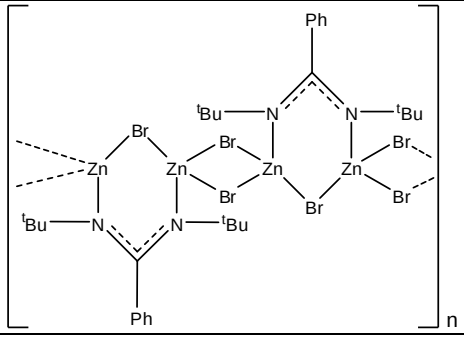	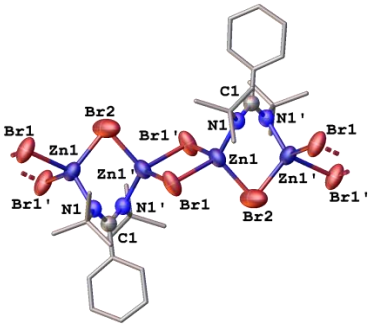

5-1-3	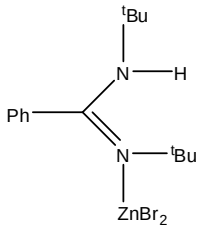	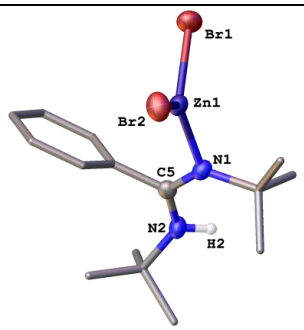
5-1-C Already known in literature	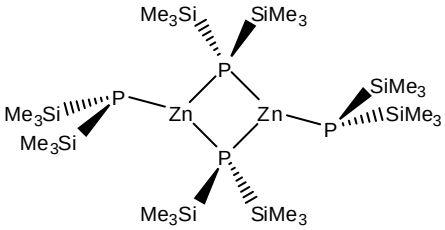	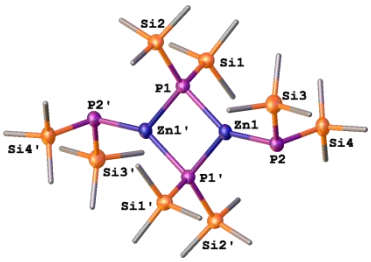
Starting material		
5-2-B	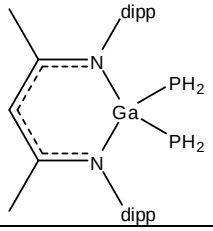	-

7.2. List of Abbreviations

NMR Spectroscopy	
NMR	Nuclear Magnetic Resonance
δ	chemical shift
ppm	part per million
Hz	Hertz, s^{-1}
J	coupling constant, Hz
s	singlet
d	doublet
t	triplet
sept	septet
m	mulitplet
VT	variable-temperature
DEPT	Distortionless enhancement by polarization transfer
Solvents and other chemicals	
THF	Tetrahydrofurane C_4H_8O
Toluene	C_7H_8
Et_2O	Diethylether $C_4H_{10}O$
Mesitylene	C_9H_{12}
HDA	Hexadecylamine $C_{16}H_{35}N$
PA	Palmitic acid $C_{16}H_{32}O_2$

Mass Spectrometry	
MS	Mass Spectrometry
$[M]^+$	molecular ion peak
m/z	mass to charge ratio
LIFDI	liquid injection field desorption ionization
EI	electron ionization
Electron microscopy and related analytic methods	
TEM	Transmission electron microscope
SEM	Scanning electron microscope
AFM	Atomic force microscope
STM	Scanning tunnel microscope
EDX	Energy dispersive X-ray spectroscopy
XRD	Powder X-ray diffraction
Substituents	
Ph	Phenyl, $-C_6H_5$
dipp	2,6-diisopropylphenyl
R	organic substituent, specified in text
Me	Methyl, $-CH_3$
*t*Bu	*tert*-Butyl, $-C_4H_9$
Other	
Å	Angstroem 1 Å = $1 \cdot 10^{-10}$ m
T	Temperature [K] or [°C]
c	Concentration [mol · L^{-1}]
n	Amount of substance [mol]
v	Wavelength [nm]
d	Distance [Å]
∢	Angle [°]
r.t.	room temperature
eq.	Equivalent
M	metal, specified in text
E	group 15 element
NP	Nanoparticle
UV	Ultraviolet range of the light spectrum v = 100 – 380 nm
VIS	Visible range of the light spectrum v = 380 – 740 nm
FT-IR	Fourier-transform infrared

7.3. Acknowledgements

In the end, I'd like to thank

- Prof. Dr. Manfred Scheer for the opportunity to do my Ph.D. thesis at his workgroup, for providing the interesting research topic and the extraordinary working conditions as well as affording my research stay in Toulouse.
- Dr. Gábor Balázs for proof-reading each of my papers and the thesis, for the DFT calculations and, most importantly, for his patience and the countless ideas, in order to find a way to reproduce those accursed (I'd really like to use a more appropriate word, but this is a Ph.D. thesis...) special silicon compounds. Thank you so much for all of your help!
- Dr. Cèline Nayral, Dr. Fabien Delpech, Dr. Edwin A. Baquero, Prof. Dr. Bruno Chaudret and all people of the work group Nanostructures and Chimie Organométallique for the teamwork in our cooperation project and for the wonderful time during my research stay. Thank you all you guys for the good work and the various experiences I was able to make! I'd especially like to thank Dominikus for inviting me to join the events every weekend! It was really great!
- Dr. Michael Seidl (my second-most favourite Michi in the whole world!) for all the proof-reading (two times!), the structure calculations and the advice for my X-ray stuff and everything.
- Georgine Stühler, Annette Schramm, Fritz Kastner and Dr. Ilya Shenderovic from the NMR department for the countless NMR spectra, normal or VT, and my special requests like the ^{29}Si spectrum.
- Wolfgang Söllner and Josef Kiermaier for their patience, their knowledge and all the solid state mass spectrometry measurements although they didn't like this method.
- Barbara Baumann and Helmut Schüller for the elemental analyses.
- Felix Riedlberger for the cyclovoltammetric measurement I needed once.
- Rudolf Weinzierl for the EPR measurements.
- The ladies and gentlemen from the glass-blowing, the electronic and the mechanic studios for their patience and their know-how for all that stuff that urgently needed to be repaired.
- The nice lady from the cleaning service, who always had a kind smile for me.
- All the former and current members of the Scheer group for all the advice and the funny times: Anna, Andi, Barbara B., Barbara, Barbara T., Bianca, Billie, Christian G., Christian S., Christoph, Claudia H., Claudia, David, Eric, Eva, Fabi, Felix L., Felix R., Gábor, Helena, Hias, Jana, Jens, Julian, Karin, Kevin, Liese, Luigi, Luis, Martin W., Martina, Matthias H., Matthias L., Mehdi, Mia, Moritz, Moni, Musch, Muschine, Nase, Olli, Petra, Pieschi, Rebecca, Sebi, Schotti, Stephan, Susanne, Vroni, Walter, Wast, Wurzl.
- My dear Andrea for all your visits in my lab, for all the hugs and the jokes, be it Coldmirror or anything else. *Ich hab Sie im Radio gesehen!*
- My most favourite lab, to Lena, Reini, Rudi and Michi, considering that I could visit you, whenever I needed a good laugh or the opportunity to tell you the events of the latest Star Wars roleplay game. Not to forget the two new players I found for the game on Mondays! Right, Reini and Rudi? *Herbert!! Leg die Waffen nieder!*
- The best Tobi, the best Helena, Felix, Claudia and Maria in the whole world for the best lunch breaks ever with exiting books, interesting discussions, the wortguru-games and the invention of the insulting mandarine! *SCHIFF!! – Echt jetz?! Die Buchstaben da ergeben noch nicht mal ansatzweise "Schiff"! – Ne, aber "Elan". – [Entnervtes Gemaule aller Anwesenden] Das Level ist doof!*
- My lovely, wonderful Pia! Thank you for your all-time support, for your kind words, your jokes, your hugs, your everything! I'm glad for all those little coincidences by which we were able to meet and my life wouldn't be the same without our countless skype-talks. *Ich bin dein größter Fan! – Und ich bin dein größter Fan! – Liebööööööh!!!*

- My beautiful, intelligent, most amazing and completely crazy girls Jeannine and Judy. Thank you for all the laughs, the cries and absolutely everything! I love you from the bottom of my heart! *Könnte das mit ganz viel Fantasie aussehen wie Ravioli...? Jaaaaa!*
- My brilliant friends Kati, Manu, Moni, Rudi, Reini, Franzi, Tobi, Frauke, Maria, Paul, Chrissimon, Johanna, Yui, Andrea, Tobi, Melli, Claudia, Maria, Helena, Chris, Stefan with Julian (Krümel), Axel, Stephan, Tassilo, Jürgen, Simon, Lara, Paul, Uschi and Sina for the parties, for the quiet evenings, for the fantastic Star Wars and Fantasy games, for the big things and the little ones! *Na, Pummelfee? – Ja, ich seh schon, du willst, dass ich dir wieder ein Schiff direkt vor die Nase setze! – Äh... nein?! – Ja, doch! Komm! Würfle! Versuch, auszuweichen...! Ach, und weißt du was? Wir werten noch einen auf! – Och... nööööö!*
- The best family in the world. Mine. To Mama, Papa, my grandparents, Michi (my most favourite Michi in the whole world!) and his wonderful Josy for all your support, the phone calls, the laughter and for making everything brighter. *Hallo!!! Ich bin wieder zuhause! – Aha. Und wann fährst du wieder? – HÖH?!*
- Markus. Because reasons. Many reasons.

"You don't have to be crazy to do this. But it sincerely helps."

Bob Ross